UTS UNIVERSITY OF TECHNOLOGY SYDNEY

Evolutionary Adaptation of Priority Pathogen *Acinetobacter baumannii* to Nanoparticulate and Ionic Forms of Silver

by Oliver McNeilly

Thesis submitted in fulfilment of the requirements for the degree of

Doctor of Philosophy

under the supervision of A/Prof Cindy Gunawan, Dr Mehrad Hamidian, and Dr Riti Mann

University of Technology Sydney
Australian Institute for Microbiology and Infection
Faculty of Science

November 2023

CERTIFICATE OF ORIGINAL AUTHORSHIP

I, Oliver McNeilly, declare that this thesis is submitted in fulfillment of the requirements for the award of Doctor of Philosophy, in the Australian Institute for Microbiology and Infection (AIMI), Faculty of Science, at the University of Technology Sydney.

This thesis is wholly my own work unless otherwise referenced or acknowledged. In addition, I certify that all information sources and literature used are indicated in the thesis.

This document has not been submitted for qualifications at any other academic institution.

The research is supported by the Australian Government Research Training Program and an Australian Research Council Discovery Project Scholarship (DP 180100474 and DP 220101819).

Production Note:
Signature removed prior to publication.

November 2023

ACKNOWLEDGEMENTS

It is a profound feeling knowing that as I make my acknowledgements it marks the culmination of this four-year-long PhD project. It is safe to say that that this experience has been both a pleasure and a privilege and one that I will not forget. The knowledge, experience, and skills I have gained throughout this journey have been undeniably rewarding and have ultimately reshaped who I am. I am profoundly grateful to all those who have supported and contributed to the completion of this thesis. Their guidance, encouragement, assistance, and friendship have played a vital role in bringing this work to fruition.

First and foremost, I extend my deepest gratitude to my core supervisor, A/Prof Cindy Gunawan, for providing me this opportunity and placing her trust in me to complete this project. I am grateful for her unwavering expertise and support throughout my entire PhD. From way back in my 2018, with my Honours project, and onwards through my PhD, Cindy has been a faithful supervisor who has guided me to become to a better scientist. Her constant feedback and recommendations regarding both experimental and written work has helped sharpen my critical thinking and academic writing skills. I am forever indebted to Cindy's accessibility and attentiveness. No matter the time of day, she was always free for a quick face-to-face meeting or answer any questions over the phone. To say Cindy is a workaholic is an understatement, but her academic and scientific drive and passion gave me the confidence and willpower to persevere through this challenging project.

I would like to express my deep appreciation to my other PhD supervisors, Dr Mehrad Hamidian and Dr Riti Mann for their expertise, constructive feedback, and assistance in the laboratory. Mehrad's extensive knowledge of the bacterial species used throughout this project was of critical value, and without him, I would have been quite lost, and completion of this work would have been near impossible. I also thank him for guiding me through the molecular work in the laboratory, particular with troubleshooting and helping improve my technique. I give my sincerest thanks to Riti who helped nurture and develop my principal laboratory and microbiological skills, for her thorough assistance with data interpretation and result discussions, and, importantly, for being my desk buddy.

All-in-all, I sincerely thank my supervisors for their immense support throughout my PhD project. Their dedication, meticulous review, and editing of my published journal articles as well as my overall thesis have significantly contributed to its overall quality. I am truly proud to have my name on this work, thanks to their insightful suggestions and constructive feedback.

I would like to thank Dr Max Cummins and Distinguished Prof Steven Djordjevic for their valued assistance with the comparative genomic analysis work and for their contributions and critiques of my first published research article, which formed the first results Chapter of this thesis. I am also thankful to Max for his friendship and for taking the time to chat in the office, whether it was for technical assistance or about what our weekend plans were.

I am also grateful to A/Prof Louise Cole and Dr Amy Bottomley of the MIF lab for their unwavering assistance with microscopy work and, most recently, for granting me the opportunity to become a SuperUser of the DV Elite fluorescence microscope. I am also very thankful to Joyce To for her assistance with biofilm-related experiments and for performing the quality control assessment for my RNA extractions.

I extend my gratitude to Igor Makunin from QCIF who performed the RNA-Seq data analysis which formed my last two results Chapters. I am very appreciative of the time he took to perform this work and for his willingness to answer any queries I had when interpreting the data.

I also give thanks to Cindy's past PhD student, Dr Elizabeth Valentin, as not only a friend but also because her experimental work and final thesis provided a skeleton for me to follow. I also thank Cindy's current PhD student, Kevin Yonathan, as well as Mehrad's students, Jonathan Koong and Liam Tobin, for their friendship and casual chats to distract us from our workloads, and for helping set up my bacterial cultures when I was not around. I also want to give a big thanks to Diren Reddy, who I met in my first year of undergrad at UTS back in 2015 and has been by my side as a close friend and colleague all the way through undergrad, Honours, and our PhD projects.

I am very thankful to the technical staff of the Level 7 Bioscience Laboratories, including Mercedes Ballesteros, Dr Luke Beebe, and Sarah Osvath, who are essential in ensuring the lab functions optimally and safely, and for providing me with assistance with the use of laboratory equipment and materials. I also give thanks to the

administrative staff, Meggie Leung, Shannon Hawkins, Shima Baradaran Vahdat, and Nikki Senyk, for their help with administrative documents and all payment/fund-related activity. I would also like to thank the HDR director, A/Prof Charles Cranefield, and the past director, A/Prof Ken Rodgers, for answering several queries regarding thesis formatting and submission.

I extend my appreciation to all those I have met throughout my candidature, including those at UTS who work/study in AIMI or in the Faculty of Science in general, as well as those I have met at various conferences and seminars, who showed great interest in my project and offered insightful ideas for future work.

Lastly, I want to express my deepest gratitude to my friends and family for their unconditional love, support, motivation, and overall interest in my PhD journey. To my High School and Uni friends, housemates, and all other friendly faces I have met over the past few years, thank you for your friendship, kindness, and means of escape from work and stress. I deeply thank my dad and step-mum, Jason and Helen, and my five siblings, Biba, Noah, Harley, Marty, and Elliott, who have all shown love and great admiration and regard for me and my work. To my partner and best-friend Joy, who I fortunately met a few months before I started my PhD. Thank you for your kind heart, your love and affection, for believing in me and motivating me, and for all the wonderfully delicious meals you made whilst I was stuck in work-mode.

Above all, I want to thank my beautiful mother, Dr Jodie McNeilly, whom without none of this would have ever been possible. I am profoundly grateful to you for shaping me into the person I am today and encouraging me to commence a PhD in the first place. Your relentless work ethic and thirst for knowledge is inspiring, which has been essential for me to successfully complete this thesis. I dedicate this work to you mum, even if you might not understand it!

LIST OF PUBLICATIONS

Journal Articles

McNeilly, O., Mann, R., Cummins, M.L., Djordjevic, S.P., Hamidian, M., Gunawan, C., 2023. Development of Nanoparticle Adaptation Phenomena in *Acinetobacter baumannii*: Physiological Change and Defense Response. *Microbiology Spectrum*, *11*(1), e02857-22. DOI: https://doi.org/10.1128/spectrum.02857-22

McNeilly, O., Mann, R., Hamidian, M., Gunawan, C., 2021. Emerging concern for silver nanoparticle resistance in *Acinetobacter baumannii* and other bacteria. *Frontiers in Microbiology*, *12*, p.652863. DOI: https://doi.org/10.3389/fmicb.2021.652863

Morel, J., McNeilly, O., Grundy, S. Brown, T., Gunawan, C., Amal, R. Scott, J., 2023. Nanoscale Titanium Surface Engineering via Low Temperature Hydrothermal Etching for Enhanced Antimicrobial Properties. *ACS Applied Materials & Interfaces, 15*(39)*,* pp. 46247–46260. DOI: https://doi.org/10.1021/acsami.3c09525

Mann, R., Mitsidis, D., Xie, Z., McNeilly, O., Ng, Y.H., Amal, R., Gunawan, C., 2021. Antibacterial activity of reduced graphene oxide. *Journal of Nanomaterials*, *2021*, pp. 1-10. DOI: https://doi.org/10.1155/2021/9941577

Mann, R., Holmes, A., McNeilly, O., Cavaliere, R., Sotiriou, G.A., Rice, S.A., Gunawan, C., 2021. Evolution of biofilm-forming pathogenic bacteria in the presence of nanoparticles and antibiotic: adaptation phenomena and cross-resistance. *Journal of nanobiotechnology*, *19*(1), pp.1-17. DOI: https://doi.org/10.1186/s12951-021-01027-8

Conference and Seminar Presentations

McNeilly, O.*, Mann, R., Cummins, M. L., Djordjevic, S. P., Hamidian, M. and Gunawan, C. “Phenotypic Modifications Induced in *Acinetobacter baumannii* Following Evolutionary Adaptation to the Nanoparticulate and Ionic Forms of Silver”. **2023 MIF Symposium** (Australia, November 2023)

McNeilly, O.*, Mann, R., Cummins, M. L., Djordjevic, S. P., Hamidian, M. and Gunawan, C. “Physiological Adaptation and Defence Responses of *Acinetobacter*

baumannii to Nanoparticulate and Ionic Forms of Silver". **ASMR NSW Annual Scientific Meeting** (Australia, June 2023)

McNeilly, O.*, Mann, R., Cummins, M. L., Djordjevic, S. P., Hamidian, M. and Gunawan, C. "Toxicological Response, Defence, and Physiological Change of *Acinetobacter baumannii* to Antimicrobial Silver Nanoparticles". **JAMS Sydney Monthly Seminar** (Australia, March 2023)

McNeilly, O.*, Mann, R., Cummins, M. L., Djordjevic, S. P., Hamidian, M. and Gunawan, C. "Understanding the Physiological and Defence Mechanisms of Silver Nanoparticle Resistance in the Bacterial Pathogen *Acinetobacter baumannii*". **EMBO Workshop: Molecular Mechanisms in Evolution and Ecology** (Germany, October 2022)

Gunawan, C.*, McNeilly, O., Mann, R., Valentin, E., Cummins, M. L., Djordjevic, S. P., Hamidian, M., and Faiz, M.B. "The Evolution of Bacteria Resistance Phenomena to Antimicrobial Nanoparticles". **ASMR NSW Scientific Meeting** (Australia, June 2022)

Gunawan, C.*, Mann, R., Holmes, A., McNeilly, O., Valentin, E., Cavaliere, R., Sotiriou, G.A., Rice, S.A., and Faiz, M.B. "Bacterial adaptation to nanoparticle toxicity and how to overcome it". **National Academy of Sciences, India – International Webinar Expert Series** (India, March 2022, virtual)

McNeilly, O.*, Mann, R., Cummins, M. L., Djordjevic, S. P., Hamidian, M. and Gunawan, C. "Understanding novel silver nanoparticle resistance in the critical level bacterial pathogen *Acinetobacter baumannii".* **Australian Prokaryote Genome & Cell Biology Symposium** (Australia, November 2021, Virtual)

McNeilly, O.*, Mann, R., Cummins, M. L., Djordjevic, S. P., Hamidian, M. and Gunawan, C. "Deciphering the molecular basis of silver nanoparticle resistance in the critical priority pathogen *Acinetobacter baumannii*". **Taylors University Graduate Research Symposium** (Malaysia, November 2021, Virtual)

McNeilly, O.*, Mann, R., Hamidian, M. and Gunawan, C. "Analysis of the Mechanisms of Adaptation to Silver Nanoparticles in *Acinetobacter baumannii*". **EMBL Australian PhD Symposium** (Australia, November 2020, Virtual) [2nd place for Poster Presentation**]**

Gunawan, C.*, Valentin, E., Mann, R., McNeilly, O., Bottomley, A. L., Sotiriou, G. A., Rice, S. A., Amal, R., Harry, E. J. "Genetically-Encoded Nanosilver Resistance in Priority Pathogen". **International Conference on Nanoscience and Nanotech** (Australia, February 2020)

Gunawan, C.*, Valentin, E., Mann, R., McNeilly, O., Bottomley, A. L., Sotiriou, G., Rice, S. A., Teoh, W. Y., Marquis, C. P., Amal, R., Harry, E. J. "Nanosilver and Priority Pathogen: Development of Resistance". **10th International Nanomedicine Conference** (Australia, June 2019)

Gunawan, C.*, Valentin, E., McNeilly, O., Bottomley, A. L., Sotiriou, G., Rice, S. A., Teoh, W. Y., Marquis, C. P., Amal, R., Harry, E. J. "The Emergence of Bacterial Resistance to Nanoparticles". **6th International Conference on Antibiotics, Antimicrobials and Resistance** (England, October 2018)

* Presenting author

TABLE OF CONTENTS

LIST OF FIGURES

LIST OF TABLES

SCIENTIFIC ABBREVIATIONS

%	Percent
°C	Degrees Celsius
µg/kg	Microgram per kilogram
µg/mL	Microgram per millilitre
µL	Microlitre
µM	Micromolar
µm	Micrometre
$\mu m^2/\mu m^3$	Micrometre squared per micrometre cubed
aa	Amino acid
Ag^+	Silver cation
Ag^{+T}	Silver cation-tolerant
Ag^0	Metallic silver
$AgNO_3$	Silver nitrate
AgSD	Silver sulfadiazine
AMR	Antimicrobial resistance
ARG	Antibiotic resistance gene
ATHA	Silver cation-tolerant high silver cation
ATLN	Silver cation-tolerant low silver cation
ATNT	Silver cation-tolerant no treatment
ATP	Adenosine triphosphate
BPEI	Branched polyethyleneimine
bp	Base pair
BR1	Biological replicate 1
BR2	Biological replicate 2
CAMHA	Cation-adjusted Mueller-Hinton agar
CAMHB	Cation-adjusted Mueller-Hinton broth
CC_{50}	50% cytotoxicity concentration
CFU/mL	Colony-forming unit per millilitre
CLSI	Clinical and Laboratory Standard Institute
CRAb	Carbapenem-resistant *Acinetobacter baumannii*

CPS	Capsular polysaccharide
CTCF	Corrected total cell fluorescence
Cu^{+}	Copper cation
d	Diameter
DEG	Differentially expressed gene
DNA	Deoxyribonucleic acid
DV	DeltaVision
eDNA	Extracellular deoxyribonucleic acid
EPS	Extracellular polymeric substance
ESBL	Extended-spectrum β lactamase
Fe^{2+}	Ferrous cation
f	Frequency
GC	Guanine-cytosine
GC1	Global clone 1
GC2	Global clone 2
GCL	Glutamate-cysteine ligase
GSH	Glutathione
GSSG	Glutathione disulfide
H_2DCFDA	2′,7′-dichlorodihydrofluorescein diacetate
H_2O_2	Hydrogen peroxide
$HgCl_2$	Mercury chloride
h	Hour/s
HIV	Human immunodeficiency virus
ICU	Intensive-care unit
IncHI-2	HI-2 incompatibility group
IS	Insertion sequence
kb	Kilobase
LC-MS	Liquid chromatography-mass spectrometry
M	Molar
MBEC	Minimum biofilm eradication concentration
MDK_{99}	Minimum duration of killing 99% of the population
$MDK_{99.99}$	Minimum duration of killing 99.99% of the population
MIC	Minimum inhibitory concentration

min	Minute/s
mg/mL	Milligram per millilitre
mL	Millilitre
mM	Millimolar
MDR	Multi-drug-resistant
MRG	Metal resistance gene
MRSA	Methicillin-resistant *Staphylococcus aureus*
n	Sample size
NADH	Nicotinamide adenine dinucleotide
NAg	Silver nanoparticles (nanosilver)
NAg^R	Nanosilver-resistant
NaOH	Sodium hydroxide
NHx	Amine
$-NH^+$	Histidine
$-NH_2^+$	Arginine
$-NH_3^+$	Lysine
ng	Nanogram
NRHN	Nanosilver-resistant high nanosilver
NRLN	Nanosilver-resistant low nanosilver
NRNT	Nanosilver-resistant no treatment
Nx	Nalidixic acid
Nx^R	Nalidixic acid-resistant
O_2	Molecular oxygen
O_2•-	Superoxide
OD_{600}	Optical density measured at 600 nanometres
OH•	Hydroxyl radical
OMP	Outer membrane protein
OXA	Oxacillinase
PALM	Photoactivated localisation microscopy
PBS	Phosphate-buffered saline
PCA	Principal component analysis
PCR	Polymerase chain reaction
PI	Propidium iodide

PNAG	Poly-β-(1-6)-*N*-acetylglucosamine
PPE	Personal protective equipment
PVP	Polyvinylpyrrolidone
PMB	Polymyxin-B
RNA	Ribonucleic acid
RNA-Seq	Ribonucleic acid sequencing
rRNA	Ribosomal ribonucleic acid
ROS	Reactive oxygen species
rpm	Revolutions per minute
RT-qPCR	Reverse transcription quantitative polymerase chain reaction
s	Second/s
$-S^-$	Thiol
SAV	Surface-area-to-volume (ratio)
SBR	Sequencing batch reactor
SEM	Scanning electron microscopy
SNP	Single nucleotide polymorphism
spp.	Species (plural)
sp.	Species
ST1	Sequence type 1
ST2	Sequence type 2
TBE	Tris-Borate-EDTA
TCLP	Toxicity characteristic leaching procedure
TEM	Transmission electron microscopy
TiO_2	Titanium dioxide
tRNA	Transfer ribonucleic acid
U/μL	Enzymatic unit of activity per microlitre
wt%	Percentage by weight
WTLA	Wild-type low silver actions
WTLN	Wild-type low nanosilver
WTNT	Wild-type no treatment
Zn^{2+}	Zinc cation
ζ	Zeta potential

ABSTRACT

The escalating threat of antimicrobial resistance (AMR) necessitates immediate, innovative solutions to combat it. Silver nanoparticles (nanosilver; NAg) have emerged as one of the most commercialised alternative antimicrobial agents, renowned for their multi-targeting and broad-spectrum antimicrobial properties. Worringly, the widespread and often indiscriminate use of these nanoparticles has raised concerns over the emergence of silver-resistant bacteria. This thesis herein describes, for the first time, the ability of *Acinetobacter baumannii*, an important Gram-negative coccobacillus bacterium, and an ESKAPE pathogen (the group of six leading hospital-acquired bacterial pathogens), to evolve stable resistance to NAg. The model ATCC 19606 strain was able to proliferate at otherwise toxic nanoparticle concentrations following prolonged exposure. Remarkably, the bacterium also demonstrated a distinct adaptation trait to the ionic form of silver (Ag^{+}), exhibiting a 'slower-to-kill' tolerance phenotype, a silver defence phenomenon also not previously seen in *A. baumannii*. Comparative whole genome analysis detected stable silver-induced gene mutations in the NAg-resistant (NAg^{R}) and Ag^{+}-tolerant (Ag^{+T}) strains. Detailed molecular studies revealed shifts in gene expression patterns in the silver-adapted strains in response to varied concentrations of the respective silver antimicrobials. The study identified tiered primary and secondary defence mechanisms that enable the bacteria to protect itself against the key cell envelope targeting and oxidative stress-mediated toxicity mechanisms of the silver agents. Notably, there were clear overlaps in defence responses between the silver-adapted bacteria to both NAg and Ag^{+}, despite their distinct adaptation characteristics. This thesis ultimately provides insights into the molecular basis of nanoparticulate and ionic silver defence in *A. baumannii* ATCC 19606, shedding light on how the bacterium physiologically evolved because of continual silver exposure. The elucidation of the adaptation phenomena can help enable future drug design that can target bacterial defence mechanisms to overcome evolutionary adaptation. The findings of this work caution against the indiscriminate use of antimicrobial silver and stress the need for implementing effective regulatory strategies to manage the responsible application silver-based products to ensure their continued and long-term use in the future.

Chapter 1: Introduction

The World Health Organisation (WHO) now considers bacterial antimicrobial resistance (AMR) to be one of the greatest public health crises facing humanity[1]. In 2019, roughly 4.95 million deaths were associated with AMR-related bacterial infection[2]. At current projected rates, it is argued that by 2050, 10 million annual deaths will be attributable to AMR, and that, between now and then, the accumulative economic cost could exceed 100 trillion USD[3]. The growing burden of global AMR can be ascribed to the misuse and overuse of antibiotic drugs, specifically including improper patient prescription, excessive agriculture/aquaculture applications[4,5], and dwindling pharmaceutical investment in antibiotic research and development[6-8].

The leading causes of nosocomial (hospital-acquired) AMR infections are a group of bacteria known as the ESKAPE pathogens (*Enterococcus faecium, Staphylococcus aureus, Klebsiella pneumoniae, Acinetobacter baumannii, Pseudomonas aeruginosa,* and *Enterobacter spp.*)[9]. These organisms represent the archetypal bacterial species responsible for infection, transmission, and adaptation, and pose a serious threat to the elderly, chronically ill, and immunocompromised[9-11]. Notably, the WHO has recently cited carbapenem-resistant *A. baumannii* (CRAb) as the top critical priority pathogen necessitating the immediate development of alternative and novel antibacterial treatment options[7].

A Gram-negative, strictly aerobic, coccobacilli, and opportunistic bacterial pathogen, *A. baumannii* has attracted considerable scientific and medical attention in recent decades[12-15]. This bacterium is frequently isolated in hospital-settings and is responsible for a range of nonspecific illnesses, such as pneumonia, wound infections, and bloodstream infections[14,16]. It is a highly successful pathogen due to its natural resistance to environmental stressors and innate ability to readily acquire resistance determinants from external sources, typically facilitated by plasmid uptake. Consequently, the emergence of multi-, extensive- and pan-drug resistant strains has become increasingly common[17,18]. These factors underline the urgent need for effective substitutes to traditional antibiotics to tackle this bacterium.

Silver nanoparticles (nanosilver; hereafter referred to as NAg) represent a highly promising alternative to traditional antimicrobials and, as such, have gained significant

commercial traction. These ultrafine nanoparticulates range in size of 1-100 nm in diameter and consist of metallic silver (Ag^0) or silver oxide (Ag_2O). Their popularity stems from their unique physiochemical properties and efficacious broad-spectrum and multi-targeting antimicrobial activity[19-22]. As a result, the healthcare sector has become one of the biggest markets for NAg, incorporating the nanoparticle as a surface coating agent in medical devices such as catheters, wound dressings, and prosthetics[22-24]. Troublingly, however, the advances in nanotechnology have enabled the widespread application of NAg in a variety of consumer products, including clothing/textiles, hygiene products, household appliances, and even infant goods[25,26]. This pervasive and indiscriminate use of NAg has raised notable concern within the scientific community over the development of silver-resistant bacteria, akin to that observed with antibiotics[25].

Bacterial resistance to cationic silver (Ag^+) has been acknowledged for some time, but NAg resistance development was considered unlikely due to its complex properties and multi-targeting toxicity mechanisms[27]. Nevertheless, recent research has demonstrated that various Gram-positive and Gram-negative bacterial species, including *Escherichia coli, P. aeruginosa, S. aureus,* and *Bacillus* spp., were capable of evolving NAg resistance[28-32]. Despite this, it is not yet clear whether *A. baumannii* has the potential to develop resistance to NAg[33]. A small selection of works have identified Ag^+ resistance traits in *A. baumannii*, including the well-known Sil Ag^+ binding/efflux system[34-36]. While both NAg and Ag^+ have shown high antibacterial efficacy against this species and its drug-resistant strains, our understanding of the interactions between the bacterium and antimicrobial silver is limited[37-41]. Therefore, it is crucial to thoroughly investigate and comprehend the antibacterial activity of NAg and Ag^+ against *A. baumannii*, with a core focus on elucidating the adaptive responses of the bacterium. This knowledge will help ensure the effectiveness of these important alterative agents are preserved in the long-term.

1.1 Scope and Aims of Thesis

This thesis investigated the potential emergence of stable NAg resistance in *A. baumannii* following prolonged and repeated exposure, in comparison with Ag^+ (as silver nitrate; $AgNO_3$). The study aimed to draw attention to the growing threat of

bacterial silver resistance and highlight that the adaptation phenomena is not species-specific. It was essential to identify unique mechanisms of adaptation that may develop to each agent and recognise any potentially shared resistance determinants. Despite the increasing overuse of NAg and other silver agents, there is limited knowledge on the interaction between *A. baumannii* and antimicrobial silver, particularly regarding adaptation. In turn, the data presented in this thesis is critical in helping better understand and subsequently address the emerging threat of bacterial silver resistance and its impact on public health.

To address the knowledge gaps and delineate the research question of this thesis, the principal objective of this work was divided into the following aims:

1. To observe the development of adaptation to NAg and Ag^+ in *A. baumannii* ATCC 19606 through prolonged exposure
2. To characterise the toxicological, physiological, and defence response/s of ATCC 19606 to NAg and Ag^+
3. To elucidate the molecular basis of adaptation of ATCC 19606 to NAg and Ag^+

This thesis contains a total of seven chapters. **Chapter 1**, herein, is an introductory chapter which briefly outlined current knowledge on the growing issue of bacterial NAg resistance, and the lack of knowledge regarding the interaction between NAg and *A. baumannii* – which together form the overarching motivation for this study – as well as the research objective and aims of this thesis. **Chapter 2** is a literature review publication which provides a comprehensive discussion of current knowledge on the physicochemical characteristics and unique antibacterial activity of NAg and Ag^+, as well as the advances in research on bacterial adaptation/s to silver which subsequently underlines the knowledge gaps in the field. Following this, **Chapter 3** provides details and justification of the materials and methodology utilised to conduct the experimental research for this project. **Chapter 4** showcases the first published evidence of NAg resistance and Ag^+ tolerance in *A. baumannii* ATCC 19606, which is followed by the identification of single nucleotide mutations in the genomes of the silver-adapted bacteria which were predicted to play a role in the physiological changes and expressed defence mechanisms exhibited by the nanosilver-resistant (NAg^R) and silver cation-tolerant (Ag^{+T}) strains. Next, in **Chapter 5** and **Chapter 6**, the toxicological and

defence responses of NAg^{R} and Ag^{+T} ATCC 19606 to the respective silver agents are described. This is followed by an explanation of the molecular basis of the defence mechanisms of the silver-adapted variants in response to NAg and Ag^{+} at the transcriptomic level, respectively. Finally, this thesis is concluded in **Chapter 7**, which delivers an overall discussion of the research findings and offers recommendations for future investigative work.

Chapter 2: Literature Review

2.1 Chapter summary

The following chapter outlines current understandings regarding the physicochemical and antimicrobial properties of silver nanoparticles (nanosilver, NAg) and discusses the growing overuse of the silver agent, the latter of which has raised concerns among the scientific community surrounding the generation of silver-resistant bacteria. Due to its proven multi-faceted and broad-spectrum antimicrobial activity, it is widely used in the medical sector, and in turn, has also seen increasing incorporation in consumer products. Consequently, over the last decade, several research inquiries have observed silver resistance traits in various bacterial species and identified many unique resistance and defence mechanisms. Nevertheless, no such studies have yet reported if the Gram-negative bacterium *Acinetobacter baumannii*, a WHO-listed critical priority nosocomial pathogen and member of the ESKAPE group, can develop resistance to NAg. The literature review herein critically assesses current knowledge and highlights the knowledge gap concerning the interaction between *A. baumannii* and NAg, particularly regarding evolutionary adaptation in the bacterium. The work presented in this literature review chapter is an annotated and partially edited reproduction of a published review article.

2.2 Declaration of publication

I, Oliver McNeilly, declare that the following publication included in lieu of this chapter meets the requirements for a thesis by compilation.

Published as:

Emerging Concern for Silver Nanoparticle Resistance in *Acinetobacter baumannii* and Other Bacteria

(https://doi.org/10.3389/fmicb.2021.652863)

Oliver McNeilly[1], Riti Mann[1], Mehrad Hamidian[1*], and Cindy Gunawan[1,2 *]

[1]Australian Institute for Microbiology and Infection, University of Technology Sydney, Broadway, NSW 2007, Australia

[2]School of Chemical Engineering, University of New South Wales, Kensington, NSW 2052, Australia

[*]Correspondence:
mehrad.hamdian@uts.edu.au; cindy.gunawan@uts.edu.au

Author Contributions: OM, MH, and CG conceptualised the paper. OM prepared the original draft. OM, RM, MH, and CG reviewed and edited the paper. MH and CG supervised the research. All authors have read and agreed to the published version of the manuscript.

Oliver McNeilly	Production Note: Signature removed prior to publication.
Riti Mann	Production Note: Signature removed prior to publication.
Mehrad Hamidian	Production Note: Signature removed prior to publication.
Cindy Gunawan	Production Note: Signature removed prior to publication.

2.3 Abstract

The misuse of antibiotics combined with a lack of newly developed options are the two main contributors to the current antibiotic resistance crisis. There is a dire need for new and alternative antibacterial options and the incorporation of nanotechnology may be a solution. Metal-based nanoparticles, particularly silver nanoparticles (NAg), have garnered widespread popularity due to their unique physicochemical properties and broad-spectrum antibacterial activity. Consequently, NAg has seen extensive incorporation in many types of products across the healthcare and consumer market. Despite clear evidence of the strong antibacterial efficacy of NAg, studies have raised concerns over the development of silver-resistant bacteria. Resistance to cationic silver (Ag^+) has been recognised for many years, but it has recently been found that bacterial resistance to NAg is also possible. It is also understood that exposure of bacteria to toxic heavy metals like silver can induce the emergence of antibiotic resistance through the process of co-selection. *Acinetobacter baumannii* is a Gram-negative coccobacillus and opportunistic nosocomial bacterial pathogen. It was recently listed as the number one critical level priority pathogen because of the significant rise of antibiotic resistance in this species. NAg has proven bactericidal activity towards *A. baumannii*, even against strains that display multi-drug resistance. However, despite ample evidence of heavy metal (including silver; Ag^+) resistance in this bacterium, combined with reports of heavy metal-driven co-selection of antibiotic resistance, little research has been dedicated toward assessing the potential for NAg resistance development in *A. baumannii*. This is worrisome, as the increasingly indiscriminate use of NAg could promote the development of silver resistance in this species, like what has occurred with antibiotics.

Keywords: antibiotic resistance, silver nanoparticles, *Acinetobacter baumannii*, silver resistance, co-selection

2.4 Introduction

The WHO has acknowledged that, alongside climate change and non-communicable disease, bacterial antibiotic resistance represents one of the most important crises to human health today[42]. It is projected that over 33,000 people in Europe alone die annually from resistant bacterial-related infections, making it a near equal health

burden to influenza, HIV, and tuberculosis combined[42,43]. In 2014, it was estimated that infection from antibiotic-resistant bacteria in the US resulted in a loss of over $20 billion in direct economic costs, and $35 billion through decline in societal productivity[9,44]. The leading cause of nosocomial infections globally is due to a league of bacteria which readily develop drug resistance, collectively referred to as the ESKAPE pathogens[10,11]. This group includes *Enterococcus faecium, Staphylococcus aureus*, *Klebsiella pneumoniae, Acinetobacter baumannii, Pseudomonas aeruginosa,* and *Enterobacter* spp. The ESKAPE organisms are the models of virulent and adaptive bacterial species, as they frequently cause severe and chronic disease and 'escape' the activity of antibiotics[10].

Of this group, *A. baumannii* has attracted significant attention over the last two decades due to the rapid onset of antibiotic resistance and worldwide spread of this species[13]. It is a Gram-negative, strictly aerobic coccobacilli and opportunistic bacterial pathogen that is generally associated with nosocomial infections, causing a range of nonspecific infections including pneumonia, soft tissue necrosis, and sepsis[17,45-47]. This bacterium became important throughout the 2001-2007 Iraqi and Afghan desert conflicts. Numerous medical and epidemiological reports documented a high incidence of multi-drug resistant *A. baumannii* infections among injured British and US soldiers, with one report stating 37% of the isolates were carbapenem-resistant[13,17,18]. International travel, including transportation of returning soldiers, is thought to be the main contributing factor in the global dissemination of resistance in *A. baumannii*[14]. This bacterium is naturally resistant to desiccation and is primarily isolated on medical equipment in hospitals, rather than in nature, and this frequently results in the infection of patients needing treatment with invasive apparatuses[48]. The recent COVID-19 pandemic has led to a significant surge in hospital and intensive-care unit (ICU) admissions. There have been numerous challenges in ensuring adequate personal protective equipment (PPE) is available for medical staff and that routine sterility management practices are maintained in COVID-19 dedicated hospitals[49,50]. Studies have reported increasing incidences of drug-resistant bacterial co-infections in COVID-19 patients, most often due to cross-contamination from other patients/staff and unsterile equipment[47,51]. Many of these incidences have included outbreaks of *A. baumannii* co-infections, particularly in ICUs, several of which have been identified as carbapenem-resistant[49,51,52]. These cases of *A. baumannii* secondary

infections throughout COVID-19 dedicated hospitals has not only further burdened already pressured medical sectors around the globe, but could also inevitably accelerate the propagation and spread of antibiotic-resistant *A. baumannii* and other priority bacterial species[53,54].

The rapid emergence of drug resistance in *A. baumannii* is owed to its receptive resistance gene acquisition and ability to adapt to environmental selective pressures[17]. Consequently, this had led to the generation of multi-, extensive-, and pan-drug-resistant strains of *A. baumannii,* the bulk of which belong to two clonal lineages, namely global clone 1 (GC1) and global clone 2 (GC2)[12,18,55]. Resistance development in *A. baumannii* is generally accomplished through three mechanisms: (1) acquisition of resistance genes (mainly *via* bacteria-to-bacteria horizontal gene transfer), which most often encode drug-inactivating enzymes, such as OXA-type β-lactamases (*e.g.* OXA-23) which hydrolyses carbapenems; (2) insertion sequence (IS)-mediated activation of resistance genes, *e.g.* insertion of ISAba1 upstream of the intrinsic *A. baumannii* gene *ampC* provides it with a strong promoter and results in resistance to 3rd generation cephalosporins; (3) genetic mutation, *e.g. gyrA* and *parC* mutations alter DNA gyrase and topoisomerase IV active sites and blocks the action of quinolones[46,56,57]. This organism was introduced as an ESKAPE member in 2009, and in 2017, the WHO and the Centers for Disease Control and Prevention (CDC) declared carbapenem-resistant *A. baumannii* as the number one critical priority antibiotic-resistant pathogen among a list of 12 bacteria requiring urgent antibacterial research and development[6,7,12]. Ultimately, antibiotic resistance in *A. baumannii* and the other priority ESKAPE pathogens highlights the need for immediate action of establishing new and alternative antibacterial agents to curb the threat of infection caused by these organisms[11].

But the current rate at which new drugs are being developed is very slow. Most major pharmaceutical companies have withdrawn from financially supporting the research and development of new antibiotics due to a lack of government incentives for these high risk investments[5,58-60]. Naturally, the need for antibiotic substitutes is dire, and nanotechnology has proven to offer effective alternatives[13]. Nanoparticles are organic (*i.e.* carbon-sources) or inorganic (*i.e.* metals) based materials, ranging from 1-100 nm in diameter[61]. Silver nanoparticles (nanosilver; herein after referred to as NAg) are currently the most widely produced nanoparticle, attributed to its unique

physicochemical characteristics and multifaceted antimicrobial mechanisms[61,62]. Many studies have demonstrated the antimicrobial efficacy of NAg against many viral, fungal, parasitic, and bacterial organisms[19,63]. The healthcare sector is one of the largest markets for NAg, with the nanoparticle being used as a coating agent in medical devices, such as intravenous catheters, wound dressings, and organ/dental implants to inhibit bacterial colonisation[23]. Worryingly, NAg has also been incorporated into hundreds of consumer products, and can, for example, be found in household appliances, textiles and clothing, cosmetics, childcare products, and food packaging and containers[23,26,64].

The widespread use of NAg has triggered concerns for the development of silver-resistant bacteria, diverging from the once commonly held perception that bacteria could not develop resistance to silver due to its complex, multi-targeting antibacterial mechanisms[25,27]. Over several years, a growing number of studies have been published describing the phenomenon of resistance in bacterial species in response to different forms of silver agents, including NAg. Silver resistance has been reported in *A. baumannii* and many other important pathogenic bacteria[29,30,32,34,65,66]. In addition, there are also human health and ecological concerns surrounding the increasing use of silver-based products, such as the systemic absorption of silver from medical devices (*i.e.* dressings and catheters), as well as wastewater and landfill silver run-off due to disposed effluent and products which can potentially affect aquatic and terrestrial ecosystems[25,26,67,68].

In this Chapter, the antibacterial actions of NAg with its multi-targeting toxicity on *A. baumannii* and other bacteria are highlighted. Current knowledge on the adaptive ability of this bacterium, and other significant bacterial species, to NAg and other silver agents are also outlined. It is important that the applicability, as well as the equally important long-term risks of the use of the nanoparticle as an alternative antimicrobial is understood. This literature review also describes the emerging phenomenon of the metal-driven co-selection of antibiotic resistance, including silver, to further stress the issue of bacterial overexposure to toxic heavy metals.

2.5 Physicochemical factors and antibacterial properties of NAg

NAg has a number of physicochemical characteristics that affect its microbiological activity and overall stability[19]. The nanoparticle exhibits distinct multi-targeting bactericidal mechanisms which are unique from common antibiotics and evidently underlines why NAg has become a popular alternative antibacterial agent[19,69].

2.5.1 Size, Shape, and Surface Properties of NAg

The physicochemical characteristics of NAg directly influence its antibacterial activity. The nanoparticles range from 1 – 100 nm size, and with their high surface-area-to-volume (SAV) ratios, each particle contains approximately 10,000 – 15,000 silver atoms, rendering them highly reactive[22,70]. Studies have shown that smaller particles have a higher SAV ratio and are generally associated with better physical nanoparticle-to-cell contact, and this allows for greater adherence to the bacterial surface which enhances their antibacterial activity[22,70,71]. NAg particulates can be synthesised into different shapes, with the most common including spheres, truncated triangles, and rods/cylinders[19,27,72]. A comparative study by Pal *et al.* found that truncated triangular shaped nanoparticles were most effective against *E. coli* when compared to spherical and rod-shaped particles[72]. The triangular shape was thought to improve reactivity of the nanoparticle due to the presence of unique active facets, which are associated with a greater concentration of silver atoms. It was also speculated that this shape enhanced particle adherence onto the bacterial surface, resulting in more extensive membrane damage and subsequent cell killing[63,72].

The morphology of NAg determines, at least in part, the particle concentration required for effective toxicity. For example, higher concentrations of rod-shaped NAg particles at 10 – 100 nm (lower SAV ratio) are needed to display comparable antibacterial activity with those of truncated triangles at 1 – 10 nm (higher SAV ratio)[22]. Moreover, higher concentrations of NAg are generally required to inhibit Gram-positive bacteria in comparison to Gram-negatives[69]. This is thought to associate with the presence of the thicker outermost peptidoglycan cell wall layer (30 – 100 nm) in Gram-positive bacteria, compared to those in Gram-negative bacteria (thin 2 – 8 nm peptidoglycan layer located between the outer and inner lipid membranes)[69,73].

Another important characteristic of NAg that affects its toxicity is the presence of functional groups on the nanoparticle surface which, in many cases, act as stabilisers (to prevent aggregation) and influence the nanoparticle net surface charge[70,74,75]. Measured as zeta potential (ζ), NAg can have a positive or negative net surface charge depending on the surface functional groups (a nominally high ζ potential reflects good colloidal stability), which affects the particle electrostatic attraction with the bacterial surface[75]. Under normal physiological conditions, the bacterial envelope has a net negative charge. The envelope itself is assembled with various biomolecules, *e.g.* proteins, sugars and phospholipids, which contain many negatively charged functional groups, including carboxyl and phosphate groups[73]. Studies have shown that nanoparticles with a highly positive ζ exhibit a greater extent of antibacterial effect than those with negative ζ, most likely due to the particle-to-bacterial envelope electrostatic interactions for the former[19,69,75]. This attraction allows for greater adherence and accumulation of NAg to the bacterial surface, with some studies hypothesising that this can induce neutralisation of the cell membrane and lead to the loss of its selective permeability[22,76]. El Badway *et al.*, for example, studied NAg with different coatings and observed the highest extent of bacterial surface interaction with a branched polyethyleneimine (BPEI)-coated nanoparticle type. This BPEI-NAg exhibited the most positive ζ (compared to negatively charged polyvinylpyrrolidone (PVP)-NAg and citrate-NAg), which was thought to interact closely with the bacterium (*Bacillus* sp.) due to electrostatic attractions[75,76].

2.5.2 General antibacterial mechanisms of NAg (cell surface)

The antibacterial activity of NAg has been studied quite extensively[19]. Four main antibacterial modes have been proposed: (**A**) bacterial envelope adhesion of the nanoparticle, resulting in envelope damage and cellular penetration, (**B**) uncoupling of the respiratory chain, (**C**) damage to cellular biomolecules and function, and (**D**) disruption of cell signalling (**Figure 2.1**)[77,78]. As briefly discussed in **Section 2.5.1**, direct physical contact of NAg with the bacterial surface is one of the initial mechanisms of its antibacterial function[63,72,77]. In Gram-negative bacteria, the 'sticking' of NAg to the outer membrane rapidly destabilises the membrane, allowing smaller-sized particles to enter the cell. This coincides with the formation of electron dense 'pits' in the thin peptidoglycan layer, which enables the nanoparticle to target

the inner membrane[10,70,76]. The pitting effect is generally slower in Gram-positives which is most likely due to the thicker outermost peptidoglycan cell wall layer[76,77,79].

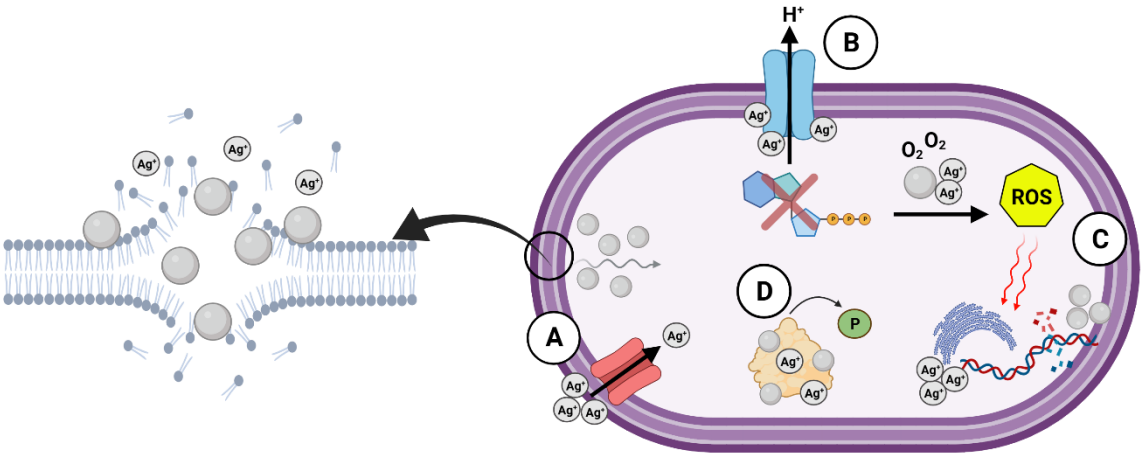

Figure 2.1 Graphical depiction of the multi-target antibacterial mechanisms of NAg on the cell surface and cell cytoplasm. (**A**) Adhesion and 'pitting' of the cell membrane, and subsequent internalisation of NAg, along with Ag^+ passage through outer membrane protein (OMP) channels, (**B**) uncoupling of the respiratory electron transport chain by Ag^+, (**C**) damage to intracellular biomolecules by silver-generated ROS and direct NAg/Ag^+ intercalation, and (**D**) disruption of cell signalling through protein dephosphorylation. Created in BioRender. Adapted from Dakal *et al.*[77].

In an aqueous environment, NAg can interact with molecular oxygen (O_2), which leads to oxidative dissolution. This causes leaching of silver ions (Ag^+) from the nanoparticle, which are crucial to the overall antibacterial activity of NAg[20,76]. Various studies note that NAg dissolution and the Ag^+ leaching rate is influenced by numerous factors. The physicochemical properties of NAg (*i.e.* morphology), presence of an aqueous solution or solid surface, nanoparticle agitation, and the use of surface coating agents, all contribute to varying rates of Ag^+ release[80-82]. One study, which performed a toxicity characteristic leaching procedure (TCLP) test of various NAg-incorporated textiles, found that the percent rate of Ag^+ leaching ranged between 7 – 162%[80]. Ag^+ leached during the dissolution process is also thought to damage the bacterial membrane and membrane-bound proteins[69,77]. Ag^+ acts as a soft acid and has a high affinity for electron donor groups in amino acid constituents of structural and enzymatic proteins. In particular, thiol ($-S^-$) groups that are present in the amino acids

cysteine and methionine, as well as amine (NH_x) groups in histidine ($-NH^+$), arginine ($-NH_2^+$) and lysine ($-NH_3^+$)[19-21,69]. Ag^+ has been found to bind to membrane-bound transport proteins in bacteria, subsequently inhibiting the proton motive force which disrupts the in-and-out transport of protons, as well as phosphate, necessary for adenosine triphosphate (ATP) synthesis[83]. Comparable to that of NAg, studies have also reported less occurrences of Ag^+ penetration in Gram-positive bacteria when compared to Gram-negative bacteria. The cations are thought to be sequestrated within the thicker negatively-charged peptidoglycan layer of the former, rendering them more tolerant to Ag^+[77,84]. However, evidence suggests that Ag^+ is more potent than NAg against both Gram-positive and Gram-negative bacteria at equivalent silver concentrations[85,86]. In Gram-negative bacteria, this could be due to the presence of molecular transport channel proteins, *e.g.* outer membrane proteins (OMPs), which facilitate transmembrane diffusion of ions, and in this case, Ag^+, into the periplasmic space[83,85,87,88].

The silver-induced 'pitting' effect on the cell wall along with altered membrane permeability inevitably allows smaller NAg particulates and Ag^+ to penetrate through the cell envelope and into the cytoplasm, while larger nanoparticles remain outside the cell[89]. Studies have also hypothesised a Trojan horse-type mechanism, whereby the nanoparticles are absorbed intracellularly and undergo further leaching of Ag^+, increasing local ion concentrations[90,91]. Taken together, these mechanisms provide access for NAg/Ag^+ to target intracellular structures and biomolecules, as described in the next section[20,70,77].

2.5.3 General antibacterial mechanisms of NAg (intracellular)

As discussed in **Section 2.5.2**, Ag^+ ions leached from NAg have been indicated to form complexes with electron donor groups, among these including thiol and amine groups present in structural proteins and enzymes[21]. In addition to the disruption of membrane-bound transport proteins, studies have also reported inhibition of respiratory chain enzymes (*e.g.* nicotinamide adenine dinucleotide [NADH] dehydrogenase) embedded in the inner membrane, which has been correlated to the complexing activity of Ag^+[20,21,92]. The latter is thought to result in the uncoupling of electron transport necessary for oxidative phosphorylation, and in turn, inhibits the bacteria respiration process and synthesis of ATP[20,93]. Furthermore, the disruption of

the respiratory chain has been hypothesised to cause electron leakage, which reduces the presence of molecular O_2 in the cytoplasm and leads to an elevated presence of NAg-induced reactive oxygen species (ROS), including superoxide ($O_2^{\bullet-}$), in bacteria[20,77,93]. Studies have also suggested that Ag^+ (and $O_2^{\bullet-}$ radicals) can target iron-sulfur (containing thiol groups) clusters in proteins, releasing Fenton-active free Fe^{2+} ions which can react with cellular hydrogen peroxide (H_2O_2) and consequently generate highly reactive hydroxyl radicals ($OH^{\bullet}$)[94,95]. Excessively generated ROS can target cellular biomolecules and cause oxidative stress. This can cause DNA damage and inhibition of replication, disruption of tRNA-30S ribosomal complexes involved in protein synthesis, as well as damage of proteins, *e.g. via* carbonylation, and lipids, *e.g. via* peroxidation, which has been observed for membrane phospholipids[82,85,96]. Interestingly, NAg has been shown to be less effective against strictly anaerobic bacteria when compared to aerobic bacteria, and this is indeed in agreement with the established role of O_2 in radical oxygen generation, and, as mentioned earlier, in the oxidative leaching of Ag^+ from the nanoparticle, both extracellularly and intracellularly[82,85,96]. Research inquiries have also suggested that NAg/Ag^+ inhibit the activity of cellular antioxidants, such as glutathione (GSH) in Gram-negative bacteria[20]. Note that, under normal conditions, ROS (including $O_2^{\bullet-}$ and H_2O_2) are naturally generated in cells as by-products of respiration, and are neutralised by antioxidant systems when they exceed the homeostatic threshold[97,98]. GSH neutralises ROS to non-toxic compounds, *e.g.* water, and in the process, GSH is oxidised to glutathione disulfide (GSSG) [20,77,99]. It is thought that NAg directly targets GSH, a glycine-cysteine-glutamic acid tripeptide (containing thiol groups), or alternatively, denatures the GSH reductase enzyme, which catalyses the GSSG-to-GSH recycling reaction[99]. For example, Singh *et al.* reported a decrease in the cellular presence of GSH (as well as cysteine) in *A. baumannii* with increasing NAg concentrations[39].

NAg and Ag^+ have been indicated to interact with nucleotides (nucleoside-phosphate groups) in DNA, intercalating between the base pairs and binding to the nucleoside structural unit[99]. Some reports have found that Ag^+ causes DNA condensation in both Gram-negative and Gram-positive bacteria, which is further linked to the observed inhibition of DNA replication[100,101]. Most reports have suggested that this condensation only occurs in the presence of Ag^+, while the nanoparticle is associated with DNA fragmentation (an outcome of hydrogen-bond disruption between

nucleotides)[19,99,100]. NAg and Ag^+ have also been found to modulate protein phosphorylation, which affects bacterial signalling pathways[77,102]. Protein phosphorylation acts as an essential signal relay mechanism in bacteria (and other domains of life) as it manages the 'on and off' switching of proteins[103]. Due to the high affinity of NAg/Ag^+ for negatively charged phosphate groups, studies have shown that phosphorylated amino acid residues (*e.g.* tyrosine) in proteins can be dephosphorylated by both forms of silver, which consequently changes protein conformity and disrupts cell function[77,104].

2.6 Combatting antibiotic resistance with NAg

A major factor to the increasing use of NAg is its proven efficacy against bacteria like *A. baumannii*, which can readily display resistance against antibiotics[19,21]. The antibacterial effect of NAg is in general unaffected by antibiotic resistance mechanisms because of the multi-targeting mechanisms of the nanoparticle[19]. Moreover, NAg has shown promising synergy with conventional antibiotics, exhibiting enhanced toxicity when compared to NAg or antibiotics alone, even against multi-resistant bacterial species[105]. The nanoparticle could also provide a solution to the current challenge of managing chronic bacterial infections, which are often associated with the colonisation of naturally resilient biofilms[87].

2.6.1 Effect of NAg on *A. baumannii* and other drug-resistant bacteria

Several reports have described the antibacterial effects of NAg on susceptible and multi-drug-resistant (MDR) *A. baumannii* (**Table 2.1**) and other various Gram-negative and Gram-positive bacteria, highlighting little difference in nanoparticle toxicity on wild-type (or non-resistant) strains when compared to resistant strains[19,21]. Lara *et al.* and Percival *et al*. performed studies to compare the bactericidal activity of NAg on various bacterial species, including several ESKAPE members, such as methicillin-resistant *S. aureus* (MRSA), ampicillin-resistant *E. coli*, and MDR *P. aeruginosa* and *Salmonella typhi*[21,106]. Each study indicated that NAg toxicity was independent of any of the antibiotic resistance traits in these bacteria, which is thought to be due to the multi-target mechanisms of the nanoparticle. Research on the activity of NAg on *A. baumannii* has also (mostly) shown comparable efficacy against both

wild-type and resistant strains[38,41,84,107]. In contrast, however, Łysakowska *et al.*, when assessing NAg activity on several wild-type and MDR *A. baumannii* strains, found that on average the resistant types were less sensitive (minimum inhibition concentration, MIC = 0.78 μg/mL) to NAg than the wild-type strains (MIC = 0.39 μg/mL)[41]. Although a minor difference in efficacy was observed, the team hypothesised there was caused by 'partial' NAg cross-resistance in the MDR strains due to the presence of in-built antibiotic resistance mechanisms, *e.g.* efflux pumps[41]. Cavassin *et al.* studied NAg with various surface coatings on carbapenem and polymyxin-B-resistant *A. baumannii*[108]. Similar to Łysakowska *et al.*, the work also found that the resistant *A. baumannii* were less sensitive to the nanoparticle than the wild-type strains[41,108]. Further, Cavassin *et al.* found little difference in the nanoparticle toxicity between citrate- (highly negative ζ) and chitosan- (highly positive ζ) coatings[41,108]. Both types were equally more effective against resistant *A. baumannii* and other tested species when compared to another coating type (PVA-coated; ζ potential was close to zero causing particle aggregation)[75,108]. This is in contrast to the observations by El Badway *et al.* who noted that positively-charged nanoparticle coatings were most often correlated with a higher extent of toxicity due to closer attraction with the negatively-charged bacterial cell surface[75].

Table 2.1 Examples of several investigations on the antibacterial activity of NAg against various MDR and non-MDR *A. baumannii* strains.

***A. baumannii* strain**	**NAg MIC [1]**	**NAg size (nm) [2]**	**Reference**
A. baumannii (carbapenem- and PMB-resistant)	3.4 μg/mL (Citrate-NAg) 6.7 μg/mL (Chitosan-NAg)	40 25	Cavassin *et al.*[108]
A. baumannii (carbapenem- and PMB- susceptible)	13.5 – ≥ 54 μg/mL (PVA-NAg) 1.6 – 3.4 μg/mL (Citrate-NAg) 1.6 – 3.4 μg/mL (Chitosan-NAg) 6.7 – ≥ 54 μg/mL (PVA-NAg)	10	
A. baumannii (MDR)	≤ 10 μg/mL	5 – 10	Chen *et al.*[38]
A. baumannii ATCC 19606	0.78 μg/mL	2 – 5	Łysakowska *et al.*[41]
Acinetobacter spp. (clinical isolates)	0.39 – 0.78 μg/mL		
A. baumannii aba1604 (carbapenem-resistant)	2.5 μg/mL	8.4	Wan *et al.*[109]
A. baumannii AIIMS 7 (planktonic) *A. baumannii* AIIMS 7 (biofilm)	16 μg/mL 2 mg/mL	8 – 12	Singh *et al.*[39]

A. baumannii SRMC 27 (biofilm)	≤ 2 mg/mL	12.05	Gaidhani *et al.*[110]
A. baumannii AIIMS 7 (biofilm)	25.6 mg/mL	60	Salunke *et al.*[111]
A. baumannii ATCC 19606	0.09 µg/mL	8 – 15	Wintachai *et al.*[37]
A. baumannii NPRCOE 160575 (MDR)	0.18 µg/mL		
A. baumannii RS307 (carbapenem-resistant)	30 µM [3]	~ 100	Tiwari *et al.*[112]
A. baumannii NCTC 13305	12.5 µg/mL	10 - 20	Ebrahimi *et al.*[113]

[1] MIC = minimum inhibitory concentration. [2] Diameter of nanoparticle in nanometres (nm). [3] MIC concentration was reported in µM.

There has been extensive evidence highlighting the synergistic benefits of nanoparticle-antibiotic combination therapies; moreover, many studies have described an enhanced antibacterial effect compared to that of NAg or antibiotics alone[39,105,114]. Some of the general hypotheses behind this synergistic activity suggest that NAg disrupts the bacterial cell envelope and in turn assists in localising antibiotics to their cellular targets, or that NAg conjugates with the biologically active hydroxyl or amino groups present in antibiotics which improves their effective concentration and toxicity[77,115,116]. Alternatively, it has been proposed that specific antibiotics can enhance the toxicity of NAg, such as penicillin, by increasing cell membrane/wall permeability to the nanoparticle[109,117]. Wan *et al.* observed increasing efficacy of the nanoparticle on *A. baumannii in vitro* when combined with polymyxin-B (PMB), a last-resort membrane permeabilising antibiotic. The study also demonstrated nanoparticle-antibiotic synergism *in vivo* using *A. baumannii* infected mouse models, increasing mice survival from 0% when treated with PMB (250 µg/kg) alone to 100% when treated with NAg-PMB (2 mg/kg + 50 µg/kg) after a 24 hour infection period[109]. This *in vivo* evidence is important, as it alludes to the therapeutic implications of potential NAg-antibiotic combination treatments for otherwise untreatable bacterial infections[105,109,117]. Some other examples of NAg-antibiotic combinations include studies by McShan *et al.*, who showed a greater extent of MDR *Salmonella typhimurium* growth inhibition with NAg-tetracycline and NAg-neomycin treatments than the nanoparticle alone, and Thomas *et al.*, who reported improved efficacy of various NAg-antibiotic combinations on *S. aureus* and MDR *Staphylococcus epidermidis*[105,109,117].

2.6.2 Effect of NAg on *A. baumannii* biofilms and other bacterial biofilms

The pathogenicity and adaptability of bacteria to antimicrobial agents is significantly attributed to their ability to form biofilms – a surface-attached biological colony made up of one or more bacterial species enclosed by a protective sticky organic matrix known as extracellular polymeric substance (EPS)[118,119]. Biofilms are the predominant mode of growth for over 99% of bacteria, conferring protection against environmental stressors, foreign agents, and toxins, and thus play an central role in antibiotic resistance and chronic human infection[120-122]. Antibiotic resistance in biofilms is garnered by several factors, including physical protection by the EPS matrix acting as a diffusion barrier, the stochastic generation of antibiotic tolerant subpopulations (persister cells), the rapid horizontal exchange of genetic material, as well as cell-to-cell communication *via* quorum sensing[121,123-127]. Quorum sensing is a process which allows bacteria to communicate with each other and regulate a range of physiological activities, including conjugation, virulence, and biofilm production[126]. Biofilm-associated bacteria produce chemical signal molecules called auto inducers which control the expression of these physiological genes[128].

There is growing attention towards the antibacterial effects of NAg on biofilms. Similar to reports on free-living (planktonic) bacterial systems, many studies have indicated that smaller-sized nanoparticles are more effective at biofilm killing when compared to larger particles, most likely due to greater SAV ratio and better EPS penetration of the former (see **Section 2.5.1**)[87,129-131]. Again however, it is important to note that the EPS of mature biofilms generally provides colonies with increased protection, rendering them more tolerant to NAg toxicity relative to their planktonic counterparts, as previously seen with *P. aeruginosa* biofilms and other bacterial species[87,132]. Studies have also correlated the anti-biofilm activity of NAg to cellular ROS generation. Qayuum *et al.*, for example, observed substantial obliteration of *E. coli* and *Streptococcus mutans* biofilms upon exposure to NAg, which was associated with a detected increase in cellular ROS within the biofilm structure, leading to bacterial cell lysis and damage to the protein, polysaccharide, and eDNA constituents of the EPS[94,95].

Studies have also indicated the possible prevention and eradication of biofilm-associated infections with NAg. Wintachai *et al.* reported over 90% inhibition of viable

MDR *A. baumannii* (NPRCOE 160575) at low NAg doses (0.09 µg/mL or 0.5 x the reported MIC), which prevented the attachment and subsequent biofilm formation of (media-suspended) *A. baumannii* on the surface of human lung epithelia (cell line A549)[37]. Indeed, the team observed negligible toxicity of the nanoparticle toward the lung cells (50% cytotoxicity concentration [CC_{50}] = 5.72 µg/mL) which is important when considering the medical application of NAg[37]. Singh *et al.* reported a greater extent of eradication of *A. baumannii* biofilms with NAg (minimum biofilm eradication concentration, MBEC = 2 mg/mL) when compared to tetracycline, erythromycin, and doxycycline, citing extensive EPS destruction and reduction in viable cells following nanoparticle treatment[39]. The work also recognised a synergistic effect between erythromycin and NAg against the biofilms, with the antibiotic's efficacy increasing 32-fold in the presence of the nanoparticle (erythromycin MBEC = 128 mg/mL; erythromycin + NAg MBEC = 4 mg/mL). This again emphasises the potential value of NAg-antibiotic combinations (see **Section 2.6.1**)[39]. Likewise, Qayuum *et al.* had shown that catheters coated in NAg hindered the formation of the *E. coli* and *S. mutans* biofilms, which further highlights the healthcare capabilities of the nanoparticle[133].

As in the case of planktonic cells (see **Section 2.5.2**), studies have also indicated greater Ag^+ toxicity on biofilms of various bacterial species when compared to NAg, most likely due to more effective penetration of the ions through the protective EPS layer relative to the nanoparticles, though there is minimal data on Ag^+ activity on *A. baumannii* biofilms overall[85,87]. A 2020 paper by Domínguez *et al.* reported Ag^+-induced protein damage (thiol group interaction) and DNA condensation on planktonic *A. baumannii* and other bacterial species, leading to subsequent cell death[84]. Vaidya *et al.* compared the individual and synergistic efficacy of Ag^+, gold (Au^+), copper (Cu^+), platinum (Pt^{2+}), and palladium (Pl^{2+}) ions on planktonic and biofilm-forming *A. baumannii* (as well as on *E. faecium* and *K. pneumoniae* planktonic and biofilm cells)[134]. Ag^+ and Ag^+ - Cu^+ were found to be most effective individual and combinational antibacterial ions against *A. baumannii* biofilms, respectively[134]. Similarly, a study by Shih and Lin reported the ability of Ag^+ - Cu^+ to inhibit planktonic and biofilm growth of *A. baumannii* (as well as other bacterial species) in a model plumbing system, providing insights into feasible bacterial biofilm control measures in water distribution systems[135].

There are a number of other studies that demonstrate effective inhibition and/or eradication of *A. baumannii* biofilms by NAg, however, each use different concentration ranges and methodologies[40,111,136]. For example, Salunke *et al*. reported ~ 98% inhibition of *A. baumannii* biofilm formation at very high NAg concentrations (25,600 µg/mL) using a 96 well-plate (5120 µg/mL per well) experimental setup, while Ramachandran and Sangeetha observed biofilm inhibition at "only" 100 µg/mL concentration of the nanoparticle in a glass test tube setup[111,136]. Albeit should not be ignored that these experiments utilised nanoparticles with different physicochemical properties (*e.g.* NAg sizes of ~ 64 nm and ~ 7 nm, respectively), these inconsistencies in methodology highlight the challenges involved in assessing the antimicrobial efficacy of NAg. Currently, there is no standard protocol to follow for researchers to directly compare the general toxicity of NAg, because different physicochemical characteristics of the nanoparticle, the bacterial growth medium, incubation conditions, and other factors, influence its antibacterial activity[22,78,137].

2.7 Bacterial adaptations to NAg

Current evidence of the bactericidal activity of NAg has underlined its proven efficacy on a broad-spectrum of microbes. However, because of the increased and widespread use of the nanoparticle in industrial and consumer products, there has been a growing concern that, just like with antibiotics, bacteria can develop resistance to NAg[25,29,30]. Bacterial resistance to silver, specifically to Ag^+, has been described quite extensively, while evidence of NAg-specific resistance is still emerging. Up to this stage, studies have described the presence of both exogenous and endogenous genetic determinants of Ag^+ resistance, which is thought to be relevant to NAg also[29-32,65]. The earliest reported case of silver resistance was in an *E. coli* strain isolated from a burn patient in 1969, who was treated with wound dressings coated in 0.5% silver nitrate ($AgNO_3$)[138]. Two strains of *Enterobacter cloacae* isolated from a burns ward by Rosenkranz *et al.* in 1974 were found to be resistant to the topical ointment silver sulfadiazine (AgSD)[139]. A year later, McHugh *et al.* reported on an *S. typhimurium* strain isolated from three burn victims with resistance to $AgNO_3$, which also displayed resistance to mercury chloride ($HgCl_2$) and various antibiotics[140].

The molecular basis of silver resistance was first described by Gupta *et al.* in 1999, who discovered an Ag^+ resistance coding region (*sil* operon) present in a 180 kb plasmid called pMG101[65]. This plasmid was extracted from the silver-resistant *S. typhimurium* strain previously isolated by McHugh *et al.* in 1975[65,140]. The first reported silver resistance mechanism, however, was by Li *et al*. who found that the loss of OMPs combined with the upregulation of copper efflux proteins (Cus system) in *E. coli,* conferred resistance to Ag^+[141,142]. Over the years, several cases of Ag^+ resistance derived from the Sil/Cus systems (and other mechanisms) have been detected in various bacterial species, including *A. baumannii*[34-36]. Gunawan *et al*. was the first to observe NAg resistance in the soil-borne bacterium *Bacillus subtilis* elicited by oxidative-stress mechanisms, which was thought to be associated by the detected presence of *sil* genes[32]. Further studies are published which provide evidence of NAg resistance determinants in different bacteria, which will be described in the following section[29-31].

2.7.1 Chromosomal (endogenous) silver resistance

The endogenous silver resistance mechanism first discovered in *E. coli* by Li *et al.* relates to the presence of the Cus efflux system and the loss of major OMPs[141,142]. Prolonged exposure of various *E. coli* strains to sub-lethal doses of $AgNO_3$ and AgSD (Ag^+ potent agents) led to the mutational development of Ag^+ resistance in the bacteria. The mutant Ag^+-resistant strains displayed a loss of the major porins OmpF or both OmpF and OmpC, along with the expression of a natural copper binding/efflux (Cus) system which conferred cross-resistance to Ag^+ (**Figure 2.2**)[85,141,142]. The *cusCFBA* operon is a gene cluster which encodes an active efflux system designed to export copper ions (Cu^+), and Ag^+[142,143]. The proteins encoded; CusA, CusB, and CusC, are subunits of a tri-component resistance-nodulation-division (RND)-type efflux system, and CusF, which is a periplasmic Ag^+/Cu^+ chaperone[85,144]. Transcription of *cusCFBA* is regulated by a dual-component system called CusRS (encoded by *cusRS* operon), which sense (CusS) and respond (CusR) to increased levels of Ag^+/Cu^+[144,145]. Exposure of *E. coli* to Ag^+ can cause a missense mutation in *cusS*, promoting gene transcription and CusS synthesis (and CusR upregulation), where CusS/R then prompts increased expression of *cusCFBA* for active Ag^+/Cu^+ binding and efflux[142]. CusF is a metal-binding chaperone, which binds Ag^+/Cu^+ ions to its methionine or

cysteine sites and delivers them to CusCBA to be shuttled out of the cell[142,143,146]. The repression of the major porins OmpF/C in the outer membrane complements the Cus system, as mentioned[87,142,146]. These porins are involved in the transport of cations and small molecules, such as drugs and toxins, across the cell membrane[147]. Transcription of *ompF/C* is regulated by EnvZ/OmpR, whereby EnvZ responds to osmotic changes (*i.e.* presence of cations) and phosphorylates the transcription unit of OmpR, which then activates the expression of OmpF/C[148]. Mutation to *envZ*/*ompR* in response to Ag^+ exposure leads to loss of function to this regulatory system, which results in a reduction of *ompF/C* expression, causing a loss in outer membrane permeability[141,142,146]. This consequently limits the cytoplasmic access of Ag^+ and reduces the susceptibility of *E. coli* to Ag^+ toxicity[87,141,142].

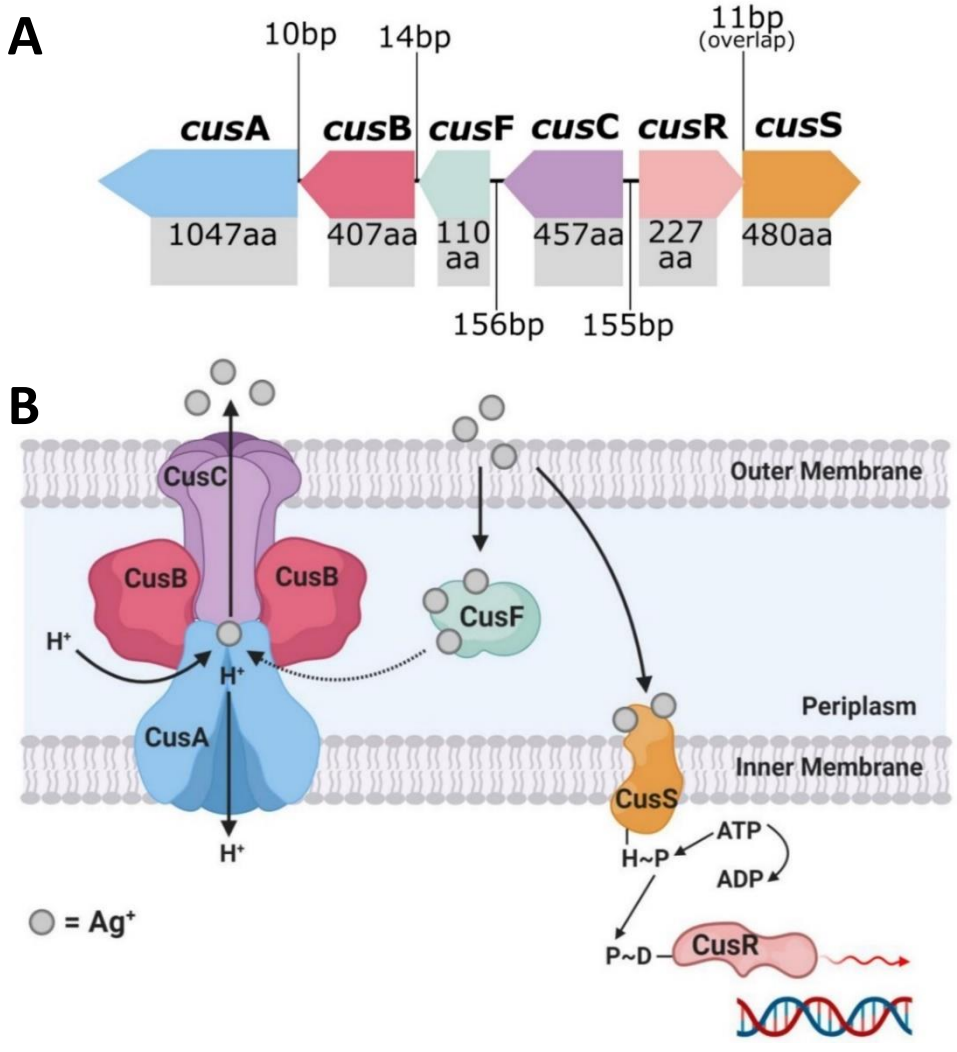

Figure 2.2 Graphical schematic of proposed Cus copper/silver efflux system. The top image (**A**) shows the genetic arrangement of the *cus* operon and includes the intergenic DNA base pair (bp) gaps/overlaps and each *cus* gene's protein product amino acid (aa) length. The bottom image (**B**) is a graphical representation of the protein arrangement and functions of the encoded membrane bound Cus efflux system. Created in Inkscape (**A**) and BioRender (**B**). Adapted from Randall *et al.*[142].

Graves *et al.* reported on induced resistance to $AgNO_3$ in another *E. coli* strain upon prolonged exposure and, in addition, observed resistance to NAg. The team found non-synonymous point mutations (results in amino acid sequence changes of the protein product) in three genes; *cusS*, as well as *purL,* which encodes the protein phosphoribylsylforml-glycineamide synthetase involved in purine nucleotide biosynthesis, and *rpoB*, which codes for an RNA polymerase beta subunit[31]. As previously discussed, CusS is part of the dual-component sensor/responder regulator for the CusCFBA Ag^+/Cu^+ efflux system[145,146]. Resistance to Ag^+ in the *E. coli* strain was significant and defined, with a > 26-fold increase in Ag^+ concentration at which the resistant bacterium could proliferate (compared to the wild-type strain), while the NAg-resistant strains could grow at a lower 1.4 – 4.7-fold increase in dose. It was unclear as to what exact mechanisms conferred the observed resistance to NAg in *E. coli*. As the leaching of Ag^+ from NAg is an integral part of the nanoparticles antibacterial activity, it is thought that the CusCFBA Ag^+ efflux system played some role in the NAg resistance effect[31].

According to Randall *et al.*, the Cus system is not unique to the *E. coli* genome and has been found in strains of other bacteria, including the soil and human gut bacterium, *Citrobacter freundii,* and the pathogenic gut bacterium, *Shigella sonnei.* However, no changes in OMP expression in these bacteria (nor loss of porins) were observed, which could perhaps explain their susceptibility to Ag^+, suggesting that the Cus system alone is not sufficient for a bacterium to confer resistance to silver[142]. The *cus* operon and OMP mechanisms are specific to Gram-negative bacteria, however, silver resistance, to both Ag^+ and NAg, have also been observed in Gram-positive bacteria. Apart from the original discovery in *B. subtilis* by Gunawan *et al.*, studies have also detected resistance in the clinically-relevant species *S. aureus* (see **Section 2.7.4**), and silver

resistance in these bacteria has been associated with *sil* genes and mutations of physiological genes[29,149,150].

Resistance to Ag^+ has been previously reported in *A. baumannii*, which will be discussed further, however, no endogenous silver resistance mechanisms have been detected to date in this bacterium[34,35,151]. Alquethamy *et al.* provided the first report of a highly conserved chromosomally-encoded copper resistance system in *A. baumannii* which was distinct from the other known copper resistance mechanisms, including the Cus system[152]. The mechanism involves two transcriptional regulators of copper-resistance, CueR and CopRS, as well as a P-type ATPase Cu^+ efflux protein called CopA[152,153]. The existence of this conserved chromosomal Cu^+ efflux system suggests a mutational response to copper exposure may have occurred at some point earlier in the phylogeny of *A. baumannii* and has been maintained through natural selection. The copper and silver efflux mechanisms, *i.e.* Cus and Sil systems, are homologous as they share common protein sequences and elicit copper/silver cross-resistance in bacteria; therefore, it is possible that the CueR/CopRS/CopA could also be involved in a silver resistance effect in *A. baumannii*.

2.7.2 Plasmid-mediated (exogenous) silver resistance

The Ag^+-resistant *S. typhimurium* strain isolated by McHugh *et al.* in 1975 is the source of the most cited and researched silver resistance mechanism to date. In 1999, Gupta *et al.* isolated the HI-2 incompatibility group (IncHI-2) plasmid pMG101 from this bacterium and found it contained various genes that encode resistance to several heavy metals and antibiotics[65,154]. The plasmid segment conferring silver resistance determinants contained the *sil* operon, which consists of nine genes that encode a Ag^+ binding and efflux system (**Figure 2.3**)[65,155,156]. In reading order, these genes are *silE, silS, silR, silC, silF, silB, silA, ORF105 (silG), and silP*, and encode their proteins in three transcriptional units (SilE, SilRS, and SilCFBAGP)[156,157]. The characterisation and organisation of the Sil system is in fact based on the earlier discovered Cus system, as the two efflux systems share close peptide homologies, as mentioned previously[85,142,143]. However, in contrast to the Cus system, the exogenous Sil system does not associate with the loss of OMP porins (*i.e.* OmpF/C) to evoke Ag^+ resistance[142].

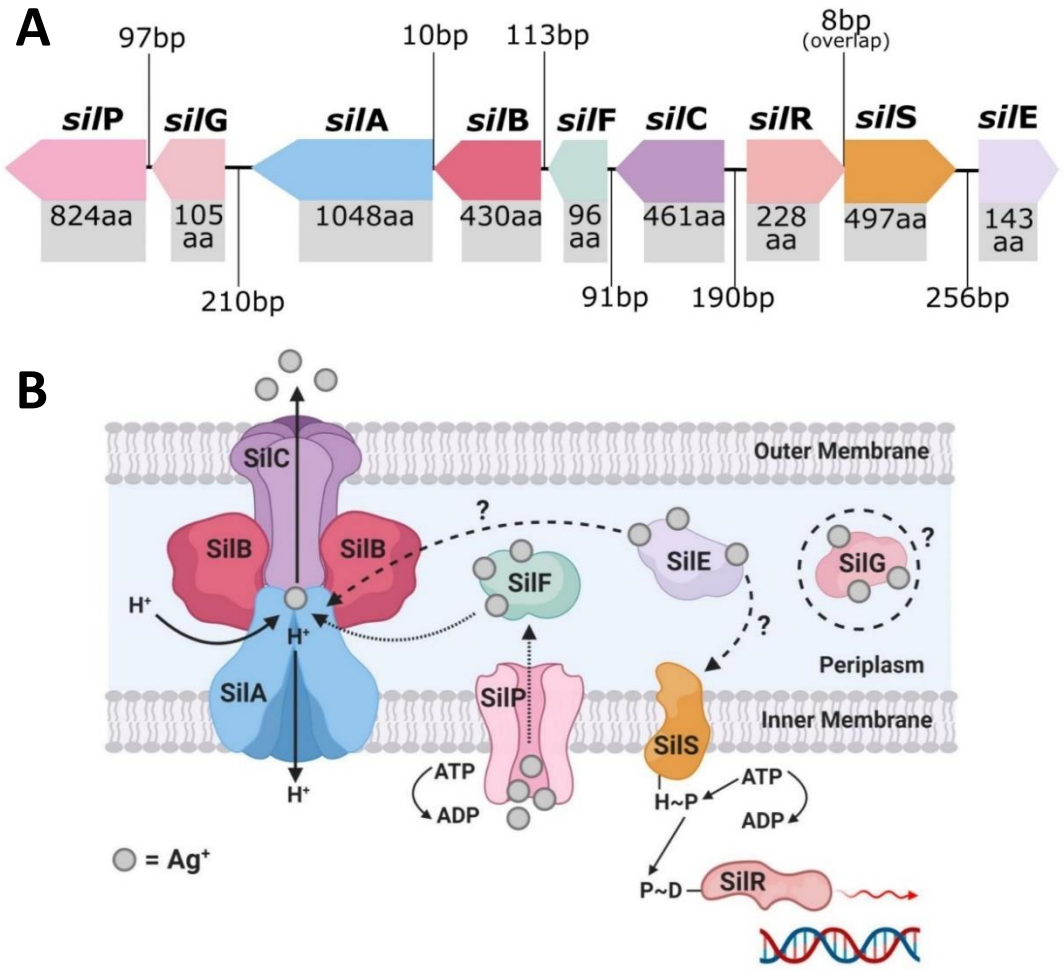

Figure 2.3 Graphical schematic of proposed Sil silver efflux system. The top image (**A**) shows the genetic arrangement of the *sil* operon and includes the intergenic DNA base pair (bp) gaps/overlaps and each *sil* gene's protein product amino acid (aa) length. The bottom image (**B**) is a graphical representation of the known and predicted protein arrangement and functions of the encoded membrane bound Sil efflux system. Created in Inkscape (**A**) and BioRender (**B**). Adapted from Randall *et al.*[142].

SilE is a periplasm-oriented protein chaperone that binds to free Ag^+ present in the periplasmic space and is currently the only Sil protein which has had its function fully validated[65,142]. SilRS are dual-component Ag^+ sensor (SilS) and responder (SilR) transcriptional regulators for SilCFBAGP, and are direct homologs of CusRS[85,156]. SilCFBA shares ~80% protein homology with CusCFBA and functions as a multi-component RND-type Ag^+ efflux system[85,142]. SilA is an inner membrane cation/proton efflux antiporter, SilB functions as a membrane fusion protein which clamps SilA together with SilC, an OMP channel[157]. SilF is another periplasmic Ag^+-

binding chaperone (similar to SilE), and binds with Ag^+ that have passed through the outer membrane from outside the cell[85]. SilP is an inner membrane-bound P-type ATPase efflux which transports Ag^+ from the cytoplasm to the periplasm for binding with the chaperones SilE/F[143]. The *sil* operon also contains an unspecific open-reading frame *ORF105* which codes for a protein with currently no defined function[65,143,157]. The encoded protein shares a ~ 45% amino acid sequence homology with the Cu^+ chaperone CopG, and both contain a CXXC motif (two amino residues between two cysteine), which is known to be involved in heavy metal binding[142,157,158]. To fit the *sil* gene nomenclature, Randall *et al.* proposed that *ORF105* be given the name *silG* and described as an Ag^+-binding chaperone, similar to SilE/F, until proven otherwise[142].

2.7.3 Presence of Sil system in *A. baumannii* and other species

The *sil* operon has been found in other IncHI plasmids like pMG101 (**Table 2.2**), and due to horizontal gene transfer of these plasmids between bacteria, whole or part of the operon has been detected among many bacterial species[143,154]. Since the initial discovery of *sil* genes in *S. typhimurium*, studies have further detected the genes in other *Salmonella* spp., and in other Gram-negative bacteria, including *E. cloacae*, *E. coli*, *P. aeruginosa, K. pneumoniae, Serratia marcescens,* and *A. baumannii*, as well as Gram-positive bacteria, such as *B. subtilis* and *S. aureus*[29,32,34,35,159]. Hosny *et al.* discovered *sil* operon-harbouring plasmids in various clinical species isolated from burns/wounds of hospital patients, including two MDR *A. baumannii* strains[34]. Conjugative horizonal transfer of the *sil* operon was observed between the silver-resistant *A. baumannii* strains and non-silver-resistant *E. coli*. This resulted in the expression of the *sil* genes and subsequent development of an Ag^+ resistance phenotype in the latter bacterium[34]. Deshpande and Chopade had in fact reported the conjugal transfer of silver resistance determinants many years prior. Their work observed the transfer of plasmid pUPI199, which contained undefined silver resistance genes, from an *A. baumannii* strain (BL88) to *E. coli* with, once again, subsequent expression of the silver resistance phenotype[35]. A study by Shakibaie *et al*. also detected the presence of another plasmid-associated silver resistance mechanism in an *A. baumannii* strain (BL54), which is unrelated to the Sil system, and was thought to be involved in the intracellular accumulation of Ag^+ and binding of the ions to metalloproteins to form inert silver complexes[151]. No follow up inquiries have been

made on either of these non-*sil* derived silver resistance determinants. Therefore, it is difficult to assess the significance and specificity of these resistance mechanisms.

Table 2.2 Properties of known IncHI plasmids containing genes coding for silver resistance, including either the complete *sil* operon or some *sil* genes.

Genus/species	Plasmid	*sil* genes	Size (bp)	Conjugative	GenBank Acc. No.	Reference
S. typhimurium	pMG101	*ESRCABGP*	14211	Y	AF067954	Gupta *et al.*[65]
Serratia marcescens	R476b	*E*	424	Y	AY009372	Gupta *et al.*[154]
		P	1362		AH011380	
		S	1154		AH011381	
Salmonella enterica	MIP233	*E*	424	Y	AY009382	Gupta *et al.*[154]
		P	1356		AH011384	
		S	1154		AH011385	
S. enterica	pWR23	*E*	424	Y	AY009387	Gupta *et al.*[154]
		P	1356		AH011388	
		S	1154		AH011389	
S. enterica	MIP235	*E*	424	Y	AY009392	Gupta *et al.*[154]
		P	1356		AH011386	
		S	1154		AH011387	
S. marcescens	R478	*ESRCABGP*	274762	Y	BX664015	Gilmour *et al.*[160]
E. coli	pAPEC-O1-R	*ESRCABGP*	241387	Y	DQ517526	Johnson *et al.*[161]
Salmonella typhi	R27	*ESRCABGP*	180461	Y	AF250878	Sherburne *et al.*[162]
A. baumannii	pUPI199	nk [1]	~50000	Y	nk [2]	Deshpande and Chopade[35]

[1] Unknown if detected silver resistance genes are *sil* genes. [2] Accession number could not be found in GenBank.

2.7.4 Other mechanism of silver resistance against NAg

Most studies have established that bacterial resistance to silver can develop through genetic mutations, as well as through horizontal gene transfer (*i.e. via* plasmids) (see **Section 2.7.1** and **2.7.2**). However, there is evidence that an increase in expression of native bacterial processes can also contribute to silver resistance. For example, a study by Muller *et al.* outlined that the redox-active metabolite pyocyanin, produced by *P. aeruginosa*, could reduce extracellular Ag^{+} to non-toxic Ag^{0} and, in turn, confer resistance to the ions[66]. Another example was the increased production of EPS by

planktonic *E. coli*, which acted as a permeability barrier to Ag^+, causing neutralisation and agglomeration of the ion into inert particulates[163]. A 2018 study by Panáček *et al.* revealed an intrinsic NAg resistance mechanism in *E. coli* involving overproduction of the protein flagellin, which led to aggregation of the nanoparticles[30]. Flagellin is an adhesive protein, forming part of the structural component in the bacterial motility organelle flagella and is known to be involved in biofilm formation[30,164,165]. This resistance mechanism was considered epigenetic, as it was independent of any genetic mutations, and provided no observable resistance to Ag^+ due to the solubility of the ions[30]. In a more recent 2021 study by Stabryla *et al.*, it was found that a hypermotile strain of *E. coli* could acquire resistance to NAg, but not Ag^+, while a non-motile strain could not develop resistance[28]. This resistance phenomenon was attributed to enhanced flagellum-based motility (allowing improved physical distancing from the nanoparticles) and complemented by expression of a mutated *cusS* copper efflux gene[28].

As mentioned in **Section 2.7.1**, evidence of silver resistance in Gram-positive bacteria have been reported, although less frequent in comparison to Gram-negative bacteria. Loh *et al.* examined the frequency of *sil* gene occurrences in 36 *S. aureus* strains isolated from human and animal sources[149]. Three strains were found to contain only the *silE* gene (95 – 100% homology with *silE* in pMG101), which appeared to confer transient resistance upon exposure to Ag^+ through ion binding, however, the exposure eventually resulted in cell death[149]. In another study, however, Hosny *et al.* isolated four clinical MDR *S. aureus* strains, each displaying stable resistance to Ag^+, and found one strain expressed the complete *sil* operon, while the remaining three expressed some of the *sil* genes[34]. The study on *B. subtilis* by Gunawan *et al.* is the only other research inquiry apart from that of Valentin *et al.* that reported the development of NAg resistance in a Gram-positive bacterium[32]. Valentin *et al.* showed the development of stable resistance to NAg (and Ag^+) in *S. aureus* (ATCC 25923) through prolonged exposure, with no known presence of the *sil* genes in its genome. The bacterium developed physiological genetic mutations, the first reported case of NAg-induced single nucleotide polymorphisms in a Gram-positive bacterium[29]. More specifically, mutations in *purR,* which encodes a purine repressor regulator protein, was hypothesised to lead to an upregulation in purine nucleotide synthesis to cope with DNA targeted NAg activity. The study also detected mutations in *tcyA*, which codes

for an L-cystine binding protein, lowering the influx of extracellular cystine which helped reduce oxidative stress by ROS generated from both high levels of intracellular cysteine and by NAg and Ag^{+}[29,166,167].

2.7.5 Silver and other metals as drivers of antibiotic resistance

While bacterial resistance to silver is in itself a troubling issue, there has been emerging evidence to show that silver and other heavy metals (*e.g.* lead, cadmium, chromium, mercury, etc.) can co-select for antibiotic resistance[168,169]. The emergence of heavy metal/antibiotic resistance was first described in 1974, when Koditschek and Guyre isolated *E. coli* from a sludge-contaminated estuarine and found it had "indirectly" acquired antibiotic resistance due to heavy metal exposure[170]. Agriculture and aquaculture practices across the globe frequently use metal-containing fertilisers, pesticides, and feed additives, and have consequently contributed to profound environmental accumulation of heavy metals. Heavy metals are stable and are not subject to rapid degradation, thus their presence in soil and water is thought to be significantly greater than antibiotics, and may therefore contribute to long-term exposure and selective pressure on bacteria[171,172]. The co-selection of antibiotic resistance by heavy metals is often associated with 'dual' metal/antibiotic resistance phenomena – cross-resistance, co-resistance, or co-regulation/co-expression (**Figure 2.4**)[171]. Cross-resistance occurs when the same genes encode resistance mechanisms to multiple agents, and in the case of metal/antibiotic resistance, one key example is the expression of Tet efflux pumps, which export tetracyclines and zinc ions (Zn^{2+})[173]. Co-resistance arises when different genes present in the same genetic element confer resistance to multiple agents at once, and are often found in mobile genetic elements (plasmids, transposons, or integrons)[171]. As an example, plasmid pMG101, from which the *sil* genes were first discovered, was found to also contain resistance genes for mercury and tellurite, and for a number of antibiotics, including ampicillin and chloramphenicol [65]. Likewise, plasmid pUPI199 isolated from *A. baumannii* by Deshpande and Chopade, which harboured (undefined) silver resistance genes, had also been found to contain resistance genes for 12 other metals and 10 antibiotics[35]. Co-regulation is when regulatory genes (in a chromosome or plasmid) of different resistance mechanisms are transcriptionally linked, meaning, in this case, exposure to a metal can trigger the expression of both metal resistance genes (MRGs) and

antibiotic resistance genes (ARGs)[171]. For example, overexpression of the gene *robA* (encodes the right origin-binding [Rob] transcriptional regulator protein) in *E. coli* was found to activate multiple mechanisms which gave rise to resistance phenotypes to silver, mercury, and cadmium, as well as various antibiotics and organic solvents[174].

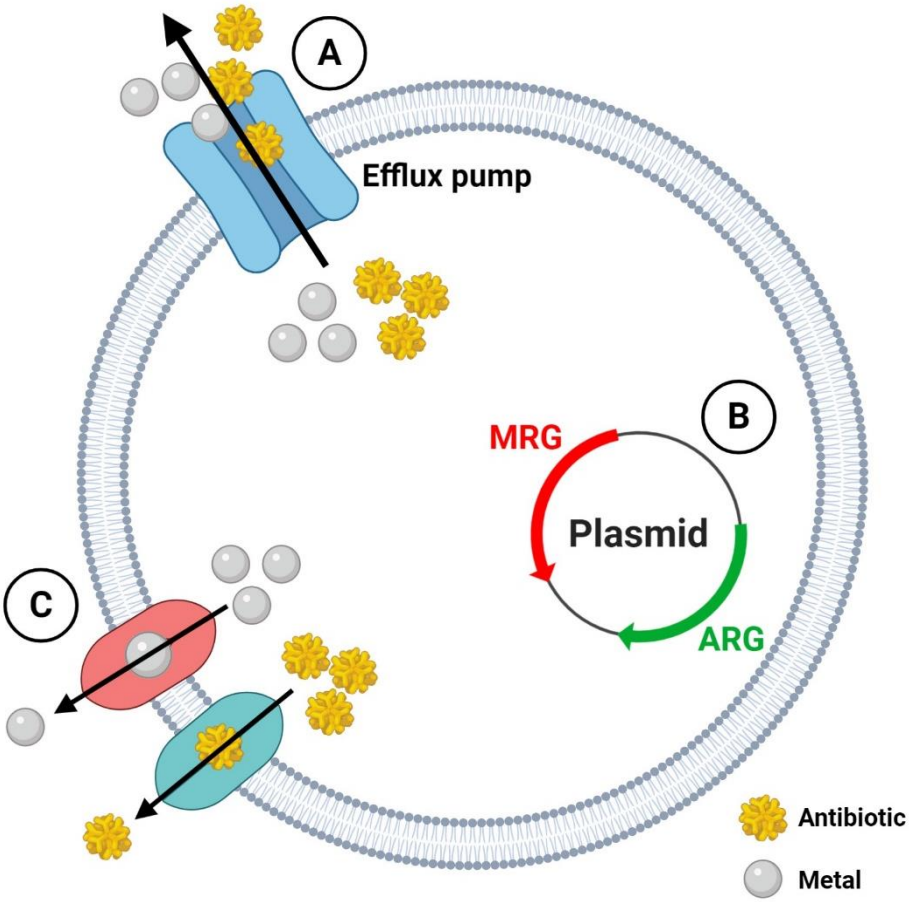

Figure 2.4 Graphical schematic highlighting the three potential mechanisms behind the co-selection of bacterial heavy metal and antibiotic resistance. (**A**) Cross-resistance: one gene/mechanism confers resistance to metals and antibiotics at once (*i.e.* efflux pumps); (**B**) Co-resistance: genes coding for metal resistance (MRG) and antibiotic resistance (ARG) are grouped together on the same genetic element (*i.e.* plasmids); (**C**) Co-regulation: expression of individual metal and antibiotic resistance systems are managed by a common gene or regulator. Created in BioRender. Adapted from Pal *et al.* (Lic. No. 4986171126814)[175].

A paper by Siddiqui *et al.* reported an increased co-selection of extended-spectrum beta lactamases (ESBLs; confer resistance to β-lactam antibiotics such as penicillins, carbapenems, cephalosporins, etc.) and silver resistance determinants (*sil* genes) in the

polluted Yamuna River in India[169]. From the collected bacterial isolates, 121 were found to be ESBL producers, including various *Acinetobacter, Enterobacterales*, and *Bacillus* species, with the most prevalent ESBL gene being $bla_{\text{CTX-M}}$ (encodes class A β-lactamases; commonly targets cephalosporins, *i.e.* cefotaxime). Out of the 73 isolates containing $bla_{\text{CTX-M}}$ genes, 53 were found to have at least one *sil* gene (*silE, silP,* or *silS*), and worryingly, the most common 'dual' presence of ESBL/*sil* genes in these isolates were $bla_{\text{CTX-M}}$ + bla_{TEM} (encodes other class A β-lactamases; commonly target penicillins) + *silE* + *silP* + *silS*. All ESBLs and *sil* genes were present in plasmids, and this work found these resistance genes could be horizontally transferred to a plasmid-free *E. coli*, rendering the bacterium resistant to β-lactams (including penicillins and cephalosporins) and Ag^{+}, confirming the co-resistance effect[169]. Another study by Deshpande *et al.* described a correlation between β-lactamase production and metal ion resistance in various clinical strains of *A. baumannii* and other *Acinetobacter* spp.[36]. The bacterial strains that were sensitive to toxic metals (including silver, mercury, and cadmium) were associated with lower levels of β-lactamase gene expression, while those that were resistant to the metals were associated with higher expression levels of the ARGs. This correlation was particularly evident in *A. baumannii*[1,36]. Deshpande and his team suggested that the resistant *A. baumannii* strains were carrying plasmids that contained both β-lactamase genes and MRGs[35,36,176]. Other bacterial species have also been found to carry plasmids that harbor *sil* genes and ARGs. For example, Gilmour *et al.* found that the plasmid R478 isolated from the opportunistic pathogenic bacterium *S. marcescens* carried the entire *sil* operon, along with mercury, tellurite, and copper resistance genes, as well as tetracycline, chloramphenicol, and kanamycin resistance genes[160]. Similarly, Johnson *et al.* also found the entire *sil* operon in plasmid pAPEC-O1-R isolated from *E. coli,* which also carried copper resistance genes and several ARGs, including gentamicin, streptomycin, and tetracycline resistance genes[161]. Most antibiotic-resistant *A. baumannii* strains belong to the GC1 complex, many of which carry a large resistance gene island (AbaR) which contains several ARGs, including ESBLs (*e.g.* bla_{TEM}), and MRGs for mercury, cadmium, and zinc, and could perhaps alternatively explain the observations made by Desphande *et al.*[55]. The high incidence of infections by MDR *A. baumannii* throughout the Iraqi and Afghan conflicts are some of the most important examples regarding heavy metal-driven antibiotic resistance co-selection in this species[13]. Destroyed infrastructure and metal-based military equipment (*i.e.*

munitions, ordnance, and explosives) are known to contaminate environments through heavy metal leaching[177,178]. It has been proposed that metal exposure on *A. baumannii* in contaminated soil or water, for example, could have promoted the co-selection of antibiotic resistance, which resulted in the increased prevalence of MDR-resistant *A. baumannii* infections in soldiers exposed to these environments during combat[179].

NAg has also been shown to promote the co-emergence of antibiotic resistance in bacteria[168,180,181]. A study by Ma *et al.* found that treatment of waste water with NAg (and Ag^{+}) using lab-scale sequencing batch reactors (SBRs), resulted in an increased shift in various ARGs among isolated *Burkholderia* spp., *Streptomyces* spp., and *Gemmatimonas* spp.[168]. More specifically, metagenomics data associated the detection of HAE1 family protein (multi-drug efflux protein), *strA* gene (encodes aminoglycoside 3'-phosphotransferase; aminoglycoside resistance), and *acrB* gene (encodes multidrug efflux pump subunit AcrB) with the increased presence of NAg, while increased abundance of undecaprenol kinase and undecaprenyl-disphosphatase (resistance to bacitracin) and the gene *ermF* (encodes rRNA adenine N-6-methyltransferase; macrolide resistance) was associated with Ag^{+} presence[168]. Interestingly, the team also found that the total abundance of MRGs (including *sil* genes) were highest in the SBRs treated with NAg, suggesting the nanoparticle has the most potential for ARG co-selection compared to Ag^{+}[168]. There is also evidence to show that the formation of biofilms functions as a mechanism for co-selecting antibiotic and metal resistance[171,181]. The EPS matrix of biofilms acts as a sequestering barrier to heavy metals and antibiotics, and alarmingly, studies have found that exposure of metals on biofilms can encourage EPS synthesis, improving the biofilms adhesive, structural and protective integrity[182,183]. Moreover, because of the proximity of biofilm-cells, there is a much greater magnitude of DNA conjugation between bacteria. Research shows these events can increase under stressful conditions (*i.e.* exposure to antibacterial agents), which is advantageous to the co-selection process[183,184]. Studies have also found that exposure of NAg/Ag^{+}, and other heavy metal agents, on biofilms can stimulate quorum sensing, increasing expression of genes involved in biofilm formation and conjugation of ARGs[182,185]. Yang and Alvarez revealed that the treatment of *P. aeruginosa* biofilms with sub-lethal doses of NAg stimulated an upregulation in quorum sensing, resulting in increased EPS production and subsequent biofilm formation. They also found it induced an up to 3.4-fold

increase in expression of the multi-drug efflux gene *mexA*[182]. The regulation and promotion of biofilm formation and change in bacterial gene expression (including lateral transfer of ARGs) has been observed in *A. baumannii* in response to cationic iron (Fe^{+}) exposure previously, for example, but not to silver (NAg or Ag^{+})[185,186].

While bacteria have been exposed to toxic heavy metals long before human existence, anthropogenic pollution of environments has evidently created prolonged selective pressures on bacteria, consequently promoting the co-emergence of heavy metal and antibiotic resistance[171]. It is therefore critical to recognise the implications heavy metals (including silver) have on bacteria in both the environment and in clinical settings, as the co-selection of ARGs and promotion of biofilm growth could further strain the healthcare system and exacerbate the current drug resistance crisis.

2.8 Knowledge gap and future remarks

Global antibiotic resistance is not a future threat, but one that has at last transpired. From improper prescriptions for non-bacterial infections and overuse in agriculture/food industries, to the diminishing pharmaceutical investment into their development, the misuse of antibiotics ultimately calls for the need of novel and alternative antibacterial agents[5-7]. Major advancement in nanotechnology has led to significant progress in designing many antibacterial nanoparticles. The metal-based silver nanoparticle (NAg) is currently the most developed nanoparticle due to its multi-targeting antibacterial mechanisms and proven efficacy against a broad-spectrum of bacteria[61]. Many studies have shown that NAg is highly toxic to several Gram-positive and Gram-negative bacterial species, including the ESKAPE pathogens – a consortium of bacteria that frequently exhibit multi-drug resistance and are the leading cause of nosocomial (hospital-related) infection[19]. Among this group, (carbapenem-resistant) *A. baumannii* is of key concern, having been recently declared the number one critical level priority pathogen. Thus calling for the immediate development of alternative antibacterial treatments for this highly infectious and resistant pathogen[12,18]. *A. baumannii* and other globally prevalent pathogens have become the main targets of the unique and effective antibacterial nanoparticle.

Notwithstanding the strong antibacterial efficacy of NAg, there has been a growing concern over the ability of bacteria to adapt to the nanoparticle due to its increasingly

widespread use[25]. Bacterial resistance to the ionic form of silver, Ag^+, has been recognised for many years, and in the last decade, research inquiries have indeed observed the development of resistance mechanisms against NAg in several environmental and clinically-relevant Gram-negative and Gram-positive bacteria[31,32,65]. Further, studies have shown that biofilms – a resilient surface-attached bacterial community, can also adapt to silver (both NAg and Ag^+) despite the effective biofilm inhibiting and eradicating activity of the silver agents compared to many conventional antibiotics[87,182]. Biofilms are a major healthcare issue, as they frequently develop in cases of uncontrolled and chronic infections[121].

So far, only the planktonic form of *A. baumannii* has been found to exhibit Ag^+ resistance characteristics due to the presence of the exogenous (plasmid-based) Ag^+ efflux Sil system, and, as found in some cases, other undefined/non-Sil related mechanisms[34,35]. No presence of endogenous (chromosomal) silver resistance mechanisms have been identified in *A. baumannii*, so far. However, it should not be ignored that chromosomally encoded copper efflux systems have been detected in this bacterium, which could infer the possibility of chromosomal silver resistance due to the similarities between copper and silver efflux mechanisms[152,153]. To date, no work has been undertaken to determine if *A. baumannii* can develop resistance or specific adaptation(s) to NAg exposure. The nanoparticles toxicity on *A. baumannii* in both its planktonic and dominant biofilm form of growth, and in turn, the adaptation characteristic(s) of the bacterium which could develop in response to prolonged exposure are currently being studied. While it is possible that the Sil system plays a role in resistance to NAg, given that the nanoparticle exerts its toxicity differently from Ag^+ it is likely that resistance to NAg involves additional mechanisms that are still largely unexplored.

In addition, evidence has emerged showcasing the potential for heavy metals to co-select for antibiotic resistance genes (ARGs), facilitated by 'dual' metal/antibiotic resistance mechanisms which are related to cross-resistance (same genes/mechanism conferring resistance to both metal and antibiotics), co-resistance (metal and antibiotic resistance determinants located in the same genetic element), or co-regulation (the regulatory genes of metal and antibiotic resistance determinants are transcriptionally linked)[171]. The combined effects of heavy metal exposure on bacteria in potentially driving both metal resistance and antibiotic resistance is a troubling issue, and further

highlights the important implications of heavy metal overexposure on bacteria and to subsequently minimise this risk. Both NAg and Ag^+ have been found to facilitate the co-selection of various ARGs, most frequently seen at this stage in polluted water systems[168,169]. Over the years, studies have indeed shown that *Acinetobacter* species (including *A. baumannii*) can display cross-resistance to Ag^+ (and other heavy metals) and several antibiotics, but there is yet to be any evidence of NAg-induced co-selection of ARGs in this bacterial genus.

The increasing prevalence of silver resistance combined with growing evidence of the co-emergence of heavy metal and antibiotic resistance highlights the serious issues behind antibacterial overuse. Knowledge of bacterial resistance to silver and other heavy metals will help equip us to study the complex adaptation mechanisms of bacteria against NAg. Elucidating the mechanisms of NAg resistance could enable the development of technologies that mitigate these problematic adaptation responses. The generated knowledge of how the nanoparticle targets bacteria, and, in turn, how bacteria develop responses to its multi-targeting mechanisms can help guide the physicochemical engineering process of NAg (*e.g.* morphology, oxidation state, surface charge) to fine tune its antibacterial activity and therefore limit bacterial adaptation. Identification of the molecular basis of NAg resistance will allow us to target the biological signalling molecules and metabolites that trigger adaptation responses, including quorum sensing molecules and/or epigenetic and genetic regulators. The generated knowledge will also help inform strategies for a better risk *versus* benefits assessment regarding the application of NAg-containing consumer products, limiting its misuse and inadequate disposal. With no discovery of new effective antibiotics over the last 30 years, the efficacy of this valuable alternative antimicrobial agent must be protected so it may continue to be used in the fight against untreatable infections.

2.9 Chapter conclusion

To address the lack of knowledge regarding the interaction between *A. baumannii* and NAg, including the antibacterial activity of NAg against the bacterium and its subsequent adaptation potential, the model *A. baumannii* strain ATCC 19606 was selected and exposed to increasing doses of NAg to establish if resistance development

was possible. This study sought to confirm that prolonged exposure of ATCC 19606 to NAg would induce adaptation and susceptibility changes which could be associated with genetic mutations (or single nucleotide polymorphisms, SNPs) identified through whole genome sequencing. However, to support the contribution of these SNPs in the NAg adaptation response/s of *A. baumannii*, whole transcriptomic analysis was performed to better elucidate the mechanisms of defence (including non-mutational or epigenetic traits), and simultaneously help improve our overall knowledge on the antibacterial activity/cell-targeting mechanisms of NAg. While resistance to Ag^+ in *A. baumannii* has been previously observed, given the oxidative leaching of Ag^+ from NAg particulates is a core feature of nanoparticle antibacterial activity, this work also included an Ag^+ adaptation study which served as a direct comparison to the NAg adaptation study.

As NAg exerts several unique antibacterial mechanisms, such as cell surface disruption and oxidative stress *via* ROS generation, it was hypothesised that the bacterium would develop physiological changes and NAg defence features which may relate to cell surface protection and antioxidant activity. Furthermore, several NAg resistance traits have been previously identified in different bacterial species, and subsequently, the potential resistance mechanism/s exhibited by *A. baumannii* were anticipated to be distinct from those reported hitherto. It was predicted that these adaptation changes would be complemented by detectable SNPs (and/or epigenetic modifications) which would likely play a role in the overall resistance effect. Likewise, prolonged exposure of ATCC 19606 to Ag^+ was also expected to induce adaptation traits which would likely be distinct from other reported Ag^+ adaptation mechanisms in the bacterium and other species. However, as there is no prevalence of conserved and/or endogenous silver resistance determinants (*e.g. sil* and/or *cus* genes) detected in the *A. baumannii* genome, the resistance mechanism/s manifested in response to NAg/Ag^+ could perhaps overlap with other unreported silver-resistant Gram-negative bacteria.

The knowledge yielded from this work will support current evidence pertaining to the potent antibacterial efficacy of NAg (and Ag^+), but in turn, will equally highlight the impact of the overuse of this highly commercialised nanoparticle agent. By understanding the toxicological and adaptation responses of priority bacterial pathogens like *A. baumannii* to NAg, it will assist future research in interpreting the complex silver-resistant mechanisms exhibited by bacteria and ultimately help guide

the physicochemical design of the nanoparticle. The latter of which is needed to limit the potential for bacterial resistance generation and ensure the efficacious long-term use of this valuable alternative antibacterial.

Chapter 3: Materials and Methods

3.1 Preparation of antibacterial agents

The silver nanoparticles (nanosilver, NAg) utilised throughout this study (6.6wt% Ag_2O [$d \approx 2$ nm] finely dispersed onto microbiologically inert TiO_2 [$d \approx 30$ nm] for support; **Figure 3.1**) were synthesised into spherical particulates *via* flame spray pyrolysis at the University of New South Wales (UNSW), as previously described by Gunawan *et al.*[32,187]. The purpose of dispersing Ag_2O onto inert TiO_2 was to increase the surface-area-to-volume ratio to enhance soluble Ag dissolution[32,42]. The nanoparticles were sterilised *via* gamma-irradiation (Cobalt-60) for 1 h at a dose rate of ~ 6 Gy/min at the Australian Nuclear Science Technology Organisation (ANSTO). A fresh stock of NAg was prepared in sterile cation-adjusted Mueller-Hinton broth (CAMHB; BD, Australia) prior to any experimentation. The NAg suspension was homogenised before each experiment *via* ultra-sonication (Vibra-cell, Sonics & Materials, Inc.) for 20 s at a sonication output of 50%. Silver nitrate ($AgNO_3$; Merck & Co. Inc.) was used as the source of cationic silver (Ag^+) and was suspended in sterile ultrapure Milli-Q water and stored in the dark at room temperature. All experiments using NAg and Ag^+ were performed in dark conditions to both photocatalytically inactivate the TiO_2 supporting the Ag_2O nanoparticles, and prevent reduction of Ag^+ to metallic silver (Ag^0)[32,187]. An antibiotic control (quinolone antibiotic nalidixic acid; Nx; Sigma-Aldrich, USA) was also utilised in this study, and was dissolved in sterile Milli-Q water with 0.1M sodium hydroxide (NaOH) and stored at 4°C.

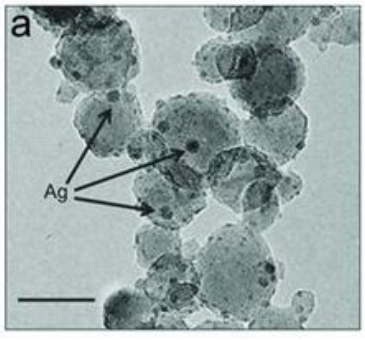

Figure 3.1 Transmission electron micrograph of TiO_2 supported Ag_2O nanocomposites. Ag_2O nanoparticles ($d \approx 2$ nm) highlighted by arrows are finely dispersed onto supportive microbiologically inert TiO_2 nanoparticles ($d \approx 30$ nm) *via* flame spray pyrolysis (scale bar = 20 nm). Image provided by Gunawan *et al.*[187].

3.2 Bacterial culture and growth conditions

The model *Acinetobacter baumannii* strain ATCC 19606 (hereafter referred to as the wild-type [WT] strain) was the bacterial organism used throughout this study. This strain was first isolated from a patient urine sample in 1948 by Schaub and Hauber[188]. A frozen (-80°C) glycerol stock of the WT strain was streaked onto a cation-adjusted Mueller-Hinton agar (CAMHA) plate and statically incubated for 16 – 18 h at 37°C. For each antibacterial exposure experiment, an overnight CAMHB culture was prepared with an isolated agar colony and incubated for 16 – 18 h at 37°C with 250 rpm orbital shaking. Following overnight growth, broth cultures were diluted 1:100 in fresh CAMHB to a cell count of ~ 2.4 x 10^8 CFU/mL and incubated for a further 2 h (37°C, 250 rpm) to pre-condition the culture. The pre-conditioning step re-establishes the active mid-exponential stage of bacterium growth, which is ideal when testing antibacterial agents[189].

3.3 Determination of the minimum inhibitory concentration (MIC) of NAg, Ag^+, and Nx

MICs were performed following a standard broth microdilution technique, and interpreted using the Clinical and Laboratory Standard Institute (CLSI) breakpoints[190,191]. Overnight pre-conditioned cultures of the WT strain were exposed to increasing doses of NAg, Ag^+, and Nx in a 96-well microtitre plate (BD Falcon, USA) at working volumes of 160 µL. The well-plates were covered in aluminium-foil to maintain dark conditions and incubated statically for 24 h at 37°C (humidified). MIC experiments were performed in three biological replicates (three isolated agar plate colonies) each in technical triplicates and included cell-only (positive) and media-only (negative) controls. The MIC is defined as the lowest dose of an antimicrobial agent which inhibits organism growth[192]. Herein, the lowest dose of each agent with no visible (turbid) growth was recorded as the MIC.

3.4 Induced adaptation response to NAg, Ag^+, and Nx *via* sequential passaging

To induce evolutionary adaptation of ATCC 19606 to each agent, the WT strain was sequentially passaged (sub-cultured every 24 h) in increasing concentrations of NAg, Ag^+, and Nx in a 24-well microtitre plate (BD Falcon, USA) and incubated for 24 h at 37°C with 150 rpm shaking. On day one, the pre-conditioned WT strain was inoculated in 0.25 x, 0.5 x, 1 x, and 2 x MIC doses of each respective agent at a working volume of 1 mL. After 24 h incubation, the highest MIC-fold dose of each agent at which growth was observed was recorded. Following this, 100 µL of surviving culture was transferred into a fresh 24-well plate (*i.e.* new exposure system) containing greater MIC-fold doses of each agent (*e.g.* 0.5 x, 1 x, 2 x, 3 x MIC). This process was repeated for a total of 30-days, and performed in two independent biological replicates, each in three technical replicates. Cell-only (positive) and media-only (negative) controls were also included, with the former passaged in the absence of any antibacterial agent in conjunction with the treated cultures to later rule out the acquisition and expression of random background adaptations traits.

3.4.1 Confirmation of stable resistance *via* MIC re-assessment

Samples of each 'adapted' culture (and cell-only control) from both passage replicates were isolated at the end of the 30-day passage experiment and stored in Cryotubes (Sarstedt, Germany) containing 20% glycerol at -80°C. The isolated cultures were streaked onto CAMHA plates containing their respective passaging agent (minimum 2 x MIC) and the surviving colonies were selected and then sub-cultured in fresh antibacterial-free CAMHB (1:100 dilution) over three-days (37°C, 250 rpm). This was to exclude cell populations exhibiting transient adaptation traits. Three isolated colonies of each of these 'stably adapted' strains were also stored in 20% glycerol at -80°C. The MICs of NAg, Ag^+, and Nx were then tested against the stable cultures to check for a minimum two-fold increase in MIC, which is indicative of resistance development[193].

3.4.2 Comparative growth rate assay

To ensure there was no variation in growth rates between the WT and silver-passaged strains (both passage replicates) which might alter their adaptation response/s, overnight (untreated) cultures were diluted to an optical density measured at 600 nm (OD_{600}) of 0.05 and incubated for 6 h in a 96-well plate at 37°C with 150 rpm shaking. Each hour, spectrophotometric readings were taken using a microplate reader (Spark 10M, Tecan, Switzerland) to capture the OD_{600} of each strain. The hourly OD_{600} was reported and plotted in a $\log_{10}$ format. Both replicates of the silver-passaged strains were included, and each growth rate assay was performed in at least two biological replicates.

3.5 Time-kill assay for non-resistant Ag^+-passaged *A. baumannii* ATCC 19606

The WT and Ag^+-passaged strains were exposed to 1.5 x MIC of Ag^+ in 50 mL of CAMHB (in conical flasks) and incubated at 37°C with 200 rpm shaking for a total of 3 h. Every 30 min, 1 mL samples of each culture were serially diluted in phosphate-buffered saline (PBS), spread onto CAMHA plates, and incubated for 24 h at 37°C. Agar plates with 30 – 300 surviving colonies were counted, and the fraction of surviving cells (CFU/mL) per 30 min time point were plotted relative to the 0 min population. Untreated cell-only controls of both strains were included and plotted against the treated populations. Determination of a tolerance or persistence response is characterised by an increase in an agent's minimum duration for killing (MDK) the bacterial population – 99% of the population for a tolerance effect (MDK_{99}), and 99.99% of the population for a persistence effect ($MDK_{99.99}$)[193,194].

3.6 Comparative whole genome analysis

3.6.1 Whole genome extraction

DNA extraction of the 'stable' media-passaged, NAg-resistant, Ag^+-tolerant, and Nx-resistant (hereafter referred to as NAg^R, Ag^{+T}, and Nx^R, respectively) ATCC 19606 strains (see **Section 3.4.1**) was performed using a DNeasy Blood and Tissue Spin-Column kit (Qiagen, Germany) following manufacturer instructions. Media-passaged

strains were included to rule out the presence of background mutations that may have developed in the absence of antimicrobial pressure and/or because of the effect of daily sub-culturing. Extracted DNA samples were eluted and stored in nuclease-free water at -20°C. In total, 24 extractions were performed, three replicates from the two sequential passage biological replicates of each respective passaged strain.

3.6.2 Whole genome sequencing and assembly

Extracted genomic DNA concentration and quality was assessed using a Quant-iT PicoGreen dsDNA assay kit (Invitrogen, USA) and agarose gel electrophoresis. Sequencing was done using the Ilumina Mi-Seq system (Illumina, USA) at the Australian Institute for Microbiology and Infection (AIMI) Sequencing Facility (UTS, Australia). Library preparation was done using an adapted Nextera Flex library preparation kit process known as Hackflex, developed by Gaio *et al.*[195]. 10 ng of DNA was used for library preparation. Tagmented DNA was amplified using the facility's custom designed i7 and i5 barcodes involving 12 cycles of polymerase chain reaction (PCR). Due to the number of samples, quality control was maintained by sequencing a pool of samples using Mi-Seq V2 nano kit (300 cycles). Following library amplification, 3 µL of each library was collated into a library pool which was then cleaned using SPRIselect beads (Beckman Coulter, USA) following the protocol published by Gaio *et al*.[195]. Based on the sequencing data generated, the read count for each sample was used to identify failed libraries (*i.e.* libraries with < 100 reads), and then normalised to ensure equal representation in the final pool. The final pool was sequenced on one lane of Illumina Novaseq S4 flow cell (2 x 150 bp) (Novogene, Singapore). For data analysis, the sequenced data were assembled in draft genome sequences using Shovill v1.0.9 (https://github.com/tseemann/shovill).

Comparative whole genome alignment was carried out using Snippy v4.6.0 using default settings. The WT strain ATCC 19606 (GenBank accession number CP045110) was used as the comparative reference genome. Manual curation of variant call files was executed to identify the location of single nucleotide polymorphisms (SNPs) in the passaged strains and the metabolic/protein product functions of these mutated genes. Unknown gene identities were confirmed through comparative analysis of other annotated references of the same ATCC 19606 strain (GenBank acc. no. CP046654 and CP059040) identified by different research groups.

3.6.3 Validation of SNPs *via* traditional Sanger sequencing

Sanger sequencing (performed by the Australian Genomic Research Facility, AGRF) was performed to confirm the presence of low frequency gene mutations. PCR was used to generate amplicons of target mutant genes using designed primers (50 µM) (Integrated DNA Technologies (IDT), USA) listed in **Table 3.1**, *Taq* polymerase (5 U/µL) and 10 x ThermoPol PCR buffer (20 mM Mg^{2+}) (New England Biolabs, USA). The following conditions were used: initial denaturation at 98°C for 1 min → 35 amplification cycles (denaturation at 95°C for 30 s; annealing at 60-62°C for 30 s; and extension at 72°C for 1 min per kbp of PCR product) → final extension at 72°C for 1 min. Amplicon quality was assessed using gel electrophoresis (1% agarose gel in 1 x TBE buffer containing Gel Red (Biotium, USA); submerged in 1 x TBE buffer). PCR products were cleaned *via* cold sodium acetate (3M) + 100% ethanol precipitation or by agarose gel extraction using the QIAquick gel extraction kit (QIAGEN, Germany).

Table 3.1 List of primers used for validation of mutations detected in the NAg^R strain.

Gene	Product size (bp)	Forward primer (5' → 3')	Reverse primer (3' → 5')	Annealing temp. (°C)
rcsC	421	GAAAACCGATTTTGCCTGAT	CCCTGTCTGGCTCTTGATTG	60
smf1-2	770	AGCTTGGACAAGTGCTGGTT	GCTGCTCTTTCGGTTGTAGG	60
csuB	920	GCCAGACGGTTTGTAGGTGT	AGTAAATGCGGGTGAAATCG	63

3.7 Biofilm growth study *via* fluorescent microscopy imaging

3.7.1 Fluorescent dye staining of biofilm

To grow biofilms of the WT, NAg^R, and Ag^{+T} ATCC 19606 strains, overnight cultures (no pre-conditioning required) were diluted 1:100 in fresh CAMHB and 200 µL was inoculated in a FluoroDish (World Precision Instruments, USA) and incubated at 37°C for 24 h (humidified). The supernatant was gently removed the following day, and the dishes were washed twice with sterile PBS. The adhered biofilms were stained with 200 µL of 5 µM SYTO-9 + 30 µM propidium iodide (PI) (Thermo Fisher Scientific, USA) for 30 min at room temperature in dark conditions. The stain was then removed, the dishes washed twice more with PBS, and then 200 µL of 80% glycerol was finally

added to each dish. Growth and staining of each biofilm culture was repeated in biological triplicates per strain.

3.7.2 Microscopy imaging of biofilm microcolonies

Fluorescent imaging was performed using a DeltaVision (DV) Elite deconvolution fluorescence microscope (GE Healthcare, USA). The fluorescence filter channel FITC excites (475/28 nm) SYTO-9-stained nucleic acid (523/48 nm emission; green colour) from all cells, and the channel TRITC excites PI-stained-nucleic acids (632/22 nm) from dead cells with compromised cell surfaces (679/34 nm emission; red colour). All images were captured at 100 x magnification in a Z-series using the DV elite SoftWoRx program and deconvolved. Ten images were captured per biological replicate per strain (total of 30 images per strain). Phase contrast images of planktonic (non-biofilm) cultures of each strain were also captured using the DV Elite Microscope at 100 x magnification.

3.7.3 Quantitative analysis of total biofilm biomass

Deconvolved fluorescent images were analysed using Imaris software v9.6.0 (Oxford Instruments, UK) to determine biofilm biomass ($\mu m^3/\mu m^2$; μm^3 = biomass volume, μm^2 = surface coverage). The SYTO-9 (green, total biomass) and PI (red, dead biomass) fluorescent stains were quantified individually to determine the viability of biofilm growth for each strain. The raw images were used to provide visualisation of biofilm biomass/cell morphology and presented as single plane 3D slices. Statistical analysis of fluorescent images was performed in Prism (GraphPad, USA) using an unpaired Student's t-test (Welch's correction), with a statistically significant *P*-value set at < 0.05.

3.8 Reactive oxygen species (ROS) generation assay

3.8.1 Generation and staining of intracellular ROS

Overnight cultures of the WT, NAg^R, and Ag^{+T} strains were resuspended in 5 mL of CAMHB to an OD_{600} (optical density at 600 nm) of 0.05 and incubated for a further 2 h to reach mid-exponential growth phase. The pre-conditioned cultures were

centrifuged at 7500 rpm for 5 min, resuspended in 1 mL of sterile saline (8 g/L NaCl + 0.2 g/L KCl) and stained with the fluorogenic ROS indicator 2′,7′-dichlorodihydrofluorescein diacetate (H_2DCFDA; 10 µM working concentration; Invitrogen, USA) for 45 min at room temperature in dark conditions. The stained cultures were centrifuged at 13000 rpm for 1 min, resuspended in 1 mL saline, and treated with 0.5 x MIC of NAg or Ag^+, respectively, for 30 min and 60 min at 37°C (200 rpm). Treated cultures were centrifuged (13000 rpm, 1 min), resuspended in 1 mL saline, and then stained with propidium iodide (PI) (30 µM working concentration; Invitrogen, USA) for 5 min (room temperature, dark conditions). Finally, the cultures were centrifuged (13000 rpm, 1 min), resuspended in 100 µL of saline, and 3 µL of each sample was pipetted onto a glass slide with a Gene Frame (Thermo Fisher Scientific, USA) containing a 30 µL 2% agarose gel pad. A positive control of 50 mM hydrogen peroxide (H_2O_2) treated cells and a negative control of untreated cells were included. This experiment was performed in three biological replicates.

3.8.2 Fluorescent cellular ROS imaging

Microscopy was performed using the DV Elite microscope (GE Healthcare, USA). The filter channel FITC was used to excite (475/28 nm) DCF-stained ROS (523/48 nm emission, green colour), the TRITC channel excites PI-stained nucleic acids (see **Section 3.7.2**). All images were captured at 100 x magnification using the DV elite SoftWoRx program and deconvolved prior to quantification. Five-to-six images were captured per biological triplicate for each treated strain.

3.8.3 Intracellular ROS quantification

Quantification of generated ROS and number of dead cells for each treatment was performed using the open-source image processor Fiji (ImageJ, USA). The fluorescent intensity (corresponds to level of cellular ROS) was quantified by calculating the corrected total cell fluorescence (CTCF). A selected cell was outlined using the freehand ROI tool, from which the "area", "integrated density", and "mean grey value" parameters were measured. This same outline was then used to measure an area of no fluorescence, or the background. The CTCF is calculated using the following formula:

Integrated Density – (Area of Selected Cell **x** Mean Fluorescence of Background)

Twenty (n = 20) cell and ten (n = 10) background readings were captured per 5 – 6 images for each triplicate treated strain. Dead cells were manually counted and recorded as a percentage of the total number of cells per image. Statistical analysis was performed in Prism (GraphPad, USA) using an unpaired Student's t-test (Welch's correction), with a statistically significant *P*-value set at < 0.05.

3.9 Transcriptomic study on NAg^R and Ag^{+T} *A. baumannii* ATCC 19606

3.9.1 Determination of working concentrations of NAg and Ag^+

Prior to commencement of the transcriptomic study, the working concentrations of NAg and Ag^+ used to treat the WT, NAg^R, and Ag^{+T} strains was determined *via* growth rate comparisons. Overnight cultures of each strain were diluted in 25 mL of fresh CAMHB to an OD_{600} of 0.05 and incubated for a further 2 h (37°C, 200 rpm). Upon reaching mid-exponential growth phase, low (sub-MIC of WT) and high (above-MIC of WT) doses of NAg and Ag^+ were added to the respective cultures accordingly. Each hour, spectrophotometric readings from each treatment system was performed to determine the OD_{600}. Untreated (cell-only) controls of each strain were also included, and each experiment was performed in at least two biological replicates. The determined working concentrations are listed in **Table 3.2** below.

Table 3.2 Determined working concentrations of NAg and Ag^+ used to treat WT, NAg^R, and Ag^{+T} *A. baumannii* ATCC 19606 prior to RNA extraction.

Treatment	*Acinetobacter baumannii* strain		
	WT	NAg^R	Ag^{+T}
NAg treatment			
Low NAg dose (sub-MIC, 0.5 x MIC)	0.5 µg/mL	0.5 µg/mL	-
High NAg dose (above MIC, 3 x MIC)	-	3 µg/mL	-
Ag^+ treatment			
Low Ag^+ dose (sub-MIC, 0.5 x MIC)	1 µg/mL	-	1 µg/mL
High Ag^+ dose (above MIC, 1.5 x MIC)	-	-	3 µg/mL

3.9.2 Bacterial culture preparation for RNA extraction

Overnight cultures of the WT, NAg^R, and Ag^{+T} strains were diluted in 25 mL CAMHB to an OD_{600} of 0.05 and incubated for 2 h (37°C, 200 rpm) to reach mid-exponential phase. Each culture was then treated with the determined low and high working concentrations of NAg and Ag^+ (see **Table 3.2**) for 30 min. The NAg^R strain was exposed to 0.5 x MIC (low dose) and 3 x MIC (high dose) of NAg, and the Ag^{+T} strain was treated with 0.5 x MIC (low) and 1.5 x MIC (high) of Ag^+. The difference in MIC-fold between the high concentrations of NAg and Ag^+ were used to ensure that the NAg^R and Ag^{+T} strains were exposed to equivalent contents of silver (3 µg Ag/mL). Untreated controls of each strain were included to serve as negative controls and each experiment was performed in three biological replicates.

3.9.3 Total RNA extraction and quality control

RNA extraction for each strain was performed using the RNeasy Mini Bacteria Kit with the RNAprotect Bacteria Reagent (Qiagen, USA) using manufacturer's instructions. Briefly, 500 µL of each treated (and untreated) culture was incubated with 1 mL of RNAprotect (5 min, room temperature) and pelleted down (7500 rpm, 10 min). The supernatant was removed, and cell pellets were treated with 20 µL of 10 mg/mL Proteinase K (Sigma-Aldrich, USA) and Qiagen lysozyme for 15 – 20 min at room temperature (with 10 s vortex every 2 min). RNA extraction of lysed cells was then performed using the RNeasy Kit and included treatment with DNase (15 min incubation, room temperature). RNA elution was done using 40 µL of RNase-free water (10000 rpm centrifuge, 1 min) and repeated using the collected elute. Total RNA quantity and purity was assessed using an Epoch microplate spectrophotometer (Agilent Technologies, USA) and a Nanodrop spectrophotometer (Thermo Fisher Scientific, USA), and RNA integrity was checked using the TapeStation System with RNA analysis ScreenTape (Agilent Technologies, USA).

3.9.4 RNA library preparation and sequencing (RNA-Seq)

Library preparation and RNA-Seq was performed at the Ramaciotti Centre for Genomics, University of New South Wales (UNSW), Australia. Briefly, 100 ng of RNA was used to prepare libraries using an Illumina Stranded Total RNA prep

Ligation Kit with Ribo-Zero Plus (Illumina, USA) as per manufacture instructions with amplification step at PCR cycle 12. Libraries were quantified using Qubit dsDNA Assay (Cat No. Q32854; Life Technologies, Australia) and size distribution was carried out using a DNA High Sensitivity Reagent with a LabChip GX Touch HT Nucleic Acid Analyser (Perkin Elmer, Australia). Libraries were pooled equimolar and sequenced on NovaSeq6000 SP 1 x 100 bp (single end read).

3.9.5 RNA-Seq data mapping and analysis

RNA-Seq mapping and analysis was performed using Galaxy Australia (https://usegalaxy.org.au) with technical assistance from Dr Igor Makunin from the Queensland Cyber Infrastructure Foundation (QCIF). The analysis workflow, including quality control of reads (see **Section 3.9.6** below), read mapping and counting, identification of differentially expressed genes (DEG), and conduction of gene ontology analysis, is visually summarised in **Figure 3.2** below. The cut-off threshold to define a DEG between pairwise comparisons was set at a $\log_2$ fold change of ≥ 0.58 ($\geq$ 1.5-fold change) with an adjusted *P*-value of < 0.01, as per the Benjamini and Hochberg false-discovery rate method[196]. DEGs with a $\log_2$-fold change of < 0.58 ($<$ 1.5-fold change) and/or adjusted *P*-value of > 0.01 were considered statistically insignificant. No test of significance relative to a fold-change threshold (TREAT) was utilised. Mapping of statistically significant DEGs to functional pathways with gene ontology was performed, however, due to the scope of this study, only the contribution of individual DEGs of interest to the evolved defence mechanisms of the NAg^{R} and Ag^{+T} strains were examined. The transcriptomic data acquired through this RNA-Seq analysis was extensive, this was attributed to the widespread and diverse gene expression changes mediated by ATCC 19606 in response to multi-targeting antimicrobial agents. Refer to **Table A1** and **Table A2** for results of gene ontology enrichment analysis of DEGs mapped to functional biological pathways.

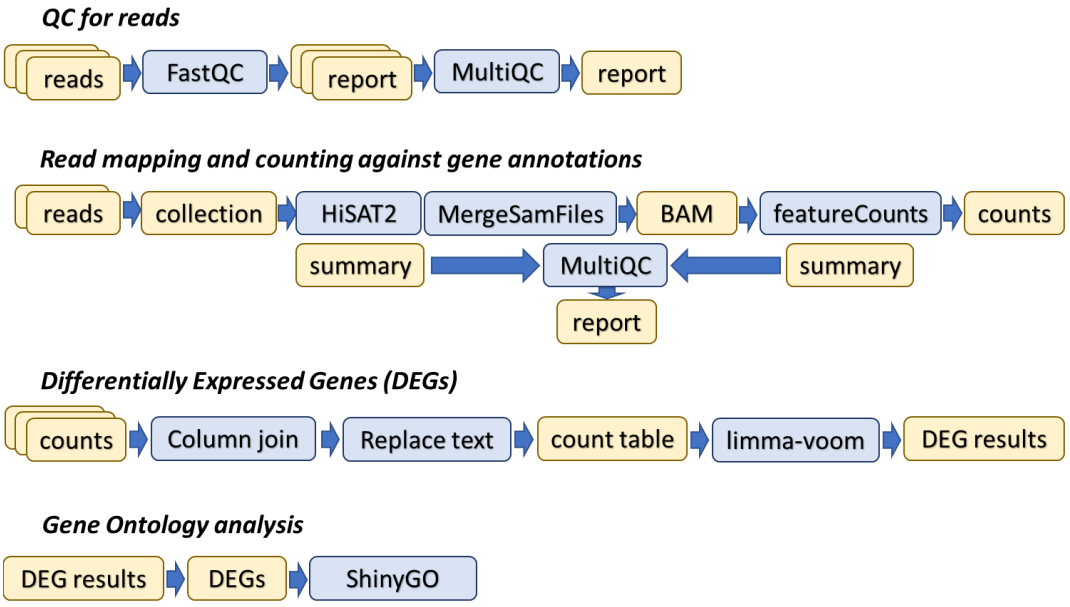

Figure 3.2 Schematic workflow summary of RNA-Seq analysis. Analysis and data mapping was performed in Galaxy Australia by Dr Igor Makunin from QCIF. Blue arrows indicate order of events starting from top (QC for reads) to bottom (Gene Ontology analysis).

3.9.6 RNA-Seq quality control *via* principal component analysis

Quality control of the RNA-Seq data was executed using a principal component analysis (PCA) to assess the extent of variation between each sample and biological replicate (**Figure 3.3**). Each coloured circular data point in the plot represents one biological replicate of each strain and respective treatment population. The distance between each sample data point corresponds to the level of dissimilarity between samples (*i.e.* further distance = dissimilar). Distinct population clustering was observed for each data point indicating minimal variation between the biological replicates of each strain and their treatment groups and that the transcriptomic study would be affected. The isolated clustering of the high NAg dose treated NAg^{R} samples (NAg^{R} high NAg) and high Ag^{+} dose treated Ag^{+T} samples (Ag^{+T} high Ag^{+}) indicates there are no significant transcriptomic differences between these treatment groups and the other treatment groups (*i.e.* non-treated and low dose treated) of the respective strains.

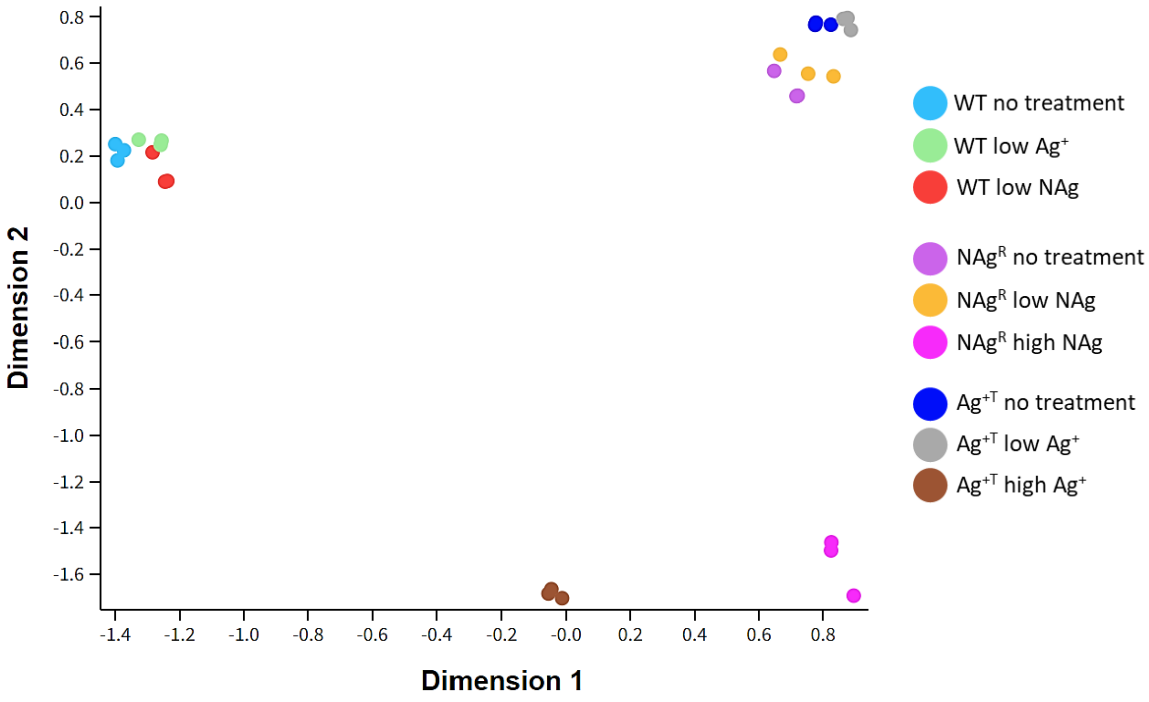

Figure 3.3 Principal component analysis (PCA) plot. The level of variation between biological triplicates of each ATCC 19606 strain and respective treatment type is displayed. Individual coloured dots represent one biological replicate of population cluster. WT = wild-type strain, NAg^{R} = NAg-resistant strain, Ag^{+T} = Ag^{+}-tolerant strain.

Chapter 4: Development of Nanoparticle Adaptation Phenomena in *Acinetobacter baumannii:* Physiological Change and Defence Response

4.1 Chapter summary

The literature review presented in **Chapter 2** offered in depth insight into the efficacious broad-spectrum and multi-targeting antibacterial activity of NAg against many important bacterial species. Simultaneously it also established that there is mounting concern for the generation of silver-resistant bacteria due to the overuse of NAg-based products. Alas, knowledge surrounding the interaction between the nanoparticle and *A. baumannii* is limited, and thus far, no studies have determined if the bacterium has the potential to develop resistance or adaptation traits to NAg. With the growing global threat of antimicrobial resistance, the need for novel and alternative agents is vital. NAg is a viable candidate, yet with continually emerging evidence of bacterial silver resistance, it is essential that our understanding of bacterial toxicity and defence response/s to nanoparticle exposure are entirely investigated and understood. These knowledge gaps are what prompted the motivation for the work in the following chapter(s). The work presented in this chapter provides the first known reported evidence of stable NAg resistance development in *A. baumannii* ATCC 19606 because of prolonged exposure. The resistance phenomenon was associated with the development of genetic mutations detected through comparative whole genome sequencing. These mutations were suggested to contribute to observed physiological changes related to biofilm formation and suppression of NAg-induced reactive oxygen species (ROS) activity. In comparison, prolonged exposure of *A. baumannii* to Ag^{+} resulted in the development of a 'slower-to-kill' tolerance trait, rather than resistance, associated with increased biofilm formation, respiratory activity, and morphological change – also potentially linked to the detected genetic mutations in the tolerant strain. The work presented in this chapter is an annotated and partially edited reproduction of a published research article.

4.2 Declaration of publication

I, Oliver McNeilly, declare that the following publication included in lieu of this chapter meets the requirements for a thesis by compilation.

Published as:

Development of Nanoparticle Adaptation Phenomena in *Acinetobacter baumannii:* Physiological Change and Defense Response

(https://doi.org/10.1128/spectrum.02857-22)

Oliver McNeilly[1], Riti Mann[1], Max Laurence Cummins[1,2], Steven P. Djordjevic[1,2], Mehrad Hamidian[1*], and Cindy Gunawan[1,3*]

[1]Australian Institute for Microbiology and Infection, University of Technology Sydney, Broadway, NSW 2007, Australia

[2]Australian Centre for Genomic Epidemiological Microbiology, University of Technology Sydney, Broadway, NSW 2007, Australia

[3]School of Chemical Engineering, University of New South Wales, Kensington, NSW 2052, Australia

[*]Correspondence:
mehrad.hamdian@uts.edu.au; cindy.gunawan@uts.edu.au

Author Contributions: OM, MH, and CG conceptualised the paper. MH and CG acquired research funding. OM, RM, MH, and CG formulated the methodology. OM performed the experimental investigation. OM and MC performed formal analysis. OM prepared the original draft. OM, RM, MC, SD, MH, and CG reviewed and edited the paper. SD, MH, and CG supervised the research. All authors have read and agreed to the published version of the manuscript.

Oliver McNeilly	Production Note: Signature removed prior to publication.
Riti Mann	Production Note: Signature removed prior to publication.

Max L. Cummins	Production Note: Signature removed prior to publication.
Steven P. Djordjevic	Production Note: Signature removed prior to publication.
Mehrad Hamidian	Production Note: Signature removed prior to publication.
Cindy Gunawan	Production Note: Signature removed prior to publication.

4.3 Abstract

The present work describes the evolution of a resistance phenotype to a multi-targeting antimicrobial agent, silver nanoparticles (nanosilver; NAg), in the globally prevalent bacterial pathogen *Acinetobacter baumannii*. The Gram-negative bacterium has been recently listed as a critical priority pathogen requiring novel treatment options by the WHO. Through prolonged exposure to the important antimicrobial nanoparticle, the bacterium developed mutations in genes that encode protein subunits of organelle structures involved in cell-to-surface attachment, as well as in a cell envelope capsular polysaccharide synthesis-related gene. These mutations are potentially correlated to stable physiological changes in biofilm growth behaviour and to an evident protective effect against oxidative stress, most likely as a feature of toxicity defence. It is furthered reported that a different adaptation response of *A. baumannii* to the cationic form of silver (Ag^+) was exhibited. The bacterium developed tolerance to Ag^+, which was associated with an indicative increase in respiratory activity and changes in biofilm formation and planktonic cell morphology, each of which are reported characteristics of tolerant bacterial populations. The findings of adaptation phenomena to NAg highlight the risks of the long-term use of the nanoparticle on a priority pathogen. The data presented herein urge for the implementation of strategies to overcome bacterial NAg adaptation to better elucidate the toxicity mechanisms of the nanoparticle and preserve the efficacy of the potent alternative antimicrobial agent in this era of antimicrobial resistance.

Key words: *Acinetobacter baumannii,* mutation, resistance, silver nanoparticles

4.4 Importance

Several recent studies have reported on bacterial resistance development to broad-spectrum antimicrobial silver nanoparticles (nanosilver; NAg). NAg is currently one of the most important alternative antimicrobial agents. However, no studies have yet established if *Acinetobacter baumannii*, a globally prevalent nosocomial pathogen, can develop resistance to the nanoparticle. The study herein describes how a model strain of *A. baumannii* (ATCC 19606), with no inherent silver resistance determinants, developed resistance to NAg following prolonged exposure. The observed stable physiological changes were correlated to mutations detected in the bacterium genome,

rendering it capable of proliferating at an otherwise toxic NAg concentration. It was also found that *A. baumannii* developed a 'slower-to-kill' tolerance trait to Ag^{+}, which highlights the unique antimicrobial activities between the nanoparticulate and ionic forms of silver. Despite the proven efficacy of the nanoparticle, the observation of NAg resistance in *A. baumannii* emphasises the potential risks of repeated overuse of this agent on a priority pathogen.

4.5 Introduction

The world is in the midst of an antimicrobial resistance (AMR) emergency, wherein many antibiotic drugs no longer have an effect against bacterial pathogens[6,43]. The widespread overuse of antibiotics across industrial and medical settings, along with significant withdrawal in financial investment into antibiotic research and development, has ultimately led to this global health crisis[5,58,60]. *Acinetobacter baumannii* is a Gram-negative coccobacillus bacterium, and a member of the ESKAPE group which include the leading nosocomial (hospital-related) antibiotic-resistant pathogens (*Enterococcus faecium*, *Staphylococcus aureus*, *Klebsiella pneumoniae*, *Acinetobacter baumannii*, *Pseudomonas aeruginosa*, and *Enterobacter* spp.)[13,17,10]. The World Health Organisation (WHO) has recently listed carbapenem-resistant *A. baumannii* (CRAb) as a critical level priority pathogen (priority level one) requiring the immediate development of new and effective treatment options[6,7]. It is difficult to control CRAb infections, given that, in addition to having resistance to carbapenems (considered last line antibiotics), these strains are also resistant to nearly all other antibiotics. The global distribution of CRAb strains is mainly due to the spread of two clonal sequence types, ST1 and ST2, also known as GC1 and GC2, respectively[18,55]. In 2019, there were 132,000 global deaths attributed to MDR *A. baumannii*, 37,700 of which were carbapenem-resistant related deaths[2]. The bacterium has an incredibly innate ability to acquire resistance to many antibiotics through the uptake of mobile genetic elements (*e.g.* transposons and plasmids) which carry AMR genes[17,56]. Carbapenem resistance in *A. baumannii* is primarily due to the horizontal

acquisition of genes encoding carbapenem-hydrolysing oxacillinases (*e.g. oxa23, oxa24, oxa58*)[57,197].

With the global spread of AMR, an increasing number of research efforts have been dedicated toward the development of alternative antimicrobials, particularly those with multi-targeting mechanisms. Silver nanoparticles (herein referred to as nanosilver or NAg) are ultrafine, less than 100 nm particulates of metallic silver (Ag^0) or silver oxide (Ag_2O). NAg is one of the most extensively commercialised alternative antimicrobial agents, due to their potent and broad-spectrum antimicrobial properties[22,62]. The nanoparticles have been used in medical devices, such as wound dressings, catheters and prosthetics, to treat and prevent infections[24,25]. NAg has also been incorporated in a vast array of every-day products and appliances, from personal care products, clothing and textiles, washing machines and fridges, to even baby products, intended to impede microbial growth[19,25,26]. This increasingly indiscriminate use of the nanoparticle has brought concern to the scientific community as to whether, just like in the case of antibiotics, bacteria could develop resistance to NAg.

While bacterial resistance to cationic silver (Ag^+) has been recognised for several decades it was commonly perceived that resistance to NAg was unlikely due to the nanoparticles multi-targeting antimicrobial mechanisms[25,29,65]. Contradicting this notion, however, there has been growing evidence over the past decade regarding the development of adaptation phenomena to NAg, observed in a number of bacterial species, including those of clinical significance, such as *Escherichia coli*, *Pseudomonas aeruginosa* and *Staphylococcus aureus*[28-32,198]. In the case of *A. baumannii,* studies have previously reported mechanisms of Ag^+ resistance in the bacterium, including the acquisition of mobile genetic elements (plasmids) that harbor the well-known Sil Ag^+ efflux system (encoded by the *sil* operon *silESRCFBAGP*)[34-36]. Nonetheless, to date there has been no reported evidence of NAg resistance in *A. baumannii*, or in any *Acinetobacter* species in fact, and only little is known regarding the bacterial species' interaction with the nanoparticle.[33]

To address this knowledge gap, the present work sought to study the toxicological and subsequent adaptation responses of *A. baumannii* to long-term NAg exposure. More specifically, this work was intended to gain insights on how the bacterium might physiologically change and exhibit defence mechanisms against the nanoparticles toxicity, that is, when in the absence of the Sil efflux system. The latter is to determine

if *A. baumannii* has the intrinsic ability to develop resistance to NAg without a native or acquired silver resistance system. Herein, the development of stable adaptation characteristics in *A. baumannii* (reference strain ATCC 19606; GenBank accession number CP045110; with no presence of *sil* genes) in response to prolonged NAg exposure was observed[199]. The bacterium evolved single nucleotide gene mutations, with evidence suggesting links between these mutations to the observed changes in the biofilm-forming ability of the bacterium, as well as, indicatively, to its protective mechanisms against NAg-induced cellular oxidative stress. The work also found that ATCC 19606 developed a different adaptation response to Ag^+, indeed with distinct physiological changes, highlighting the unique microbiological activities of the nanoparticulate *versus* ionic forms of silver. A parallel evolutionary study with the quinolone antibiotic nalidixic acid (Nx) was also included, to compare the extent of resistance development with a single-target model antibiotic.

4.6 Results and Discussion

4.6.1 Toxicological and adaptation responses of *A. baumannii* ATCC 19606 to NAg, Ag^+, and Nx

To investigate the adaptation responses of *A. baumannii* ATCC 19606 to NAg, Ag^+ (supplied as $AgNO_3$) and the model antibiotic Nx, the minimum inhibitory concentration (MIC) of each antibacterial agent was first determined. From the dose-dependent growth inhibition studies, the MIC was observed at 1 μg/mL for NAg and 2 μg/mL for Ag^+ (**Figure 4.1A**). NAg and Ag^+ are known to target the bacterial cell envelope, which in the case of Gram-negative bacteria like *A. baumannii*, involves damage to phospholipid moieties in their outer and inner membranes[98]. The targeting of the inner membrane is thought to disrupt bacterial respiratory components (embedded within the membrane). For instance, Ag^+ can form complexes with electron donor groups in proteins (*i.e.* thiol and amine groups), including those that are present in the respiratory enzyme NADH dehydrogenase[20,22,77,93,133]. This membrane-targeting activity likely causes electron leakage from respiratory components, which can result in the generation of reactive oxygen species (ROS) which further damage biomolecules, including DNA, lipids, and other proteins[22,98]. Although there are some similarities, studies have shown that NAg exerts unique antimicrobial mechanisms when compared to Ag^+. In an aqueous environment, NAg can undergo oxidative

dissolution, releasing Ag^+ ions, which can interact with various moieties (including halides, sulphides, and organics) and transform into other distinct silver species, each with their own toxicity[33,35]. Previous studies have shown that Ag^+, in general, exerts a higher extent of antibacterial activity when compared to NAg, as the activity of the nanoparticle is determined by its physicochemical characteristics, such as size, shape, and surface charge[75,77,143,200]. The results, however, are indeed consistent with reported NAg MICs of 0.39 – 2.5 µg/mL on *A. baumannii*, as well as with one Ag^+ study reporting an MIC of 4 µg/mL[41,84,109]. Nx is a single-target fluoroquinolone antibiotic that inactivates the DNA gyrase subunit GyrA, an enzyme that plays a role in the unwinding of DNA during cell replication[201]. Herein, a 5 µg/mL MIC for Nx was observed (**Figure 4.1A**).

A

MIC testing on WT *A. baumannii* ATCC 19606

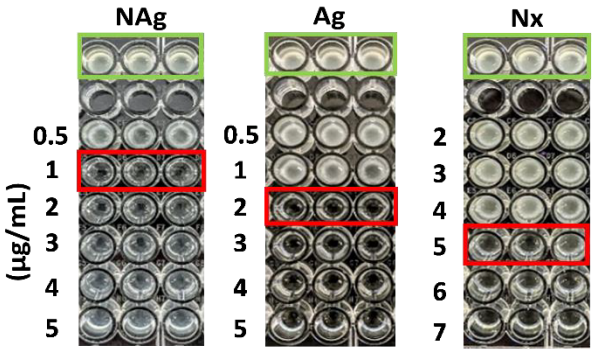

Antibacterial agent	MIC (µg/mL)
NAg	1
Ag^+	2
Nx	5

B

Prolonged antibacterial exposure via sequential passaging

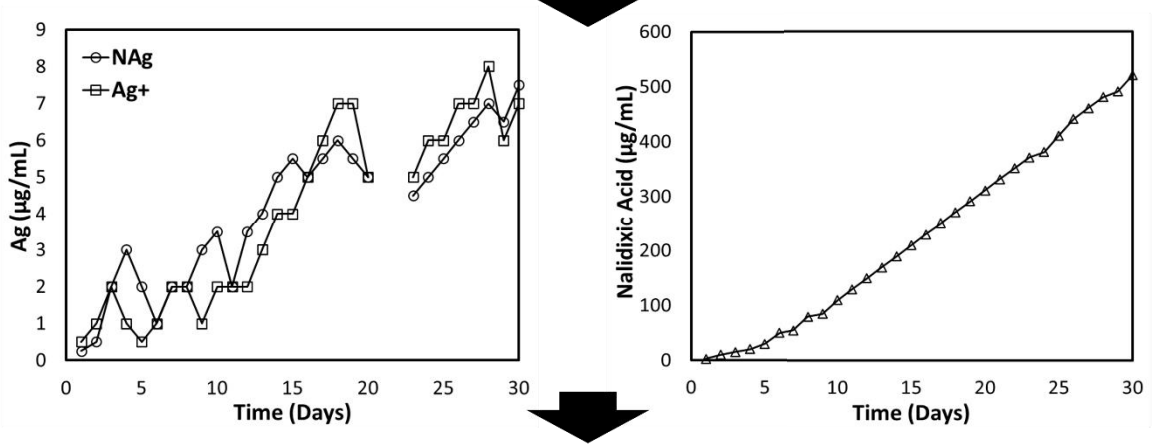

C

Evolved stable adaptation phenotypes

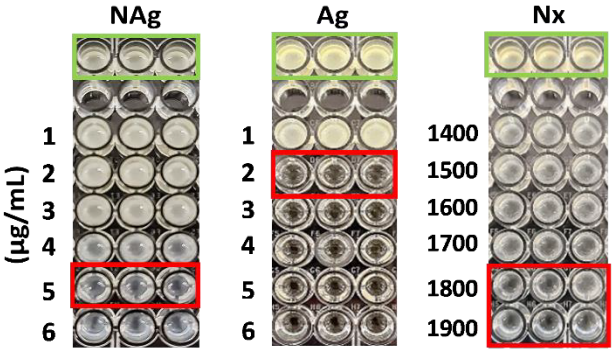

Antibacterial agent	MIC (µg/mL)
NAg	5
Ag^+	2
Nx	1800-1900

D

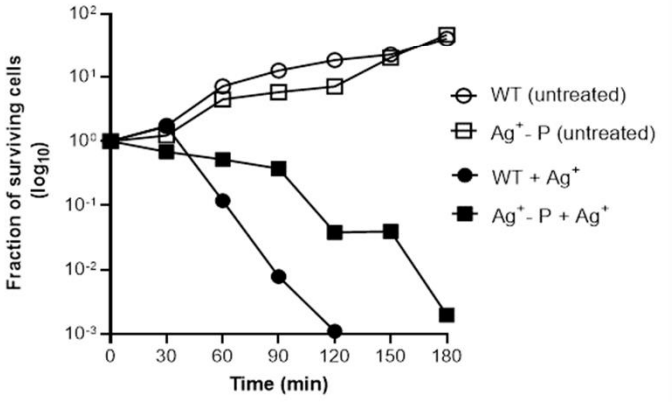

Strain	MDK_{99}
WT *A. baumannii*	~ 90 min
Ag^+-passaged *A. baumannii*	~ 135-165 min

Figure 4.1 Susceptibility and evolutionary adaptation potential of *A. baumannii* ATCC 19606 to NAg, Ag^+, and Nx. (**A**) Determination of the initial minimum inhibitory concentrations (MICs) of NAg, Ag^+, and Nx on wild-type (WT) ATCC 19606. The experiments were performed in three biological replicates (independent bacterial inoculum from three individual colony isolates per antibacterial agent; each with three technical replicates). One biological replicate per treatment system is shown (green outline = cell-only control; red outline = MIC point; media-only control not shown). (**B**) Sequential passaging experiments (sub-culturing every 24 h) showing the progressive shifts in the highest concentrations of NAg, Ag^+, and Nx at which the bacterium could proliferate (over 30-days). The experiments were performed in two biological replicates (for each agent) and included a cell-only control passaged culture (no antimicrobial agent), each condition including three technical replicates. Note the three-day passaging gap in the NAg/Ag^+ exposure experiments were due to laboratory closure. See **Figure S1** for passaging results of the second biological replicate. (**C**) NAg, Ag^+, and Nx MIC re-assessment on the passaged cultures (isolates obtained at end point of passage). Shown here are the results of the first biological replicate passaging culture, see **Figure S1** for MIC results of the second biological passaged replicate. (**D**) Killing kinetics of WT and Ag^+-passaged (Ag^+-P) strains when exposed to 1.5 x MIC Ag^+ dose to determine the minimum duration of killing 99% (MDK_{99}) of the cell populations. The graph plot shows one technical time-kill assay replicate of the first biological passaged replicate (for the Ag^+-P strain), see **Figure S1** for all other biological and technical replicates.

Next, the ability of ATCC 19606 to evolve adaptation characteristics to NAg, Ag+, and Nx was investigated. The bacterium was exposed to progressively increasing concentrations of each agent through sequential passaging (sub-culturing) every 24 h over 30-days. For this experiment, a 30-day timeframe was selected firstly due to time sensitivity and because previous long-term *in vitro* bacterial evolution studies (involving various antibacterial agents) have also utilised a 30-day sequential passaging methodology[202,203]. The prolonged exposures saw progressive shifts in the highest antimicrobial doses at which the bacterium could proliferate. On day one, *A. baumannii* was only able to grow at a maximum concentration of 0.25 and 0.5 µg/mL of NAg and Ag^+, respectively. At the conclusion of the exposure courses, the

bacterium could proliferate at 7 µg/mL of NAg (day 30), and 8 µg/mL of Ag^+ (day 28) (**Figure 4.1B**). For Nx, the bacterium was proliferating at an extremely high concentration of 520 µg/mL by day 30, from 2.5 µg/mL on day one (**Figure 4.1B**). To assess for the development of stable resistance traits, the MICs of each agent were tested against the sequentially passaged cultures. It was found that the MIC of NAg had increased to 4 – 5 µg/mL (4 – 5 x MIC of that observed for the wild-type (WT) strain) and to 1800 – 1900 µg/mL for Nx (360 – 380 x MIC of that of the WT), while the MIC of Ag^+ was unaffected, remaining like that of the WT strain at 2 µg/mL (**Figure 4.1C**, **Figure S1**). A resistance effect develops when a bacterial population is able to proliferate at an otherwise toxic concentration of an agent[5]. This effect is confirmed when there is a two-fold or higher increase in the MIC of an agent on an exposed bacterial strain[193]. As described in **Section 2.6.2**, there are no standardised CSLI-like MIC values for NAg (and Ag^+) due to their complex antibacterial activity and correlated physicochemical properties. Silver resistance development was defined by a two-fold or more increase in MIC relative to that of the baseline MIC values for the corresponding WT strain. Thus herein, it was concluded that *A. baumannii* ATCC 19606 had developed stable resistance to NAg, and as expected, to Nx, due to prolonged antibacterial exposure. It should also be noted that the sequentially passaged bacterial isolates were cultured in antimicrobial-free media (for three-days) prior to the MIC re-assessment. This was to exclude any cell population with transient adaptation traits[204]. *A. baumannii* is known to develop resistance to Nx through single point mutations in the *gyrA* gene, which was also detected in the present work following the Nx passaging experiment, as later described (see **Section 4.6.2**)[205]. Exceptionally high Nx MICs (> 1000 µg/mL), as observed in this study, have been previously reported in other Nx-resistant *A. baumannii* strains[206,207]. The inclusion of the Nx resistance study was not only to investigate the distinct adaptation responses of *A. baumannii* to the antibiotic, but also validate the sequential passaging experiment. As per current knowledge, this is the first reported evidence of (stable) NAg resistance evolution in any *A. baumannii* strain.

Earlier studies have reported (cationic) silver resistance in the bacterium[34-36,151]. Hosny *et al.* detected the presence of the Ag^+ efflux Sil system in two *A. baumannii* strains isolated from patient wounds that were treated with 1% silver sulfadiazine[34]. This well-established silver efflux mechanism is encoded by a nine-gene *sil* operon, which is

often found in mobile genetic elements, such as plasmids[33,65,154]. The *silE, silS, silR, silC, silF, silB, silA*, ORF105 (*silG*) and *silP* genes encode functional proteins in three transcriptional units (SilE, SilRS, and SilCFBAGP)[156,157]. The efflux mechanism responds to the presence of intracellular Ag^+, binding the ions to chaperone/s, then exporting the ions out of the cell *via* a membrane-bound P-type ATPase efflux[65,143,156,157]. Recalling the absence of Ag^+ resistance development in the present *A. baumannii* strain, it was confirmed that there was no *sil* genes present in the bacterium genome. The strains isolated by Hosny, *et al.* had likely acquired their *sil* genes through uptake of mobile genetic elements (hence acquiring exogenous genes)[34]. As discussed in **Chapter 2**, no endogenous presence of *sil* genes have been reported in the *A. baumannii* genome before[33].

Although no increase in the Ag^+ MIC was seen for the Ag^+-passaged strain, the bacterial growth that was observed at increasing Ag^+ doses during the passaging experiment (**Figure 4.1B**) indicated that some form of adaptation phenotype had developed, potentially associated with tolerance or persistence. In contrast to resistance, tolerance is the ability of a bacterial population to survive a lethal antimicrobial exposure for a longer time (with no MIC increase) due to a slower killing rate (conferred environmentally or through mutation), while persistence only affects a minute fraction of a clonal bacterial population[193,194]. The slower killing effect is characterised by an increase in an agents minimum duration for killing (MDK) the bacterial population; 99% of the population for a tolerance effect (MDK_{99}), and 99.99% of the population for a persistence effect ($MDK_{99.99}$)[193,194,198]. A time-kill assay was performed to determine if the Ag^+-passaged strain had developed tolerance or persistence to Ag^+. The killing kinetics of Ag^+ (1.5 x MIC dose) on the passaged strain saw an increase in the MDK_{99} (~ 135 – 165 min) when compared to that observed for the WT strain (~ 90 min), which signifies a tolerance trait (**Figure 4.1D**, **Figure S1**). Presumably, this is the first reported case of Ag^+ tolerance in *A. baumannii* in response to prolonged Ag^+ exposure. Tolerance to other heavy metals have been reported in *A. baumannii*, with one study highlighting a link between copper tolerance to upregulation of copper efflux genes, including both endogenous (*e.g. cueR*) and exogenous (*e.g. copRS*) genes[208].

No reduction in the growth rate of the (untreated) Ag^+-tolerant (Ag^{+T}) strain was observed, which exhibited a similar growth profile as the WT strain (**Figure 4.1D**).

This indicates that prolonged Ag^+ exposure did not induce a 'tolerance by slow-growth' effect, which is a characteristic feature often seen in antibiotic-tolerant strains as a means to passivate antibiotics that target actively-proliferating bacteria[193,209]. Studies have also described other antimicrobial tolerance mechanisms in bacteria, including changes in biofilm growth behaviour and cellular ROS-associated physiological changes[210,211]. As shown later, this study investigated these behaviours to gain clues on the mechanisms that could play a role in the Ag^+ tolerance trait.

Note that there was no cross-adaptation observed between NAg and Ag^+. The MIC of NAg for the Ag^+-tolerant (Ag^{+T}) strain, and vice versa, the MIC of Ag^+ for the NAg-resistant (NAg^R) strain, were comparable to their respective MICs for the WT strain (**Figure S3**). The adaptation to NAg and Ag^+ also did not provide cross-protection to Nx. The MIC of Nx for the NAg^R and Ag^{+T} strains were akin to that seen with the WT strain (**Figure S3**). These findings are not surprising considering the diverse antimicrobial mechanisms of NAg, Ag^+, and the model antibiotic.

4.6.2 Genetic mutations and physiological changes in silver-adapted *A. baumannii* ATCC 19606

Comparative genomic analysis was carried out to detect potential gene mutations in the silver-adapted strains. Various unique silver-induced single nucleotide polymorphisms (SNPs) were identified in the NAg^R and Ag^{+T} strains (**Table 4.1**), which excludes random 'background' mutations. The latter are SNPs that were identified in the cell-only passaged cultures (passaged with no antimicrobial agent), which most likely developed due to the effect of repeated sub-culturing (**Table S1**)[29]. The detected silver-induced SNPs were stable, given that the adapted strains were cultured in antimicrobial-free media for several days prior to the genome sequencing. This suggests that ATCC 19606 had evolved physiological changes that could contribute to defence against silver toxicity. Mutations were indeed detected in *gyrA* in the Nx^R strain, further validating the sequential passaging experiment. Two point mutations (associated with change in the protein amino acid sequence) were seen in the gene (**Table 4.1**); one nucleotide substitutional mutation (f = 100%, n = 6) resulting in a Ser81Leu change (serine at position 81 to leucine), and another substitutional mutation (f = 50%, n = 6) associated with an Arg70Gly change. Studies have shown that point mutations in *gyrA* lead to conformational changes in the GyrA protein, with

the most frequently reported amino acid change being Ser83Leu, blocking Nx from accessing its active site[205,212-214]. Several more SNPs were detected in other genes in the Nx^R strain (**Table S2**), which are most likely unrelated to the Nx resistance trait.

Table 4.1 Gene mutations detected in the Nx-resistant (Nx^R, only mutations detected in the target gene *gyrA* are shown), NAg-resistant (NAg^R), and Ag^+-tolerant (Ag^{+T}) *A. baumannii* ATCC 19606 strains.

Strain	Mutation	Genome pos.[1]	AA change	Gene	Locus tag	*f* (%)[2]	Protein product
Nx^R	SUB (G > A)	3108662	Ser81Leu	*gyrA*	FQU82_02986	100	DNA gyrase subunit A
	SUB (T > C)	3108695	Arg70Gly	*gyrA*	FQU82_02986	50 [3]	DNA gyrase subunit A
NAg^R	SUB (G > A)	659811	Ser196Phe	*rcsC* [4]	FQU82_00629	16.7 [3]	Sensor histidine kinase RcsC
	DEL (TG > T)	2146107	Ala129fs [5]	*smf1-2*	FQU82_02066	33.3 [6]	Major fimbrial subunit SMF1
	SUB (G > A)	2669300	Ala20Val	*csuB*	FQU82_02552	33.3 [6]	Csu pili biogenesis protein CsuB
	INS (C > CATA)	2669301	Tyr19dup [7]	*csuB*	FQU82_02552	16.7 [3]	Csu pili biogenesis protein CsuB
Ag^{+T}	DEL (GA > G)	133861	Lys4fs [5]	*atr2*	FQU82_00141	100	Acyltransferase
	DEL (GA > G)	135040	Met150fs [5]	*gtr6*	FQU82_00142	33.3 [8]	Glycosyltransferase
	SUB (G > A)	2753686	Gly352Arg	*adeF*	FQU82_02642	16.7 [6]	Multidrug efflux RND transporter subunit AdeF
	SUB (G > A)	3407963	Arg58Cys	*trpB*	FQU82_03235	100	Tryptophan synthase beta chain subunit
	SUB (C > T)	3878684	Gly39Arg	*gshA*	FQU82_03694	100	Glutamate-cysteine ligase
	DEL (TG > T)	3927318	Val10fs [5]	*iclR*	FQU82_03739	16.7 [3]	IclR family transcriptional regulator

[1] Position of gene mutation in the ATCC 19606 genome. [2] *f* = frequency of mutation (%) in isolated strain. [3] Detected in only the first biological passage replicate of respective strain. [4] Mutation to gene also detected in Nx^R strain (see **Table S2**). [5] fs = frameshift. [6] Detected in

only the second biological passage replicate of respective strain. [7] dup = duplication. [8] Detected in each biological passage replicate of respective strain. Note: Refer to **Table S2** for the complete list of mutations detected in the Nx^R strain. Random 'background' gene mutations that were detected in the cell-only passaged control (see **Table S1**) have been excluded.

As shown in **Table 4.1**, several SNPs were detected in the NAg^R strain in genes related to biofilm formation. A mutation was detected in the gene *rcsC* (substitution – *f* = 16.7%, n = 6), which encodes the sensor histidine kinase RcsC. This protein forms part of the Rcs pathway, which regulates the synthesis of capsular polysaccharide (CPS), a unique cell envelope component highly conserved in *A. baumannii*. Studies have supported a role for CPS involvement in biofilm formation, that is, in maintaining cell membrane integrity during bacterial attachment to surfaces[215,216]. Next, a mutation was detected in the gene *smf1-2* (deletion – *f* = 33.3%, n = 6), which encodes the major fimbrial subunit SMF1 (**Table 4.1**). This peritrichous hair-like polymeric protein structure is used by bacteria to attach to surfaces and help initiate biofilm formation[217]. Finally, mutations (substitution – *f* = 33.3%, n= 6; insertion – *f* = 16.7%, n = 6) were detected in the gene *csuB* (**Table 4.1**). This gene encodes the Csu pili protein subunit CsuB and is part of a six-gene operon *csuA/BABCDE*, which collectively code for the Csu Type 1 chaperone-usher pili[16]. Pili, like fimbriae, are also hair-like protein structures, which project from the bacterial envelope. Pili are known to aid in cell-to-cell DNA transfer during bacterial conjugation, but reports have indicated that bacteria also use these structures to attach to surfaces for biofilm growth[16]. The Csu pili is, in fact, one of the most conserved biofilm-associated protein structures in globally disseminated *A. baumannii* clones[218,219].

Mutations were also detected in the genome of the Ag^{+T} strain (**Table 4.1**), and indeed, at least one of these SNPs is in a gene that has been previously linked to biofilm formation. A mutation was detected in the gene *gshA* (substitution – *f* = 100%, n = 6), which encodes the enzyme glutamate-cysteine ligase (GCL) that is involved in the biosynthesis of the antioxidant glutathione (GSH)[220]. GSH is essential for maintaining redox balance in Gram-negative bacteria, scavenging for excess ROS to control oxidative stress, and also reportedly plays a key role in certain transition-metal homeostasis, namely *via* metal ion binding and periplasmic sequestration, such as with cadmium[220,221]. Interestingly, studies have recognised a link between *gshA* function

and biofilm formation. Wongsaroj, *et al.* for instance, reported a higher extent of biofilm formation in a *gshA*-knockout mutant, relative to the WT strain, in *P. aeruginosa*[222]. The study also observed reduced motility with the mutant. The *gshA* mutation detected herein could also relate to the known oxidative stress-related toxicity of Ag^{+}[223,224]. Therefore, the mutation is hypothesised to contribute to the Ag^{+} tolerance trait, of which the phenotypic features (biofilm growth and cellular ROS response) were later investigated in this Chapter. Notably, mutations in other genes in the Ag^{+T} strain (**Table 4.1**; f = 16.7 – 100%, n = 6) were detected, but with limited correlations to Ag^{+} toxicity defence. For example, a mutation was detected in the gene *adeF* (substitution – f = 16.7%, n = 6), which encodes the protein AdeF, a subunit of the RND multi-drug efflux system AdeFGH[225]. This efflux system is reported to contribute to ß-lactam (antibiotic) resistance, as well as to other biocides, such as benzalkonium, in *E. coli*[225]. Nevertheless, there is no evidence, at this stage, to suggest the role of AdeF in heavy metal efflux.

Considering the potential link between the detected SNPs to biofilm formation phenotypes, it was hypothesised that there could be changes in the biofilm growth behaviour of the silver-adapted strains, possibly as a stable physiological feature that developed in response to the prolonged exposure events. Biofilms are surface-attached microbial communities. Bacterial populations in biofilms are protected by an adhesive matrix structure known as EPS, rendering the colony resilient to many external stressors, including antimicrobial exposure[118,119,226]. The biofilm growth behaviour of the NAg^{R} and Ag^{+T} strains in the absence of silver were assessed. The latter was to see if the (hypothesised) physiological changes were stable, and therefore still manifested even without silver. Increased extent of biofilm formation have been observed in bacteria in response to external stress, including silver toxicity[155,182,198], Such silver-induced changes in growth activity have yet to be reported in *A. baumannii*[33]. For the biofilm-formation study, the silver-adapted isolates which carry the (earlier described) specific mutations in biofilm-associated genes were studied. For the NAg^{R} strain, an isolate with mutations in the highly conserved biofilm-associated genes *rcsC* and *csuB* (insertional mutation for the latter gene) was selected (**Table 4.1**; GenBank accession number JAPYLV000000000), whereas for the Ag^{+T} strain, an isolate with a mutation in *gshA* was selected (**Table 4.1**; GenBank accession number JAPYLT000000000), considering the gene's more established role in biofilm formation.

As shown in **Figure 4.2**, it was found that the long-term silver exposures had altered the biofilm-forming ability of the bacterium. Under the experimental conditions tested, the NAg^R strain formed ~ 15% more biofilm biomass (487 $\mu m^2/\mu m^3$ mean total (live/dead) biomass) when compared to the WT strain (422 $\mu m^2/\mu m^3$ mean total biomass, $P < 0.05$). The fluorescent microscopy images (**Figure 4.2A**, red arrows) highlight the greater extent of biofilm growth. The observations suggest that the evolved NAg-induced mutations – seen in the CPS synthesis regulatory pathway gene *rcsC* and the Csu pili subunit gene *csuB* – could be associated with increased biofilm growth in the strain. These mutations in the capsule envelope (CPS) synthesis and external motility organelle (pili) are hypothesised to enhance the surface attaching ability of the bacterium (as described earlier) and promote further colonisation. The greater biofilm-forming ability of the NAg^R strain suggests it would require a higher NAg dosage to control when compared to the WT strain, thereby acting as a resistance trait. Earlier studies have also correlated NAg resistance to cell envelope (motility) organelles. Panáček, *et al.* reported increased production of flagellin (a major protein component of flagella) in *E. coli*, with the epigenetic/non-mutational changes associated with aggregation of NAg, which was thought to hinder nanoparticle activity[30]. In another *E. coli* study, Stabryla, *et al.* suggested a link between improved flagella-based motility and the development of NAg resistance. A stable resistance phenotype was only seen in the hyper-motile strain following prolonged exposure, while resistance was absent in the non-motile strain[28]. It should be noted that at this stage, the potential role of the lesser studied *A. baumannii* fimbrial subunit gene *smf1-2* in the altered biofilm-forming physiology of the NAg^R strain is not excluded. Further molecular-focussed investigations, as later described in **Chapter 5**, were performed to better understand the role/s of this gene (and others) in the NAg resistance trait.

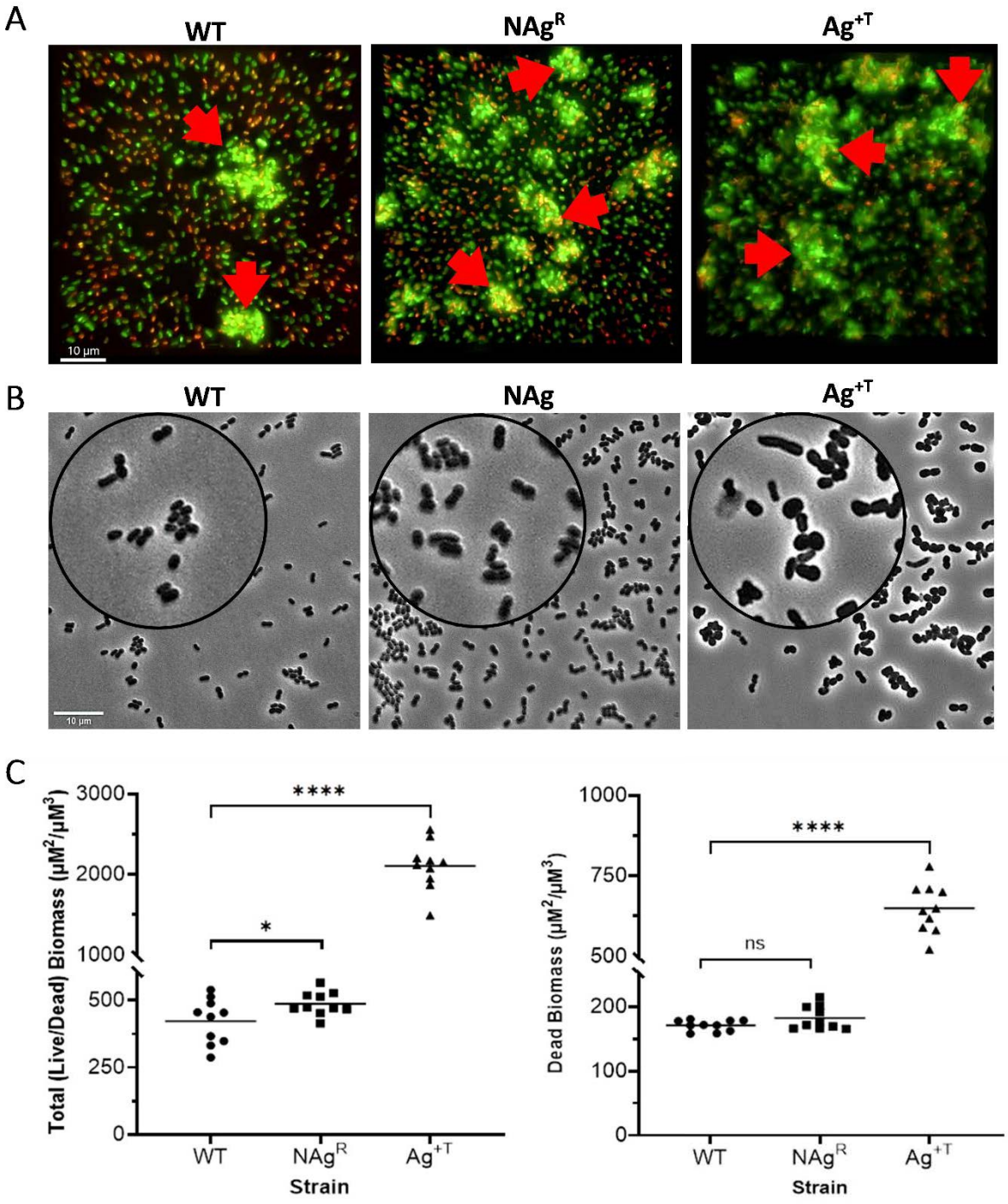

Figure 4.2 Evolved physiological changes in NAg^{R} and Ag^{+T} *A. baumannii* ATCC 19606 strains. (**A**) Fluorescent microscopy images of live (green) and dead (red) biofilm biomass from the WT, NAg^{R}, and Ag^{+T} strains. Red arrows highlight biofilm biomasses. Images are sectional Z-stacks compressed together into single plane 3D slices (scale bar = 10 µm). (**B**) Phase contrast images of planktonic WT, NAg^{R}, and Ag^{+T} *A. baumannii* cells (scale bar = 10 µm). Magnified inset images provide closer details of cell morphology. (**C**) Analysis of total biomass (live and dead, left plot) and

dead biomass (right plot) biomass ($\mu m^2/\mu m^3$) from the fluorescent microscopy images for each strain; ten images were captured for each biological replicate (30 images total for three biological replicates per strain). Each symbol (circle, square, triangle) represents the average of three analysed images for the respective strain, with the horizontal bars representing the average of all 30 analysed images per strain. (*****) indicates a statistically significant increase in NAg^R and Ag^{+T} biofilm biomass, relative to the WT (***** = $P < 0.05$, ******** = $P < 0.0001$).

Biofilm growth studies performed on the Ag^{+T} strain yielded interesting results. Under the experimental conditions, the strain formed ~ 5-fold higher biofilm biomass (2107 $\mu m^2/\mu m^3$ mean total biomass) relative to the WT strain ($P < 0.0001$) (**Figure 4.2C**). The observations suggest a potential link between the *gshA* mutation in the tolerant strain to its increased biofilm growth. The Ag^+-induced mutation in the GSH synthesis gene *gshA* is thought to decrease bacterial motility. The latter phenotype, as earlier mentioned, has been reported in a (*P. aeruginosa*) *gshA*-knockout mutant (Δ*gshA*), with the mutant also forming more biofilm than the WT strain. However, the exact link between motility and the changes in biofilm growth behaviour is still unclear[222]. Herein observed, the greater biofilm-forming ability of the Ag^{+T} strain may require longer time to control when compared to the WT strain, and hence could correspond to the tolerance effect.

Further examination revealed notable morphological changes in the Ag^{+T} strain, not seen with the NAg^R strain (**Figure 4.2B**). In comparison to the ~ 1 μm coccobacillus (length) of the WT strain, many Ag^{+T} cells were engorged with irregular shapes, with some exhibiting an elongation of more than 2-fold the length of the WT cells. Research inquiries have reported morphological changes in bacteria in response to antibacterial treatment[77,227,228]. One study described the shortening and lengthening of *E. coli* cells following prolonged Ag^+ exposure[229]. This oscillation in morphology appeared to associate with a suppression in metabolic activity (similar to tolerant/persistent behaviour), which seemed to protect the bacterium from Ag^+ toxicity[229]. In *A. baumannii*, a number of antibiotic-adapted strains have also been reported to undergo morphological changes[228]. It is therefore reasonable to suggest that the morphological changes seen with the Ag^{+T} strain is a contributing factor in the bacterium tolerance response to the ions.

Taken together, the SNP evidence indicates that ATCC 19606 evolved the gene mutations in response to prolonged NAg (and Ag^{+}) exposure. A number of these mutations appear to correlate to the increased biofilm-forming ability seen with both silver-adapted strains. The stable physiological changes most likely contribute to the bacterium adaptation behaviour, that is, the 'harder-to-kill' resistance trait in the case of NAg, and the 'slower-to-kill' tolerance trait against Ag^{+}. The latter adaptation effect also seems to involve morphological changes in the bacterium. Finally, it is noteworthy to mention that these SNPs had been validated through re-sequencing of the PCR-amplified genes of interest. Next, the defence responses of the silver-adapted strains, which manifest in the presence of silver, were studied.

4.6.3 Cellular ROS-related defence in silver-adapted *A. baumannii* ATCC 19606

The mutations that developed in silver-adapted ATCC 19606 could play a role in the defence mechanisms against NAg and Ag^{+}. Herein, the defence traits were studied in the presence of silver. This was intended to see how the NAg^{R} and Ag^{+T} strains protected themselves from oxidative stress, one of the major toxicity paradigms of silver. For this study, the same silver-adapted isolates (used for the biofilm work) were examined, to gain insights on the potential roles of the same mutations of interest in oxidative stress defence. To first confirm the ROS-associated antibacterial activity of NAg on the bacterium, the WT strain was exposed to a sub-MIC dose of the nanoparticle (0.5 x MIC at 0.5 µg/mL, 1 h exposure), and indeed, higher intracellular ROS presence was detected (presented as corrected total cell fluorescence (CTCF), $P < 0.001$) relative to the untreated (cell-only) WT control (**Figure 4.3C**). Apart from the earlier mentioned cell envelope targeting route, there are alternative pathways that can also promote silver-induced ROS generation in bacteria. Studies have shown that both NAg particulates and leached soluble silver can stimulate cellular ROS generation[98,133,224]. Ag^{+}, for instance, can attack iron-sulfur clusters that are present in many critical proteins, releasing Fenton-active ferrous (Fe^{2+}) ions, which can then react with cellular H_2O_2 to generate highly reactive hydroxyl radicals ($OH^{\bullet}$)[29,98]. The ROS-generating mechanism/s of solid NAg particulates remains under debate, however evidence indicates they generate comparable levels of ROS to that of soluble Ag^{+} leachate[98,230]. However, further work is needed to elucidate the mechanism of ROS generation by NAg alone, which is rather difficult considering nanoparticles

undergo continuous oxidative dissolution and cannot be easily separated from Ag^{+} leachate[98,187,230].

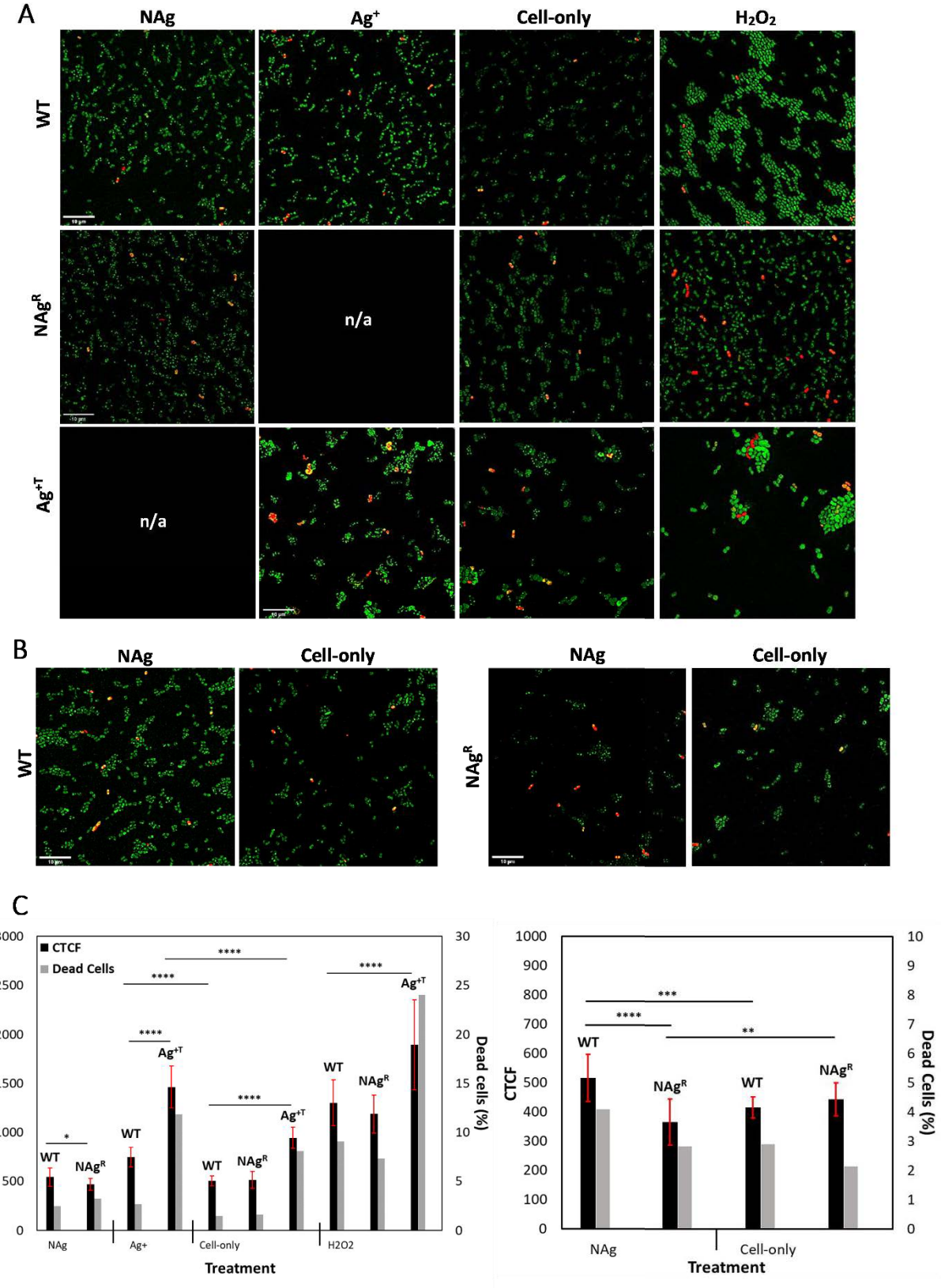

Figure 4.3 Cellular ROS-related defence in NAg^R and Ag^{+T} *A. baumannii* ATCC 19606 strains. (**A**) Fluorescent microscopy images of intracellular ROS (green) and dead cells (red) detected in the WT, NAg^R, and Ag^{+T} strains following exposures to NAg and Ag^+ (30 min). Also shown are the cell-only (untreated) and H_2O_2-treated samples (n/a = not applicable). Scale bar = 10 µM. (**B**) Detection of cellular ROS (and dead cells) in the WT and NAg^R strains after 1 h NAg exposure. (**C**) Quantitative analysis of cellular ROS presence (as corrected total cell fluorescence, CTCF) and dead cells in the WT, NAg^R, and Ag^{+T} strains following 30 min of NAg, Ag^+, and H_2O_2 exposures (left). The quantitative ROS/dead cells analysis following 1 h NAg exposure (for WT and NAg^R strains) are also shown (right). For each strain, each of the exposure experiments were performed in three biological replicates, with five-to-six images captured per replicate and 20 individual cells analysed per image. Red error bars represent standard deviation. (*) indicates statistical significance for differences in cellular ROS level detected in the respective culture samples (* = $P < 0.05$, ** = $P < 0.01$, *** = $P < 0.001$, **** = $P < 0.0001$).

When exposed to a similar NAg dose (0.5 µg/mL), there was less cellular ROS detected in the NAg^R strain relative to the WT. The statistically significant lower ROS level in the resistant strain was evident within just 30 min of NAg exposure ($P < 0.05$) (**Figure 4.3C**), with the difference becoming even more significant after 1 h of exposure ($P < 0.0001$) (**Figure 4.3C**). The findings are indicative of a NAg-induced ROS-associated defence mechanism in the resistant strain, which may relate to the detected mutation in the CPS synthesis-related *rcsC* gene (**Table 4.1**). Increased CPS expression in *A. baumannii* has been linked to protection from antimicrobial targeting, including antibiotics and oxygen radicals[231,232]. Studies have in fact reported increased expression of the *cps* gene (encodes CPS synthesis) as a result of *rcsC* mutation, in *E. coli*[233,234]. It is therefore reasonable to suggest that the NAg-induced *rcsC* mutation detected in this study could correlate to the observed lower cellular ROS presence in the NAg^R strain. It is hypothesised that this links to a more compact occurrence of CPS structures on the NAg^R cell envelope, hence limiting penetration of the toxic NAg particulates and leached soluble silver into the cell. Exposure of the NAg^R strain to ROS-generating H_2O_2 (30 min) also appeared to result in less cellular ROS in the resistant strain when compared to the WT, although this was not statistically significant (**Figure 4.3C**).

The cellular ROS studies with the Ag^{+T} strain revealed entirely different results. Firstly, the ROS-associated antibacterial activity of Ag^{+} was indeed evident with detection of a higher cellular ROS presence in the Ag^{+}-exposed WT strain (0.5 x MIC dose, 1 μg/mL, 30 min exposure, $P < 0.0001$) relative to the untreated WT control (**Figure 4.3C**). With regard to the Ag^{+T} strain, earlier studies have reported on the upregulation of defence mechanisms in tolerant bacteria in response to (antibiotic-induced) cellular oxidative stress[210]. It was therefore hypothesised that the Ag^{+T} strain would also exhibit cellular ROS-related defence mechanism/s, possibly associated with the evolved mutation in the antioxidant GSH synthesis gene *gshA*. However, as shown in **Figure 4.3C**, exposure of Ag^{+T} *A. baumannii* to Ag^{+} (1 μg/mL) resulted in a higher level of detected cellular ROS relative to the WT strain after just 30 min of exposure ($P < 0.0001$), which contrasts that seen with the NAg^{R} strain. This unexpected observation could perhaps relate to enhancement in respiratory activity in the tolerant strain, a known phenomenon in a number of microbial tolerance cases[235,236]. A study by McBee, *et al.*, for instance, reported a significantly higher cellular presence of superoxide radical ($O_2^{\bullet-}$) in an antibiotic-tolerant *Mycobacterium* spp., which appeared to result from enhanced respiration (as ROS is a natural by-product of aerobic respiration), independent of antibiotic-induced oxidative stress[236,237]. Indeed, a higher level of cellular ROS was detected in the untreated Ag^{+T} strain when compared to the WT ($P < 0.0001$) (**Figure 4.3C**), which supports the hypothesis that heightened respiratory activity has occurred, independent of the silver-induced oxidative stress. It is still not clear at this stage, however, if the predicted increase in respiratory activity in the Ag^{+T} population correlates to any of the Ag^{+}-induced SNPs (**Table 4.1**), as no studies have yet reported any link between this phenotype and any specific gene mutations. Increased respiratory activity has been indicated to occur stochastically in tolerant cells, with this phenotype thought to assist the population in resuming normal growth upon removal of antimicrobial pressure[235]. Higher cellular ROS presence was also seen in the Ag^{+T} strain following H_2O_2 treatment (30 min), relative to the WT strain ($P < 0.0001$) (**Figure 4.3C**).

In summary, it is evident that the NAg^{R} strain developed a defence mechanism against nanoparticle-induced cellular oxidative stress. The Ag^{+T} strain, on the other hand, exhibited a different cellular ROS-related response, which offers insights into the tolerant adaptation features of the bacterium. The tolerant strain appears to have

physiologically transformed, displaying an apparent 'over-active' respiration phenotype – a recognised characteristic of tolerant populations[235].

4.7 Conclusions

For the first reported time, the Gram-negative opportunistic bacterial pathogen *A. baumannii* ATCC 19606 exhibited the ability to establish a stable resistance phenotype to silver nanoparticles (NAg), while notably, also developing tolerance to cationic silver (Ag^{+}). The adaptation mechanisms were indicated to associate with stable physiological changes to protect the bacterium from silver toxicity. The NAg-resistant (NAg^{R}) strain evolved mutations in genes that encode protein subunits of cell envelope organelles that mediate cell attachment on surfaces, as well as a mutation in a cell envelope capsular polysaccharide (CPS) synthesis-related gene. These mutations are suggested to correlate with the observed increase in biofilm growth with the resistant strain and play a role in the suppression of oxidative stress (seen with the resistant strain). The 'slower-to-kill' Ag^{+}-tolerant (Ag^{+T}) strain also exhibited an enhancement in biofilm formation, but on the other hand, also appeared to develop known tolerant features, including increased respiratory activity and changes in cell morphology. At this stage, however, it remains unclear as to how these latter features are linked to the detected mutations in the Ag^{+T} strain. Note that the evolutionary adaptation studies were validated by the confirmed development of resistance to the model antibiotic nalidixic acid (Nx), with detection of SNPs in the target gene *gyrA* (reported involvement in Nx resistance). In closing, the findings highlight the risks of prolonged nanoparticle use, presenting the need to overcome bacterial adaptation to ensure the successful long-term use of this important alternative antimicrobial agent. Further molecular work (**Chapter 5** and **Chapter 6**) was performed to reveal other physiological changes and defence responses to silver toxicity, including any epigenetic (non-mutational) mechanisms. The upcoming work was also intended to help clarify the differences in the adaptation responses of *A. baumannii* ATCC 19606 to the nanoparticulate and ionic forms of silver, providing further insights into the roles of the gene mutations detected in the present study, and to identify any compensatory mutations for fitness effects.

4.8 Chapter conclusion

The identification of novel adaptation responses to NAg and Ag^+ in *A. baumannii* ATCC 19606 following prolonged exposure to the respective silver agents, complemented by unique genetic mutations and phenotypic changes, which raised several important inquiries. Although potential correlations were established between the mutated genes and the observed physiological alterations, particularly in biofilm formation and silver-induced oxidative stress responses, the exact genetic mechanisms were inconclusive. Therefore, the remainder of this study endeavoured to explore and compare the transcriptomic profiles of the evolved *A. baumannii* ATCC 19606 strains with that of the WT strain through RNA sequencing (RNA-Seq) analysis. To achieve this, the silver-adapted strains were subjected to varying doses of their respective agents, and the degree of differential gene expression between the adapted strains and the WT bacterium were compared. The objective was to identify upregulated genes and encoded mechanisms which potentially enhance the defence capabilities of the evolved strains against NAg and Ag^+, respectively.

Importantly, the transcriptomic profiles of each strain will also be assessed and compared to the WT bacterium when in optimal conditions, or without silver pressure. This will reveal how the evolved bacteria were stably and physiologically altered because of long-term exposure to their respective agents. It will also help showcase what modified genes and potentially encoded defence mechanisms are now inherent to silver-adapted ATCC 19606. The knowledge generated from this investigation will not only shed light on the consequences of antimicrobial silver overuse but also provide insights into the evolutionary defence mechanisms that a priority bacterial pathogen can develop so that they may be overcome in the future. **Chapter 5** of this thesis presents the first known transcriptomic study of *A. baumannii* ATCC 19606 (WT and NAg^R strains) following exposure to NAg and provides compelling evidence into the potentially relevant defence mechanisms responsible for conferring NAg resistance in this bacterium.

4.9 Supplementary information

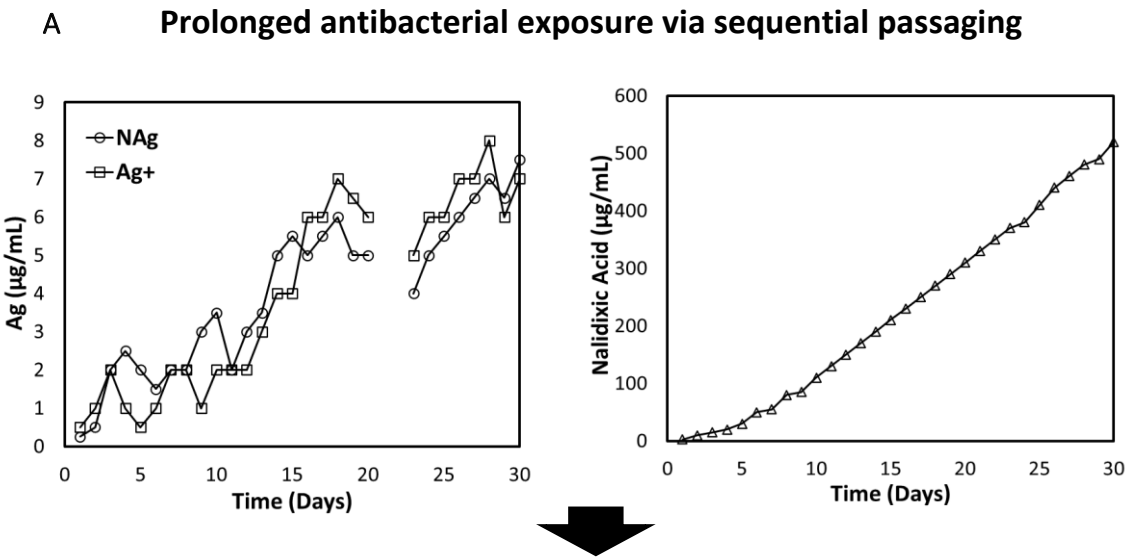

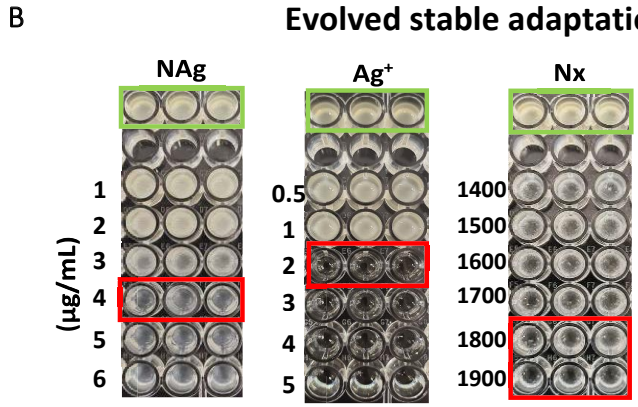

Antibacterial agent	MIC (µg/mL)
NAg	4
Ag^+	2
Nx	1800-1900

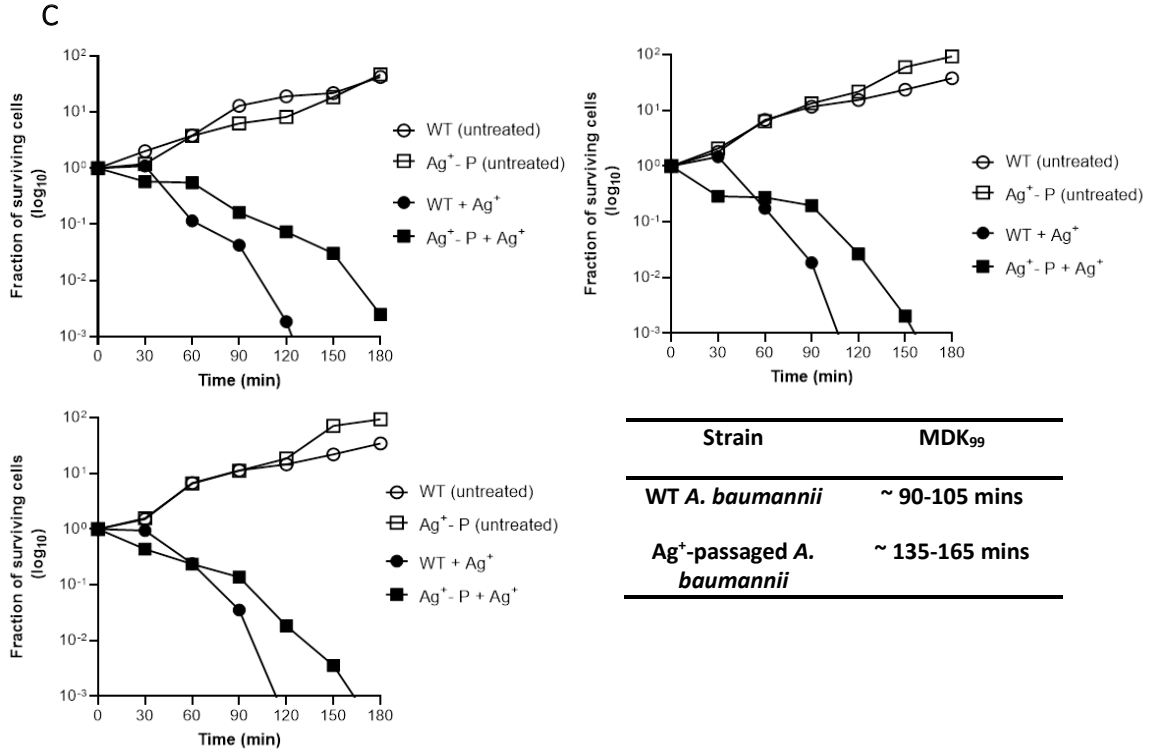

Strain	MDK_{99}
WT *A. baumannii*	~ 90-105 mins
Ag^+-passaged *A. baumannii*	~ 135-165 mins

Figure S1 Evolution of adaptation phenotypes to NAg, Ag^+, and Nx in *A. baumannii.* (**A**) Second biological replicate of sequentially passaged *A. baumannii* in the presence of progressively increasing NAg, Ag^+, and Nx concentrations over 30 days. (**B**) NAg, Ag^+, and Nx minimum inhibitory concentration (MIC) assessments for the second biological replicate of sequentially passaged *A. baumannii* (green outline = cell-only control; red outline = MIC point). (**C**) Killing kinetics of WT and Ag^+-passaged (Ag^+-P) *A. baumannii* when exposed to 1.5 x Ag^+ MIC dosage, for determination of the minimum duration of killing 99% (MDK_{99}) of the cell populations. The plots show the second technical replicate of the first biological passaged replicate (for the Ag^+-P strain) (top left), and the first technical replicate (lower left) and second technical replicate (right) of the second biological passaged replicate (for the Ag^+-P strain).

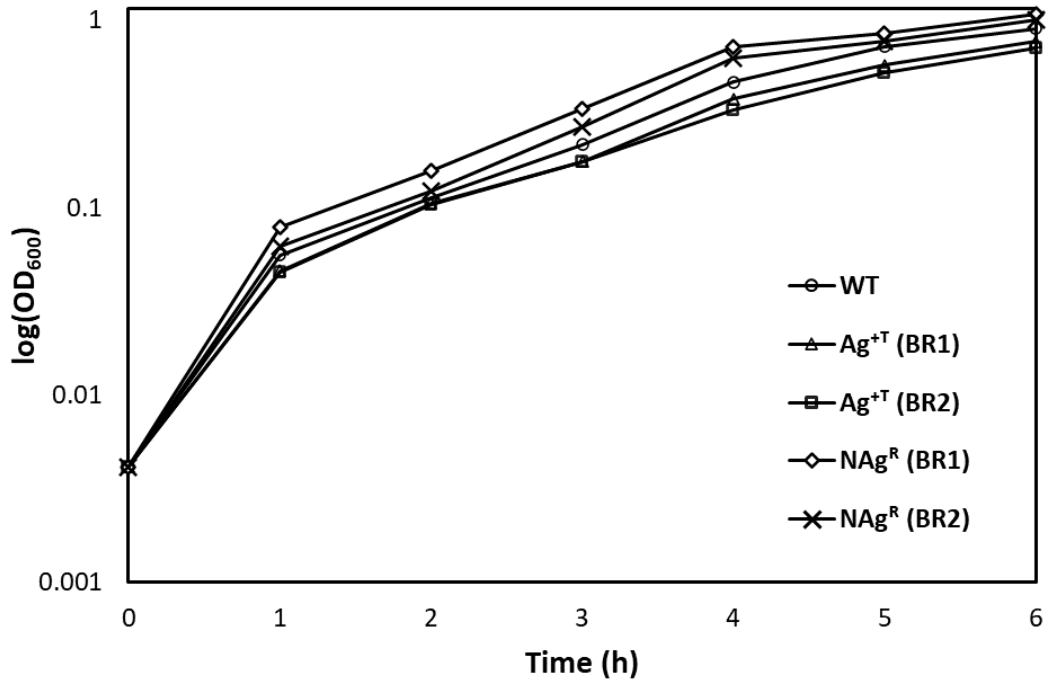

Figure S2 Comparative growth rates of WT, NAg-resistant (NAg^R), and Ag^+-tolerant (Ag^{+T}) *A. baumannii.* Shown are the 6 h growth profiles of the NAg^R and Ag^{+T} strains from biological replicate 1 and 2 (BR1 and BR2) of the passage. Note the initial OD_{600} (optical density at 600 nm) of 0.05 for each culture system.

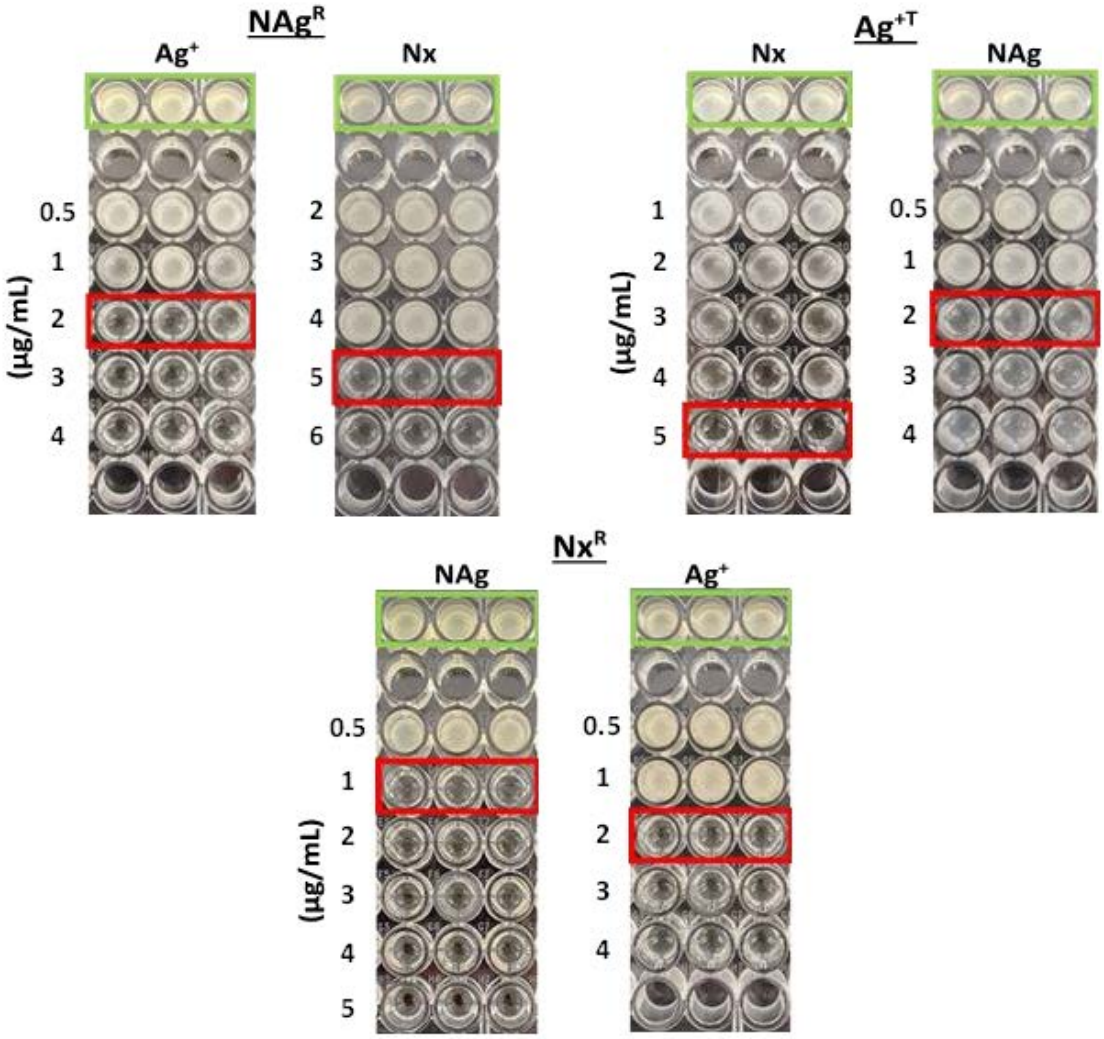

Strain	Antibacterial agent		
	NAg	Ag^{+}	Nx
NAg^{R}	-	S	S
Ag^{+T}	S	-	S
Nx^{R}	S	S	-

Figure S3 Comparative cross-adaptation study between the NAg-resistant (NAg^{R}), Ag^{+}-tolerant (Ag^{+T}), and Nx-resistant (Nx^{R}) strains. Each adapted strain was tested for an increase in MIC between to their respective non-passaged agent to determine if a cross-adaptation effect had developed during the sequential passage experiment. Green outline = cell-only control; red outline = MIC point. The table highlights the susceptibility profile (sensitive = S, resistant = R) of each strain following MIC testing with the respective agents. Each biological passage replicate was tested in this cross-adaptation study and produced identical results. Only the results of the one biological replicate are shown.

Table S1 'Background' gene mutations detected in the cell-only passaged control culture (containing no antimicrobial).

Mutation	Genome pos.[1]	AA change	Gene	Locus tag	Protein product
SNP (G > A)	787051	Gly195Ser	*rstA*	FQU82_00751	Transcriptional regulator protein RstA
Del (AT > A)	1438692	Phe444fs [2]	*actP*	FQU82_01385	Copper-transporting P-type ATPase
SNP (T > C)	1879011	Gln222Arg	*hrtE*	FQU82_01809	Outer membrane usher protein HtrE
Ins (C > CATTAAAAAT)	2090006	Asn90dup [3]	*yjiE*	FQU82_02014	HTH-type transcriptional regulator YjiE
SNP (G > A)	2156407	Val67Ile	*sasA*	82_02072	Adaptive-response sensory-kinase SasA
SNP (G > A)	2665349	Ser58Leu	*csuE*	82_02549	Csu pili tip adhesin CsuE
SNP (C > A)	2980241	Trp273Leu	*gltR*	82_02866	HTH-type transcriptional regulator GltR
SNP (G > A)	3166695	Ala320Val	*blp1*	82_03028	Blp1

[1] Position of gene mutation in the *A. baumannii* genome. [2] fs = frameshift. [3] dup = duplication

Table S2 The complete list of gene mutations detected in the Nx^R strain.

Mutation	Genome pos. [1]	AA change	Gene	Locus tag	Protein product
SUB (C >T)	620945	Ala165Thr	*macA*	FQU82_05595	Macrolide export protein MacA
SUB (A > G)	658605	Leu598Pro	*rcsC* [2]	FQU82_00629	Sensor histidine kinase RcsC
SUB (A > G)	659115	Ile428Thr	*rcsC* [2]	FQU82_00629	Sensor histidine kinase RcsC
SUB (C > T)	708108	Cys275Tyr	*gigA*	FQU82_00676	RsbU family protein phosphatase GigA
SUB (C > T)	708291	Leu214Pro	*gigA*	FQU82_00676	RsbU family protein phosphatase GigA
SUB (A > G)	718107	-	INTERGENIC [3]	-	-
SUB (C > T)	1114223	Ala9Val	-	FQU82_01057	Hypothetical Protein [4]
SUB (C > T)	1118624	-	INTERGENIC [3]	-	-
SUB (A > G)	1338851	Ala330Ala	nk [5]	FQU82_01287	ATP-binding protein
SUB (C > T)	1497310	Arg1782Cys	nk [5]	FQU82_01459	GNAT family N-acetyltransferase
INS (T > TG)	1526729	Leu104fs	*yigZ*	FQU82_01486	IMPACT family member YigZ
SUB (G > A)	1531871	His815Tyr	*mutS*	FQU82_01493	DNA mismatch repair protein MutS
SUB (C > T)	1726410	Asp352Asp	nk [5]	FQU82_01662	DCAP-like protein
INS (G > GC)	1776690	His256fs	*mdcE*	FQU82_01714	Biotin-independent malonate decarboxylase
SUB (C > T)	1889732	Met48Ile	-	FQU82_01822	Hypotheical Protein [4]
SUB (C > T)	1974783	Ala134Ala	nk [5]	FQU82_01906	Glutathione S-transferase
SUB (A > G)	2046714	Leu339Leu	*metZ*	FQU82_01973	O-succinylhomoserine sulfhydrylase
SUB (C > T)	2153492	Val204Met	*acrB*	FQU82_02069	Multidrug efflux pump subunit AcrB
SUB (C > A)	2154730	Gly197Cys	*mexA*	FQU82_02070	Multidrug resistance protein MexA
DEL (GA > A)	2156077	Lys217fs	*srrA*	FQU82_02071	Transcriptional regulatory protein SrrA
DEL (GA > A)	2360141	Lys515fs	*cydA*	FQU82_02258	Cytochrome bd upiquinol oxidase subunit 1
INS (A > AC)	2384649	Ile228fs	nk [5]	FQU82_02286	EAL domain-containing protein
DEL (TA > T)	2517316	-	INTERGENIC [3]	-	-
INS (C > CA)	2572117	Ala484fs	*kdpD*	FQU82_02458	Sensor protein KdpD
SUB (G > A)	2622129	Gly110Arg		FQU82_02505	Ribosomal protein L11 methyltransferase
SUB (T > C)	2744324	-	INTERGENIC [3]	-	-
DEL (CA > C)	2990495	-	INTERGENIC [3]	-	-
SUB (T > C)	3005539	Tyr294Tyr		FQU82_02886	Nitronate monooxygenase
SUB (T > C)	3017346	Leu302Leu	*uvrB*	FQU82_02897	UvrABC system protein B
DEL (CA > C)	3121018	Lys146fs	nk [5]	FQU82_02998	Tim44 domain-containing protein
SUB (G > A)	3191294	Ala667Thr	*carB*	FQU82_03583	Carbamoyl-phosphate synthase large chain
INS (A > AG)	3363303	-	INTERGENIC [3]	-	-
INS (G > GA)	3659282	-	INTERGENIC [3]	-	-
SUB (G > A)	3666751	-	INTERGENIC [3]	-	-
SUB (T > G)	3751924	Ser183Arg	*rhaS*	FQU82_03583	HTH-type transcriptional activator RhaS

[1] Position of gene in *A. baumannii* genome. [2] Mutation to gene(s) also detected in NAg^R strain. [3] Mutation occurred in the intergenic region/s of genome (no open-reading frame present). [4] No putative function allocated for gene/protein. [5] nk = gene name not known. Note: Mutations to *gyrA* gene (**Table 4.1**) and random 'background' mutations (**Table S1**) have been excluded.

Chapter 5: Toxicological and Defence Responses and Physiological change to NAg

5.1 Chapter summary

Despite the proven antimicrobial efficacy of NAg, there has been mounting evidence showcasing the evolution of NAg resistance in various bacterial species. However, as discussed in **Chapter 2**, there have been no studies indicating the potential emergence of NAg resistance in *A. baumannii*. The findings outlined in **Chapter 4** revealed the first known evidence of stable NAg resistance development in *A. baumannii* ATCC 19606 following prolonged *in vitro* exposure of the bacterium to the nanoparticle. The resistance trait was associated with various genetic mutations thought to confer physiological changes and defence mechanisms. The work of this chapter involved a whole transcriptomic study of the WT and NAg^R ATCC 19606 strains to identify potential NAg defence mechanisms and elucidate the physiological changes manifested in the resistant bacterium. RNA-Seq analysis of the WT strain grown under sub-lethal (or sub-MIC) NAg stress revealed several differentially expressed genes (DEGs) indicated to confer defence against the main antibacterial paradigms of the nanoparticle, including physical cell surface disruption and cellular oxidative stress. These toxicological response mechanisms collectively form what is defined herein as the **primary defence system**. Most of the upregulated primary defence genes were found to be further upregulated in the NAg^R strain. This enhancement of primary defence-related gene expression formed what was defined as the **advanced primary defence system**, which suggested these intrinsic 'first tier' mechanisms were key to NAg defence in ATCC 19606. Further RNA-Seq analysis of the NAg^R strain revealed a plethora of gene expression changes which were unique from the WT strain. The identified upregulated genes were indicated to encode mechanisms which contribute to the general stress response, physical cell surface protection, oxidative stress defence, and DNA repair. These DEGs were correlated to the evolved **secondary defence system**, which likely developed because of the evolutionary adaptation of ATCC 19606 to NAg. Nearly all the advanced primary and secondary defence-related genes

associated were found to be stably upregulated in the resistant bacterium when grown in optimal conditions (in the absence of NAg pressure).

5.2 Introduction

With the issue of AMR growing immensely globally, NAg has become one the most commercialised and important alternative antimicrobial agents due to its proven multi-targeting and broad-spectrum antimicrobial activity. Despite this, there is mounting evidence highlighting that bacterial resistance to silver agents (including NAg) is possible and of legitimate concern. There is sufficient evidence demonstrating the emergence of NAg resistance in a variety of bacterial species, including *E. coli*, *P. aeruginosa, S. aureus,* and *Bacillus* spp. As outlined in **Chapter 2**, it is unclear whether the Gram-negative nosocomial pathogen *A. baumannii* is capable of developing NAg resistance, as previous studies have only highlighted the acquisition of plasmid-oriented resistance to silver cations (Ag^{+})[33-35]. This work presented in **Chapter 4** revealed, for the first time, the ability of this bacterial species to develop a resistance trait against NAg following 30-days of continual exposure. In turn, the next step, as revealed in the subsequent Chapter, was to gain clearer insight into the molecular basis of this resistance phenomenon by characterising the defence mechanisms at the transcriptomic level. Specifically, RNA sequencing (RNA-Seq) analysis was utilised to identify changes in gene expression in the resistant strain in response to varied NAg loads, and when in optimal conditions, in comparison to the WT strain. This was intended to help link the mutated genes and other identified genes of interest to the evolved physiological changes and NAg defence mechanisms observed in the NAg^{R} bacterium in the previous Chapter.

Previous studies have performed whole transcriptomic analyses on a variety of bacterial species in response to NAg toxicity *via* RNA-Seq[238-241]. Such inquiries have identified a multitude of gene expression changes in these bacteria and correlated them to various potential NAg defence mechanisms. Transcriptomic analysis of WT ATCC 19606 exposed to low levels of NAg revealed various DEGs associated with the intrinsic 'first tier' primary defence system against NAg toxicity. The NAg^{R} exhibited extensive gene expression change, first showing further upregulation of majority of the primary defence-related genes as part of its advanced primary defence system,

while additionally exhibiting upregulation of genes that were distinct from the WT and thus associated to the evolved secondary NAg defence system. Further transcriptomic analysis revealed that these defence-related genes were constitutively expressed in the NAg^R bacterium even in the absence of NAg. This indicated that the resistant ATCC 19606 strain had physiologically changed in response to long-term NAg treatment, and that the permanently upregulated defence-associated genes were likely now inherent to the evolved NAg resistance response.

5.3 Results and Discussion

5.3.1 Toxicological response of WT *A. baumannii* ATCC 19606 to NAg

5.3.1.1 Comparative growth rate of untreated and NAg-treated WT ATCC 19606

Comparative growth rate assays between NAg-treated and untreated (no NAg) WT *A. baumannii* were performed prior to transcriptomic analysis to determine the effective working (sub-MIC or low) concentrations of NAg (see **Table 3.2**)**.** This lower concentration of NAg was utilised to, firstly, induce a toxicological response in the strain, and secondly, ensure it did not adversely impact bacterial growth. This was essential in avoiding potential overlapping gene expression changes which might affect growth rate. Treatment of the WT strain with low concentrations of NAg (0.5 µg/mL; 0.5 x MIC) resulted in a comparable growth rate (0.602/h) to that of the untreated WT strain (0.603/h; **Figure 5.1**). Conclusively, the working concentration of NAg needed to elicit a toxicological response in WT *A. baumannii*, without disturbing cell behaviour, was determined to be 0.5 x MIC of NAg.

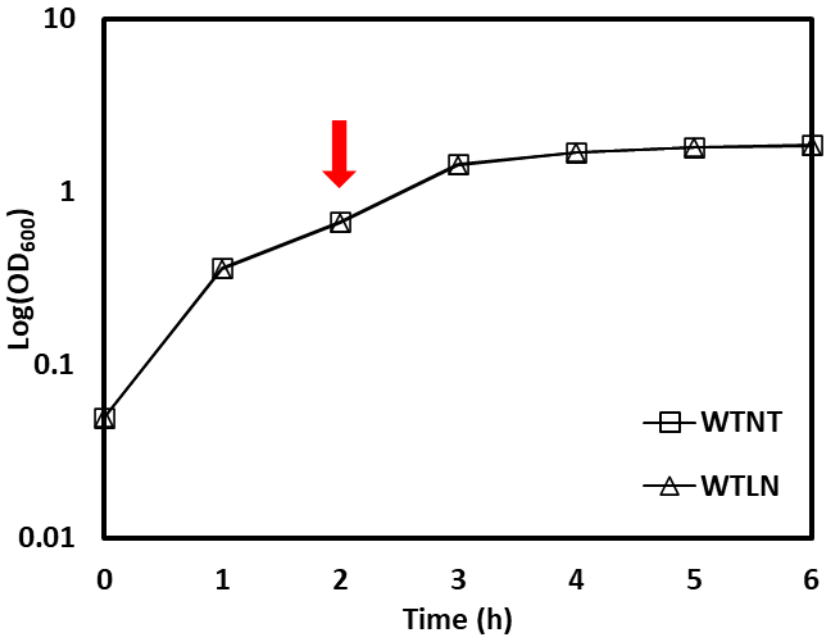

Figure 5.1 Comparative growth rates of WT ATCC 19606 when treated with low NAg concentration (0.5 µg/mL; 0.5 x MIC) and untreated (no NAg) over 6 h. WTNT = wild-type no treatment (square); WTLN = wild-type low NAg (triangle). The red arrow indicates the time point (2 h) at which NAg was added to (WTLN) culture. RNA was extracted 30 min (2.5 h time point) after addition of NAg. Initial OD_{600} at time 0 began at 0.05. Each data point represents mean of at least two biological replicates.

5.3.1.2 Differentially expressed genes in NAg-treated WT ATCC 19606

As stated above, WT *A. baumannii* ATCC 19606 was treated with an NAg dose of 0.5 x MIC for 30 min to elicit a toxicological response prior to RNA extraction. Gene expression of the NAg-treated WT strain (hereafter referred to as Wild-Type Low NAg; WTLN) was compared against that of untreated WT *A. baumannii* (hereafter referred to as Wild-Type No Treatment; WTNT) to examine the difference in transcription in response to NAg toxicity. See **Section 3.9.5** for cut-off threshold values which define a differentially expressed gene (DEG) between the pairwise comparisons. Refer to **Table A1** in the appendix for the complete gene ontology analysis of the DEG data of NAg-treated WT ATCC 19606.

Transcriptomic analysis of the WTLN strain revealed a total of 34 statistically significant DEGs when compared to WTNT (**Table 5.1**). Of these 34 transcripts, 29

were found to be upregulated, while 5 were downregulated. Earlier studies have reported variable DEG findings in NAg-treated bacterial species. For instance, one RNA-Seq study reported over 300 DEGs in *E. coli* following NAg treatment, while a doctoral study identified a total of 44 DEGs in *S. aureus* after sub-lethal NAg treatment[239,241]. These variations in the number of DEGs detected can be attributed to several factors, including differences in the physicochemical properties of the NAg particulates used, species-specific responses to NAg, and the working concentration and duration of NAg treatment involved. Refer to **Section 2.5** for information on the influence of NAg physicochemical properties on its antibacterial activity.

Table 5.1 Number of DEGs (upregulated and downregulated genes) identified in WT *A. baumannii* treated with 0.5 x MIC dose of NAg (WTLN) in comparison to untreated WT *A. baumannii* (WTNT).

Comparison	Upregulated	Downregulated	Total
WTLN *versus* WTNT	29	5	34

The modified expression of these 34 transcripts is a direct result of the toxicological response of *A. baumannii* to sub-lethal NAg exposure. To elucidate the biological significance of these DEGs in the bacterium response to NAg, the following discussion will focus on specific gene expression changes that could encode defence mechanisms against recognised NAg toxicity features. However, understanding the complete global transcriptional changes in the bacterium in response to the nanoparticle are beyond the scope of this study. As knowledge on the interaction between *A. baumannii* and NAg is limited, further research is needed to gain a more comprehensive grasp of the potential mechanistic defence characteristsics of the bacterium. This is particularly important since there is a lack of studies on bacterial transcriptomics in response to NAg toxicity, and further, no such analyses have been conducted on *A. baumannii* in response to NAg exposure.

5.3.1.3 Toxicological responses to NAg

As outlined in **Chapter 2** and **Chapter 4,** cell surface disruption and oxidative stress-related activity are among the major toxicity paradigms of NAg. Of the 34 DEGs detected, several upregulated genes were associated with the toxicological responses of the WT bacterium to these NAg toxicity mechanisms and are hence suggested to contribute to the intrinsic 'first tier' **primary defence system** of ATCC 19606. More specifically, out of the 29 upregulated DEGs, seven of these were linked to this proposed primary NAg defence response (**Figure 5.2**). RNA-Seq analysis revealed that these seven upregulated genes encode various outer membrane proteins (OMPs), copper efflux pumps, and an oxidative stress response protein. Note that the identified downregulated DEGs have no putative function (encode hypothetical proteins), and therefore, only upregulated genes were examined.

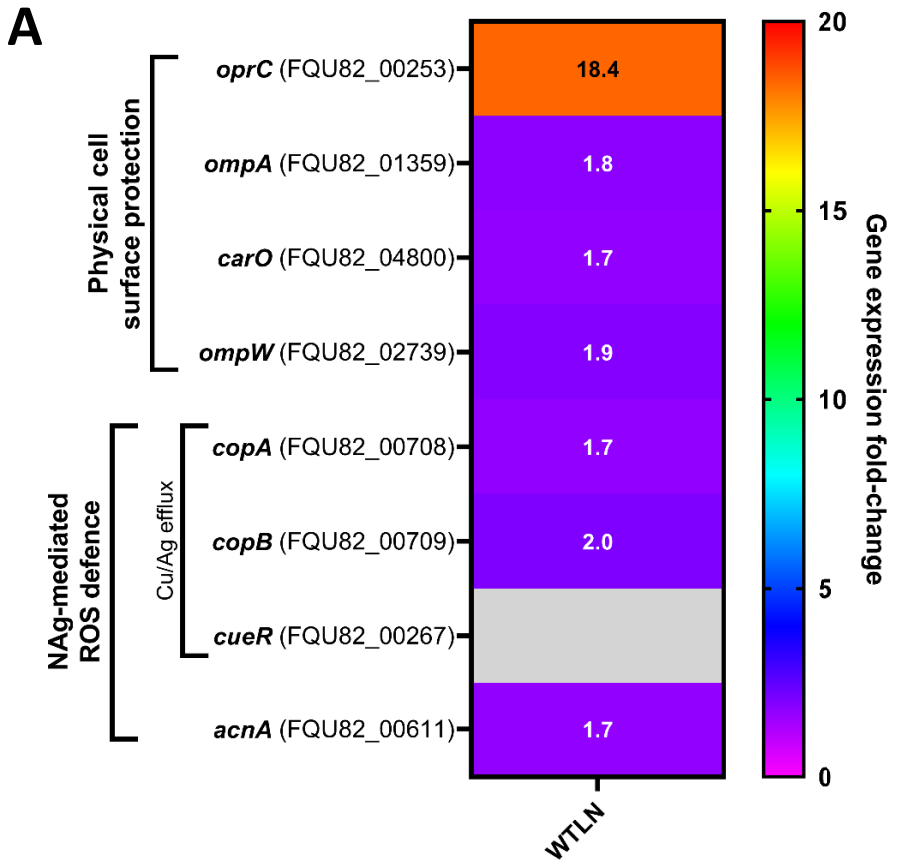
A
oprC (FQU82_00253)
ompA (FQU82_01359)
carO (FQU82_04800)
ompW (FQU82_02739)
copA (FQU82_00708)
copB (FQU82_00709)
cueR (FQU82_00267)
acnA (FQU82_00611)
Physical cell surface protection
NAg-mediated ROS defence
Cu/Ag efflux
18.4
1.8
1.7
1.9
1.7
2.0
1.7
WTLN
20
15
10
5
0
Gene expression fold-change

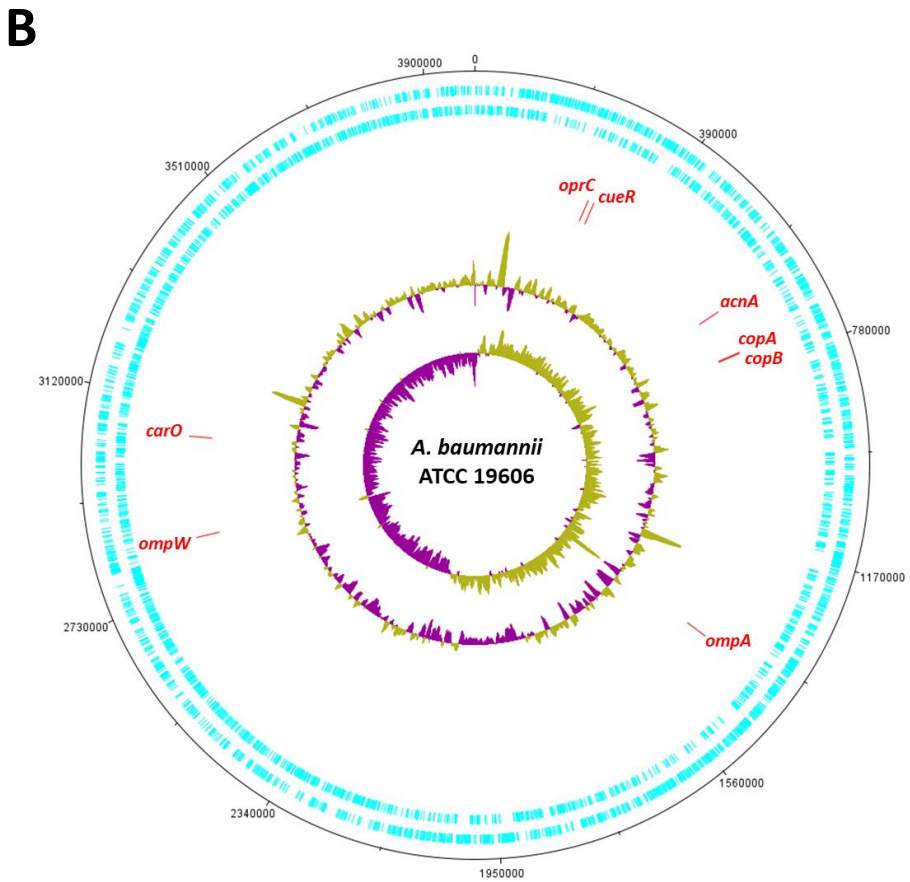
B
3900000
0
390000
780000
1170000
1560000
1950000
2340000
2730000
3120000
3510000
oprC
cueR
acnA
copA
copB
carO
ompW
ompA
A. baumannii
ATCC 19606

Figure 5.2 Differentially expressed genes (DEGs) identified in WT *A. baumannii* ATCC 19606 in response to low (sub-lethal) NAg doses. (**A**) Heat-map representing expression fold-change in genes of interest hypothesised to contribute to the primary NAg defence system of the WT strain. Grey cells indicate statistically insignificant DEGs. Pairwise comparison: WTLN *versus* WTNT. (**B**) Map of *A. baumannii* ATCC 19606 chromosome indicating sequence positions of DEGs of interest. Forward and reverse reading frames are shown by the cyan-coloured bars. The two internal rings indicate the chromosome's GC skew (the innermost ring) followed by the chromosome's GC content.

Among the upregulated OMP genes identified in WTLN relative to WTNT, the RNA-Seq analysis detected increased expression of the gene *oprC* (FQU82_00253) by ~ 18.4-fold which encodes the putative outer membrane copper receptor OprC (a TonB-dependent copper receptor; **Figure 5.2**). OprC has been associated with increased to copper ion (Cu^{+}) resilience in *A. baumannii*, which is suggested to involve uptake and sequestration of the toxic heavy metal within the periplasmic space[208,242]. As Cu^{+} and Ag^{+} are both soft acids and are isoelectronically comparable metals, it is hypothesised that low dose NAg exposure stimulated increased upregulation of *oprC* as seen herein[243,244]. Previous work has linked the upregulation of copper homeostasis mechanisms to the presence of silver pressure, with one study suggesting that *oprC* may be involved in silver uptake, based on protein structural data[239,245]. Therefore, this upregulation of *oprC* could result in periplasmic sequestration of silver, ultimately acting as a mechanism of physical protection against NAg activity. In addition, studies have noted that superoxide dismutase enzymes (specifically SodC) can enter the bacterial periplasmic space and enact ROS scavenging, which could potentially occur in response to sequestered silver and generated ROS[246]. However, this process has only been associated with host virulence, designed to scavenge for superoxide ($O_2^{\bullet-}$) generated by responding macrophages, rather than with antimicrobial defence[246,247]. Ultimately, further evidence is required to suggest a link between NAg (or antimicrobial) presence and ROS scavenging within the periplasm.

Several other OMP-encoding genes were found to be upregulated in WTLN, albeit at a lower extent, in comparison to WTNT, including *ompA* (encoding OmpA; FQU82_01359), *carO* (encodes CarO; FQU82_04800), and *ompW* (encodes OmpW;

FQU82_02739), each of which had expression changes between ~ 1.7 – 1.9-fold (**Figure 5.2**). Studies have associated increased OmpA expression and greater drug resistance in various *A. baumannii* strains (including against last line antibiotics, such as colistin and polymyxin B)[248-250]. This resistance mechanism is thought to relate to improved cell membrane integrity, along with increased drug shuttling (coupled with efflux pumps), which has been demonstrated in ATCC 19606[250,251]. OmpW also has reported functions in macrophage phagocytosis resistance in *E. coli*[252]. In turn, the upregulation of *ompW* in the WT strain is thought to confer increased cell membrane integrity, thus providing physical protection against NAg activity. CarO is a highly conserved carbapenem-associated porin in *A. baumannii,* and studies have reported a link between increased CarO expression and greater cell-to-surface adherence and biofilm formation in this bacterium, which may also play a role in physical NAg penetration protection[248,253,254]. Indeed, studies have also associated functions of both OmpA and OmpW in *A. baumannii* biofilm formation[248,255]. Overall, it is currently hypothesised that the upregulation of *oprC*, *ompA, ompW,* and *carO* in WT ATCC 19606 are associated with physical cell surface protection to NAg toxicity, specifically involving periplasmic sequestration of nanoparticles (*via oprC*) and improved cell membrane integrity (*via ompA* and *ompW*). However, the potential roles of the upregulated OMP genes (including *carO*) in increased biofilm formation of ATCC 19606 has not been overlooked, and the involvement of this phenotype in NAg defence is explored within the evolved NAg^R strain, as later described in **Section 5.3.2.3**.

RNA-Seq analysis also revealed a ~ 1.7 – 2-fold expression level increase of two copper efflux genes in WTLN, *copA* (FQU82_00708) and *copB* (FQU82_00709; **Figure 5.2**). CopA and CopB are cytoplasmic (inner membrane)-bound P-type ATPase copper efflux proteins, which are known to facilitate bacterial resistance to copper and silver ions[152,256]. The presence of both CopA and CopB have been detected in copper-resistant (or tolerant) *A. baumannii* strains, and it is likely that these proteins confer similar protection mechanisms to silver in this species[152,257]. Previous transcriptomic studies have also observed increases in *copA* expression in many bacterial species in response to nanoparticulate and ionic silver exposure[238,240,241]. Upregulation of *copA* has also been linked to Cu^+-induced oxidative stress protection in *A. baumannii,* whereby increased expression of the efflux pump removes excess copper, hindering the generation of intracellular ROS[152]. This counteraction of copper-

induced ROS generation by CopA/CopB efflux is thought to also function against silver in ATCC 19606 herein. Studies have reported on the role of the HTH-type transcriptional regulator CueR in positively regulating *copA* (and potentially *copB*) expression in *A. baumannii*[152,153,257]. However, there was no statistically significant change in expression of *cueR* (FQU82_00267) observed in WTLN, which instead, was upregulated in the NAg^R strain (along with *copA/copB*) as later described in **Section 5.3.2.3**. The gene *acnA* (FQU82_00611), which encodes the aconitate hydratase enzyme AcnA, was also upregulated by ~ 1.7-fold (**Figure 5.2**). AcnA is an enzyme involved in citric acid cycle homeostasis. Increased synthesis of this protein reportedly helps maintain the citric acid cycle during exposure to (or recovery from) cellular oxidative stress, which has been observed in *A. baumannii*[258-260]. It was therefore deduced that upregulation of *acnA* may have protective functions against NAg-mediated oxidative stress in WT ATCC 19606 by conserving cellular metabolic function.

To summarise, the RNA-Seq analysis revealed seven DEGs indicated to be involved in the toxicological response of WT *A. baumannii* ATCC 19606 following sub-lethal NAg treatment. These upregulated genes are hypothesised to contribute to the primary NAg defence system of the bacterium, and encode various OMPs, two copper efflux pumps, and an oxidative stress response protein. The maintenance of cell membrane integrity *via* OMP upregulation may impede NAg penetration through the cell surface, while the upregulation of the *copA*/*copB* efflux pumps are thought to help expel excess intracellular silver (including leached Ag^+) and protect the cell from silver-mediated ROS generation. In addition, activation of the oxidative stress response gene *acnA* may help uphold normal cell function by maintaining the citric acid cycle. Next up, this thesis will discuss the gene expression changes and proposed defence responses of NAg^R ATCC 19606 in response to NAg toxicity.

5.3.2 Defence response of NAg^R *A. baumannii* ATCC 19606 to NAg

5.3.2.1 Comparative growth rate of NAg-treated WT and NAg^R ATCC 19606

A comparative growth study between the WT and NAg^R strains when exposed to sub-MIC (low) doses of NAg (0.5 µg/mL; 0.5 x MIC; see **Table 3.2**), was performed to determine if growth rate of the NAg^R strain had been altered in comparison to the WT

strain. A comparison of growth rates between the NAg^R strain when untreated (no NAg), when exposed to a low NAg dose (0.5 µg/mL; 0.5 x MIC), and an above-MIC (high) dose of NAg (3 µg/mL; 3 x MIC; see **Table 3.2**), was also performed to observe any potential growth behaviour changes in the bacterium under varied NAg loads. The growth rates of the low dose treated WT strain (0.602/h), untreated resistant strain (0.608/h), and low dose and high dose treated resistant strain (0.602/h and 0.608/h, respectively) were all found to be comparable (**Figure 5.3**). This indicated that both the low and high NAg doses were suitable for inciting a defence response in the respective strains without disrupting growth behaviour.

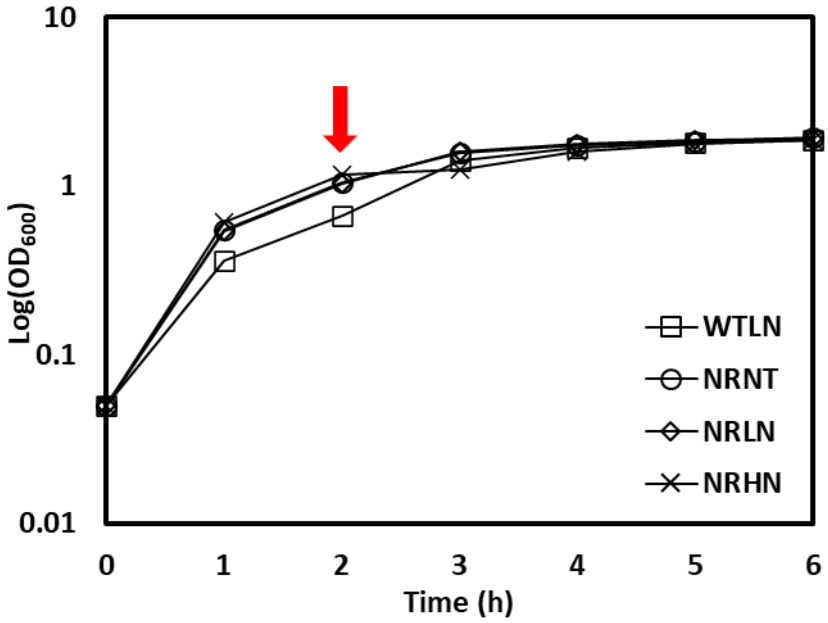

Figure 5.3 Comparative growth rates of WT and NAg^R ATCC 19606 strains treated with low and high NAg doses over 6 h. WTLN = wild-type no treatment (square); NRNT = NAg-resistant no treatment (circle); NRLN = NAg-resistant low NAg (diamond); NRHN = NAg-resistant high NAg (cross). The red arrow indicates the time point (2 h) at which NAg was added to the respective cultures. RNA was extracted 30 min (2.5 h time point) after addition of NAg. Initial OD_{600} at time 0 began at 0.05. Each data point represents mean of at least two biological replicates.

5.3.2.2 Differentially expressed genes between NAg-treated WT and NAg-treated NAg^R ATCC 19606

To identify changes in gene expression which could contribute to the evolved NAg defence response of NAg^R *A. baumannii* ATCC 19606, the resistant strain was

exposed to both low (0.5 x MIC) and high (3 x MIC) doses of the nanoparticle (refer to **Table 3.2**). The transcriptomic profile of WTLN was compared against that of low dose NAg-treated NAg^R strain (hereafter referred to as Nanosilver-Resistant Low Nanosilver; NRLN) to observe alterations in gene expression patterns between the WT and adapted bacteria. The untreated NAg^R strain (hereafter referred to as Nanosilver-Resistant No Treatment; NRNT) was compared against both NRLN and high dose NAg-treated NAg^R strain (hereafter referred to as Nanosilver-Resistant High NAg; NRHN), respectively. Gene expression changes between NRLN and NRHN were also compared. See **Section 3.9.5** for cut-off threshold values which define a differentially expressed gene (DEG) between the pairwise comparisons. Refer to **Table A1** in the appendix for complete gene ontology analysis of DEG data of NAg-treated WT and NAg^R ATCC 19606.

RNA-Seq analysis revealed a total of 1121 DEGs in NRLN when compared to WTLN (**Table 5.2**). A total of 559 genes were upregulated while 562 genes were downregulated. Between NRLN and NRNT, the analysis revealed only 7 DEGs, 5 of which were upregulated while 2 were downregulated. A total of 1797 DEGs were identified in NRHN in comparison to NRNT, with 1004 genes upregulated and 793 genes downregulated. Finally, the RNA-Seq analysis revealed a total of 1834 DEGs in NRHN when compared to NRLN, 1013 of which were upregulated while 821 were downregulated. This data highlights that the NAg^R strain exhibits significantly higher changes in gene expression when exposed to low and high doses of NAg in comparison to that of the low dose treated WT strain (*i.e.* WTLN *versus* WTNT; see **Table 5.1**).

Table 5.2 Number of DEGs (upregulated and downregulated genes) identified in NAg^R *A. baumannii* treated with a low dose (0.5 x MIC) of NAg (NRLN) and a high dose (3 x MIC) of NAg (NRHN).

Comparison	Upregulated	Downregulated	Total
NRLN *versus* WTLN	559	562	1121
NRLN *versus* NRNT	5	2	7
NRHN *versus* NRNT	1004	793	1797

NRHN *versus* NRLN	1013	821	1834

In the context of silver defence, DEGs with known (or hypothetical) functions in antibacterial defence, particularly against the toxicity paradigms of NAg (*e.g.* cell envelope targeting and ROS generation) were examined. This included changes in expression of the DEGs linked to the primary NAg defence system of the WT strain described in **Section 5.3.1**. This was to determine if any of the primary defence mechanism are further enhanced in the resistant bacterium as part of its adapted defence response. In **Section 4.6.2**, the NAg^R strain developed stable mutations in the genes *rcsC, smf1-2,* and *csuB* following prolonged exposure to the nanoparticle. Therefore, expression modifications of these mutated genes were also examined to elucidate their potential role in the NAg resistance phenomena. Due to the large number of DEGs identified in the NAg^R strain, the following section will primarily focus on the contributions of upregulated genes in the defence response of the resistant bacterium.

5.3.2.3 Evolved defence responses to NAg

As discussed in **Chapter 4**, *A. baumannii* ATCC 19606 was subjected to increasing dose of NAg over 30 days to induce an adaptation response. The adapted bacterium was able to proliferate at an otherwise toxic concentration of NAg (above the WT strain MIC; two-fold or more increase), which was indicative of stable resistance development to the nanoparticle. In the RNA-Seq study herein, the transcriptomic profile of the NAg^R strain, following exposure to low dose (0.5 x MIC of WT) and high dose (3 x MIC of WT) NAg, was examined to identify changes in gene expression which might facilitate the evolved defence response. Of the seven DEGs correlated to the primary NAg defence system of the WT strain (see **Figure 5.2**), all genes exhibited varied expression levels in the NAg^R bacterium in response to different NAg doses. The primary defence-related genes which showed further upregulation in the resistant strain were correlated to what is defined in this study as the **advanced primary defence system**. A total of 19 other DEGs only detected in the NAg^R strain (unique from the WT) were linked to the **secondary defence system** and encoded mechanisms involved in the general stress response, physical cell surface protection, and NAg-

mediated oxidative stress defence. These latter gene expression modifications are the result of evolutionary change in ATCC 19606 due to long-term NAg exposure.

It is important to note that only seven DEGs (five upregulated and two downregulated genes) were detected in the low dose treated NAg^R strain (NRLN) relative to the untreated resistant strain (NRNT; **Table 5.2**). As majority of the gene expression fold-changes identified in NRLN relative to NRNT were statistically insignificant, the DEG results of this comparison are not reported in this Chapter, unless stated otherwise. It is thought that the sub-lethal NAg concentration (0.5 µg/mL) was not sufficiently toxic to induce extensive transcriptomic modification in the NAg^R strain (compared to its untreated counterpart). A previous RNA-Seq analysis of *E. coli* treated with sub-lethal Ag^+ doses also resulted in little gene expression change relative to an untreated control sample[261]. Indeed, it was hypothesised that the limited gene expression changes between the low dose treated and untreated cultures is indicative of the fact that the NAg^R strain has undergone stable physiological change involving permanent gene expression modification even in optimal conditions (without NAg pressure). This concept is explored in the final section of this Chapter (**Section 5.3.3**).

5.3.2.3.1 Advanced primary defence system

As described in **Section 5.3.1.3**, 8 upregulated genes were detected in the ATCC 19606 WT strain (*i.e.* WTLN), indicated to be involved in the toxicological response of the bacterium to sub-lethal NAg, herein referred to as the primary defence response. Upregulation of these genes are thought to confer physical protection, *via* increased expression of OMPs, and oxidative stress defence, *via* silver efflux and citric acid cycle homeostasis for optimal cell function. Further RNA-Seq analysis of the NAg^R strain revealed, in general, a higher extent of expression of these genes upon exposure to the nanoparticle, contributing to what is defined herein as the advanced primary NAg defence response (**Figure 5.4**).

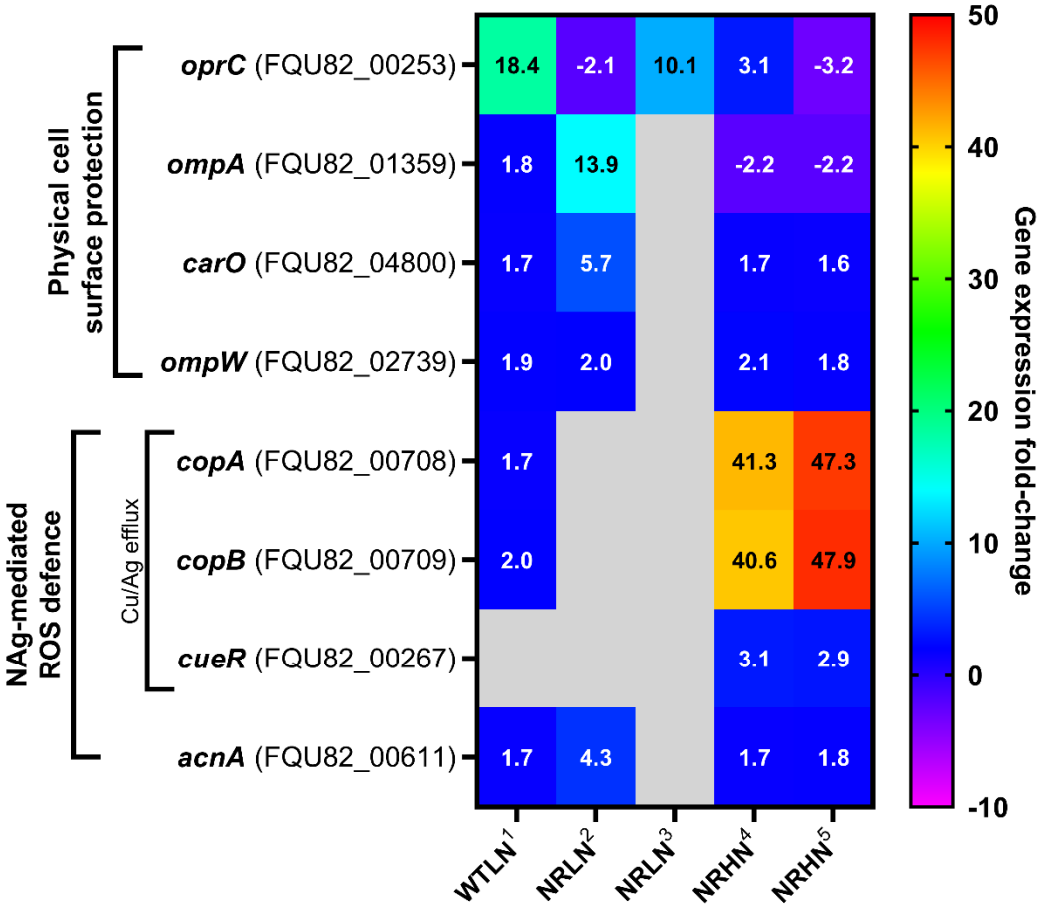

Figure 5.4 Differentially expressed genes (DEGs) identified in WT and NAg^{R} *A. baumannii* ATCC 19606 in response to low (sub-lethal) or high (lethal) NAg doses. Heat-map represents expression fold-change in genes of interest hypothesised to contribute to the primary and advanced primary NAg defence systems of the WT and NAg^{R} strains, respectively. Grey cells indicate statistically insignificant DEGs. Pairwise comparisons: [1] WTLN *versus* WTNT, [2] NRLN *versus* WTLN, [3] NRLN *versus* NRNT, [4] NRHN *versus* NRNT, [5] NRHN *versus* NRLN.

In NRLN, the genes *ompA*, *carO*, and *ompW* were upregulated by ~ 13.9-fold, ~ 5.7-fold, and ~ 2.0-fold, respectively, relative to WTLN. The expression levels of *ompW* and *carO* were further upregulated in NRHN by ~ 1.8 – 2.1-fold and ~ 1.6 – 1.7-fold when compared to NRNT and NRLN, respectively. Enhanced expression of these OMPs are thought to contribute to the (earlier described) potential improvement in cell membrane integrity, as well as increased cell-to-surface attachment and biofilm formation[248,262]. This aligns with the observed enhanced biofilm-forming capabilities of the resistant strain, as described in **Section 4.6.2**. Specifically, the NAg^{R} strain

formed more biofilms than that of the WT strain, even in the absence of NAg, which is most likely the result of evolutionary physiological changes that occurred due to prolonged NAg exposure. This improved biofilm-forming phenotype might contribute to increased defence against NAg toxicity[263]. Interestingly, *ompA* was slightly downregulated by ~ 2.2-fold in the high dose treated resistant strain in comparison to both NRNT and NRLN. The reason for the downregulation of *ompA* at higher NAg concentrations is unclear at this stage.

The NAg^R strain exhibited upregulation of *oprC* by ~ 10.1-fold in response to low NAg doses, relative to NRNT, and interestingly, only by ~ 3.1-fold in the high dose treated culture relative to NRNT. The observed reduction in expression levels of this porin in response to increasing nanoparticle concentration is thought to be a defence strategy. Specifically, it may occur to restrict the periplasmic sequestration of toxic silver levels, thereby preventing intracellular accumulation. Indeed, a ~ 3.2-fold downregulation of the gene was detected in NRHN, relative to NRLN, and a ~ 2.1-fold downregulation was also seen in NRLN, relative to WTLN.

Next, the NAg^R strain exhibited upregulation of the copper/silver efflux *copA* and *copB* genes, by ~ 40.6 – 47.9-fold in NRHN relative to NRNT and NRLN (**Figure 5.4**). The high NAg dose treated strain also exhibited upregulation of the associated transcriptional regulator gene *cueR* by ~2.9 – 3.1-fold in comparison to NRNT/NRLN, indicating a regulatory link to the increased expression levels of *copA/copB*. Note that, when compared to the low dose exposed WT strain, a ~ 1.7 – 2.1-fold downregulation of both *copA* and *copB* were observed in NRLN, which indicates that a higher toxicity 'threshold' (*i.e.* higher NAg concentrations) is needed to induce enhanced upregulation of the copper efflux genes.

Lastly, the oxidative stress-related citric acid cycle gene *acnA* was also upregulated in the NAg^R strain. At lower NAg doses, the gene was upregulated by ~ 4.3-fold in the resistant bacterium in comparison to WTLN. The gene was further upregulated by ~ 1.7-fold and ~ 1.8-fold in the high dose treated NAg^R strain relative to both NRNT and NRLN, respectively (**Figure 5.4**). Enhanced expression levels of *acnA* may contribute to the improved NAg-mediated oxidative stress defence observed in the NAg^R bacterium shown in **Figure 4.3**[260,264].

5.3.2.3.2 Secondary defence system

The observed increase in expression levels of the OMP-related genes, *ompA, carO,* and *ompW,* the copper efflux genes *copA*, *copB*, (and transcriptional regulator *cueR*), along with and the oxidative stress response-related gene *acnA*, indicate the involvement of physical cell surface protection and ROS defence in the advanced primary defence system of the NAg^R bacterium. Further transcriptomic analysis revealed several other statistically significant DEGs indicated to contribute to the evolved secondary defence response of the resistant bacterium. Specifically, 19 DEGs were identified and indicated to be involved in the general stress response, physical cell surface protection, and NAg-mediated oxidative stress defence (**Figure 5.5**). The secondary defence system likely manifested because of the evolutionary adaptation of ATCC 19606 to prolonged NAg treatment and is therefore unique to the NAg^R strain and not observed in the WT bacterium.

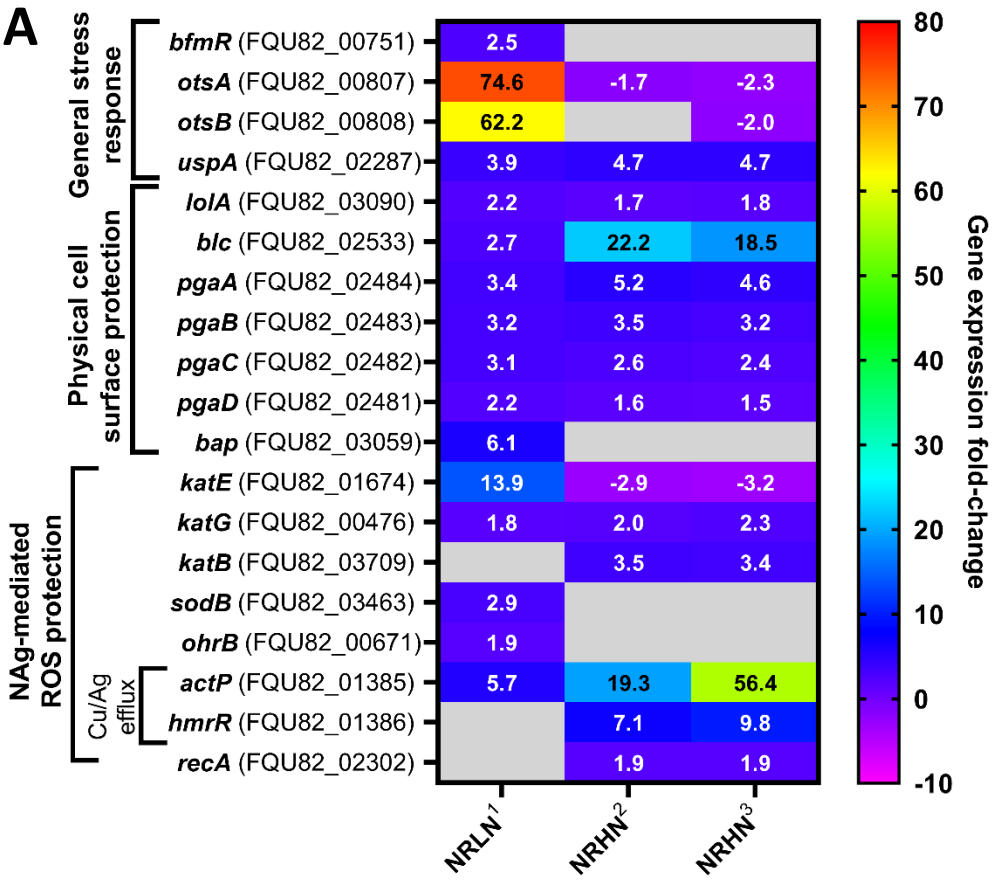
A
General stress response
Physical cell surface protection
NAg-mediated ROS protection
Cu/Ag efflux
bfmR (FQU82_00751)
otsA (FQU82_00807)
otsB (FQU82_00808)
uspA (FQU82_02287)
lolA (FQU82_03090)
blc (FQU82_02533)
pgaA (FQU82_02484)
pgaB (FQU82_02483)
pgaC (FQU82_02482)
pgaD (FQU82_02481)
bap (FQU82_03059)
katE (FQU82_01674)
katG (FQU82_00476)
katB (FQU82_03709)
sodB (FQU82_03463)
ohrB (FQU82_00671)
actP (FQU82_01385)
hmrR (FQU82_01386)
recA (FQU82_02302)
2.5
74.6 -1.7 -2.3
62.2 -2.0
3.9 4.7 4.7
2.2 1.7 1.8
2.7 22.2 18.5
3.4 5.2 4.6
3.2 3.5 3.2
3.1 2.6 2.4
2.2 1.6 1.5
6.1
13.9 -2.9 -3.2
1.8 2.0 2.3
3.5 3.4
2.9
1.9
5.7 19.3 56.4
7.1 9.8
1.9 1.9
NRLN1
NRHN2
NRHN3
80
70
60
50
40
30
20
10
0
-10
Gene expression fold-change

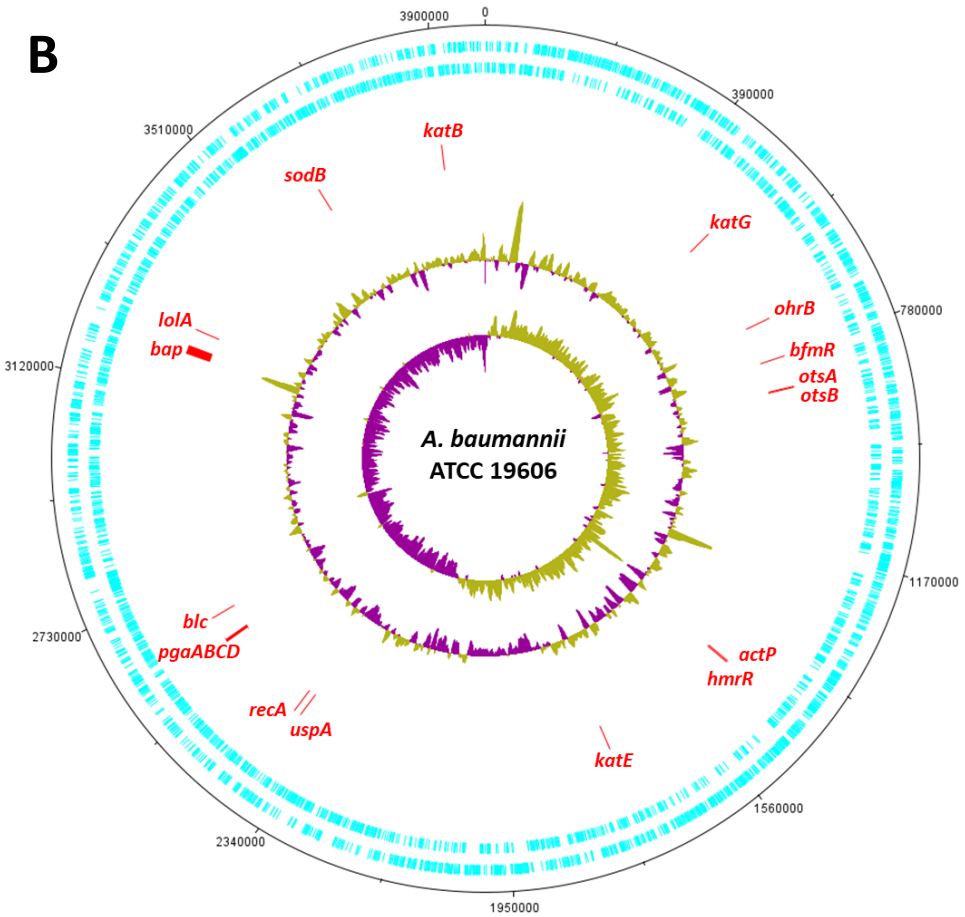
B
3900000
0
390000
780000
1170000
1560000
1950000
2340000
2730000
3120000
3510000
katB
sodB
katG
ohrB
bfmR
otsA
otsB
lolA
bap
blc
pgaABCD
recA
uspA
katE
actP
hmrR
A. baumannii
ATCC 19606

Figure 5.5 Differentially expressed genes (DEGs) identified in NAg^R *A. baumannii* ATCC 19606 in response to low (sub-lethal) or high (lethal) NAg doses. (**A**) Heat-map representing expression fold-change in genes of interest hypothesised to contribute to the secondary NAg defence system of the resistant strain. Grey cells indicate statistically insignificant DEGs. Pairwise comparisons: [1] NRLN *versus* WTLN, [2] NRHN *versus* NRNT, [3] NRHN *versus* NRLN. NRLN *versus* NRNT comparative DEG data not shown. (**B**) Map of *A. baumannii* ATCC 19606 chromosome indicating sequence positions of DEGs of interest. Forward and reverse reading frames are shown by the cyan-coloured bars. The two internal rings indicate the chromosome's GC skew (the innermost ring) followed by the chromosome's GC content.

General stress response – Several stress response related genes were upregulated in the NAg^R strain (**Figure 5.5**). In response to low NAg concentrations, the gene *bfmR* (FQU82_00751), which encodes the response transcriptional regulator factor BfmR, was found to be upregulated by ~ 2.5-fold when compared to WTLN. In *A. baumannii*, BfmR is part of the two-component regulatory system BfmR/S which is involved in regulating stress by modulating the expression of various stress response and virulence genes. No statistically significant change in expression of *bfmR* was noted in NRHN when compared to both NRLN and NRNT. BfmR is known to regulate expression of the osmotic stress response genes *otsA* and *otsB* (FQU82_00807 and FQU82_00808, respectively)[260]. These latter genes, which are involved in the trehalose synthesis pathway and encode the enzymes trehalose-6-phosphate synthase and trehalose-6-phosphate phosphatase respectively, were indeed, highly upregulated by ~ 62.2 – 74.6-fold in NRLN in comparison to WTLN[265,266]. Trehalose is a simple disaccharide with structural and functional roles, and is synthesised by bacteria under stressful conditions[267]. In *A. baumannii*, trehalose synthesis has been associated with increased CPS density and thickness, which is thought to enhance cell envelope integrity[266]. In **Section 4.6.2**, it was hypothesised that the NAg^R strain exhibited increased CPS production and therefore, improved cell envelope integrity, based on the initial genomic data (**Table 4.1**). This was thought to contribute to the higher extent of biofilm growth (see **Figure 4.2**) and apparent protection against ROS activity in the resistant strain (see **Figure 4.3**), relative to the WT strain. Increased expression of CPS

synthesis genes have been previously observed in *E. coli* and *S. aureus* in response to NAg toxicity[238,240]. The herein observed upregulations of *bfmR*, as well as *otsA/B*, are consistent with this hypothesis. In NRHN, these genes were slightly downregulated by ~ 1.7 – 2.3-fold relative to NRNT/NRLN. The latter is thought to correlate to the statistically insignificant expression change of the transcriptional regulator *bfmR* in NRHN (relative to NRNT and NRLN). Next, the gene *uspA* (encodes the universal stress protein UspA; FQU82_02287) was found to be upregulated by ~ 3.9 – 4.7-fold in the NAg^R strain in response to both low and high NAg concentrations, across all pairwise comparisons. The precise role of universal stress proteins in NAg defence remains unclear; however, studies have indicated that UspA offers protective effects against oxidative stress in bacteria, including *A. baumannii*, while Δ*uspA* mutants exhibit increased susceptibility to environmental stressors[268,269]. Additionally, *uspA* has also been shown to regulate the expression of other stress response genes, including upregulation of DNA repair genes, the latter of which was also linked to the secondary defence of the resistant strain, as later described[270].

Physical cell surface protection – An array of cell surface protection mechanisms, which are distinct from those earlier described in the primary and advanced primary defence systems, were herein identified, and correlated to the secondary defence of the resistant bacterium (**Figure 5.5**). The NAg^R strain exhibited upregulation of *lolA* (FQU82_03090), which encodes the outer membrane lipoprotein-carrier protein LolA, by ~ 1.7 – 2.1-fold in response to higher NAg doses, relative to NRNT and NRLN. No statistically significant changes in the expression of *lolA* was noted in NRLN when compared to WTLN. LolA forms part of the LolABCDE protein complex which helps maintain structural integrity of the outer membrane (OM) in Gram-negative bacteria[271,272]. LolCDE is an ATP-binding cassette transporter system responsible for releasing newly synthesised lipoproteins from the inner membrane and directing them to LolA. LolA acts as a chaperone, shuttling lipoproteins to the OM for biogenesis, which is mediated by LolB[271]. Increased expression of the Lol system in *E. coli* and *P. aeruginosa* has been reported to confer increased resistance to a range of antibacterial agents, including lipoprotein inhibitors, as well as globomycin, an antifungal agent with bactericidal activity against Gram-negatives[271,272]. While no statistically significant change in expression of the other *lol* genes (*lolBCDE)* were noted in the resistant strain, the upregulation of *lolA* is hypothesised to increase

lipoprotein delivery to the OM, and in turn, improve membrane integrity to enhance protection of known NAg cell membrane targets[33,98]. Next, upregulation of the gene *blc* (FQU82_02533) by ~ 2.6-fold was exhibited by the low dose treated strain in comparison to the WT strain. This gene was then further upregulated by ~ 18.5 – 22.2-fold in the high dose treated bacterium relative to NRNT and NRLN. This gene encodes the lipocalin Blc which is an OM lipoprotein-carrier[273]. Studies have shown that lipocalins are highly expressed in Gram-negative bacteria, such as *E. coli*, when exposed to stressors, including starvation and oxidative stress, to boost lipoprotein transport for membrane repair[273-275]. The increased expression of *blc* could, at least in part, complement the upregulation of *lolA*, simultaneously improving OM lipoprotein transport for added cell surface defence against the nanoparticle.

Recalling the findings in **Chapter 4**, the resistant strain demonstrated a greater extent of biofilm formation in comparison to the WT bacterium, even in optimal conditions (refer to **Figure 4.2**). Herein, the resistant strain exhibited upregulation of genes that encode membrane-bound proteins involved in exopolysaccharide (EPS) production. The *pgaABCD* operon (FQU82_02484, 02483, 02482, and 02481, respectively) was upregulated by ~ 2.2 – 3.4-fold in the low dose treated resistant strain in comparison to WTLN, and then further upregulated by ~ 1.5 – 5.2-fold in the bacterium in response to high dose NAg relative to the untreated and low dose treated cultures. This operon encodes the membrane-bound proteins PgaABCD which collectively synthesise the exopolysaccharide poly-β-(1-6)-*N*-acetylglucosamine (PNAG) – an important EPS constituent in *A. baumannii* biofilms, as well as other bacteria[276]. Studies have linked upregulation of the *pga* operon to improved biofilm EPS formation, and in turn, to increased biofilm-mediated antimicrobial defence[121,277]. Studies have also reported that the negatively-charged EPS can drive the biosorption and sequestration of positively-charged heavy metals to detoxify the surrounding environment, which is hypothesised to function against silver[278,279]. Moreover, the gene *bap* (FQU82_03059), which encodes the biofilm-associated protein Bap, was upregulated in NRLN by ~ 6.1-fold in comparison to WTLN. However, no statistically significant increase in *bap* expression was noted in the high dose treated NAg^R strain relative to NRNT and NRLN. Bap is one of the largest and most conserved biofilm-related proteins in *A. baumannii* and is essential for cell surface attachment and maturation of biofilm colonies[280].

Oxidative stress response – A variety of ROS scavenger and oxidative stress response genes were also upregulated in the NAg^R strain (**Figure 5.5**). In NRLN, the genes *katE* (FQU82_01674) and *katG* (FQU82_00476) were upregulated by ~ 13.9-fold and ~ 1.7-fold, respectively, when compared to WTLN. The gene *katE* encodes the enzyme catalase HPII, while *katG* encodes catalase HPI, both of which are hydroperoxidases which catalyse the degradation of excess intracellular hydrogen peroxide (H_2O_2)[281]. Excess H_2O_2 removal is critical in preventing its conversion into other oxygen radicals, such as superoxide ($O_2^{\bullet}$-) or hydroxyl ($^{\bullet}OH$) through the Fenton-active ferrous iron (Fe^{2+}) reaction, which helps delay the onset of oxidative stress[98]. However, in NRHN, *katE* was downregulated by ~ 3.0 – 3.2-fold when compared to the untreated and low dose treated NAg^R strains, while alternatively, expression levels of *katG* and another catalase-encoding gene *katB* (FQU82_03709) had increased by ~ 2.0 – 3.5-fold in the bacterium following high dose exposure[282]. No statistically significant expression change of *katB* was observed in NRLN in comparison to WTLN. Upregulation of both *katE* and *katG* have been previously reported to facilitate oxidative stress defence (in response to H_2O_2) in *A. baumannii*, with evidence suggesting that *katG* may evoke a more dominant scavenging role than *katE*[283]. Studies have highlighted that *katE* is typically expressed in response to lower cellular H_2O_2 levels, while *katG* is upregulated at higher H_2O_2 levels[281,283,284]. This could relate to the observed upregulation of *katG*, and potentially, the downregulation of *katE* in NRHN, as it is thought that higher NAg concentration exposure may lead to elevated oxidative stress, therefore demanding an increase in *katG* expression, with simultaneous *katE* downregulation. Moreover, the transcriptional regulator BfmR has been shown to positively regulate *katE* expression in *A. baumannii*[260]. As described earlier in the **general stress response** section above, no statistically significant change in *bfmR* expression levels was observed in NRHN, relative to NRNT and NRLN, which could be associated with the downregulation of *katE* seen in NRHN herein. Next, the gene *sodB* (FQU82_03463) was upregulated by ~ 3.0-fold in NRLN in comparison to WTLN. This genes encodes superoxide dismutase SodB which catalyses the dismutation of $O_2^{\bullet}$- radicals to molecular O_2 and H_2O_2[285]. The gene *ohrB* (FQU82_00671), which encodes the organic hydroperoxide resistance protein OhrB, was also upregulated in NRLN, relative to WTLN, by ~ 1.9-fold. OhrB, alongside the catalase enzymes, also helps control intracellular H_2O_2 levels[286]. Expression levels of *sodB* and *ohrB* were not further enhanced in response to higher NAg concentration, exhibiting statistically insignificant expression changes

in NRHN, relative to NRNT and NRLN. Taken together, it is reasonable to suggest that these identified oxidative stress response DEGs contribute to the improved ROS defence phenotype observed in the NAg^R strain, as described in **Section 4.6.3** (see **Figure 4.3**).

The resistant strain exhibited upregulation of a copper transport protein, which also was correlated to protection from silver-induced ROS stress, as similarly observed with the upregulation of *copA* and *copB* in the primary and advanced primary defence systems. The gene *actP* (FQU82_01385) increased in expression by ~ 5.7-fold in NLRN relative to WTLN, and even further by ~19.7-fold and ~ 55.7-fold in the high dose treated NAg^R strain when compared to NRNT and NRLN, respectively (**Figure 5.5**). This gene encodes a copper-transport P-type ATPase efflux pump (ActP), similar to that of CopA and CopB[287,288]. While less studied, it is hypothesised that ActP, like the above-mentioned copper efflux pumps, is also involved in silver efflux, as indicated by its higher extent of expression at higher NAg concentrations, and because of the chemical similarities between copper and silver. This upregulation may be linked to the detected increase in expression of *hmrR* (FQU82_01386) which encodes the heavy metal response transcriptional regulator HmrR, which was also upregulated by ~ 7.1 – 9.8-fold in NRHN compared to NRNT/NRLN. HmrR reportedly responds to excess copper presence and positively regulates expression of ActP[287]. It is hypothesised this may also occur in response to silver. Contrarily, expression change of this gene was insignificant in NRLN relative to WTLN, which might explain the lower observed expression increase of *actP* in the resistant strain when exposed to a lower NAg dose compared to higher concentrations.

The NAg^R strain also exhibited increased expression of a DNA repair gene (**Figure 5.5**). NAg dissolution is known to induce oxygen radical generation which can cause oxidative DNA damage in bacteria[94,98]. Oxygen radicals such as $^{\bullet}OH$ can target H-bonds in nucleotide base pairs, as well as sugar moieties in the sugar-phosphate backbone[289]. Upregulation of the gene *recA* (FQU82_02302), which encodes the DNA recombinase enzyme RecA, occurred in NRHN by ~ 1.9-fold when compared to NRNT and NRLN. While in NRLN, there was no statistically significant change in its expression in comparison to WTLN. The RecA enzyme is involved in homologous recombinational DNA repair in bacteria following DNA cleavage caused by oxidative stress and other stressors[290]. RecA upregulation has been shown to effectively confer

oxidative stress defence in various bacteria, including *A. baumannii*[291,292]. Studies have also indicated that upregulation of *recA* is regulated by the universal stress response system, which links to the observed upregulation of *uspA* in the NAg^R strain, as described earlier[293].

Evolutionary gene mutations – Comparative whole genome sequence analysis between the NAg^R and WT strains revealed that the resistant bacterium had evolved four single nucleotide mutations across three genes, including *smf1-2* (FQU82_02066)*, csuB* (FQU82_02552), and *rcsC* (FQU82_00629) as shown in **Table 4.1**. The gene *smf1-2* encodes the major fimbrial subunit SMF1, which mediates cell-to-surface attachment to initiate biofilm formation[217]. The RNA-Seq analysis was expected to offer deeper insight into the potential role of the mutation in this lesser studied gene (in *A. baumannii* biology) in the resistance phenotype, and more specifically, the enhanced biofilm-forming ability of the NAg^R strain as observed in **Chapter 4**[263]. However, it was found that expression of *smf1-2* was downregulated by ~ 2.6-fold in NRLN *versus* WTLN and exhibited no statistically significant expression changes in the high dose treated strain when compared to NRNT and NRLN (data not shown). These observations suggest that the single nucleotide deletional mutation (Ala129fs, **Table 4.1**) negatively affected the expression of the gene, which suggests that the gene mutation does not contribute to the increased biofilm-forming ability of the resistant strain.

Next, the gene *csuB*, which encodes the Csu pili biogenesis subunit CsuB, is part of the operon *csuA/BABCDE* which collectively code for Csu type 1 pili biogenesis – the most conserved biofilm-associated organelle in *A. baumannii*[218,263]. Two mutations (substitutional, Ala20Val; and insertional, Try19dup; **Table 4.1**) were detected in this gene. It was initially predicted that the increased biofilm-forming ability of the NAg^R strain was influenced by the *csuB* mutations[263]. However, transcriptomic analysis found that expression change of *csuB* was not statistically significant in NRLN when compared to WTLN (data not shown). This was also the case for the remaining genes in the operon (*csuA/B, A, C, D,* and *E*; data not shown). While in NRHN, *csuB* expression was in fact downregulated by ~ 4.3-fold and ~ 3.2-fold when compared to NRLN and NRNT, respectively. The expression of all other genes in the *csu* operon were also either downregulated by ~ 1.9 – 4.3-fold or statistically insignificant in the high dose treated bacterium relative to NRLN and NRNT. As observed with *smf1-2*, it

is likely that the two mutations to *csuB* correlate with the observed downregulation of gene, and that the mutations do not play a role in the enhanced biofilm-forming phenotype of the resistant strain.

The gene *rcsC* encodes the sensor histidine kinase RcsC, forming part of the Rcs pathway which regulates CPS synthesis. It was initially hypothesised that the detected substitutional mutation (Ser196Phe; see **Table 4.1**) to the *rcsC* gene could increase CPS production in the resistant strain, and in turn, contribute to its enhanced biofilm formation phenotype and cell surface defence against NAg targeting[215,263]. However, RNA-Seq analysis found no statistically significant changes in *rcsC* expression in NRLN (relative to WTLN) nor in NRHN (relative to NRNT and NTLN; data not shown). In turn, it appears that the substitutional mutation to *rcsC* did not alter its expression. Further transcriptomic analysis revealed that the expression changes of various *cps* cluster genes (likely regulated by the Rcs pathway), including *pgm, gpi, ugd, wza, wzb, wzx, wzy,* and *gna*, were either downregulated or statistically insignificant in all NRLN and NRHN pairwise comparisons (data not shown)[215,294]. Even so, these results do not contradict the earlier described upregulation of the CPS-associated stress response genes *otsA/otsB* in the resistant strain (see **general stress response** paragraph), as the latter genes are not reportedly regulated by the Rcs pathway. Overall, based on the RNA-Seq results herein, it was determined that *smf1-2*, *csuB* (and the remaining *csu* genes), and *rcsC* likely do not contribute to the evolved NAg defence in the resistant strain. Nonetheless, further studies are needed to fully rule out the contribution of these genes, and their respective stable mutations, to the resistance trait of the NAg^R bacterium.

In summary, the present RNA-Seq analysis revealed a variety of gene expression changes in NAg^R *A. baumannii* ATCC 19606 which have likely manifested as a result its evolutionary adaptation to prolonged NAg exposure. The data outlined herein has provided mechanistic insights into the evolved advanced primary and secondary NAg defence systems of the resistant bacterium. In **Section 5.3.1**, the toxicological response of the WT strain to NAg was investigated, which led to the identification of various upregulated primary defence mechanisms related to cell surface protection and oxidative stress defence. These mechanisms included OMPs, copper efflux pumps, and an oxidative stress response protein. Subsequently, the evolution of NAg resistance in ATCC 19606 led to the development of the advanced primary defence system. This

involved enhanced expression of majority of the primary defence-related genes in the resistant strain, highlighting the significance of these intrinsic 'first tier' defence mechanisms in ATCC 19606 against NAg toxicity. The resistant strain also exhibited a secondary defence system, not seen in the WT strain. In addition to various general stress responses, the resistant strain upregulated several cell surface protection and oxidative stress defence mechanisms, the latter of which includes ROS scavengers. Expression levels of most defence genes in the resistant bacterium increased with increasing NAg doses. Importantly, upregulation of several secondary defence-related genes was correlated to the observed enhancement in biofilm formation and oxidative stress defence of the resistant strain as reported in **Chapter 4**. There was a notable absence of statistically significant DEGs in NRLN relative to NRNT. This may suggest that the evolved bacterium has experienced permanent physiological change, resulting in stable genetic modifications which are expressed even in the absence of silver. This concept will be further examined in the subsequent section.

5.3.3 Physiological change between WT and NAg^R *A. baumannii* ATCC 19606

5.3.3.1 Comparative growth rate of untreated WT and NAg^R ATCC 19606

Comparisons of growth rate between the WT and NAg^R strains in the absence of NAg exposure (untreated) were also performed prior to the transcriptomic study. This was to rule out any stable growth rate changes in the NAg^R strain which might exhibit even without NAg pressure. The growth rate of untreated WT *A. baumannii* (0.603/h) was found to be comparable to that of the untreated NAg^R strain (0.608/h, **Figure 5.6**). Therefore, the growth behaviour of the NAg^R strain did not appear to be altered by prolonged NAg exposure during the sequential passage evolution study.

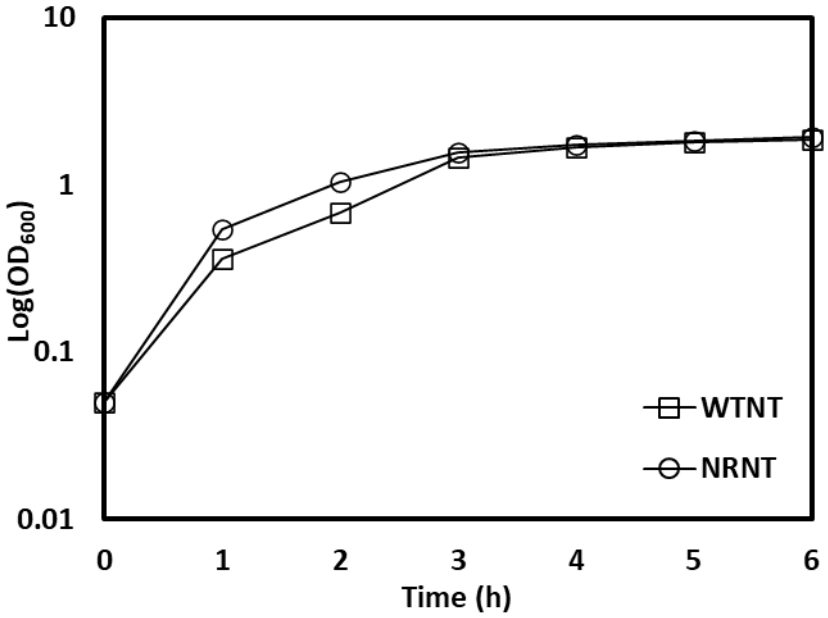

Figure 5.6 Comparative growth rates of untreated (no NAg) WT and NAg^R ATCC 19606 strains over 6 h. WTNT = wild-type no treatment (square); NRNT = NAg-resistant no treatment (circle). RNA was extracted at the 2.5 h time point. Initial OD_{600} at time 0 began at 0.05. Each data point represents mean of at least two biological replicates.

5.3.3.2 Differentially expressed genes between untreated WT and NAg^R ATCC 19606

As discussed in **Chapter 4**, the NAg^R strain had undergone genetic and phenotypic modifications which are thought to contribute to its NAg resistance trait. Therefore, it was important to conduct a comparative transcriptomic analysis between the WT and NAg^R strains when in optimal conditions. More specifically, the objective was to identify stable alterations in gene expression (or DEGs) that had occurred in the NAg^R strain due to prolonged (30-day) NAg exposure and assess whether these expression patterns persisted in the absence of NAg. The transcriptomic profiles of the untreated NAg^R strain (NRNT) relative to the untreated WT strain (WTNT) were compared to gain insight into potential physiological modifications undergone by resistant ATCC 19606. See **Section 3.9.5** for cut-off threshold values which define a differentially expressed gene (DEG) between the pairwise comparisons. Refer to **Table A1** in the appendix for complete gene ontology analysis of DEG data of untreated WT and NAg^R ATCC 19606.

In total, 1314 statistically significant DEGs were detected in NRNT when compared to WTNT. Interestingly, an equivalent number of upregulated and downregulated genes were present at 657 each (**Table 5.3**). These DEGs were detected in the NAg^R strain even in the absence of NAg exposure and demonstrates that the bacterium experienced significant stable genomic modification due to prolonged silver exposure.

Table 5.3 Number of DEGs (upregulated and downregulated genes) identified in untreated NAg^R *A. baumannii* (NRNT) in comparison to untreated WT *A. baumannii* (WTNT).

Comparison	Upregulated	Downregulated	Total
NRNT *versus* WTNT	657	657	1314

The DEGs identified in **Section 5.3.2**, hypothesised to contribute to the advanced primary and secondary defence systems of NAg^R ATCC 19606, will be the focus of this section. In addition, potential expression changes in the mutated genes of interest described in **Chapter 4**, specifically *rcsC, smf1-2,* and *csuB,* will also be examined. Although these genes were not upregulated in the NAg^R strain when treated with the nanoparticle (see **Section 5.3.2.3.2**), their potential contribution to the altered physiology of the resistant bacterium needed to be investigated. Overall, the objective of this analysis was to confirm if any identified resistant defence mechanisms are permanently expressed in the NAg^R bacterium even in the absence of NAg pressure, demonstrating that the silver-adapted ATCC 19606 strain has undergone stable evolutionary physiological change.

5.3.3.3 Physiological change due to NAg

The following section sought to decipher which genes involved in the advanced primary and secondary defence systems of the NAg^R strain, as described in **Section 5.3.2.3**, were persistently expressed even in the absence of NAg stress. The upregulated genes linked to the primary and advanced primary defence systems in the WT and NAg^R strains, respectively, encoded OMPs for cell surface protection, copper efflux pumps, and an oxidative stress response protein. The gene expression changes

only observed in the resistant strain, which were correlated to the secondary defence system of the bacterium, were, in addition to general stress responses, thought to also be involved in cell surface protection and oxidative stress defence, the latter of which involves a copper efflux pump and ROS scavengers. Of the 27 DEGs associated with the advanced primary and secondary defence responses of NAg^R ATCC 19606, 20 of these genes were constitutively upregulated in bacterium even in the absence of silver (**Figure 5.7**). It should be noted that the growth rate of the resistant strain was found to be comparable to that of the WT strain (see **Figure 5.6**), which suggests the absence of compensatory mechanisms (as fitness costs), sometimes observed with other antibiotic adaptation phenomena in bacteria[295].

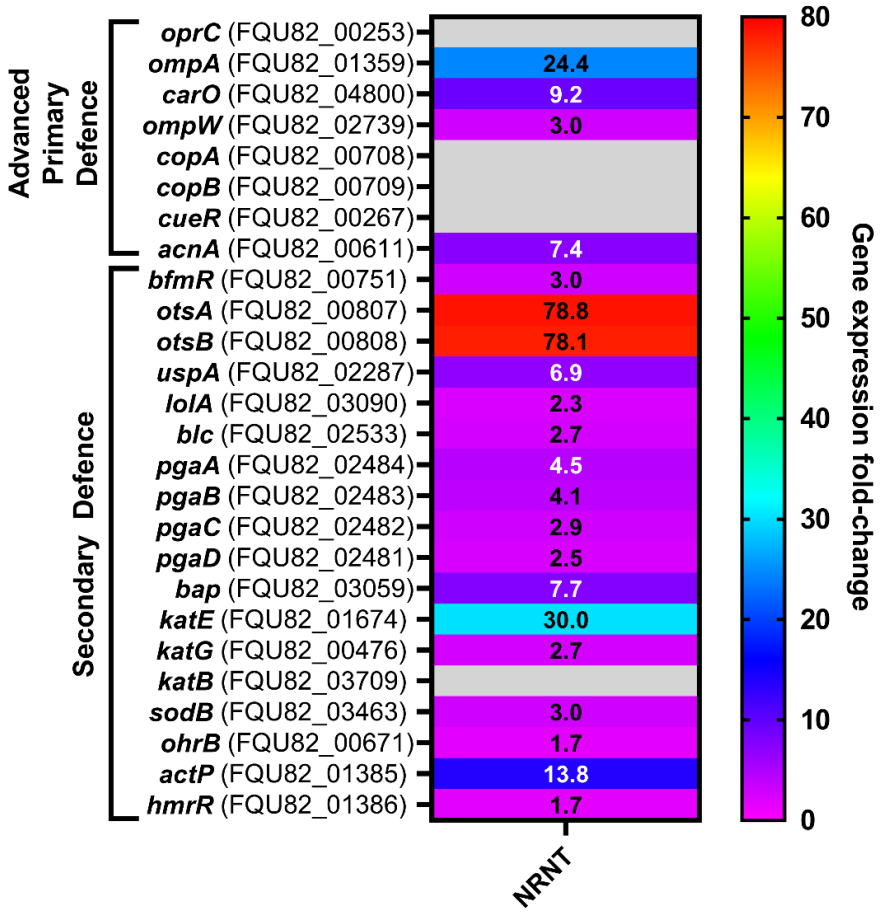

Figure 5.7 Differentially expressed genes (DEGs) identified in NAg^R *A. baumannii* ATCC 19606 which manifest under optimal conditions (no NAg present). Heat-map represents expression fold-change in genes of interest hypothesised to contribute to the advanced primary and secondary NAg defence systems of the resistant strain. Grey cells indicate statistically insignificant DEGs. Pairwise comparison: NRNT *versus* WTNT.

Relative to the untreated WT strain, the RNA-Seq analysis revealed that four out of the eight primary/advanced primary defence-related DEGs remained stably upregulated in the untreated NAg^R strain (**Figure 5.7**). These included *ompA* (~ 24.4-fold), *ompW* (~ 3.0-fold), *carO* (~ 9.2-fold), and *acnA* (~ 7.4-fold). Upregulation of the OMP-related genes *ompA, ompW,* and *carO* are thought to contribute to improved biofilm-forming activity, which is consistent with the higher extent of biofilm formation observed in the resistant strain, relative to the WT, when in the absence of NAg, as demonstrated in **Figure 4.2**[250,263,296,297]. While stable upregulation of *acnA* aligns with the observed enhancement in NAg-mediated oxidative stress defence in the NAg^R strain (see **Figure 4.3**). Contrarily, changes in expression of *oprC*, *copA, copB,* and the copper response regulator *cueR,* were found to be statistically insignificant in NRNT in comparison to WTNT. It is reasonable to deduce that increased expression levels of the latter genes contribute to the 'active' defence responses of the resistant bacterium and are hence only upregulated when in the presence of NAg, as observed in both the WT and resistant strains (**Figure 5.4**).

The genes indicated to contribute to the secondary NAg defence system of the resistant bacterium encoded mechanism associated with general stress responses, physical cell surface protection, and oxidative stress defence through ROS scavenging and copper efflux, as well as DNA repair (see **Section 5.3.2.3.2**). These observations suggest that the NAg^R strain is equipped with a more sophisticated defence response to the nanoparticle compared to the WT bacterium, and these defence mechanisms could be physiologically stable as part of the resistance trait. Firstly, recalling the general stress responses observed in the resistant bacterium, the untreated NAg^R strain exhibited upregulation of the regulatory transcription factor gene *bfmR* by ~ 3.0-fold, and indeed, the two trehalose synthesis genes *otsA* and *otsB* (expressions are regulated by BfmR) by ~ 78.1 – 78.8-fold, relative to WTNT (**Figure 5.7**). As discussed earlier, it is hypothesised that the stable upregulation of *otsA/otsB* might improve CPS density, contributing to improved biofilm formation phenotype and cell capsule defence against NAg-mediated ROS activity[238,266,267]. BfmR is known to also regulate expression of the stress response gene *acnA*, which is consistent with earlier mentioned stable upregulation of the latter gene in the untreated resistant strain[260]. Increased expression of the universal stress protein gene *uspA* (~ 6.9-fold) was also noted in NRNT relative to WTNT.

Regarding the secondary defence physical cell surface protection mechanisms, the NAg^R strain exhibited upregulation of all previously described genes when in the absence of NAg (**Figure 5.7**). The two lipoprotein-carrier protein-encoding genes *lolA* and *blc* were upregulated by ~ 2.3-fold and ~ 2.7-fold, respectively, relative to WTNT. Likewise, the biofilm-associated genes *pgaABCD* were upregulated by ~ 2.5 – 4.5-fold, along with the gene *bap*, which increased in expression by ~ 7.7-fold in NRNT compared to WTNT. The upregulation of these latter biofilm-related genes is again linked to the observed physiologically enhanced biofilm-forming ability of the NAg^R bacterium, as shown in **Figure 4.2**.

Nearly all genes involved in the secondary oxidative stress defence response were also stably upregulated in the untreated NAg^R bacterium (**Figure 5.7**). Expression of the catalase hydroperoxidase genes *katE* and *katG* increased by ~ 30.0-fold and ~ 2.7-fold, respectively in NRNT relative to WTNT, while contrarily, *katB* expression change was statistically insignificant. Upregulation of the superoxide dismutase gene *sodB* and the organic hydroperoxide resistance protein gene *ohrB* also increased by ~ 3.0-fold and ~ 1.7-fold in NRNT compared to WTNT. The untreated NAg^R strain also exhibited upregulation of the copper efflux gene *actP*, as well as its transcriptional regulator gene *hmrR*, by ~ 13.8-fold and ~ 1.7-fold, respectively, relative to WTNT. Recalling the statistically insignificant changes in expression of the other copper efflux pumps, *copA* and *copB*, and their response regulator *cueR*, in NRNT, the subsequent upregulation of *actP* and *hmrR* herein is intriguing. Studies have reported permanent expression of efflux pumps in bacteria previously, which has been attributed to changes in expression levels (and/or due to mutation) of their respective response regulators, as indicated herein[298,299]. Though no mutation to any response regulator genes was observed in the present work. Taken together, it is evident that the resistant strain has evolved an inherent oxidative stress defence system which manifests even in the absence of NAg pressure. This aligns with the improved NAg-mediated ROS defence observed in the resistant strain in **Figure 4.3**. No statistically significant change in expression of *recA* was noted in untreated resistant strain relative to the untreated WT strain. It is hypothesised that upregulation of the DNA recombinase gene also occurs only in response to NAg presence, as observed in the high dose treated NAg^R strain in **Figure 5.5**. Lastly, no statistically significant expression changes were identified in the mutated genes *rcsC* and *csuB* in NRNT relative to WTNT, while a ~

2.4-fold downregulation was detected in *smf1-2* (data not shown). Despite this, as highlighted earlier, further studies are required to elucidate the roles of the genes and their stable mutations in the resistant trait of NAg^R ATCC 19606.

The findings reported in this section have ultimately given insight into how NAg^R *A. baumannii* ATCC 19606 physiologically transformed at the transcriptomic level because of its evolutionary adaptation to the nanoparticle. This section aimed to determine which of the advanced primary and secondary NAg defence-associated genes were permanently upregulated in the resistant strain even in optimal conditions (without NAg pressure). It was found that majority of the evolved defence mechanisms identified in **Section 5.3.2.3**, including those linked to the general stress response, physical cell surface protection, and the oxidative stress response, were stably upregulated in the untreated NAg^R strain. Defence mechanisms that exhibited no statistically significant expression change were thought require the presence of NAg to be activated/upregulated. Notably, several defence-related genes correlated to biofilm formation and oxidative stress defence were stably upregulated in the bacterium, even in the absence of NAg pressure. These results aligned with the enhanced biofilm-forming and NAg-mediated ROS defence phenotypes observed in the resistant strain in **Chapter 4**. Ultimately, it can be concluded that the stable increase in expression of defence-associated genes in the untreated NAg^R strain are intrinsically linked to the nanoparticle resistance trait following evolutionary adaptation. As a reminder, no changes in expression of the mutated genes identified in **Section 4.6.2** were noted in the NAg^R strain (under both NAg stress and when in optimal conditions). Thus, at this stage, these mutated genes do not appear to contribute to the evolved NAg resistance trait.

5.4 Chapter conclusion

Whole transcriptomic analysis of NAg^R *A. baumannii* ATCC 19606 revealed an abundance of gene expression changes which are indicated to contribute to the evolved nanoparticle resistance phenotype.

RNA-Seq analysis of the WT strain, treated with sub-lethal (or low) NAg doses, identified several upregulated genes as a part of its toxicological response, which

encode mechanisms hypothesised to contribute to the primary NAg defence system. These mechanisms included OMPs which confer physical cell surface protection, as well as two copper efflux pumps and a citric acid cycle homeostasis protein, which were linked to oxidative stress defence. Further RNA-Seq analysis found that majority of the primary defence mechanisms were enhanced in the NAg^R strain, which were linked to the evolved advanced primary defence system, highlighting the importance of these intrinsic 'first tier' NAg defence mechanisms in ATCC 19606.

Further transcriptomic analysis of the NAg^R strain following exposure to low and high NAg concentrations identified several upregulated defence-related genes which were distinct from the WT strain. These upregulated genes were indicated to contribute to the evolved secondary defence system of the resistant strain, which likely developed following prolonged NAg exposure. The encoded secondary defence mechanisms encompassed cell surface protection and biofilm formation, oxidative stress defence *via* a copper efflux pump and ROS scavengers, as well as recombinational DNA repair. In addition, the analysis revealed that even in the absence of NAg pressure (*i.e.* in optimal growth conditions) the resistant bacterium exhibited upregulation of most advanced primary and secondary defence-related genes. This indicated that the resistant strain had experienced permanent physiological change because of its evolutionary adaptation to NAg. Notably, various upregulated defence-related genes associated to biofilm formation and the oxidative stress response, were indicated to contribute to the respective phenotypic changes of the resistant strain as observed in **Chapter 4**. The RNA-Seq analysis also demonstrated that the mutated genes (*rcsC, smf1-2, csuB*; see **Table 4.1**) were either downregulated or exhibited no statistically significant expression change in the resistant bacterium, suggesting that the mutations negatively affected expression or had no notable transcriptional effect. At this stage, this indicates that the mutated genes played no role in the evolved NAg defence response of the resistant strain. See **Figure 5.8** below for a combined heat-map summary of all primary/advanced primary and secondary NAg defence-related DEGs identified in this RNA-Seq study.

The work herein reported the first known evidence of NAg resistance development in *A. baumannii* (ATCC 19606) following prolonged exposure, as well as the first known transcriptomic assessment of NAg-treated *A. baumannii*[263]. Even so, there remains several knowledge gaps and unclear hypotheses regarding the mechanistic function/s

of the NAg resistance phenomenon. It is therefore critical that follow-up work is performed to validate these proposed defence and resistance mechanisms. Reverse transcriptase quantitative PCR (RT-qPCR) is a useful tool to validate RNA-Seq data. However, inquiries have highlighted that RNA-Seq methods alone are often robust enough for whole transcriptomic analysis[300,301]. Valuable follow-up studies could include whole proteomic and metabolomic assessments. This would help gain better mechanistic insight into the function and regulation of the bacterium defence systems at the protein and metabolite levels[302,303]. Furthermore, confirming the link between an upregulated gene (and its encoded protein) and a particular NAg resistance mechanism in the resistant strain can be executed through gene editing/knockout methods[304]. Alternatively, utilisation of Transposon Directed Insertion Sequencing or TraDIS is another useful technique to complement RNA-Seq data. This technique helps identify essential and non-essential genes, including those that confer bacterial survival advantages under desired environmental conditions, *i.e.* defence-related genes against NAg toxicity[305]. Furthermore, phenotypic studies, such as super resolution microscopy, can help visualise physical changes in cell surface (*e.g.* outer membrane and CPS density) or biofilm structures of the adapted bacterium[306,307].

The RNA-Seq investigation presented in this study has yielded a plethora of compelling findings which contribute to better understanding the underlying molecular basis of NAg resistance in *A. baumannii* ATCC 19606. The knowledge generated has the potential to advance scientific comprehension of bacterial nanoparticle defence mechanisms. Equally this knowledge emphasises the importance of implementing effective management strategies for proper NAg usage and disposal to maintain the successful long-term utilisation of this valuable alternative antimicrobial agent in the long-term. The findings from this study may also aid in the development of more effective nanoparticle antimicrobials to mitigate the risks of bacterial adaptation in the future.

In **Chapter 4**, ATCC 19606 also developed a tolerance trait to Ag^{+} following prolonged exposure. **Chapter 6** will delve into the transcriptomic analysis of the Ag^{+}-tolerant (Ag^{+T}) bacterial to elucidate potential evolved Ag^{+} defence mechanisms. Due to the distinct adaptation traits of the NAg^{R} and Ag^{+T}, it was expected that unique and diverse gene expression patterns which contribute to the defence capabilities of tolerant bacterium would be identified. However, while the nanoparticulate and ionic

forms of silver exert distinct antibacterial mechanisms, they do share similar toxicity paradigms, and it was therefore anticipated that overlapping defence traits between the silver-adapted strains would be observed.

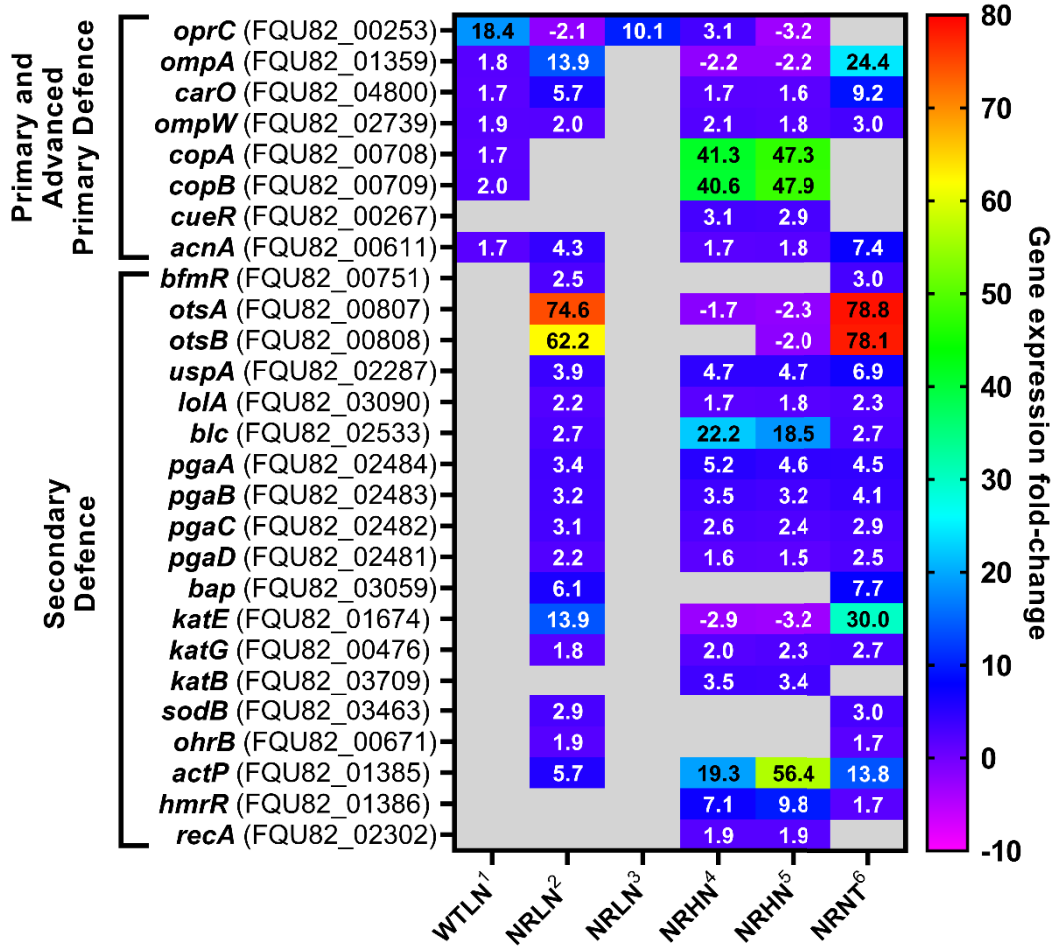

Figure 5.8 Combined heat map of primary, advanced primary, and secondary NAg defence-associated DEGs identified in WT and NAg^{R} ATCC 19606. Grey cells indicate statistically insignificant DEGs. Pairwise comparisons: [1] WTLN *versus* WTNT, [2] NRLN *versus* WTLN, [3] NRLN *versus* NRNT, [4] NRHN *versus* NRNT, [5] NRHN *versus* NRLN, [6] NRNT *versus* WTNT.

Chapter 6: Toxicological and Defence Responses and Physiological change to Ag^+

6.1 Chapter summary

As discussed in **Chapter 2**, Ag^+ resistance traits have been previously identified in *A. baumannii*, and bacterial resistance to Ag^+ alone has been recognised for some time. However, no such studies had previously shown *A. baumannii* to exhibit a tolerance trait to the cations following prolonged *in vitro* exposure, until first demonstrated in the work presented in **Chapter 4**. This identified tolerance trait was associated with changes in biofilm formation and the oxidative stress response, predicated to be correlated to unique genetic mutations. The work presented in this Chapter details an analysis of the transcriptomic profile of Ag^{+T} *A. baumannii* ATCC 19606, in comparison to the WT bacterium. This analysis was aimed to identify defence mechanisms developed against Ag^+ toxicity and to shed light on the physiological changes because of adaptation in the bacterium. Initial RNA-Seq analysis of the WT bacterium revealed an abundance of gene expression changes following exposure to low (sub-lethal) Ag^+ concentrations. The upregulated DEGs identified were indicated to encode mechanisms that confer 'first tier' defence against Ag^+ toxicity, including physical cell surface protection and active removal *via* copper and antibiotic efflux pumps. These toxicological responses of the WT strain collectively contribute to what is defined herein as the **primary defence system**. Like that of the NAg^R strain, it was anticipated that these same primary Ag^+ defence-related mechanisms would be enhanced in the Ag^{+T} strain, as part of its **advanced primary defence system**. Notably, expression patterns of the identified DEGs were varied in the tolerant strain and appeared to be concentration-dependant. Nevertheless, an assortment of other upregulated genes, unique to the tolerant strain, encoding mechanisms thought to facilitate the general stress response, physical cell surface defence, and active cation removal and counteraction, which were collectively linked to the **secondary defence system**. These upregulated genes included two genes that were mutated by prolonged Ag^+ exposure. These secondary defence mechanisms were unique to the evolved bacterium (*i.e.* not identified in the WT strain) which suggested they likely manifested

as a result of evolutionary adaptation. Under optimal conditions (without Ag^+ stress), the transcriptomic analysis revealed that many of the advanced primary and secondary defence-associated genes remained stably upregulated in the tolerant bacterium. This indicated that ATCC 19606 had experienced physiological modification in response to long-term Ag^+ treatment. It was concluded that these permanently upregulated defence-associated genes were now intrinsically involved in the Ag^+ tolerance trait, and were predicted to contribute to the observed changes in biofilm formation, respiratory activity, and (potentially) morphology, as earlier observed in **Chapter 4**.

6.2 Introduction

With the expanding and often indiscriminate use of silver antimicrobials, there is increasing concern over the generation of silver-resistant bacteria. In **Chapter 2**, it was established that the development of bacterial NAg resistance is possible and not species specific – as subsequently demonstrated with *A. baumannii* ATCC 19606 in **Chapter 4**[29-32]. Likewise, there is sufficient evidence showcasing the emergence and prevalence of endogenous and exogenous Ag^+ resistance traits across a variety of bacterial species[65,141,142,150,159]. Previous studies have identified plasmid-oriented Ag^+ resistance acquisition in other *A. baumannii* strains, but the work presented in **Chapter 4** revealed the first evidence of Ag^+ tolerance development in this species following long-term exposure. The tolerance trait was complemented by various single nucleotide gene mutations and correlated to physiological changes in biofilm-formation and oxidative stress defence. Successively, the aim of this Chapter was to characterise the molecular basis of this tolerance phenotype at the transcriptomic level, to gain clearer insight into the mechanistic function of defence against Ag^+ toxicity.

Transcriptomic profiling of Ag^+-treated bacteria has been performed using RNA-Seq previously, and these studies have identified a variety of potential Ag^+ defence-associated DEGs[239,261]. However, no RNA-Seq analyses of *A. baumannii* when exposed to Ag^+ have been previously published, making this a novel study. This work was intended to form links between changes in gene expression and potential Ag^+ defence mechanisms. In **Chapter 5**, NAg^R ATCC 19606 was found to exhibit an abundance of gene expression changes which were correlated to various NAg-specific defence mechanisms. Due to the complex nature of tolerance, relative to resistance, it

was anticipated the Ag^{+T} bacterium would exhibit more unique gene expression patterns compared to that of the NAg^{R} strain.

Whole transcriptomic analysis of WT ATCC 19606 treated with low doses of Ag^{+} revealed various gene expression changes linked to the toxicological response of the bacterium, which represented the 'first tier' primary defence system. RNA-Seq assessment of the Ag^{+T} strain, exposed to both low and high Ag^{+} concentrations, demonstrated a distinct shift in gene expression. The primary defence-associated genes were further upregulated in the tolerant strain as part of its advanced primary defence response, but expression patterns were dependent on Ag^{+} concentration. Further analysis of the tolerant bacterium revealed DEGs that were unique to the strain and were suggested to encode Ag^{+} tolerant-specific mechanisms as part of its secondary defence system. These mechanisms encompassed general stress responses, physical cell surface protection, and active cation removal and counteraction, these of which also appeared to be concentration-dependant. Notably, even in the absence of Ag^{+} pressure, the Ag^{+T} strain maintained stable expression of several advanced primary and secondary Ag^{+} defence-related genes, which is indicative of permanent physiological change due to adaptive evolution.

6.3 Results and Discussion

6.3.1 Toxicological response of WT *A. baumannii* ATCC 19606 to Ag^{+}

6.3.1.1 Comparative growth rate of untreated and Ag^{+}-treated WT ATCC 19606

A comparison of growth rates between Ag^{+}-treated and untreated (no Ag^{+}) WT *A. baumannii* ATCC 19606 was performed prior to transcriptomic analysis to determine the effective working concentrations (sub-MIC or low) of Ag^{+} needed to induce a toxicological response in the bacterium while not disrupting growth behaviour (see **Table 3.2**). This was to exclude any potential gene expression changes exhibited because of growth rate changes. The growth profiles between the untreated (0.603/h) and Ag^{+}-treated (0.585/h) WT strain were overall similar, but there was an slight disturbance in growth of the WT strain following addition of low Ag^{+} dose (0.5 µg/mL; 0.5 x MIC) at the 2 h mark (**Figure 6.1**). However, growth rates between the two cultures within the 30 min exposure time (2 – 2.5 h, *i.e.* prior to RNA extraction) was found to be comparable (see inset plot). Therefore, the working concentration of

Ag^+ needed to elicit a toxicological response in the WT strain was determined to be 0.5 x MIC of Ag^+ (or 0.5 µg/mL).

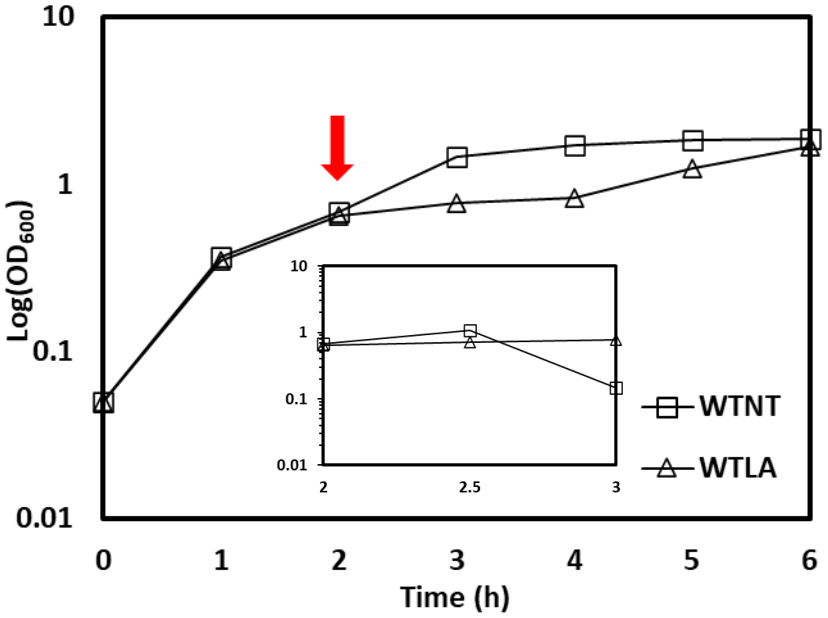

Figure 6.1 Comparative growth rates of WT ATCC 19606 strain when treated with low Ag^+ concentration (1 µg/mL; 0.5 x MIC) and untreated (no Ag^+) WT ATCC 19606 over 6 h. WTNT = wild-type no treatment (square); WTLA = wild-type low Ag^+ (triangle). The red arrow indicates the time point (2 h) at which NAg was added to culture. RNA was extracted 30 min (2.5 h time point) following addition of Ag^+. The inset plot displays an expanded time range from 2 – 3 h to show the closely comparable growth profiles of the untreated and treated bacterium. Initial OD_{600} at time 0 began at 0.05. Each data point represents mean of at least two biological replicates.

6.3.1.2 Differentially expressed genes in Ag^+-treated WT ATCC 19606

As discussed, the WT bacterium was treated with a 0.5 x MIC dose of Ag^+ for 30 min to induce a toxicological response prior to RNA extraction. The low dose Ag^+-treated WT strain (hereafter referred to as Wild-Type Low Ag^+; WTLA) was compared to that of its untreated counterpart (hereafter referred to as Wild-type No Treatment; WTNT) to examine gene expression changes in response to Ag^+ toxicity. See **Section 3.9.5** for cut-off threshold values which define a differentially expressed gene (DEG) between

the pairwise comparisons. Refer to **Table A2** in the appendix for complete gene ontology analysis of DEG data of Ag^+-treated WT ATCC 19606.

RNA-Seq analysis of WTLA revealed a total of 124 DEGs relative to WTNT (**Table 6.1**). Of these 124 transcripts, 71 genes were upregulated, while 53 genes were downregulated. Interestingly, there was a greater occurrence of DEGs detected in the Ag^+ treated WT strain in comparison to the NAg-treated WT bacterium (see **Table 5.1** in **Section 5.3.1.2**). It is generally understood that Ag^+ is more reactive and exerts broader antibacterial mechanisms than the nanoparticle alone, particularly because the physicochemical properties NAg and its surrounding aqueous environment influences its toxicity[85,86]. The cations are also known to actively react and bind with DNA more readily than NAg particulates, which could perhaps result in greater gene modifications and subsequent transcriptional alterations at sub-lethal Ag^+ concentrations[33,100]. Also, as shown in **Figure 4.1**, the MIC of NAg was determined to be lower than that of Ag^+ against WT ATCC 19606, which means the total silver content exposed to the WT strain was greater when treated with sub-lethal Ag^+. This may be indicative of the diverse gene expression patterns to allow the bacterium to cope with higher silver content.

Table 6.1 Number of DEGs (upregulated and downregulated genes) identified in WT *A. baumannii* ATCC 19606 treated with 0.5 x MIC dose of Ag^+ (WTLA) in comparison to untreated WT ATCC 19606 (WTNT).

Comparison	Upregulated	Downregulated	Total
WTLA *versus* WTNT	71	53	124

Like the RNA-Seq study conducted on the WT and NAg^R strains (see **Chapter 5**), comprehending the biological significance of all DEGs involved in the toxicological response of the WT strain to Ag^+ presents significant challenges. Thus, this study also focussed on gene expression changes which can be correlated to antimicrobial defence responses. Also, because nearly all downregulated genes were found to encode either uncharacterised proteins or proteins not associated with antimicrobial defence, only the potential roles of upregulated genes in Ag^+ defence were examined. It was expected

that crossovers in gene expression (and encoded mechanisms) would be identified between the NAg-treated and Ag^+-treated bacterium, because of known overlaps in antibacterial activity of the silver agents. Again, due to the scale of this study and limited prior knowledge, elucidating the global transcriptional profile of ATCC 19606 in response to cationic silver will require further investigation beyond this work. This is essential considering that no RNA-Seq analysis of Ag^+-treated *A. baumannii* has been performed previously.

6.3.1.3 Toxicological responses to Ag^+

In **Chapter 2** and **Chapter 4**, the antibacterial activity of Ag^+ was discussed. In general, most studies highlight that inactivation of the inner membrane respiratory chain and damage to intracellular biomolecules (*e.g.* proteins, lipids, DNA), either through ROS generation or direction interaction with Ag^+, are among the main mechanisms of action of the cation[93,150,223]. Analysis of the 124 DEGs detected in WTLA relative to WTNT revealed several notable gene expression changes, which are indicated to contribute to the toxicological response of ATCC 19606 against Ag^+. Of the 71 identified upregulated genes, 13 genes were indicated to play a role in the intrinsic **primary defence system** of ATCC 19606 to Ag^+ toxicity (**Figure 6.2**). These 13 upregulated genes were hypothesised to confer physical cell surface protection to Ag^+ intrusion and active cation efflux. Importantly, several of these defence mechanisms were also linked to the primary/advanced primary NAg defence systems of WT and NAg^R ATCC 19606.

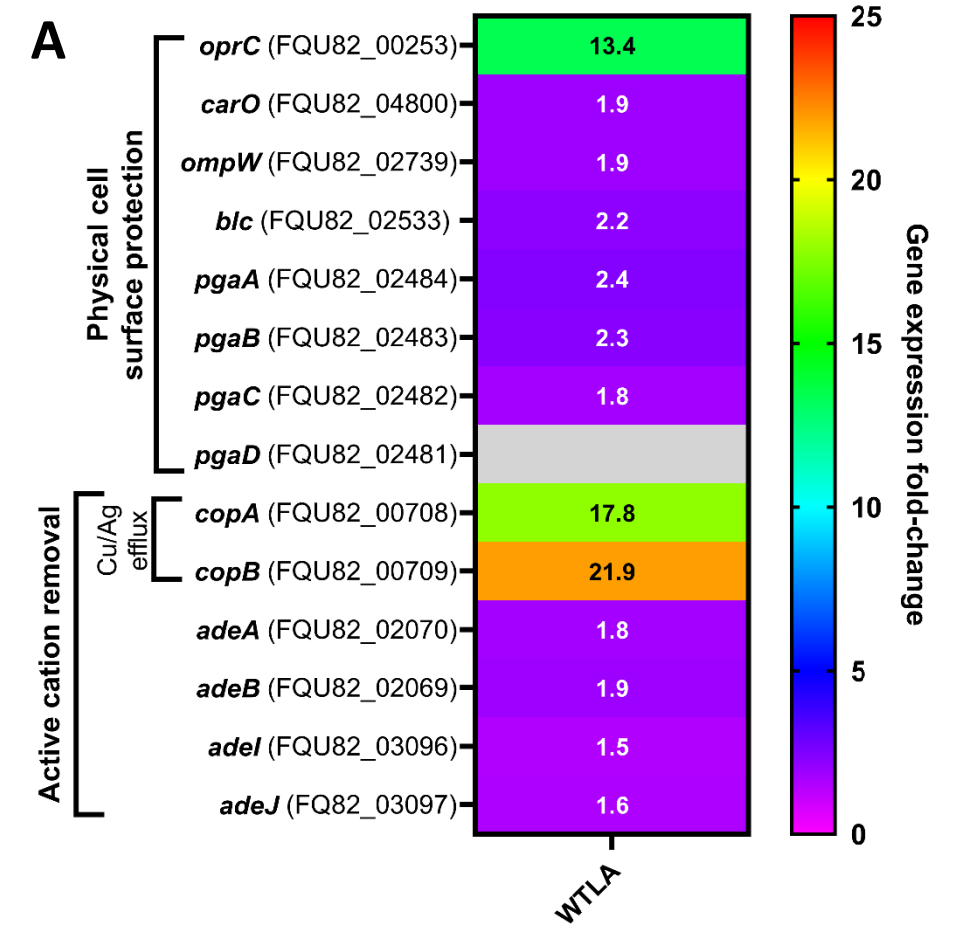
A
oprC (FQU82_00253)
carO (FQU82_04800)
ompW (FQU82_02739)
blc (FQU82_02533)
pgaA (FQU82_02484)
pgaB (FQU82_02483)
pgaC (FQU82_02482)
pgaD (FQU82_02481)
copA (FQU82_00708)
copB (FQU82_00709)
adeA (FQU82_02070)
adeB (FQU82_02069)
adeI (FQU82_03096)
adeJ (FQ82_03097)
13.4
1.9
1.9
2.2
2.4
2.3
1.8
17.8
21.9
1.8
1.9
1.5
1.6
Physical cell surface protection
Active cation removal
Cu/Ag efflux
WTLA
25
20
15
10
5
0
Gene expression fold-change

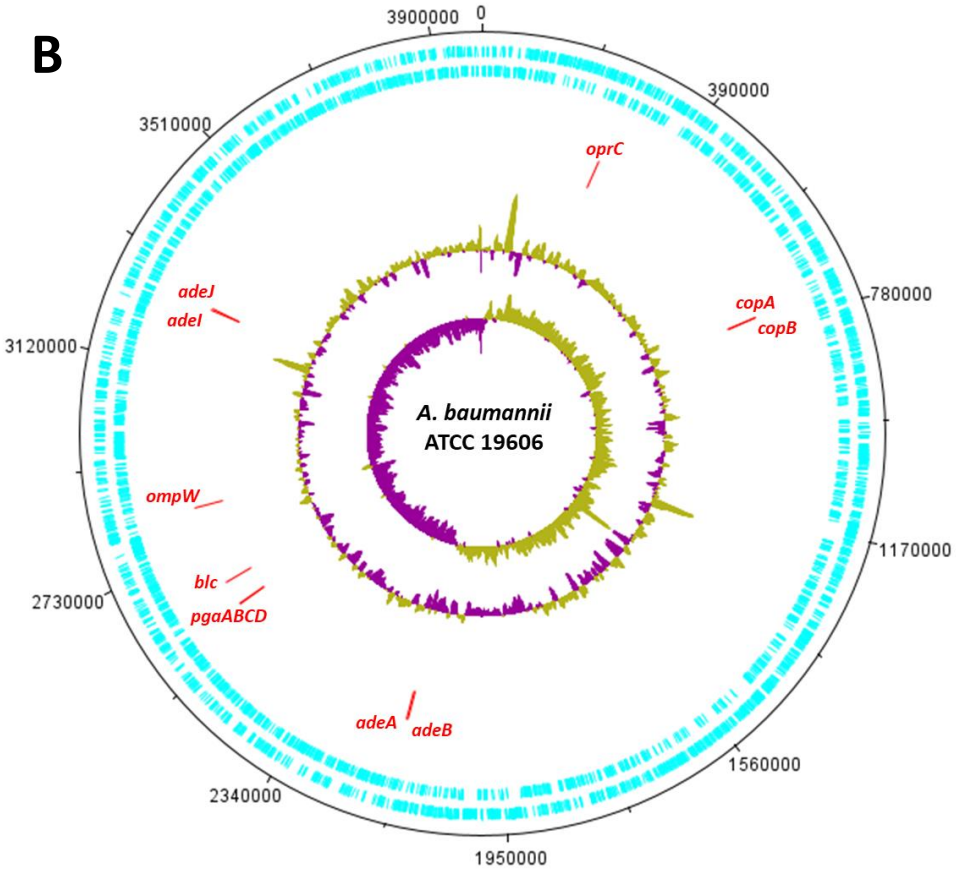
B
3900000
0
390000
780000
1170000
1560000
1950000
2340000
2730000
3120000
3510000
oprC
copA
copB
adeJ
adeI
ompW
blc
pgaABCD
adeA
adeB
A. baumannii
ATCC 19606

Figure 6.2 Differentially expressed genes (DEGs) identified in WT *A. baumannii* ATCC 19606 in response to low (sub-lethal) Ag^+ doses. (**A**) Heat-map representing expression fold-change in genes of interest hypothesised to contribute to the primary Ag^+ defence system of the WT strain. Grey cells indicate statistically insignificant DEGs. Pairwise comparison: WTLA *versus* WTNT. (**B**) Map of *A. baumannii* ATCC 19606 chromosome indicating sequence positions of DEGs of interest. Forward and reverse reading frames are shown by the cyan-coloured bars. The two internal rings indicate the chromosome's GC skew (the innermost ring) followed by the chromosome's GC content.

Several upregulated genes were indicated to encode physical cell surface protection mechanisms to Ag^+ in the WT bacterium (**Figure 6.4**). Firstly, the gene *oprC* was upregulated by ~ 13.4-fold in the WT bacterium following exposure to low dose Ag^+, relative to its untreated counterpart. Upregulation of this gene was also noted in the NAg-treated WT strain (WTLN) in **Section 5.3.1.3**. As described earlier, *oprC* encodes the putative outer membrane copper receptor OprC which was predicted to confer cross-defence between Cu^+ and Ag^+ *via* periplasmic sequestration, due to isoelectronic similarities between the heavy metal ions[208,239,243-245]. Two OMP-encoding genes, *carO* and *ompW*, were also upregulated by ~ 1.9-fold in WTLA in comparison to WTNT. Increased expression levels of these genes were also noted in the WTLN samples, with studies correlating upregulation of these genes to enhanced OM integrity, as well as biofilm formation[248,297]. These mechanisms, along with cation sequestration by OprC, are thought to protect the WT bacterium from Ag^+ targeting and intracellular diffusion.

Another OM-associated gene, *blc*, was also upregulated by ~ 2.2-fold in WTLA relative to WTNT. The encoded protein Blc is a lipoprotein-carrier lipocalin, which delivers newly synthesised lipoproteins to the OM to assist in membrane biogenesis or repair in response to environmental stress[273,274]. This mechanism is thought to strengthen the OM and behave as a physical barrier against Ag^+ penetration. Studies have also correlated enhanced lipoprotein transport to multi-drug resistance[308]. This mechanism may help provide a physical barrier to Ag^+ penetration through the OM. Various biofilm-associated genes were also upregulated in the low Ag^+ dose treated WT bacterium. Three genes which compose the *pga* locus, specifically *pgaA, pgaB,*

and *pgaC*, were upregulated by a range of ~ 1.8 – 2.4-fold, while no statistically significant expression change of the final gene *pgaD* was noted. Upregulation of these genes in the secondary defence system of the NAg^R strain also occurred (refer to **Figure 5.5**). The *pga* operon is involved in the synthesis of the exopolysaccharide PNAG, which is an essential EPS component in biofilms of *A. baumannii* and other bacteria[276]. Increased production of PNAG (and formation of EPS) has been associated with biosorption and sequestration of toxic heavy metals[278,279]. The present study did not directly explore the association between enhanced biofilm formation and Ag^+ defence in WT ATCC 19606. However, it is possible that the upregulation of the *pga* genes and overproduction of PNAG could lead to increased biosorption of positively-charged Ag^+ into the net negatively-charged EPS, as a defence mechanism[279].

Two of the highest expression fold-changes occurred in the copper efflux genes *copA* and *copB*, which were upregulated by ~ 17.8 and ~ 21.9-fold, respectively, in the low dose treated WT strain relative to WTNT. Interestingly, as with the case of the primary NAg defence system (WTLN vs WTNT, **Figure 5.2**), no statistically significant expression changes of the copper response transcriptional regulator gene *cueR*, which regulates *copA* (and likely *copB*) expression, was noted in WTLA compared to WTNT. The efflux pumps are known to confer copper and silver cross-resistance, and as earlier described, were indicated to also contribute to the primary and advanced primary NAg defence in WT and NAg^R ATCC 19606 (**Chapter 5**)[256]. In addition, various antibiotic efflux pump genes, which were not detected in the NAg exposure systems, were upregulated in the Ag^+ exposed WT bacterium, including two known *A. baumannii* RND multi-drug efflux pump operons, *adeABC* and *adeIJK*. Specifically, the genes *adeA* (FQU82_02070), *adeB* (FQU82_02069), *adeI* (FQU82_03096), and *adeJ* (FQU82_03097) were all upregulated by a range of ~ 1.5 – 1.9-fold in the low Ag^+ exposed WT bacterium relative to the untreated culture (**Figure 6.4**). Changes in expression of the remaining genes in each respective locus, *adeC* and *adeK*, were statistically insignificant. The latter observation is surprising considering these genes (*adeABC, adeIJK*) are clustered as operons. These tripartite RND efflux systems reportedly confer multi-drug resistance to a variety of antibiotics in *A. baumannii*, including β-lactams, aminoglycosides, tetracyclines, and other compounds[309]. Apart from the opportunistic or responsive roles of RND efflux pumps in the removal of antimicrobial agents, studies have noted their endogenous roles in bacterial biology,

with research highlighting they may contribute to virulence, nutrient acquisition, and potentially biofilm formation, though the latter contribution is still under debate[310,311]. While no studies have reported on the activity of these efflux pumps against heavy metals previously, considering the multi-drug efflux capabilities of these pumps, a cross-defence effect against Ag^+ is possible[312]. Taken together, the contributions of the copper and antibiotic efflux pumps are thought to aid in the defence against Ag^+, supporting the earlier described cell surface protection mechanisms.

In summary, RNA-Seq analysis of the WT bacterium following exposure to sub-lethal Ag^+ concentrations revealed 13 upregulated defence-related genes of interest. The upregulated genes were indicated to contribute to the toxicological response, or herein defined primary defence system, of ATCC 19606 to Ag^+, encoding mechanisms associated with OM integrity, periplasmic sequestration of Ag^+, promotion of biofilm growth, and active cation removal *via* copper and multi-drug efflux pumps. Interestingly, nearly all the primary Ag^+ defence-related DEGs of interest were also detected in the NAg exposure systems reported in **Chapter 5**. While NAg and Ag^+ exhibit unique antibacterial mechanisms, the findings highlight some degree of similarities in their toxicity features, and therefore, potential overlapping bacterial defence mechanisms against the nanoparticulate and ionic forms of silver. This is consistent with the known oxidative dissolution phenomena of NAg, with the leaching of Ag^+ being among the key contributors to the nanoparticle toxicity[86].

6.3.2 Defence response of Ag^{+T} *A. baumannii* ATCC 19606 to Ag^+

6.3.2.1 Comparative growth rate of Ag^+-treated WT and Ag^+-treated Ag^{+T} ATCC 19606

A comparison of growth profiles between WT *A. baumannii* ATCC 19606, when exposed to sub-MIC (low) doses of Ag^+ (0.5 µg/mL; 0.5 x MIC; see **Table 3.2**), and the Ag^{+T} strain when treated with low Ag^+, were performed to see if the tolerant bacterium experienced changes in its growth behaviour. A comparison of growth rates between the Ag^{+T} strain when untreated (no Ag^+), when exposed to a low Ag^+ dose (0.5 µg/mL; 0.5 x MIC), and to an above-MIC (high) dose of NAg (3 µg/mL; 1.5 x MIC; see **Table 3.2**), were also performed. The growth rates between the low dose treated WT strain (0.585/h), untreated tolerant strain (0.598/h), and low dose treated tolerant strain (0.589/h) were all found to be comparable (**Figure 6.3**). The high dose

treated tolerant strain showed a gradual reduction in cell growth over the 6 h time course (growth rate = 0.409/h), but this was expected considering the strain exhibits tolerance rather than resistance and therefore the above-MIC (lethal) Ag^+ dose would eventually lead to cell death. However, the bacterium showed no notable growth reduction for at least the 30 min exposure time prior to RNA extraction (see inset plot, **Figure 6.3**). The low and high Ag^+ doses were concluded to be sufficient for inducing a defence response in the respective strains.

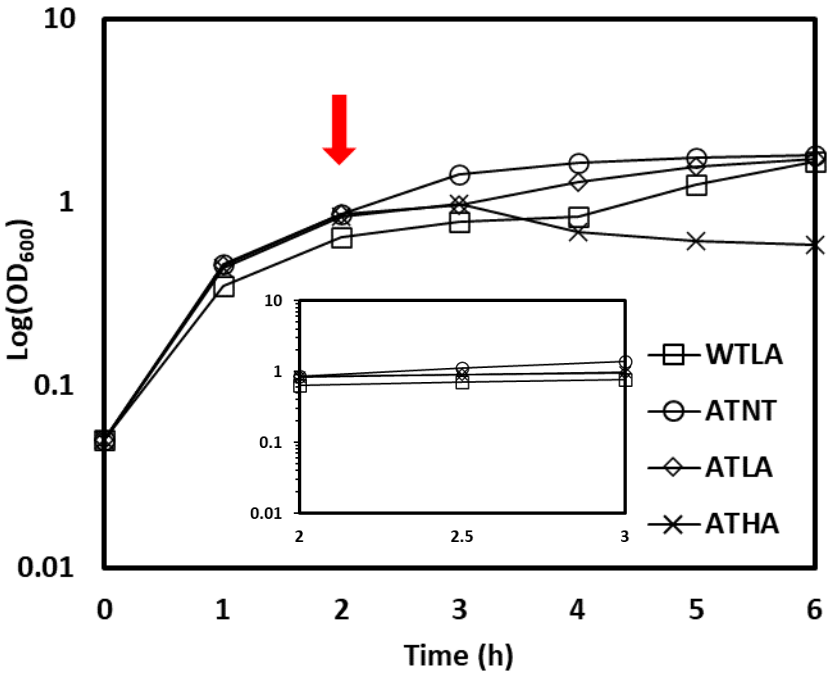

Figure 6.3 Comparative growth rates of WT and Ag^{+T} ATCC 19606 strains treated with low and high Ag^+ doses over 6 h. WTLA = wild-type low Ag^+ (square); ATNT = Ag^+-tolerant no treatment (circle); ATLA = Ag^+-tolerant low Ag^+ (diamond); ATHA = Ag^+-tolerant high Ag^+ (cross). The red arrow indicates the time point (2 h) at which Ag^+ was added to the respective cultures. RNA was extracted 30 min (2.5 h time point) after the addition of Ag^+. The inset plot displays an expanded time range from 2 – 3 h to show the closely comparable growth profiles of each culture. Initial OD_{600} at time 0 began at 0.05. Each data point represents mean of at least two biological replicates.

6.3.2.2 Differentially expressed genes between Ag^+-treated WT and Ag^{+T} ATCC 19606

To understand the unique evolutionary adaptation trait of the Ag^{+T} strain, the bacterium was exposed to both low (0.5 x MIC) and high (1.5 x MIC) doses of Ag^+ to

incite a defence response (see **Table 3.2**). The transcriptomic profile of the low Ag^{+} dose treated WT strain was compared to that of low dose treated Ag^{+T} strain (hereafter referred to as Ag^{+}-Tolerant Low Ag^{+}; ATLA) to observe differences in gene expression patterns. RNA-Seq analysis of the untreated Ag^{+T} strain (hereafter referred to as Ag^{+}-Tolerant No Treatment; ATHA) was compared to that of ATLA, as well as the high Ag^{+} dose treated Ag^{+T} strain (hereafter referred to as Ag^{+}-Tolerant High Ag^{+}; ATHA). In addition, analysis was also performed on ATHA relative to ATLA. See **Section 3.9.5** for cut-off threshold values to define which differentially expressed gene (DEG) between the pairwise comparisons. Refer to **Table A2** in the appendix for complete gene ontology analysis of DEG data of Ag^{+}-treated WT and Ag^{+T} ATCC 19606.

In the comparison between ATLA and WTLA, a total of 1202 DEGs were identified. Among these, 660 genes were upregulated while 542 genes were downregulated. When comparing ATLA to ATNT, only 8 DEGs were found, all of which were upregulated. On the other hand, a total of 2121 DEGs were identified in ATHA when compared to ATNT. Among these, 1110 genes were upregulated, and 1011 genes were downregulated. In comparison to ATLA, 2098 DEGs were identified in ATHA, with 1098 upregulated genes and 1000 downregulated genes (**Table 6.2**). Comparing these results to the DEGs identified in the WT bacterium (WTLA *versus* WTNT, see **Table 6.1**), it is evident that the Ag^{+T} strain exhibits significant gene expression changes under low and high Ag^{+T} doses. This suggests that the bacterium has experienced notable molecular change to develop a defence system to tolerate Ag^{+} toxicity.

Table 6.2 Number of DEGs (upregulated and downregulated genes) identified in Ag^{+T} *A. baumannii* ATCC 19606 treated with a low dose (0.5 x MIC) of Ag^{+} (ATLA) and a high dose (1.5 x MIC) of Ag^{+} (ATHA).

Comparison	Upregulated	Downregulated	Total
ATLA *versus* WTLA	660	542	1202
ATLA *versus* ATNT	8	0	8
ATHA *versus* ATNT	1110	1011	2121
ATHA *versus* ATLA	1098	1000	2098

Due to the extent of identified DEGs in this RNA-Seq analysis, DEGs with known (or hypothetical) functions in antibacterial defence, specifically against the main toxicity mechanisms of Ag^{+} (*e.g.* ROS generation, respiratory electron chain uncoupling, and biomolecule damage) were examined. The potential contribution of the WT strain primary Ag^{+} defence-related genes (see **Section 6.3.1**) in the evolved defence response of the Ag^{+T} strain were also investigated. Again, only upregulated genes were, in general, analysed to assess their contribution to Ag^{+} defence. The work presented in **Chapter 4** revealed that various genetic mutations arose in the tolerant bacterium (see **Table 4.1**). In turn, changes in expression of these mutated genes were also examined to interpret their potential contribution to the adapted defence of the Ag^{+T} strain. It is important to note that ATCC 19606 developed Ag^{+} tolerance after long-term exposure, rather than resistance, which is a previously unobserved adaptation phenomenon in *A. baumannii* against this agent. Therefore, identifying the specific mechanisms that facilitate this tolerance trait may pose a challenge due to the complexity of the adaptation trait, and further investigation beyond this transcriptomic analysis is necessary to fully elucidate the molecular basis of Ag^{+} defence in this bacterium, as later outlined.

6.3.2.3 Evolved defence responses to Ag^{+}

In conjunction with NAg, as described in **Section 4.6.1**, ATCC 19606 was also exposed to sequential Ag^{+} treatment for 30-days to incite an adaptation response. The

bacterium developed a tolerance trait to the cations, indicated by an increase in the minimum duration of killing 99% (MDK_{99}) of the population when compared to the WT strain. The transcriptomic profile of the tolerant strain, when exposed to low (0.5 x WT MIC) and high (1.5 x WT MIC) doses of Ag^+, was examined to uncover what mechanisms confer the tolerant defence response in the bacterium. A total of 13 DEGs were correlated to the primary Ag^+ defence system of the WT strain (see **Figure 6.1**). Majority of these primary defence-related genes showed further but variable upregulation in the tolerant strain, and expression increases appeared to correspond to varied Ag^+ doses. Nonetheless, enhancement of these genes was thought to contribute to the **advanced primary defence system**. 22 other DEGs, which were only upregulated in the Ag^{+T} bacterium (*i.e.* unique from the WT), were linked to the **secondary defence system** and encoded mechanisms involved in the general stress response, physical cell surface protection, and active cation removal and counteraction. These latter gene expression modifications are the result of evolutionary change to ATCC 19606 in response to long-term Ag^+ exposure and included two genes, *gshA* and *adeF*, which underwent genetic mutation (refer to **Table 4.1**).

As a reminder, only eight DEGs were identified in the Ag^+ strain following treatment with low dose Ag^+ (ATLA) when compared to that of the untreated (no Ag^+) tolerant bacterium (ATNT; **Table 6.2**). Majority of the gene expression fold-changes identified in ATLA relative to ATNT were determined to be statistically insignificant. Therefore, unless otherwise stated, the DEG results of this comparison are not reported throughout this Chapter. It was hypothesised that the dose of Ag^+ was also too low to promote substantial gene expression change in the tolerant strain, as similarly observed in NRLN relative to NRNT (**Table 5.2**). It is likely that the Ag^{+T} strain has undergone physiological change, like that of the NAg^R bacterium. This is indicated by stable and permanent change in gene expression levels in the evolved bacterium even in the absence of Ag^+ stress, as potentially highlighted by the limited DEG variation between low dose treated and untreated cultures. The final section of this Chapter (**Section 6.3.3**) will explore and discuss the basis of this concept.

6.3.2.3.1 Advanced primary defence system

The toxicological gene expression changes exhibited by the WT bacterium, as described in **Section 6.3.1.3,** encoded mechanisms which were linked to the primary

defence response against Ag^+. These mechanisms involved cell surface protection to Ag^+ penetration, *via* OM integrity and biofilm formation, and active efflux of Ag^+. It was next found that the Ag^+-tolerant strain amplified many of these mechanisms, most likely due to its evolutionary adaptation to Ag^+, and interestingly, in a concentration-dependent manner. This augmentation of the primary defence gene expression is referred to herein as the **advanced primary defence** system (**Figure 6.4**).

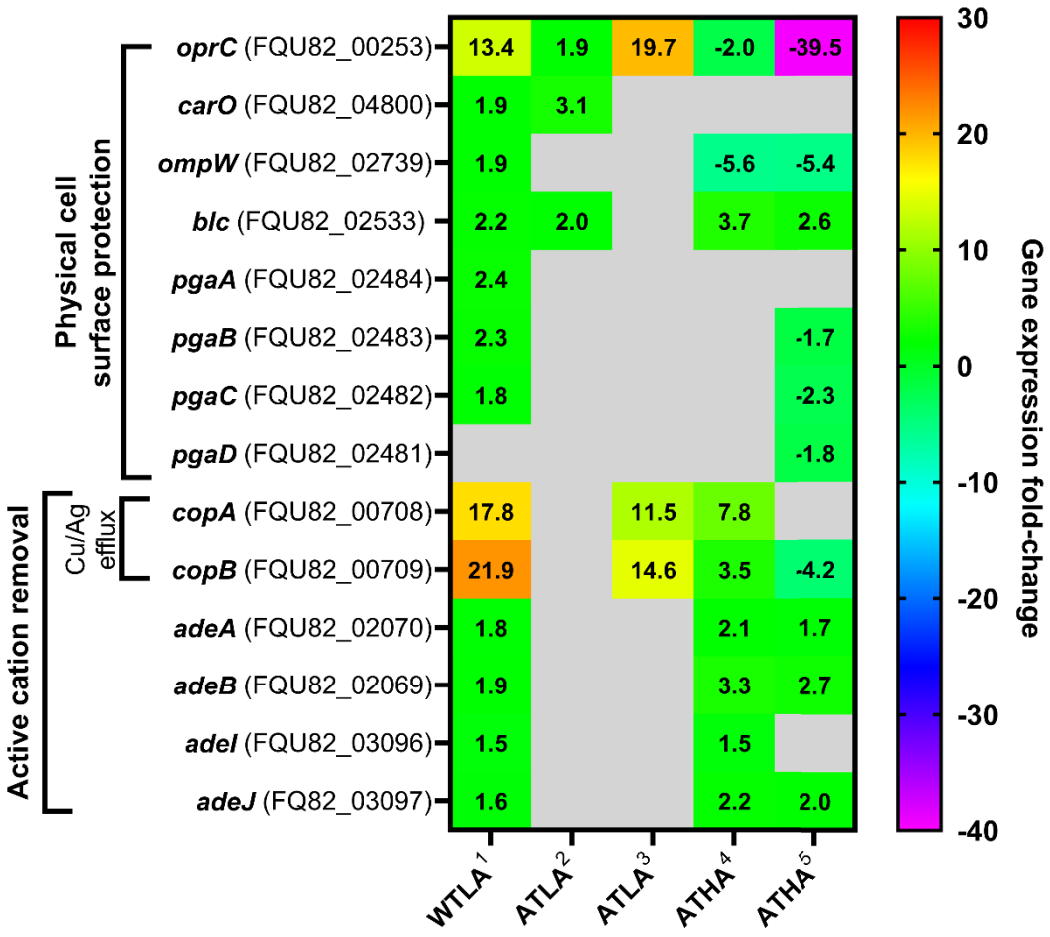

Figure 6.4 Differentially expressed genes (DEGs) identified in WT and Ag^{+T} *A. baumannii* ATCC 19606 in response to low (sub-lethal) or high (lethal) Ag^+ doses. (**A**) Heat-map representing expression fold-change in genes of interest hypothesised to contribute to the primary and advanced primary Ag^+ defence system of the WT and Ag^{+T} strains, respectively. Grey cells indicate statistically insignificant DEGs. Pairwise comparisons: [1] WTLA *versus* WTNT, [2] ATLA *versus* WTLA, [3] ATLA *versus* ATNT, [4] ATHA *versus* ATNT, [5] ATHA *versus* ATLA.

The OMP-synthesis genes *oprC* and *carO*, and the lipoprotein transport gene *blc,* were upregulated by ~ 1.9-fold, ~ 3.1-fold, and ~ 2.0-fold, respectively, in the Ag^{+} strain when exposed to low cation doses relative to WTLA (**Figure 6.4**). Interestingly, *oprC* was upregulated by ~ 19.7-fold in ATLA in comparison to ATNT. But when treated with higher Ag^{+} doses, expression of this gene was downregulated by ~ 2.0-fold and ~ 39.5-fold when compared to ATNT and ATLA, respectively. It is hypothesised that repressed *oprC* expression at the higher Ag^{+} dose is to reduce periplasmic sequestration, and in turn, cellular build-up of the toxic cation. Note that downregulation of *oprC* was also observed in the NAg^{R} strain in response to high NAg doses (see **Section 5.3.2.3.2**). Likewise, *ompW* was also downregulated by ~ 5.4 – 5.6-fold, while *carO* expression change was statistically insignificant, in ATHA relative to ATNT and ATLA. Downregulation or statistically insignificant expression of the *pga* operon was also noted in the high dose treated tolerant bacterium in comparison to ATNT/ATLA. These results indicate that *ompW, carO,* and the *pga* locus may not contribute to an enhanced biofilm-forming defence phenotype in the tolerant bacterium in response to higher Ag^{+} doses. In fact, when treated with higher Ag^{+} doses, the tolerant strain only exhibited upregulation of the gene *blc* (~ 2.6 – 3.7-fold) when compared to untreated and low dose treated Ag^{+T} strain cultures. This data indicates that *blc* is the only cell surface defence-associated gene upregulated in response to increasing Ag^{+} concentrations. The increased transport of lipoproteins to enhance OM integrity is thought to be a physical defence mechanism against higher Ag^{+} stress. This observation aligns with the NAg^{R} strain, which also exhibited upregulation of *blc* when exposed to high dose NAg (see **Section 5.3.2.3.2**).

The copper efflux pump genes, *copA* and *copB*, were upregulated by ~ 3.5 – 7.8-fold in the Ag^{+} strain at high Ag^{+} doses relative to ATNT (**Figure 6.4**). But interestingly, when compared to the untreated bacterium, expression of both genes had further increased by ~ 11.5 – 14.6-fold in ATLA. In fact, the copper efflux genes were either downregulated (*copB* by ~ 4.2-fold) or had similar expression levels (*copA*) in ATHA, relative to ATLA. Likewise, no statistically significant changes in *copA* and *copB* expression were detected in ATLA relative to WTLA (**Figure 6.4**). These observations contrast those seen in the NAg^{R} strain, which exhibited significant upregulation of both genes at high dose nanoparticle treatment (**Figure 5.4**). Overall, this data indicates that the Ag^{+T} strain exhibited no enhanced upregulation of *copA* and *copB* compared to the

WT. While the reason for this is unclear at this stage, it should be noted that no statistically significant expression change of the transcriptional activator gene *cueR* was noted in the Ag^{+T} strain (at low or high Ag^{+} doses; data not shown), unlike that of the NAg^{R} strain (see **Figure 5.4**). This inactivity of the transcriptional regulator (*cueR*) might explain the lack of enhanced activation of *copA/copB* in the tolerant bacterium relative to the WT. Contrarily, *adeA/adeB* and *adeI/adeJ* increased in expression by ~ 1.7 – 3.3-fold and ~ 1.5 – 2.2-fold in ATHA when compared to the untreated and low dose treated tolerant bacterium (**Figure 6.4**). But no statistically significant changes in expression of *adeA/B* and *adeI/J* were seen in ATLA relative to WTLA. In turn, this indicates that, unlike *copA/copB*, enhanced expression of the *ade* genes in the Ag^{+T} strain occurs in response to more lethal doses of Ag^{+}, which further supports the hypothesis that these multi-drug efflux pumps are involved in silver defence.

6.3.2.3.2 Secondary defence system

The RNA-Seq analysis revealed concentration-dependent changes in expression levels of the primary Ag^{+} defence-related genes in the Ag^{+T} bacterium. At lower Ag^{+} doses, the cell surface defence genes *oprC, carO,* and *blc,* were upregulated, while at higher Ag^{+} doses, the lipoprotein transport gene *blc* and the multi-drug efflux pump genes *adeAB* and *adeIJ,* were upregulated, which collectively form the advanced primary Ag^{+} defence system. Further transcriptomic analysis revealed a total of 22 of DEGs not seen in the WT bacterium which were indicated to play roles in the secondary defence response of the Ag^{+T} strain. These encoded secondary defence mechanisms were thought to encompass general stress responses, physical cell surface protection, and active cation removal and toxicity counteraction (**Figure 6.5**). The secondary defence system most likely manifested because of evolutionary adaptation of *A. baumannii* ATCC 19606 to prolonged Ag^{+} exposure as it is not observed in the WT bacterium. Additionally, two of the identified DEGs in this defence system, *gshA* and *adeF*, underwent mutation in the tolerant strain due to long-term Ag^{+} exposure (see **Table 4.1**). Furthermore, several of the secondary defence mechanisms were also detected in the NAg^{R} bacterium, further highlighting the overlap in NAg and Ag^{+} toxicity and potential for cross-defence effects against the silver agents.

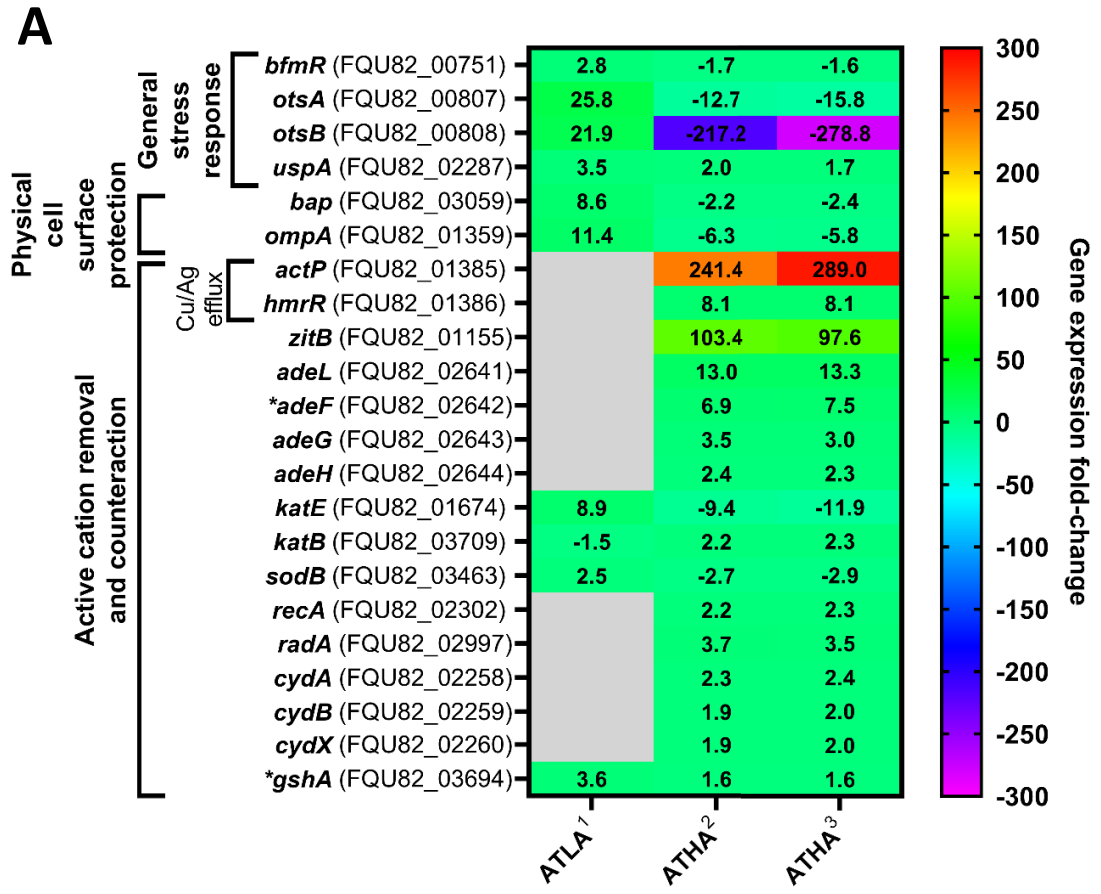
A
General stress response
Physical cell surface protection
Cu/Ag efflux
Active cation removal and counteraction
bfmR (FQU82_00751) 2.8 -1.7 -1.6
otsA (FQU82_00807) 25.8 -12.7 -15.8
otsB (FQU82_00808) 21.9 -217.2 -278.8
uspA (FQU82_02287) 3.5 2.0 1.7
bap (FQU82_03059) 8.6 -2.2 -2.4
ompA (FQU82_01359) 11.4 -6.3 -5.8
actP (FQU82_01385) 241.4 289.0
hmrR (FQU82_01386) 8.1 8.1
zitB (FQU82_01155) 103.4 97.6
adeL (FQU82_02641) 13.0 13.3
*adeF (FQU82_02642) 6.9 7.5
adeG (FQU82_02643) 3.5 3.0
adeH (FQU82_02644) 2.4 2.3
katE (FQU82_01674) 8.9 -9.4 -11.9
katB (FQU82_03709) -1.5 2.2 2.3
sodB (FQU82_03463) 2.5 -2.7 -2.9
recA (FQU82_02302) 2.2 2.3
radA (FQU82_02997) 3.7 3.5
cydA (FQU82_02258) 2.3 2.4
cydB (FQU82_02259) 1.9 2.0
cydX (FQU82_02260) 1.9 2.0
*gshA (FQU82_03694) 3.6 1.6 1.6
ATLA1
ATHA2
ATHA3
300
250
200
150
100
50
0
-50
-100
-150
-200
-250
-300
Gene expression fold-change
B
3900000
0
390000
780000
1170000
1560000
1950000
2340000
2730000
3120000
3510000
gshA
sodB
katB
bap
radA
bfmR
ostA
ostB
adeFGH
adeL
zitB
ompA
actP
hmrR
recA
uspA
cydABX
katE
A. baumannii
ATCC 19606

Figure 6.5 Differentially expressed genes (DEGs) identified in Ag^{+T} *A. baumannii* ATCC 19606 in response to low (sub-lethal) or high (lethal) Ag^{+} doses. (**A**) Heat-map representing expression fold-change in genes of interest hypothesised to contribute to the secondary Ag^{+} defence system of the tolerant strain. Grey cells indicate statistically insignificant DEGs. * Genes detected with point mutations as listed in **Table 4.1**. Pairwise comparisons: [1] ATLA *versus* WTLA, [2] ATHA *versus* ATNT, [3] ATHA *versus* ATLA. ATLA *versus* ATNT comparative DEG data not shown. (**B**) Map of *A. baumannii* ATCC 19606 chromosome indicating sequence positions of DEGs of interest. Forward and reverse reading frames are shown by the cyan-coloured bars. The two internal rings indicate the chromosome's GC skew (the innermost ring) followed by the chromosome's GC content.

General stress response – Four stress response-related genes were upregulated in the Ag^{+T} strain, which were also identified in the NAg^{R} strain (refer to **Figure 5.7**). Notably, the genes *otsA* and *otsB*, responsible for trehalose synthesis, exhibited a ~ 21.9 – 25.8-fold expression increase in ATLA when compared to WTLA. Trehalose is a disaccharide which supports CPS formation and increases density under stressful environmental conditions[265-267]. Expression of *otsA/otsB* is transcriptionally regulated by BfmR, which was also upregulated in ATLA by ~ 2.8-fold relative to WTLA[260,264]. Intriguingly, both *otsA* and *otsB* (and *bfmR*) were downregulated by ~ 12.7 – 278.8-fold (~ 1.6 – 1.7-fold) in the high dose treated bacterium when compared to ATNT/ATLA (**Figure 6.5**). Slight downregulation of *otsA/otsB* was also noted in the high dose treated NAg^{R} strain (see **Figure 5.5**). The reason for this reduction in *otsA*/*otsB* expression in the tolerant bacterium is not currently clear. However, it is hypothesised that there may a diversion of energy to more critical defence mechanisms in response to higher cation doses. Moreover, *otsB*, specifically, is involved in the final dephosphorylation step in trehalose synthesis, and it is thought that significant downregulation of this gene (~ 217.2 – 278.8-fold), compared to *otsA* (~12.7 – 15.8-fold; **Figure 6.5**) is required to effectively halt the synthesis reaction[266]. Conversely, the universal stress protein gene *uspA* was also upregulated in the Ag^{+T} strain, increasing in expression by ~ 3.5-fold in ATLA relative to WTLA and even further by ~ 1.7 – 2.0-fold in ATLA when compared to ATNT/ATLA (**Figure 6.5**). Increased upregulation of *uspA* also occurred in the high NAg dose treated NAg^{R} strain (see **Figure 5.5**). Studies have indicated that upregulation of universal stress proteins offer

increased protection against oxidative stress, DNA damage, and respiratory chain uncoupling, which are key antimicrobial mechanisms of Ag^+, and has been shown to regulate DNA repair gene expression, which was linked to the secondary Ag^+ defence as later highlighted[270,293].

Physical cell surface protection – The RNA-Seq analysis revealed two upregulated genes associated with physical cell surface defence against Ag^+ penetration. In response to low cation stress, the biofilm-associated gene *bap* was upregulated by ~ 8.6-fold in the tolerant bacterium when compared to WTLA. This highly conserved gene plays a critical role in the formation and maturation of biofilms in *A. baumannii*[280]. The gene *ompA*, which encodes outer membrane protein A, was also upregulated by ~ 11.4-fold in ATLA relative to WTLA. OmpA is important for OM structural integrity and also plays a prominent role in *A. baumannii* biofilm formation[249,250]. Increased expression of *bap* was also seen in the low dose treated NAg^R strain, as part of its secondary defence (refer to **Figure 5.5**), while *ompA* was upregulated in both the primary and advanced primary defence systems of the WT and the NAg^R strains, respectively (see **Figure 5.2**, **Figure 5.4**). As outlined in **Section 4.6.2**, the Ag^{+T} strain exhibited a higher extent of biofilm growth compared to the WT bacterium, even in the absence of Ag^+ pressure[263]. It was thus hypothesised that the upregulation of *bap* and *ompA* might contribute to the stably improved biofilm-forming ability of the Ag^{+T} strain. However, further RNA-Seq analysis showed that both genes were downregulated in the tolerant bacterium when exposed to a higher Ag^+ concentration, with *bap* and *ompA* decreasing in expression by ~ 2.2 – 2.4-fold and ~ 5.8 – 6.3-fold, respectively, relative to ATNT and ATLA (**Figure 6.5**). The reason for the partial downregulation of *bap* at higher Ag^+ doses is currently unclear, but repression of OMP expression have been observed in bacteria, including *E. coli*, as a defence strategy to limit silver diffusion through the cell surface, which might explain the downregulation of *ompA*[141,142,313]. The latter conclusion, however, is hypothetical at this stage.

Active removal *via* efflux – In ATHA, the copper resistance efflux pump gene *actP* exhibited significant upregulation ~ 241.4 – 289.0-fold relative to the untreated and low dose treated bacterium (**Figure 6.5**). The heavy metal transcriptional regulator *hmrR* (involved in *actP* expression regulation) was also upregulated by ~ 8.1-fold in ATHA relative to ATNT and ATLA. Interestingly, no statistically significant changes

in expression of *actP* (and *hmrR*) were detected in ATLA when compared to WTLA. The data suggests that upregulation of this copper efflux pump more readily occurs in response to higher Ag^+ concentrations. While *actP* has not been associated with silver defence previously, the upregulation of this gene at lethal Ag^+ doses aligns with the observed overexpression of this gene in the secondary defence system of the NAg^R strain when exposed to higher NAg doses (see **Figure 5.5**).

Several other efflux transporters were also upregulated in the high dose treated tolerant bacterium. The zinc transporter ZitB, encoded by *zitB* (FQU82_01155), was upregulated in ATHA by ~ 97.6 – 103.4-fold when compared to ATNT and ATLA (**Figure 6.5**). In *E. coli*, basal level expression of *zitB* is reportedly involved in zinc transport to maintain homeostasis under normal growth conditions. But upregulation of *zitB* in environments with toxic zinc concentrations has been shown to confer zinc defence[314]. In the bacterium *Streptomyces coelicolor*, overexpression of the transporter has also been indicated to interrupt heavy metal differentiation and subsequently confer tolerance to iron, cobalt and nickel[315]. While no studies have suggested that this zinc defence mechanism can confer cross-defence against silver, the notable upregulation of *zitB* at high Ag^+ concentrations herein indicate there may be a loss of metal differentiation and silver could be targeted. ATLA exhibited no statistically significant change in *zitB* expression when compared to WTLA, which indicates that this gene is specifically involved in the secondary defence against more lethal Ag^+ doses.

Another operon of *ade* efflux pump genes, *adeFGH* (FQU82_02642, 02643, 02644, respectively) were also upregulated in secondary defence system of the tolerant strain. This operon was upregulated by a range of ~ 2.3 – 7.5-fold in the high dose treated Ag^{+T} bacterium relative to ATNT and ATLA (**Figure 6.5**). Similar to that of the *adeABC* and *adeIJK* systems, which were indicated to contribute to the primary and advanced Ag^+ defence systems (see **Section 6.3.1.3** and **Section 6.3.2.3.1**), the *adeFGH* operon also encodes a tripartite RND multi-drug resistance efflux system which is highly prevalent across *A. baumannii* clones[225,316]. Activation of *adeFGH* is reportedly induced by the LysR-type transcriptional regulator *adeL*, which was also upregulated in ATHA by ~ 13.0 – 13.3-fold when compared to ATNT and ATLA[225]. Previous studies have not indicated that *adeFGH* (like *adeABC* and *adeIJK*) confer heavy metal efflux in *A. baumannii* or any other bacterial species. But their observed

upregulation at higher silver doses combined with their multi-drug targeting capabilities suggest a possible cross-tolerance effect to Ag^{+}. No statistically significant expression change of *adeFGH* was noted in ATLA relative to WTLA, further underscoring their potential role in Ag^{+} efflux at higher silver concentrations. It is also important to note that a point mutation to *adeF* was detected in the Ag^{+T} strain, as shown in **Table 4.1**, which may be a contributing factor to the enhanced expression of this specific gene. This hypothesis is discussed in the **evolutionary gene mutations** paragraph below.

Toxicity counteraction – A range of oxidative stress response genes were upregulated in the Ag^{+T} strain. Under lower Ag^{+} stress, the catalase HPI gene *katE*, which facilitates degradation of excess H_2O_2, was upregulated by ~ 8.9-fold in the tolerant bacterium relative to WTLA[282,283]. Likewise the superoxide dismutase gene, *sodB*, which is involved in the dismutation of $O_2^{\bullet-}$ radicals to O_2 and H_2O_2, was upregulated by ~ 2.5-fold in ATLA relative to the WT strain[285]. But in response to higher Ag^{+} concentrations, both genes were downregulated by ~ 9.4 – 11.9-fold and ~ 2.7 – 2.9-fold, respectively, relative to ATNT and ATLA (**Figure 6.5**). Alternatively, the major catalase gene *katB* was upregulated by ~ 2.2 – 2.3-fold in ATHA in comparison to the untreated and low dose treated tolerant cultures (**Figure 6.5**). These ROS scavenger gene expression patterns align with that of the NAg^{R} strain, which exhibited upregulation of *katE* and *sodB* only in response to low dose NAg (NRLN), while *katB* was upregulated at higher NAg concentrations (NRHN; see **Section 5.3.2.3.2**). Studies indicate that *katE* is typically upregulated in response to lower H_2O_2 concentrations and is regulated by the transcriptional regulator gene *bfmR*, which was also only upregulated in the low dose treated Ag^{+T} strain, as described in the **general stress response** paragraph above (**Figure 6.5**)[260,317]. Conversely, the upregulation of *katB* in both the NAg^{R} and Ag^{+T} strains when exposed to higher silver doses indicates this catalase gene plays a role in the oxidative stress defence against higher silver-induced ROS levels. Taken together, it is reasonable to suggest that these identified ROS scavenging DEGs contribute to an improved concentration-dependent oxidative stress defence trait in the Ag^{+T} strain.

As described in **Chapter 2**, a main toxicity feature of Ag^{+} is damage to biomolecules, such as DNA, through direct base-pair intercalation or by generated ROS activity[150,223]. Hence, RNA-Seq analysis found two genes encoding DNA repair

mechanisms in the Ag^{+T} bacterium. In response to high Ag^{+} levels, the DNA recombinase gene *recA* was upregulated by ~ 2.2 – 2.3-fold in comparison to ATNT and ATLA (**Figure 6.5**). RecA plays a critical role in mediating homologous DNA recombination, particularly following DNA cleavage caused by environmental stressors (*e.g.* oxygen radicals)[292]. Another DNA repair gene, *radA* (FQU82_02997), was also upregulated by ~ 3.5 – 3.7-fold in ATHA relative to ATNT/ATLA (**Figure 6.5**). RadA works in conjunction with RecA by initiating hydrolysis of ATP to drive the homologous DNA pairing mechanism (facilitated by RecA)[318]. Contrarily, no statistically significant change in *recA* or *radA* expression was noted in ATLA when compared to WTLA. These findings are consistent with that observed in the NAg^{R} strain (for *recA* specifically; see **Figure 5.5**). This overall indicates that higher doses of silver may induce DNA damage which necessitates recombinational repair. Moreover, activation of *recA* (and potentially *radA*) is reportedly regulated by the universal stress gene *uspA* in response to DNA damage, the latter of which saw further upregulation in the high dose treated Ag^{+T} bacterium, as described in the **general stress response** paragraph (**Figure 6.5**)[293].

In **Section 4.6.3**, an inference regarding changes to respiratory activity in the Ag^{+T} strain was made, as evidenced by the increased detection of intracellular ROS (see **Figure 4.3**). As Ag^{+} is known to target bacterial membrane-bound respiratory enzymes, it was thought that alterations in respiratory-associated gene expression would occur as a defence response[98]. The transcriptomic analysis found that *cydABX* (encodes the cytochrome *bd* oxidase complex CydABX; FQU82_02258, 02259, and 02260, respectively), were upregulated in ATHA by ~ 1.8 – 2.3-fold in comparison to ATNT and ATLA (**Figure 6.5**). The cytochrome *bd* complex is a terminal oxidase in the respiratory chain which catalyses the reduction of O_2 into water and drives the proton motive force for ATP generation[319]. It is hypothesised that upregulation of *cydABX* in the Ag^{+T} strain serves as a compensatory mechanism to counteract electron chain disruption by Ag^{+}, preserving respiration and ATP production for normal cell function. This potential case of heightened respiration may explain the 'elevated' ROS levels observed in the Ag^{+T} strain, compared to the WT strain (even in the untreated control; see **Figure 4.3**), because of the natural respiratory by-production of H_2O_2[237,319]. No statistically significant change in expression of *cydABX* was observed

in ATLA when compared to WTLA, indicating this mechanism is activated in response to higher Ag^{+} concentrations as a function of tolerance.

Evolutionary gene mutations – As outlined in **Section 4.6.2**, comparative whole genome sequence analysis of the Ag^{+T} strain identified six mutated genes (see **Table 4.1**). Notably, three of these genes, *gshA* (FQU82_03694), *atr2* (FQU82_00141), and *trpB* (FQU82_03235) underwent mutation with a 100% frequency in all sequenced biological replicates of the tolerant strain. The gene *adeF* (part of *adeFGH* operon), which was upregulated in the secondary defence system (refer to **Figure 6.5**), also experienced mutation, but only occurred in 16.7% of sequenced isolates. In turn, for simplicity, only the potential expression changes of these four mutated genes were examined.

The gene *gshA*, which encodes the enzyme glutamate cysteine-ligase (GCL), was upregulated in the Ag^{+T} strain by ~ 3.6-fold in response to low Ag^{+} doses when compared to WTLA, and then further upregulated by ~ 1.6-fold at higher doses relative to ATNT and ATLA (**Figure 6.5**). GCL is involved in the biosynthesis of the antioxidant glutathione (GSH) which plays a key role in ROS scavenging[220]. Due to higher levels of intracellular ROS detected in the tolerant bacterium (in comparison to the WT strain; see **Section 4.6.3**), it was difficult to interpret the role of *gshA* in the oxidative stress response[263]. Even so, it is hypothesised that the substitutional mutation (Gly39Arg) resulted in enhanced expression of *gshA* which may now play a role in Ag^{+}-mediated oxidative stress defence of the tolerant bacterium. Additionally, research on *E. coli* has indicated that sulfur groups of GSH can form complexes with certain heavy metal ions, such as cadmium, mercury, and lead. These complexes are then sequestered into the periplasmic space, where they are then removed *via* efflux pumps[320,321]. While there is no evidence that GSH can complex with silver and undergo sequestration, it is possible that this mechanism might function against Ag^{+} in the tolerant bacterium considering its upregulation at a higher Ag^{+} dose (**Figure 5.1**). Moreover, one study noted that a Δ*gshA P. aeruginosa* mutant displayed reduced motility and biofilm-forming activity, while a separate study indicated that GSH production is essential in activating virulence factors needed for bacterial biofilm development[322,323]. It is therefore reasonable to suggest that upregulation of *gshA* in the Ag^{+T} bacterium may contribute to its enhanced biofilm-forming phenotype, as shown in **Figure 4.2**.

The gene *adeF*, which is a subunit in the multi-drug efflux pump operon *adeFGH*, was also mutated in the Ag^{+T} strain[225]. Expression of this gene had increased by ~ 6.9 – 7.5-fold in the bacterium following treatment with high dose Ag^{+}, relative to ATNT/ATLA, as described in the **active removal *via* efflux** paragraph above (**Figure 6.5**). This represented the largest expression increase among each gene in the *adeFGH* operon. The substitutional mutation to this gene (Gly352Arg) was only detected in 16.7% of all sequenced replicates (see **Table 4.1**). It is therefore difficult to conclude if the mutation to *adeF* resulted in a non-synonymous sequence change and enhanced expression, or if the mutation 'randomly' occurred in a single isolate. This is because expression of *adeG* and *adeH,* along with the transcriptional regulator gene *adeL*, had also increased without mutation, implying that the regulator and/or efflux system is inherently stimulated by the presence of silver. Therefore, further assessment on the molecular impact of this gene mutation is required.

The *atr2* gene encodes an enzyme belonging to the acetyltransferase family, which is primarily responsible for post-translational protein modification through the acetylation of lysine residues[324]. In the Ag^{+T} strain, expression of *atr2* was repressed in all pairwise comparisons, with the most significant downregulation occurring in the ATLA *versus* WTLA comparison, which exhibited a significant ~ 23.8-fold decrease in expression (data not shown). It is possible that the deletional gene mutation (Lys4fs) caused expression instability and/or non-functional protein translation, potentially leading to homeostatic repression of the gene through negative feedback loops[325]. Moreover, the gene *trpB* encodes a tryptophane synthase beta chain subunit involved in the two-step tryptophan biosynthesis reaction, which is an essential amino acid in bacterial cell function[326]. This gene underwent a substitutional mutation (Arg58Cys) but exhibited no statistically significant expression change in the tolerant strain across all RNA-Seq comparisons (data not shown). As such, at this stage, it appears that *atr2* and *trpB* likely play no role in the evolved secondary defence system of the Ag^{+T} strain. Despite this, further investigation is needed to elucidate the effect of the stable mutations to both genes and confirm the potential mechanistic defence functions of each gene.

In summary, the whole transcriptomic analysis revealed widespread differential gene expression changes in the Ag^{+T} strain which likely developed because of the evolutionary adaptation of ATCC 19606 to prolonged Ag^{+} exposure. The data depicted

herein has provided mechanistic insights into the evolved advanced primary and secondary Ag^+ defence systems of the tolerant bacterium. In **Section 6.3.1.3**, the toxicological response of the WT strain was examined, and a variety of upregulated genes, linked to the intrinsic primary Ag^+ defence system, were identified. These genes encoded various OM- and biofilm-related mechanisms, as well as copper/silver and antibiotic efflux pumps. The Ag^{+T} tolerant strain demonstrated a concentration-dependent enhancement in expression of the primary defence-related genes, as part of its advanced primary defence system. Only the antibiotic efflux pumps and the lipocalin Blc were further upregulated in the tolerant bacterium when exposed to lethal Ag^+ concentrations, highlighting the importance of these intrinsic mechanisms in Ag^+ defence for ATCC 19606. Further RNA-Seq analysis identified other upregulated genes which were indicated to contribute to the secondary defence system of the Ag^{+T} strain, which were distinct from the WT strain, and likely manifested following adaptation to Ag^+. The secondary defence mechanisms encompassed the general stress response, physical cell surface protection, and active cation removal and toxicity counteraction. Gene expression patterns were also Ag^+ concentration-dependent, as similarly observed with the advanced primary Ag^+ defence system. Under lower Ag^+ stress, genes correlated to the general stress response and cell surface protection were in general upregulated, while at higher Ag^+ concentrations genes encoding efflux pumps, ROS scavengers, DNA repair proteins, and respiratory chain enzymes were upregulated. Additionally, two of the secondary defence-related genes of interest, *gshA* and *adeF*, underwent mutation due to prolonged Ag^+ exposure, which may have enhanced gene expression and subsequent transcription levels. Importantly, various genes involved in biofilm formation and the respiratory chain were upregulated, which were thought to be correlated to the respective phenotypic changes observed in the tolerant bacterium as reported in **Chapter 4**. There was a notable lack of statistically significant DEGs between NRLN and NRNT. This suggested that the Ag^{+T} bacterium may have undergone permanent physiological change, in comparison to the WT, leading to stable gene expression modifications which exhibit even in the absence of silver. This concept is explored further in the following section.

6.3.3 Physiological change between WT and Ag^{+T} *A. baumannii* ATCC 19606

6.3.3.1 Comparative growth rate of untreated WT and Ag^{+T} ATCC 19606

A comparison between the growth profiles of WT and Ag^{+T} in the absence of Ag^{+} was performed prior to this transcriptomic study. This was to ensure there no changes in the growth behaviour of the Ag^{+T} strain which manifest without silver pressure. The growth rate of untreated WT strain (0.603/h) was near equivalent to that of untreated tolerant strain (0.598/h, **Figure 6.6**). Thus, the growth behaviour of the Ag^{+T} strain was determined to not have been altered due to evolutionary adaptation.

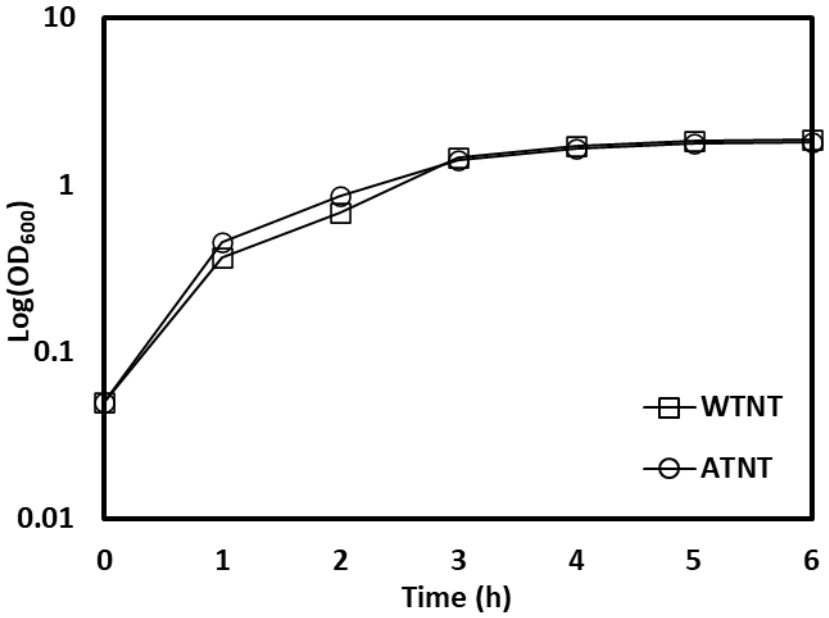

Figure 6.6 Comparative growth rates of untreated (no Ag^{+}) WT and Ag^{+T} ATCC 19606 strains over 6 h. WTNT = wild-type no treatment (square); ATNT = Ag^{+}-tolerant no treatment (circle). RNA was extracted at the 2.5 h time point. Initial OD_{600} at time 0 began at 0.05. Each data point represents mean of at least two biological replicates.

6.3.3.2 Differentially expressed genes between untreated WT and Ag^{+T} ATCC 19606

The aim of this RNA-Seq analysis was to identify stable gene expression changes which exhibited in the Ag^{+T} strain even in the absence of Ag^{+} pressure. The transcriptomic profiles of the untreated Ag^{+T} strain (ATNT) was compared to that of the untreated WT strain (WTNT) to identify DEGs which exhibit in optimal conditions

to elucidate how the tolerant bacterium physiologically changed due to adaptation. See **Section 3.9.5** for cut-off threshold values which define a differentially expressed gene (DEG) between the pairwise comparisons. Refer to **Table A2** in the appendix for complete gene ontology analysis of DEG data of untreated WT and Ag^{+T} ATCC 19606.

A total of 1351 statistically significant DEGs were identified in ATNT relative to WTNT (**Table 6.3**). 722 genes were found to be upregulated, while 629 genes were downregulated. These gene expression changes were detected in the Ag^{+T} strain even in the absence of Ag^{+} pressure which indicated that stable genetic modification occurred following prolonged silver treatment. The high degree of DEGs detected in the untreated Ag^{+T} strain also aligns with the transcriptomic data of the untreated NAg^{R} bacterium (see **Table 5.3**), which also exhibited notable gene expression change in optimal conditions (without NAg pressure).

Table 6.3 Number of DEGs (upregulated and downregulated genes) identified in untreated Ag^{+T} *A. baumannii* ATCC 19606 (ATNT) in comparison to the untreated WT strain (WTNT).

Comparison	Upregulated	Downregulated	Total
ATNT *versus* WTNT	722	629	1351

The DEGs identified in **Section 6.3.2**, indicated to be involved in the advanced primary and secondary defence systems of Ag^{+T} ATCC 19606, will be the focus of the following section. Additionally, the potential expression changes of the mutated genes described in **Section 4.6.2**, explicitly *atr2, adeF*, and *gshA*, will also be investigated. Change in *trpB* expression was statistically insignificant across all pairwise comparisons and was therefore deemed irrelevant in the Ag^{+T} strains defence and physiological change at this stage. Ultimately, the objective of this study was to confirm if any identified tolerant defence mechanisms are continually expressed in the Ag^{+T} bacterium even in the absence of Ag^{+} pressure, to demonstrate that the silver-adapted ATCC 19606 strain has undergone permanent physiological change due to long-term Ag^{+} exposure.

6.3.3.3 Physiological change due to Ag^{+}

The following section highlights which advanced primary and secondary defence-related genes (see **Section 6.3.2.3**) were constitutively expressed in the Ag^{+T} bacterium even in optimal growth conditions. The upregulated genes linked to the primary and advanced primary defence systems in the WT and Ag^{+T} strains, respectively, encoded OM- and biofilm-related proteins indicated to be involved cell surface protection, as well as copper and multi-drug resistance efflux pumps. The upregulated genes only observed in the tolerant strain, which were correlated to the secondary defence system, were thought to contribute to the general stress response, cell surface protection and active cation removal and toxicity counteraction, the latter of which included a copper efflux pump and multi-drug efflux pumps, ROS scavengers, DNA repair proteins, and respiratory chain enzymes. Of the 36 genes linked to the respective defence systems, 19 genes exhibited stable upregulation in the untreated tolerant bacterium (**Figure 6.7**). As seen in **Figure 6.6**, the growth rate of the tolerant strain appeared to be comparable to that of the WT strain and therefore unchanged by its evolutionary adaptation to Ag^{+}. This implied there was an absence of 'fitness cost' compensatory mechanisms which are occasionally identified in other bacterial adaptation phenomena studies (to antibiotics)[295].

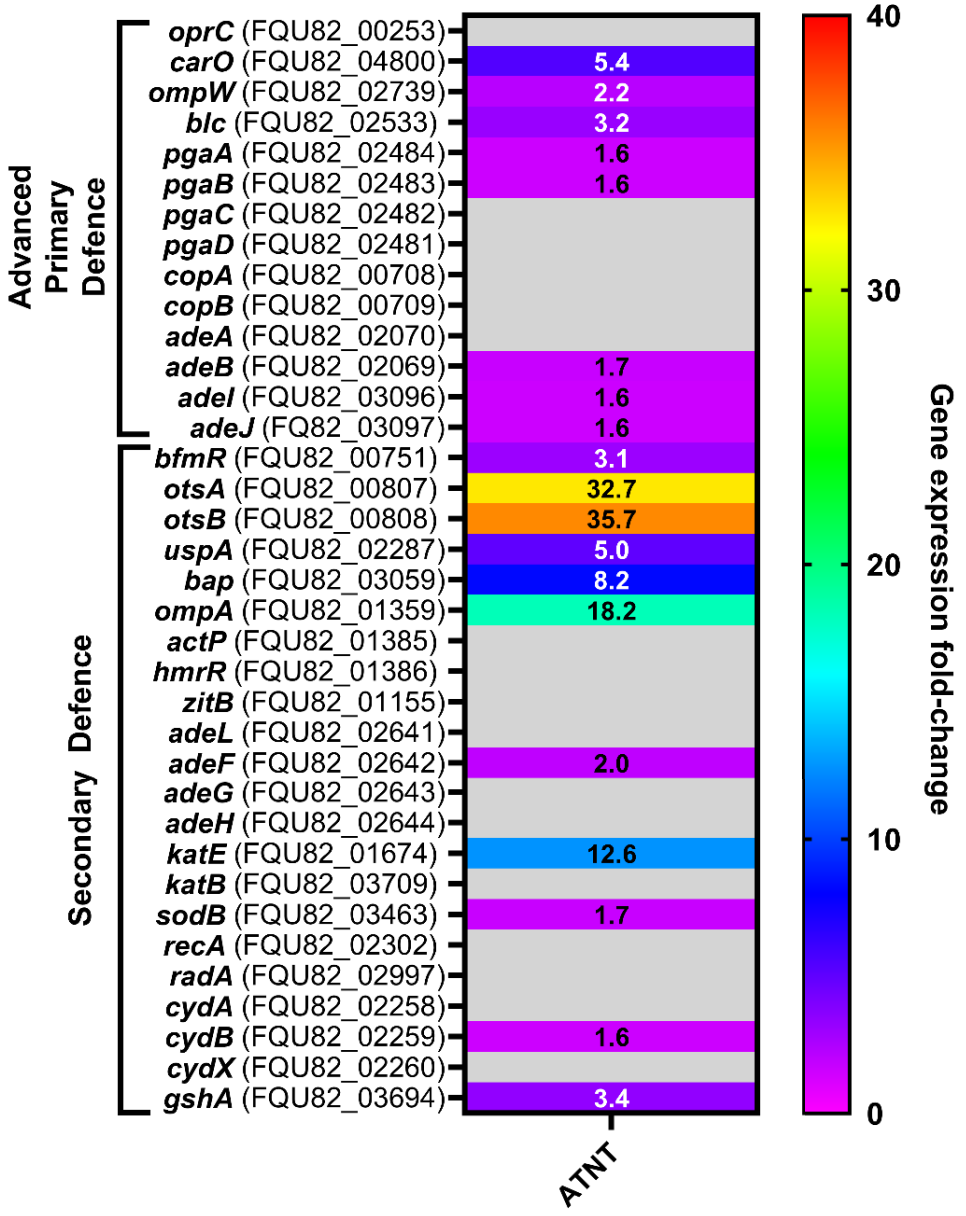

Figure 6.7 Differentially expressed genes (DEGs) identified in Ag^{+T} *A. baumannii* ATCC 19606 which exhibit in optimal conditions (no Ag^{+} present). Heat-map represents expression fold-change in genes of interest hypothesised to contribute to the advanced primary and secondary Ag^{+} defence systems of the tolerant strain. Grey cells indicate statistically insignificant DEGs. Pairwise comparisons: ATNT *versus* WTNT.

The transcriptomic analysis revealed that 8 advanced primary defence-related genes were stably upregulated in the untreated tolerant bacterium, relative to WTNT. The OM-related genes *carO, ompW,* and *blc* increased in expression by ~ 5.4-fold, ~ 2.2-fold, and ~ 3.2-fold, respectively. Stable upregulation of the two OMP genes (*carO*

and *ompW*) are indicated to contribute to biofilm formation, which aligns with the enhanced biofilm-forming ability of the Ag^{+T} strain compared to the WT (in optimal conditions; see **Figure 4.2**)[296,297]. The upregulation of the lipoprotein-carrier gene *blc* is thought to help maintain OM integrity of the tolerant strain and in turn protect it against initial Ag^{+} targeting[273,308]. Permanent upregulation of *carO, ompW,* and *blc* was also observed in the physiologically changed NAg^{R} strain (NRNT *versus* WTNT; see **Figure 5.7**). Furthermore, among the *pga* operon, upregulation of *pgaAB* occurred by ~ 1.6-fold, while expression change of *pgaCD* was insignificant in the untreated tolerant bacterium compared to the WT strain. It is not clear why only *pgaAB* was upregulated, but studies show that *pgaCD* are responsible for periplasmic synthesis of PNAG, while *pgaAB* facilitate the extracellular export of PNAG biofilm EPS formation[276,327]. It is hypothesised that upregulation of the latter genes (and potentially increased PNAG exportation) herein may also contribute to the enhanced biofilm-forming phenotype of the tolerant bacterium (**Figure 4.2**). Most of the *ade* efflux genes linked to the advanced primary defence system also exhibited upregulation in ATNT relative to WTNT (**Figure 6.7**). The genes *adeB, adeI* and *adeJ* exhibited a ~ 1.6 – 1.7-fold expression increase, while expression change to *adeA* was statistically insignificant. It is not currently clear why only *adeA* exhibited no expression change, but the upregulation of the other *ade* genes was interesting, as it was thought that activation of these efflux pump genes is stimulated by Ag^{+} presence. Nonetheless, further investigation is needed to fully ascertain the roles of these mult-drug efflux pumps in silver defence. In contrast, the copper response protein *oprC*, and the copper efflux pump genes *copA* and *copB*, showed no statistically significant expression changes in the untreated tolerant bacterium compared to WTNT. This is understandable considering that these three defence genes were hypothesised to require the presence of silver for transcriptional activation, as also seen in the NAg^{R} strain in **Chapter 5**.

The RNA-Seq analysis revealed that several of the secondary Ag^{+} defence-related genes were also stably expressed in the physiologically changed tolerant bacterium. These secondary Ag^{+} defence mechanisms involved the general stress response, physical cell surface protection, and cation removal and toxicity counteraction through efflux pumps and ROS scavenging, as well as DNA repair and respiratory chain maintenance (see **Section 6.3.2.3.2**). The identification of these mechanisms

highlights that the Ag^{+T} strain exhibits a more refined defence response to cationic silver compared to the WT bacterium. These findings also imply that these defence mechanisms may be physiologically stable, contributing to the now inherent tolerance trait. Firstly, the genes *otsA* and *otsB* (and their transcriptional regulator *bfmR*), responsible for trehalose synthesis, were upregulated by ~ 32.7 – 35.7-fold (and ~ 3.1-fold) in the untreated Ag^{+T} strain relative to the WTNT (**Figure 6.7**). It was deduced that *otsA*/*otsB* upregulation may play a crucial role in the bacterium response to initial Ag^{+} activity, specifically increasing trehalose synthesis and thereby improving CPS density and integrity[265,266]. Additionally, the universal stress protein gene *uspA* was also upregulated by ~ 5.0-fold in the untreated Ag^{+T} strain (**Figure 6.7**). It was hypothesised this gene may also help regulate *otsA*/*otsB* expression due to its regulatory role in the global stress response[268,269,293]. In **Section 4.6.2**, it was noted that the cell morphology (size and shape) of the Ag^{+T} strain had been permanently altered, and the reason for this was unclear (see **Figure 4.2**). Studies have reported on the role of the regulatory factor BfmR in cell morphology regulation in *A. baumannii*[328,329]. It is thought that the increased expression of *bfmR*, and subsequent transcriptional upregulation of *otsA/otsB*, leading to changes in the cell capsule, might in turn contribute to the morphological alterations of the tolerant bacterium[329].

The two genes linked to physical cell surface protection in the secondary defence system, *bap* and *ompA* (see **Section 6.3.2.3.2**), each exhibited upregulation by ~ 8.2-fold and ~ 18.2-fold, respectively, in ATNT compared to WTNT. These genes have substantiated roles in bacterial biofilm formation, and their stable upregulation is thought to contribute to the improved biofilm-forming capabilities of the Ag^{+} bacterium, which manifests without the presence of Ag^{+} (refer to **Figure 4.2**)[251,280]. Furthermore, changes in expression in *ompA* specifically could be correlated to the morphological changes seen in the Ag^{+T} strain (see **Section 4.6.2**). This OMP is recognised for its role in anchoring the outer membrane (of Gram-negative bacteria) to the cell wall by interacting with peptidoglycan[330]. Peptidoglycan is a major constituent of the cell wall, critical in maintaining its strength and integrity, which is ultimately responsible for dictating cell shape[331]. The increased expression of OmpA in the untreated Ag^{+T} strain could perhaps change the peptidoglycan anchorage mechanism, consequently altering the cell wall shape, and in turn, cell morphology, as

seen herein this study[330,332]. This, however, is currently hypothetical and further phenotypic investigation is needed to confirm this association.

Nearly all the secondary defence-related efflux pumps showed no statistically significant change in expression in the untreated tolerant bacterium (**Figure 6.7**). This included the heavy metal efflux pump genes (*actP, hmrR*, and *zitB*) as well as the multi-drug antibiotic efflux pump genes (*adeL, adeG,* and *adeH*). The lack of expression change in these genes was expected, considering no silver was present to stimulate efflux pump activation. Interestingly, *adeF* alone was upregulated by ~ 2.0-fold. A substitutional point mutation was detected in *adeF* (see **Table 4.1**), which may contribute to the stable expression increase of this gene in the Ag^{+T} strain. The precise role of *adeF* in the *adeFGH* operon is not yet fully established, but studies indicate it encodes a membrane fusion protein similar to *adeA* (part of well-defined *adeABC* efflux system) which is responsible for 'opening and closing' the drug transporter (encoded by *adeB*)[316]. Increased translation of the AdeF membrane fusion protein may have been due to the amino acid substitution, improving support for the 'opening/closing' mechanism of the transporter (likely AdeG) to allow for heightened Ag^{+} efflux. Nevertheless, further assessment is necessary to gain a better understanding of the contribution of the mutation to *adeF* and the precise role of these antibiotic efflux pumps in Ag^{+} defence.

Majority of the oxidative stress response-related genes had increased in expression in ATNT in comparison to WTNT. Specifically, *katE, sodB,* and *gshA*, each demonstrated a ~ 12.6-fold, ~ 1.7-fold, and ~ 1.6-fold increase in expression, respectively, while *katB* exhibited no statistically significant expression change (**Figure 6.7**). Upregulation of *katE* and *sodB* (and insignificant expression change of *katB*) was also observed in the untreated NAg^{R} strain (NRNT *versus* WTNT; see **Figure 5.7**). The upregulation of the antioxidant gene *gshA* could coincide with the detected substitutional point mutation to the gene (refer to **Table 4.1**). This may have induced a non-synonymous sequence change, potentially enhancing translation of GCL and subsequent biosynthesis of GSH in the event of Ag^{+}-mediated oxidative stress[220]. Furthermore, the stable upregulation of *gshA* is hypothesised to contribute to the improved biofilm-forming ability of the tolerant bacterium (see **Figure 4.2**)[222]. Taken together, it appears that the Ag^{+T} bacterium has evolved a more improved

oxidative stress defence system compared to the WT bacterium, which manifests even in the absence of silver.

Nearly all DNA repair and respiratory chain maintenance genes exhibited statistically insignificant expression changes in ATNT compared to WTNT. Both DNA recombinase genes *recA* and *radA* showed no statistically significant changes in expression (**Figure 6.7**). This is expected considering that no Ag^{+} (or generated ROS) was present to inflict DNA damage, which aligns with that seen in the untreated NAg^{R} strain, wherein no statistically significant change in *recA* expression was detected (see **Figure 5.7**). Between the three cytochrome *bd* complex genes (*cydABX*) only *cydB* showed an increase in expression of ~ 1.6-fold (**Figure 6.7**). It is not currently understood why overexpression of *cydB* and not *cydA* occurred considering they are both cytochrome *bd* oxidase subunits[333]. However, research indicates that the *cydB* gene sequence is far more divergent across bacterial species, compared to *cydA*, and that *cydB* upregulation is typically associated with resistance to respiratory chain toxins[334]. This could imply that the stable upregulation of *cydB* herein is related to this sequence diversity and correlated to respiratory chain defence. Moreover, the hypothesised heightened respiratory activity of the Ag^{+T} strain, as indicated by the higher extent of intracellular ROS (including in the untreated culture; see **Figure 4.3**), may be due to permanently increased cytochrome *bd* enzyme activity in the respiratory chain (because of CydB upregulation). Lastly, the mutated gene *atr2* exhibited a ~ 24.3-fold downregulation in ATNT relative to WTNT (data not shown). As hypothesised earlier, it appears the deletional mutation may have negatively affected gene function, triggering a homeostatic negative feedback loop to decrease its expression[325]. Despite this, as highlighted earlier, further studies are required to substantiate this claim and elucidate the role/s of the stably mutated gene in the tolerance trait of Ag^{+T} ATCC 19606.

The RNA-Seq data presented herein offers valuable insight into the evolution, adaptation, and physiological changes of ATCC 19606 in response to prolonged exposure to Ag^{+}. The purpose of this section was to identify which mechanisms associated with the advanced primary and secondary Ag^{+} defence systems were permanently expressed in the Ag^{+T} strain and manifested even in the absence of silver pressure. This was to highlight that the bacterium had experienced stable physiological change, relative to the WT strain, due to evolutionary adaptation. The untreated Ag^{+T}

strain (ATNT) demonstrated persistent upregulation of several of the defence-related genes linked to the general stress response and physical cell surface protection. Additionally, various multi-drug efflux pump subunit genes, ROS scavenger genes, and a cytochrome *bd* complex subunit gene, were also upregulated. These included two genes (*gshA* and *adeF*) which underwent mutation because of the bacterium adaptation to Ag^{+}. Defence mechanisms that exhibited no statistically significant expression change were thought to require the presence of Ag^{+} to be activated. Importantly, genes related to biofilm formation, respiratory activity, and (potentially) cell morphology, were persistently upregulated in the untreated Ag^{+T} strain. These observations align with the enhanced biofilm-forming ability and morphological changes, as well as the hypothesised increase in respiratory activity, seen in the tolerant strain in **Chapter 4**. Overall, it can be surmised that in the untreated Ag^{+T} bacterium, the stable expression level increase of the described defence-associated genes are now intrinsically linked to the Ag^{+} tolerance trait. As a reminder, downregulation, or statistically insignificant expression change of the mutated genes, *atr2* and *trpB*, were observed. Thus, at this stage, these mutated genes do not appear to contribute to the evolved Ag^{+} tolerance trait of ATCC 19606.

6.4 Chapter conclusion

Whole transcriptomic analysis of Ag^{+T} *A. baumannii* ATCC 19606 revealed that the bacterium exhibited a diverse extent of gene expression changes which are hypothesised to contribute to the evolved tolerant defence trait against Ag^{+} activity.

The RNA-Seq assessment of the WT strain, following treatment with low or sub-lethal doses of Ag^{+}, led to the identification of gene expression changes which were linked to the primary Ag^{+} defence system. These defence-related genes were suggested to confer physical cell surface defence against Ag^{+} intrusion, through OMPs and biofilm formation, and active cation removal *via* copper/silver and multi-drug efflux pump expression. Enhanced expression of these primary defence-associated genes in the Ag^{+T} strain appeared to be cation concentration-dependent, as function of its evolved advanced primary defence system. Specifically, at lower cation doses, cell surface defence mechanisms were upregulated, while at higher Ag^{+} concentrations, a lipoprotein-carrier and multi-drug efflux pumps exhibited enhanced expression levels.

Intriguingly, further upregulation of the copper/silver efflux pumps was not observed in the Ag^{+T} bacterium, relative to the WT strain. Even so, the heightened upregulation of the primary defence genes in the Ag^{+T} strains highlights the significance of these intrinsic 'first tier' Ag^{+} defence mechanisms in ATCC 19606. See **Figure 6.8** below for a combined heat-map summary of all primary/advanced primary and secondary Ag^{+} defence-associated DEGs identified in this study.

Further RNA-Seq analysis of the tolerant strain, following exposure to low and high concentrations of Ag^{+}, uncovered a multitude of gene expression changes which were unique from the WT bacterium. The encoded mechanisms of these DEGs were linked to the secondary defence system, which likely manifested as result of the evolutionary adaption of ATCC 19606 to Ag^{+}. These secondary defence mechanisms encompassed the general stress response, physical cell surface protection, and active cation removal and toxicity counteraction (*via* oxidative stress responses, DNA repair, and respiratory chain maintenance). Importantly, the exhibition of these mechanisms was also concentration-dependent, as similarly observed with the advanced primary defence system. At lower Ag^{+} doses, the general stress response and cell surface protection genes were, in general, upregulated, while at higher Ag^{+} concentrations, genes encoding efflux pumps, ROS scavengers, DNA recombinases, and respiratory chain enzymes were upregulated. Additionally, the RNA-Seq analysis also revealed that just over half of the advanced primary and secondary defence-related genes were persistently upregulated in the Ag^{+T} strain even in optimal conditions (without Ag^{+} pressure). This included two mutated genes (*gshA* and *adeF*; see **Table 4.1**), which reinforces notion that the mutations had permanently altered gene expression and that these genes are key contributors to the evolved Ag^{+} defence of the tolerant strain. It was ultimately concluded that Ag^{+T} ATCC 19606 had experienced stable physiological change because of its evolutionary adaptation to long-term Ag^{+} exposure. Additionally, several of the defence-related genes were also indicated to contribute to the observed changes in biofilm formation, morphology, and respiratory activity in the tolerant bacterium, as shown in **Figure 4.2** and **Figure 4.3**.

Notably, many of the Ag^{+} defence mechanisms identified in the Ag^{+T} bacterium were also detected in the NAg^{R} strain. This included, but was not limited to, cell surface-related genes (including OMPs and biofilm-related proteins), a copper/silver efflux pump, and various ROS scavengers. Although NAg and Ag^{+} exhibit distinct

antimicrobial toxicity mechanisms, there is overlap in their overarching toxicity paradigms[85]. Considering that the oxidative dissolution of NAg particulates results in the leaching of soluble Ag^{+} (refer to **Figure 2.1**), it is reasonable to suggest that shared defence mechanisms in ATCC 19606 could manifest against both silver agents. Even so, no direct cross-adaptation effects (*i.e.* changes in MIC) were observed between the NAg^{R} and Ag^{+T} strain when treated with each respective silver agent (see **Figure S3**). However, further assessment into the molecular basis of cross-defence needs to be performed. This is important considering that bacterial cross-resistance between NAg and Ag^{+} is evidentially possible[29,85,87].

As this study provided the first reported identification of acquired Ag^{+} tolerance in ATCC 19606, the transcriptomic analysis of the tolerant bacterium has delivered a strong basis for deciphering this bacterial adaptation phenomena against silver cations. Nonetheless, understanding the transcriptomic profile of the Ag^{+T} bacterium was more challenging in comparison to the NAg^{R} strain, specifically because tolerance is considered a more complex adaptation trait than that of resistance[335]. In turn, there remains several knowledge gaps and unclear hypotheses, thus further work is needed to validate the proposed Ag^{+} defence mechanisms. As briefly outlined in the conclusion of **Chapter 5** (**Section 5.4**), an assortment of follow-up experimental work can be performed to fully elucidate the molecular basis of defence in silver-adapted ATCC 19606. Such work might include RT-qPCR to confirm the level of transcriptomic change of genes of interest, though research indicates that RNA-Seq data alone is generally robust enough to confirm changes in gene expression patterns[300]. Performing proteomic and metabolomic studies can offer insight into the function and regulation of the defence mechanisms at the protein and metabolite levels, and gene knockout work is useful in proving the link between an upregulated gene and a predicted defence trait (*e.g.* silver efflux)[302-304]. Alternatively, TraDIS can also be used to determine the link between gene function and fitness in specific conditions and can allow for multiple potential defence-related gene sequences to be targeted at once[305]. High resolution microscopy studies may also be performed to help visualise phenotypic changes in the improved biofilm structure of the tolerant bacterium, as well as the morphological changes exhibited in its planktonic form[306,307].

The RNA-Seq analysis of the Ag^{+T} strain yielded a plethora of promising leads in helping decipher the molecular basis of Ag^{+} tolerance acquisition in bacteria. The

notable overlap in defence mechanisms between the NAg^{R} and Ag^{+T} bacteria underscores the toxicological similarities between NAg and Ag^{+} and sheds light on the potential for cross-defence against each silver agent. The generated knowledge can help improve understanding of the unique adaptation and defence responses of bacteria against different silver agents. This could provide a basis for continual research and development into alternative antimicrobial design which might assist in overcoming the potential for evolutionary adaptation. Ultimately, this work highlights the importance of minimising the overuse of these important alternative agents, specifically through implementation of strategies to manage both the application and disposal of silver-based products to sustain their long-term use in the future.

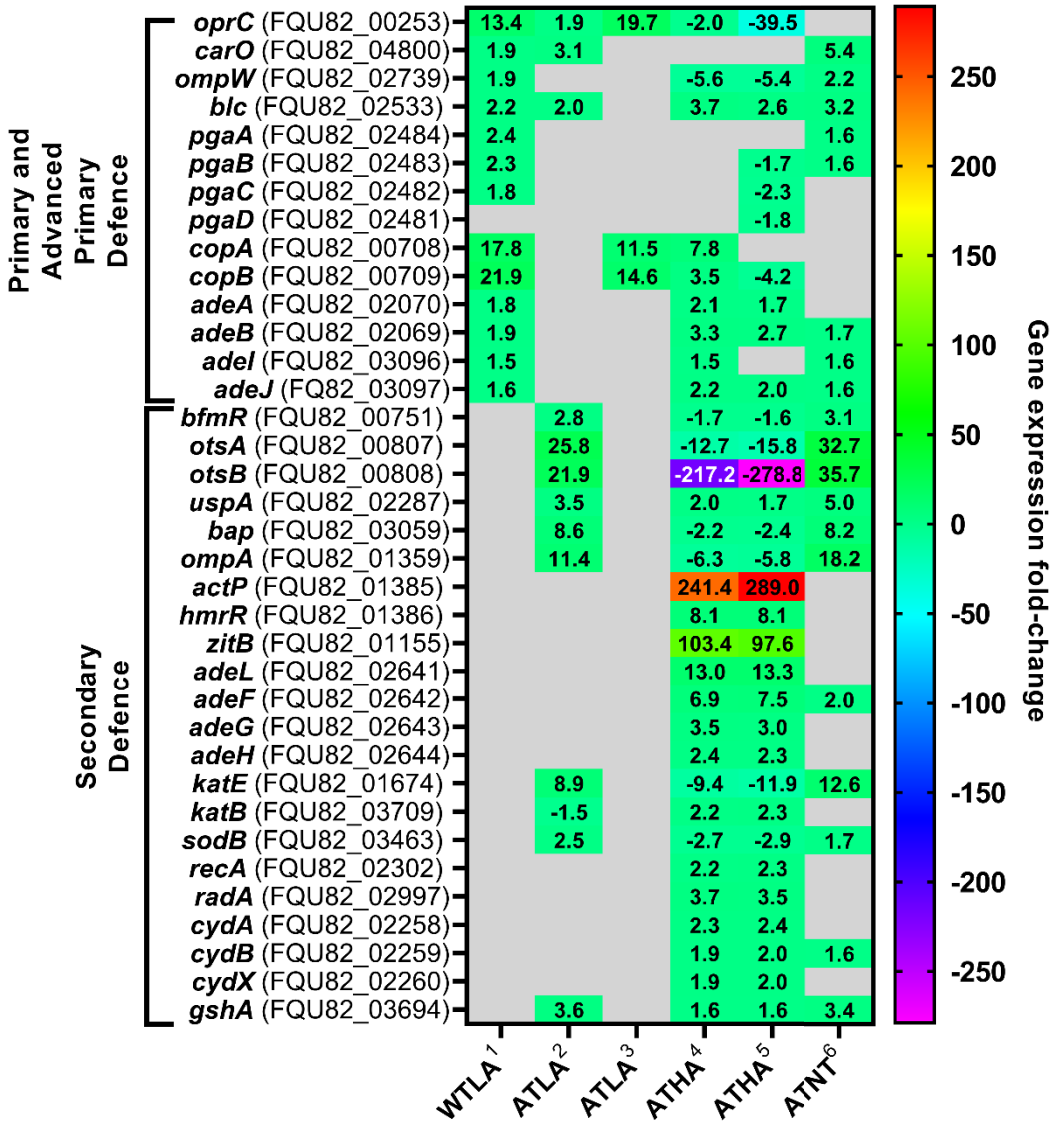

Figure 6.8 Combined heat map of primary, advanced primary, and secondary Ag^{+} defence-associated DEGs identified in WT and Ag^{+T} ATCC 19606. Grey cells indicate statistically insignificant DEGs. Pairwise comparisons: [1] WTLA *versus* WTNT, [2] ATLA *versus* WTLA, [3] ATLA *versus* ATNT, [4] ATHA *versus* ATNT, [5] ATHA *versus* ATLA, [6] ATNT *versus* WTNT.

Chapter 7: General Discussion, Overall Conclusions, and Future Directions

7.1 General Discussion and Conclusions

Antimicrobial resistance (AMR) has become one of the greatest public health challenges facing humanity today, resulting from the medical and commercial overuse of antimicrobials, coupled with diminishing investment into drug development[5-7]. Consequently, there is an urgent need for novel and alternative antimicrobial agents. In recent years, the use of nanotechnology has gained significant momentum in the biomedical sector[61,62]. Silver nanoparticles (or nanosilver; NAg) have become one of the most commercially successful nanotechnology products, owing to their broad-spectrum antimicrobial properties and unique physicochemical properties, making them distinct from traditional antibiotics[19,22,89]. In turn, NAg has become increasingly used in medical devices and commercial products as a means of inhibiting microbial contamination[22,23]. Silver-based agents, such as silver nitrate and silver sulfadiazine, which are sources of cationic silver (Ag^+), have been employed for medical purposes for decades[139,140]. Despite the high antimicrobial efficacy of silver, the growing indiscriminate use of these agents has heightened concern for the generation of silver-adapted bacteria. Bacterial resistance to Ag^+ has been recognised for many years, with most studies highlighting that expression of the silver efflux Sil system or copper efflux Cus system are the main mechanism/s of silver resistance[65,141,154]. However, over the last 10 years, evidence underscoring the emergence of NAg resistance in an array of Gram-negative and Gram-positive bacterial species has grown[29-32,263].

Even so, as outlined in **Chapter 2**, no previous studies had identified if the Gram-negative coccobacillus bacterium *Acinetobacter baumannii* had the potential to develop resistance to NAg[33]. This species is a member of the ESKAPE pathogens group, and in particular, carbapenem-resistant *A. baumannii* (CRAb) has been listed by the WHO as the number one critical priority pathogen requiring novel treatment options[7,9]. Previous inquiries have identified Ag^+ resistance in *A. baumannii*, including expression of the Sil efflux system, but the work presented in **Chapter 4** revealed the first reported evidence of the evolutionary development of NAg resistance in this

species (strain ATCC 19606) following prolonged *in vitro* nanoparticulate exposure[263]. Likewise, this study reported on the development of Ag^{+} tolerance in ATCC 19606 which has also not been shown previously[263]. These distinct adaptation responses were associated with various gene mutations which were linked to physiological and defence changes in the bacterium that manifested due to adaptation to the nanoparticulate and ionic forms of silver. Subsequently, a plethora of gene expression modifications were identified in the resistant and tolerant strains, as discussed in **Chapter 5** and **Chapter 6**, respectively. These were correlated to the proposed silver defence mechanisms and physiological changes of the evolved bacteria. A summary and portrayal of the working models depicting the mechanistic function of the hypothesised defence mechanisms of WT and silver-adapted ATCC 19606 are presented throughout this final Chapter.

7.1.1 The mechanisms of NAg defence in WT and NAg^{R} *A. baumannii*

The study herein revealed, for the first time, that *A. baumannii* ATCC 19606 developed stable resistance to NAg following 30-days of prolonged exposure (refer to **Chapter 4**). This resistance trait was confirmed by an observed 4 – 5 times increase in the minimum inhibitory concentration (MIC) of NAg when compared to the WT strain. The development of NAg resistance was confirmed by the parallel evolution of resistance to the quinolone antibiotic nalidixic acid (Nx) in the bacterium (360 – 380 x MIC; **Figure 4.1**). The NAg^{R} strain evolved stable mutations in the genes *rcsC*, *smf1-2*, and *csuB*, which were initially thought to be responsible for its enhanced biofilm-forming ability and oxidative stress defence (see **Figure 4.2** and **Figure 4.3**). Subsequently, the transcriptomic work in **Chapter 5** revealed no notable expression changes in these mutated genes. Therefore, it was concluded at this stage that these mutated genes have no apparent roles in the NAg resistance trait until further confirmatory research is conducted. Alternatively, the RNA-seq study identified changes in expression patterns of several other genes in the NAg^{R} strain, when compared to the WT, which were correlated to the physiological and defence changes observed in the evolved bacterium.

7.1.1.1 Primary NAg defence response of WT strain

Transcriptomic analysis was conducted on WT ATCC 19606 to investigate potential intrinsic defence mechanisms triggered in response to sub-lethal NAg stress. A variety of upregulated genes were identified in the WT bacterium following treatment with a low (sub-lethal) dose of NAg (0.5 μg/mL; refer to **Table 3.2**). These upregulated genes encoded mechanisms that are designated to the 'first tier' primary defence of the WT bacterium. The primary NAg defence mechanisms comprised of physical cell surface protection against the cell surface targeting activity of NAg, which was mediated by the OMP-encoding genes *oprC*, *ompA, carO,* and *ompW*. While yet to be confirmed, increased expression of the latter three genes may also contribute to an improved biofilm-forming phenotype in the WT strain[248,297]. The primary defence system also involved silver-mediated oxidative stress defence *via* upregulation of the copper efflux pump genes *copA* and *copB* and the homeostasis gene *acnA*, which helps maintain the citric acid cycle for optimal cell function (refer to **Section 5.3.1.3**)[259]. The schematic below shows the working model for the primary (and advanced primary) NAg defence system of WT (and NAg^R) *A. baumannii* ATCC 19606 (**Figure 7.1**).

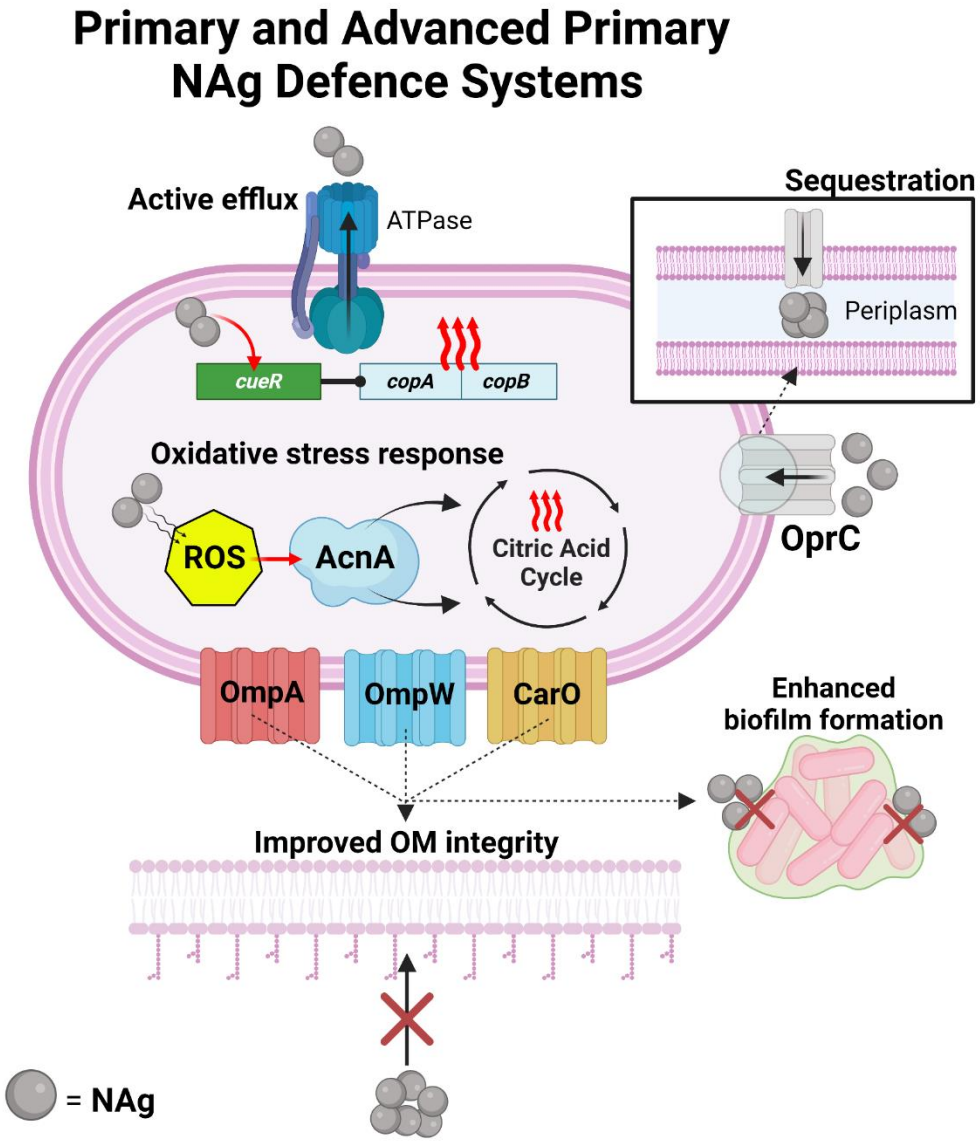

Figure 7.1 Working model depicting the hypothesized inherent 'first tier' primary and advanced primary defence mechanisms against NAg toxicity in WT and NAg^{R} *A. baumannii* ATCC 19606. The mechanisms of NAg defence include physical cell surface protection to NAg penetration, which involves periplasmic sequestration of NAg particulates and increased OMP expression to aid in improved OM integrity and biofilm formation, and oxidative stress prevention *via* active NAg efflux and homeostatic oxidative stress response. Note that expression of *oprC* and *ompA* were not further enhanced in the NAg^{R} strain in response to high NAg dose exposure. Created in BioRender.

7.1.1.2 Advanced primary and secondary defence response of NAg^R strain

The RNA-Seq analysis revealed that nearly all genes linked to the primary defence response were further upregulated in the nanosilver-resistant strain (see **Section 5.3.2.3.1**), which was referred to herein as the advanced primary defence system (**Figure 7.1**).

In response to low NAg concentrations, the genes *ompA, carO*, and *ompW*, exhibited increased expression levels in the NAg^R strain. Additionally, the oxidative stress response gene *acnA* was also further upregulated (see **Figure 5.5**). It is suggested that the increased expression levels of the OMP genes might correlate to the improved biofilm-forming ability of the resistant strain (see **Figure 4.2**). Likewise, upregulation of *acnA* could, at least in part, contribute to the enhanced ROS defence observed in the NAg^R bacterium (see **Figure 4.3**). At higher (lethal) NAg concentrations (3 μg/mL; see **Table 3.2**), the resistant strain only exhibited further upregulation of *carO, ompW,* and *acnA*, while *ompA* and *oprC* were downregulated (see **Figure 5.4**). The reason for *ompA* downregulation remains unclear, while the downregulation of *oprC* is hypothesised to serve as a defence strategy, specifically involving reduced periplasmic sequestration to prevent cellular build-up of toxic silver. The copper efflux pump genes, *copA* and *copB*, along with the transcriptional regulator gene *cueR*, were also further upregulated in the NAg^R strain in response to the higher NAg dose (**Figure 5.4**), which indicate key roles of the copper efflux systems in defence against high concentration nanoparticle exposure. Indeed, no statistically significant expression changes of *copA/B* and *cueR* were detected in the resistant strain in response to lower NAg doses when compared to the WT strain (**Figure 5.4**).

Further RNA-Seq studies revealed several other DEGs detected only in the NAg^R strain – unique from the WT bacterium – which were linked to the secondary NAg defence system. The proposed mechanisms of secondary NAg defence also comprised of physical cell surface protection to NAg invasion, and NAg-induced oxidative stress defence *via* ROS scavenging and active efflux, as well as DNA repair (see **Figure 5.5**). The resistant strain also activated a general stress response which was not observed in the WT bacterium. In response to low NAg doses, upregulation of the general stress response CPS-related genes *otsA* and *otsB* was exhibited by the NAg^R strain. The stress response transcriptional regulator, BfmR, along with the universal stress protein UspA, were also upregulated at low NAg doses, which are thought to positively regulate

otsA/otsB expression[260,269,293]. Upregulation of the trehalose-synthesis *otsA/otsB* genes are thought to improve CPS density and hence confer better cell surface integrity to NAg penetration, while also potentially contributing to the enhanced biofilm-forming ability and silver-mediated ROS defence in the resistant strain (see **Figure 4.2** and **Figure 4.3**)[265-267]. Slight downregulation of *otsA* and *otsB* were observed in the NAg^R strain when treated with high dose NAg (see **Figure 5.5**). The reason for this is not entirely clear, but may correlate to the statistically insignificant expression change of the transcriptional factor BfmR at the higher NAg concentration.

Several other biofilm-associated genes were upregulated in the NAg^R bacterium, *pgaABCD* and *bap*, which support the improved biofilm formation phenotype of the adapted strain (**Figure 4.2**)[276,280]. Previous studies have linked biofilm formation to NAg defence in bacteria. For instance, Panáček, *et al.* reported increased expression of flagellin in *E. coli*, a core protein of flagella, which was correlated to an observed NAg resistance phenotype[30]. Flagellin is crucial in biofilm formation because of its role in facilitating cell-to-surface adhesion[336]. Mann *et al.* observed augmented biofilm formation in gentamicin-resistant *P. aeruginosa* (PAO1) which exhibited greater defence against NAg penetration compared to the WT PAO1 strain[198]. In response to lower NAg doses, *pgaABCD* and *bap* were upregulated in the NAg^R bacterium, but when exposed to higher NAg doses, only *pgaABCD* showed further upregulation, while *bap* showed no statistically significant expression change. The Pga protein complex synthesises the biofilm EPS constituent PNAG, and the enhanced upregulation of this protein complex at higher NAg concentrations thought to facilitate sequestration of the positively-charged metal (including leached Ag^+) by the negatively-charged EPS[276,278]. The NAg^R strain also exhibited increased expression of the lipoprotein transport genes *blc* and *lolA*, at lower NAg doses and even further at higher concentrations (**Figure 5.5**). These lipoprotein-carriers transfer newly synthesised lipoproteins to the OM, which, as indicated in some studies, forms a part of cell membrane repair mechanism[272,273]. Upregulation of these transporters are suggested to provide cell surface defence, in this case, against nanoparticle penetration. Increased expression of lipoprotein-carrier proteins have been indicated to confer resistance to OM-targeting antibiotics[337].

Several genes correlated to secondary oxidative stress defence exhibited increased expression in the resistant strain. Firstly, the NAg^R strain upregulated the catalase

genes *katE, katG,* and *katB,* the superoxide dismutase gene *sodB,* and organic hydroperoxide gene *ohrB*, each of which have been previously linked to both antibiotic and/or silver-induced oxidative stress responses[98,241,281,282,338]. Expression levels of *katB* and *katG* increased in response to higher NAg concentrations, while the other genes were either downregulated or exhibited no statistically significant expression changes (see **Figure 5.5**). Next, the copper efflux pump gene *actP* was also upregulated in the NAg^R bacterium, along with the transcriptional regulator gene *hmrR*. While *actP* expression has not been previously linked to silver defence, expression of this gene had increased in response to higher doses of NAg (**Figure 5.5**)[287,288]. The observed upregulation of these oxidative stress response-related genes in the NAg^R strain are consistent with the observed NAg-mediated ROS defence of the resistant strain, with less intracellular ROS detected compared to the WT strain (at comparable NAg doses; see **Figure 4.3**). The oxidative stress response is also consistent with the observed upregulation of the DNA repair gene *recA* in the resistant strain[291,292]. For the latter, previous studies have indicated oxidative DNA damage in silver-exposed bacteria[99,223]. The schematic below shows the working model for the secondary NAg defence system of NAg^R ATCC 19606 (**Figure 7.2**).

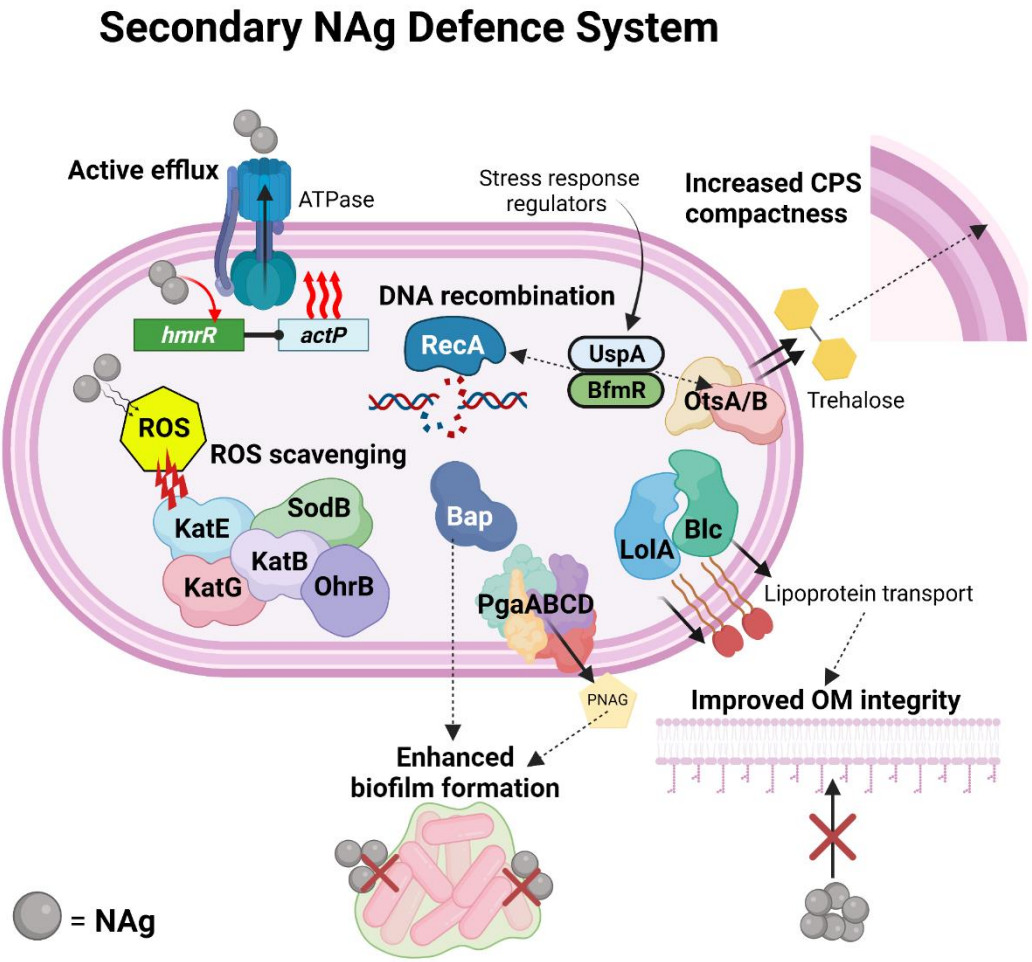

Figure 7.2 Working model depicting the hypothesised mechanisms which confer the secondary defence to NAg toxicity in NAg^{R} *A. baumannii* ATCC 19606. The mechanisms of defence and/or resistance include regulation of the general stress response which involves enhanced trehalose production for added CPS compaction, physical cell surface protection to NAg penetration *via* improved biofilm formation and OM integrity maintenance, oxidative stress prevention *via* ROS scavenging, active silver efflux, as well as recombinational DNA repair. Created in BioRender.

The extent of gene expression changes in the resistant strain, when compared to the WT bacterium, suggested that the resistant strain had physiologically transformed because of its evolutionary adaptation to NAg. Transcriptomic analysis of the resistant bacterium when proliferating in optimal growth conditions (*i.e.* in the absence of NAg pressure) revealed that nearly all DEGs associated with the advanced primary and

secondary defence systems remained stably upregulated. The exceptions being *oprC*, *copA*, *copB*, *cueR*, *katB*, and *recA* (refer to **Figure 5.7**). Upregulation of these defence mechanisms was thought to require stimulation by nanoparticle presence. Notably, the genes involved in OM lipoprotein transport, *blc* and *lolA,* the biofilm-associated genes, *ompA*, *carO, ompW, bap*, and *pgaABCD*, and the oxidative stress defence-related genes, including *acnA, katE, katG, sodB*, *ohrB*, *actP* (and its transcriptional regulator *hmrR*) were all constitutively upregulated in the untreated NAg^R bacterium. Permanent upregulation of these genes was correlated to the improved cell surface defence, enhanced biofilm-forming ability, and greater ROS defence capabilities of the resistant strain. In addition, stable upregulation of *otsA* and *otsB* (as well as the stress response regulators *bmfR* and *uspA*) were also observed, and it was hypothesised that overproduction of trehalose for improved CPS density might also potentially contribute to these respective phenotypic changes[231].

7.1.2 The mechanisms of Ag^+ defence in WT and Ag^{+T} *A. baumannii*

In parallel to NAg, *A. baumannii* ATCC 19606 was also subjected to long-term cationic silver (Ag^+) exposure over 30-days with the aim of inducing adaptation. Rather than developing resistance, the bacterium evolved a tolerance trait, as evidenced by an increase in the minimum duration of killing 99% (MDK_{99}) of the population with Ag^+ (see **Section 4.6.1**, **Figure 4.1**). Various genetic point mutations were identified in the Ag^{+T} strain (refer to **Table 4.1**), and the bacterium exhibited distinct changes in its biofilm-forming ability, cell morphology, oxidative stress response, and potential respiratory activity (see **Section 4.6.2** and **Section 4.6.3**). Among the mutated genes, *gshA* was initially associated with the observed changes to biofilm formation and oxidative stress response. However, the mechanistic link underlying the alterations in cell morphology and respiratory function could not be determined. Subsequently, the transcriptomic study presented in **Chapter 6** aimed to identify alterations in gene expression patterns in the Ag^{+T} strain, when compared to the WT strain, with the intention of unravelling the underlying tolerant mechanisms and elucidate the phenotypic changes observed in the adapted bacterium.

7.1.2.1 Primary Ag^+ defence response of WT strain

RNA-Seq analysis of WT *A. baumannii* ATCC 19606 was performed to identify defence mechanisms that were activated in response to low (sub-lethal) Ag^+ exposure (1 µg/mL; refer to **Table 3.2**). Several upregulated genes were detected, encoding mechanisms designated to the 'first tier' primary Ag^+ defence system of the bacterium. The primary mechanisms comprised of cell surface defence to Ag^+ targeting and active removal of the cation *via* efflux pumps (see **Section 6.3.1.3**).

Regarding cell surface defence, various genes encoding OMPs and biofilm-associated proteins were upregulated in WT ATCC 19606 (refer to **Figure 6.4**). The OM-related genes *oprC*, *ompA*, *ompW*, and *blc*, along with the biofilm-associated operon *pgaABC* (excluding *pgaD*) were upregulated in WT bacterium in response to low dose Ag^+, Increased expression of the copper efflux pump genes *copA* and *copB* was also observed in the low Ag^+-treated WT bacterium. Notably, increased expression of *oprC, ompA,* and *ompW* and both copper efflux genes was noted in the low NAg-treated WT strain (**Figure 5.2**). The detection of overlapping defence mechanisms between the NAg- and Ag^+-exposed WT bacteria highlights the similarities in toxicity mechanisms between the two silver agents (refer to **Figure 2.1**) and indicates the possibility of cross-defence effects. Furthermore, genes unique to the Ag^+-treated WT bacterium were also upregulated, which included the highly conserved *A. baumannii* RND multidrug efflux pump genes *adeAB* (excludes *adeC*) and *adeIJ* (excludes *adeK)*[309,316]. While these efflux pumps have not been previously associated with heavy metal efflux, expression of these genes were later found to be further increased in the Ag^{+T} strain (see **Figure 6.4**) which indicated an involvement in silver efflux. The working model of the primary (and advanced primary) Ag^+ defence system in *A. baumannii* ATCC 19606 is shown below in **Figure 7.3**.

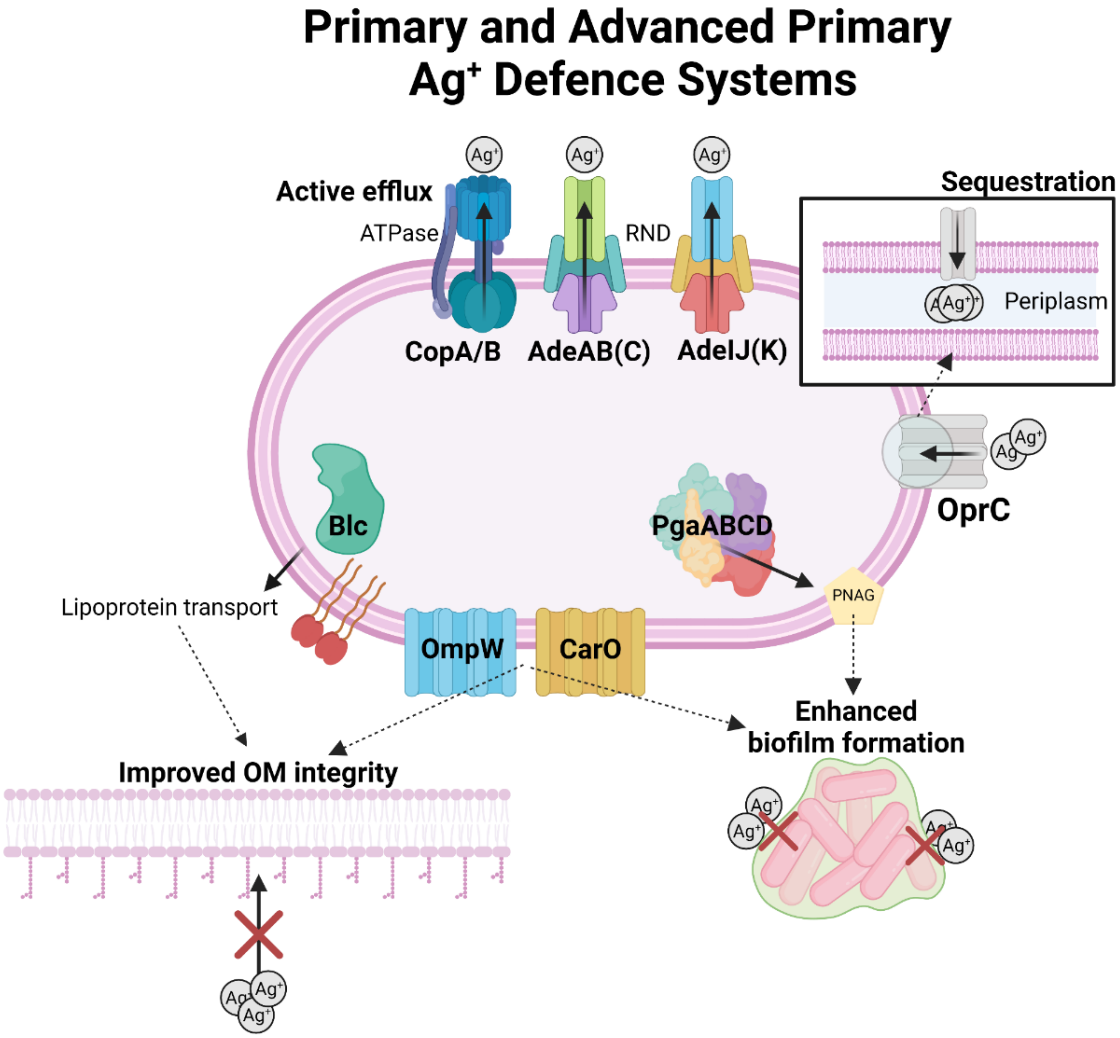

Figure 7.3 Working model depicting the hypothesised mechanisms which confer 'first tier' primary and advanced primary defence to Ag^{+} toxicity in WT and Ag^{+T} *A. baumannii* ATCC 19606. The mechanisms of defence include physical cell surface protection to Ag^{+} penetration *via* periplasmic sequestration of cations, and enhanced biofilm formation of OM integrity maintenance, and active removal of the cations *via* copper and antibiotic efflux pumps. In the Ag^{+T} strain, the mechanisms of physical cell surface protection appeared to respond to lower (sub-lethal) doses of Ag^{+}, while increased antibiotic efflux pump expression occurred at higher (lethal) Ag^{+} doses. Note that further upregulation of the copper efflux pumps beyond the WT bacterium was not observed in the Ag^{+T} strain. Created in BioRender.

7.1.2.2 Advanced primary and secondary defence response of Ag^{+T} strain

Deciphering the mechanistic basis of tolerance posed challenges, as this adaptation trait is less understood and considered more complex than that of resistance[193,335]. Whole transcriptomic analysis of the Ag^{+T} strain, following exposure to both low and high concentrations of Ag^{+}, revealed notable shifts in gene expression patterns in comparison to the WT bacterium (refer to **Section 6.3.2.3**). The primary Ag^{+} defence-related genes were further upregulated in the tolerant strain as part of its advanced primary defence system, but in a concentration-dependent manner (see **Section 5.3.2.3.1**). Specifically, genes related to non-specific physical defence were enhanced in expression at lower doses of Ag^{+}, while following treatment with higher Ag^{+} doses, genes encoding antibiotic efflux pumps and an OM lipoprotein-carrier were further upregulated (see **Figure 7.3**).

In response to lower Ag^{+} concentrations, the physical cell surface defence-related genes, *oprC*, *carO*, and *blc* exhibited further upregulation in the Ag^{+T} strain (see **Figure 6.4**). All other primary defence-associated genes, including the copper and antibiotic efflux pump genes, showed no statistically significant expression change. In contrast, only *blc* and the antibiotic efflux pumps *adeAB* and *adeIJ* exhibited increased expression in the Ag^{+T} strain when exposed to higher Ag^{+} doses (3 μg/mL; see **Table 3.2**; and see **Figure 6.4**). Enhanced upregulation of *blc*, as well as *carO*, was also observed in the NAg^{R} strain in response to higher NAg concentrations (see **Figure 5.4** and **Figure 5.5**). Overall, it is indicated that increased lipoprotein transport for OM maintenance is critical in cell surface defence to Ag^{+} diffusion, while the antibiotic efflux pumps are required to remove excess cations that have breached through to the cytoplasm. These observations support the hypothesis that the antibiotic efflux pumps may play a role in cross-defence against silver. On the other hand, notable downregulation of *oprC* was seen in the high Ag^{+}-treated tolerant bacterium, but this was thought serve as a defence strategy to reduce periplasmic accumulation of toxic silver, as similarly observed in the high NAg-treated NAg^{R} strain (see **Figure 5.4**)[242]. Moreover, the downregulation or insignificant expression change of the biofilm-related genes *pgaABCD* in the high dose treated bacterium was unexpected, considering that the Ag^{+T} strain exhibited an enhanced biofilm-forming phenotype (see **Figure 4.2**). This contrasts that of the NAg^{R} strain, which exhibited increased expression change of *pgaABCD* in response to high NAg concentrations. Nonetheless,

the reason for the downregulation of this operon in the tolerant bacterium is currently unclear and further assessment is needed.

Further RNA-Seq analysis of the Ag^{+T} strain identified several other DEGs, unique from the WT bacterium, which were linked to the evolved secondary Ag^{+} defence system. The suggested mechanisms of secondary defence also encompassed physical cell surface protection to Ag^{+} diffusion, and active cation removal and toxicity counteraction, as well as the general stress response (see **Section 6.3.2.3.2**). As similarly observed in the NAg^{R} strain, the Ag^{+T} strain exhibited increases in expression of *otsA* and *otsB*, along with transcriptional regulator and universal stress response genes, *bfmR* and *uspA,* respectively, when exposed to low doses of Ag^{+} (see **Figure 6.5**). Intriguingly, the tolerant bacterium displayed significant downregulation of *otsA*/*otsB*, as well as *bfmR*, when treated with higher Ag^{+} doses. While the reason for this is not fully clear, it is hypothesised this mechanism is 'switched-off' in order to divert resources to more critical defence mechanisms, such as efflux pumps and ROS scavengers (see **Section 6.3.2.3.2**, **Figure 6.5**). Slight downregulation of *otsA/otsB* (and insignificant expression change of *bfmR*) was also observed in the high NAg-treated resistant strain, but not to the same extent as the tolerant bacterium herein (see **Figure 5.5**). Alternatively, *uspA* was further upregulated in the high Ag^{+} dose treated bacterium (like that of the NAg^{R} strain; **Figure 5.5**), indicating its likely important role in regulating the universal stress response. Notably, two key biofilm-associated genes, *ompA* and *bap*, were also upregulated in the low dose treated Ag^{+T} bacterium, which supports the observed enhancement in biofilm formation of the tolerant strain as shown in **Figure 4.2**. A decrease in expression levels of both biofilm-related genes was noted when the strain was exposed to higher Ag^{+} concentrations (**Figure 6.5**). The reason for the downregulation of *bap* is not currently clear, but decreased *ompA* expression could be linked to the known *E. coli* defence mechanism involving repressed *ompF*/*C* expression to limit silver passage through the OM[141,142]. A decrease in *ompA* expression and statistically insignificant change in *bap* expression was also noted in the NAg^{R} strain when exposed to higher NAg doses (**Figure 5.4**), but the reason for these observations is also unclear this stage.

The Ag^{+T} strain also exhibited significant expression changes in genes encoding efflux pumps, ROS scavengers, respiratory chain enzymes, and DNA recombinases (see **Figure 6.5**). The copper efflux pump gene *actP*, its transcriptional regulator *hmrR*, and

the zinc transporter gene *zitB* all exhibited upregulation when the bacterium was exposed to high Ag^+ doses. Expression levels of these genes were statistically insignificant in the low Ag^+ exposure system. Overexpression of *actP* (and *hmrR*) was also noted in the high NAg-treated NAg^R strain (refer to **Figure 5.5**), which support its hypothesised involvement in silver efflux. Research indicates that significant overexpression of the zinc transporter can disrupt heavy metal differentiation, implying ZitB can permit efflux of Ag^+[315]. The RND multidrug efflux pump operon *adeFGH*, and the transcriptional regulator *adeL*, were also upregulated only following high Ag^+ dose treatment[225]. Increased expression levels of the advanced primary defence-related *ade* efflux genes at higher Ag^+ doses supported the hypothesis that the multi-drug efflux pumps can confer Ag^+ defence (see **Figure 6.4**). It is also important to highlight that the gene *adeF* was mutated in the tolerant bacterium (see **Table 4.1**), and this mutation may have affected its expression and is thought to be key to the evolved Ag^+ tolerant activity of the bacterium. However, further assessment is needed to confirm the significance of this mutation and prove the contribution of these multi-drug efflux pumps in silver defence.

Changes in expression of various oxidative stress response genes were also observed, and included *katE*, *katB*, *sodB*, and the antioxidant gene *gshA* (see **Figure 6.5**). Both *katE* and *sodB* appear to be activated at lower Ag^+ doses, which was also noted in the NAg^R strain when treated with sub-lethal NAg doses (refer to **Figure 5.4**). Contrarily, *katB* and *gshA* were overexpressed following high Ag^+ dose treatment. These expression levels were linked to reported evidence that *katE* (and possibly *sodB*) is typically activated in response to lower ROS concentrations, while *katB* may be upregulated at higher concentrations. This also aligns with the observed upregulation of *katB* in the NAg^R bacterium in response to high NAg doses (**Figure 5.4**). Notably, a point mutation to *gshA* was detected in the Ag^{+T} strain (**Table 4.1**), and it was suspected that this stable mutation permanently altered gene expression. This mutated gene is predicted to play a role in the oxidative stress response and enhanced biofilm-forming capabilities of the tolerant bacterium described in **Chapter 4**. In addition, there is a potential association with increased GSH production and binding with silver to subsequently induce periplasmic sequestration[221,222,321,322]. Collectively, the overlapping expression changes in ROS scavenging genes between the Ag^{+T} and NAg^R strains underscores the importance of bacterial oxidative stress defence in response to

silver[33,98]. Moreover, upregulation of the two DNA recombinase genes, *recA* and *radA*, also only occurred in the tolerant bacterium following high Ag^{+} dose exposure. Increased expression of *recA* was also observed in the NAg^{R} strain, and this indicated that activation of DNA repair mechanisms is necessary in the counteraction of silver toxicity (see **Figure 5.4**)[292,318]. Lastly, genes encoding the respiratory chain cytochrome *bd* complex operon, namely *cydABX*, was also upregulated in the tolerant bacterium. The upregulation of *cydABX* was thought to counteract Ag^{+} toxicity by maintaining respiratory activity and ATP generation in the Ag^{+T} strain. This in turn would lead to higher H_2O_2 generation as a respiratory by-product as indicated by the greater intracellular ROS levels (measured as CTCF) in the Ag^{+T} strain in **Figure 4.3**[20,33,319,334]. The working model portraying the secondary Ag^{+} defence mechanisms in Ag^{+T} *A. baumannii* ATCC 19606 is shown in **Figure 7.4** below.

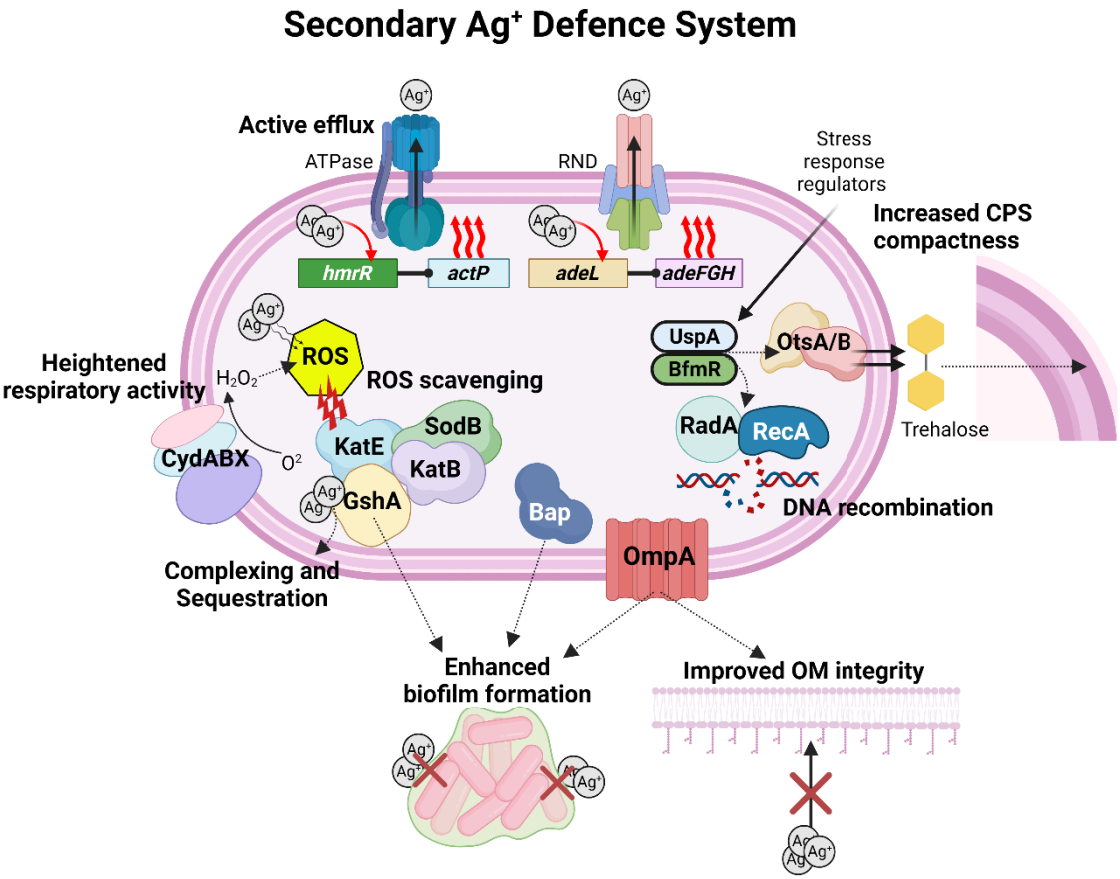

Figure 7.4 Working model depicting the hypothesised mechanisms which confer the secondary defence to Ag^+ toxicity in Ag^{+T} *A. baumannii* ATCC 19606. The mechanisms of Ag^+ defence and/or tolerance include general stress responses involving stress response regulation which stimulates increased trehalose production for added CPS compaction, physical cell surface protection to Ag^+ penetration *via* enhanced biofilm formation and improved OM integrity, active cation removal and counteraction *via* copper and antibiotic efflux pumps, ROS scavenging, recombinational DNA repair, and heightened respiratory activity. In general, under low Ag^+ dose exposure, the general stress response and physical cell surface protection mechanisms were upregulated, while at higher Ag^+ doses, the efflux pumps, ROS scavengers, DNA recombinases, and respiratory chain enzymes were upregulated. Created in BioRender.

As similarly observed in the NAg^R strain, the extent of gene expression changes in the Ag^{+T} strain, relative to the WT bacterium, indicated that the tolerant strain had physiologically transformed due to prolonged Ag^+ exposure. This was confirmed by the stable upregulation of roughly half of the advanced primary and secondary Ag^+

defence-associated genes in the tolerant bacterium when grown in optimal conditions (without Ag^+ presence; refer to **Figure 6.7**). Genes that exhibited no stable upregulation were thought to be stimulated by the presence of silver.

Genes correlated to cell surface defence and biofilm formation and were stably upregulated in the untreated Ag^+ strain, including *carO*, *ompW*, *blc*, *pgaA/B* (excluding *pgaC/D*), *otsA*/*otsB*, *ompA*, *bap*, the mutated gene *gshA*, as well as the stress response regulators *bfmR* and *uspA*. Stable expression increases of these genes are thought to contribute to the physiologically enhanced biofilm-forming phenotype observed in the tolerant bacterium (see **Figure 4.2**). It is therefore thought that improved biofilm formation functions at the frontline of tolerant defence against initial Ag^+ pressure. In addition, it was also hypothesised that upregulation of *otsA*/*otsB*, and their transcriptional regulator *bfmR*, could relate to the observed morphology alterations due to changes in CPS density[329]. Furthermore, the anchorage of OmpA to the inner peptidoglycan cell wall is known to dictate cell morphology, and in turn it was hypothesised that overexpression of the porin could result in changes in cell wall rigidity and potentially alter cell size and shape[330,332]. Nonetheless, further assessment is needed to properly interpret the morphological changes observed in the tolerant strain.

Upregulation of *adeB* and *adeIJ*, but not *adeA*, was noted in the untreated tolerant strain, and considering that these efflux pump genes are clustered as operons (*i.e. adeABC, adeIJK*) this observation is surprising and the reason is currently unclear. Moreover, expression of *adeF* was also increased, but not in *adeL* nor *adeGH*, though this was linked with the detected point mutation to the former gene (see **Table 4.1**), which might have permanently altered its expression. Additionally, stable upregulation of *katE* and *sodB* was also observed. The permanent overexpression of these ROS scavenger genes was linked to evidence that they are activated in response to lower ROS levels, thus, they are hypothesised to act in the first-line of defence to silver-generated ROS. Interestingly, the *cydB* subunit exhibited slight upregulation in the untreated Ag^{+T} strain, while *cydA* and *cydX* showed no statistically significant expression change. This upregulation of *cydB* was correlated to its genetic sequence diversity and reported evidence that overexpression of this gene confers defence against respiratory chain toxins (see **Figure 6.7**)[334]. It was also hypothesised that the proposed heightened respiratory activity demonstrated by the Ag^{+T} strain may be

associated with permanent upregulation of *cydB* (see **Figure 4.3**), however continual investigation to understand this phenotype is required.

7.2 Overall conclusions

This study presented novel findings on the simultaneous stable evolution of resistance to antimicrobial silver nanoparticles (NAg) and tolerance to cationic silver (Ag^+) in *A. baumannii* ATCC 19606. The silver-adapted strains evolved genetic mutations and initial investigation associated these molecular changes to alterations in biofilm formation and oxidative stress-related defence. Through comparative global transcriptomic analyses, broader insights into the molecular mechanisms underlying these adaptation traits and physiological changes in the adapted bacteria was gained. Importantly, this study represents the first transcriptomic investigation of an *A. baumannii* strain in response to NAg and Ag^+ toxicity. It should be noted that, for this thesis, the ATCC 19606 strain (first isolated in 1948) was selected over a more modern strain because it is biologically well-established, its genome has been fully sequenced, and it has been widely utilised for studying antimicrobial resistance evolution in *A. baumannii*[199,339]. Considering this was a novel silver evolution study, it was also imperative to use a strain that is 'antibiotic susceptible' (which is often difficult to source) to limit the interference of non-intrinsic antibiotic resistance mechanisms which could potentially confer unwanted cross-defence against the silver agents[199].

The NAg-resistant (NAg^R) bacterium exhibited significant changes in expression of genes which encode mechanisms indicated to confer NAg resistance. The enhanced expression of primary NAg defence-related genes (identified in WT ATCC 19606) in the resistant strain constituted what was labelled herein as the advanced primary defence system. Further gene expression changes in the NAg^R strain were hypothesised to contribute to a secondary defence system, which was unique to the evolved strain and likely manifested as result of evolutionary adaptation to NAg. Notably, majority of these defence mechanisms were stably upregulated in the NAg^R bacterium, even in optimal growth conditions, indicating that substantial physiological changes occurred in the bacterium due to its adaptation to the nanoparticle. Genes that were not constitutively upregulated were expected to only be activated when in the

presence of silver. These changes encompassed enhanced biofilm formation and improved oxidative stress defence capabilities and demonstrated that the permanently upregulated defence-related genes were now inherently linked to the NAg resistance phenotype. Based on the RNA-Seq data reported herein, the genetic mutations identified in the NAg^R strain were, at this stage, concluded to not directly contribute to the NAg defence response of the evolved bacterium. It should also be noted that, despite in depth literature reviews, any indirect roles of these mutated genes to the physiology and/or active defence of the resistant strain could not be identified.

In contrast, the Ag^+-tolerant (Ag^{+T}) strain demonstrated far more unique gene expression patterns when compared to the NAg^R bacterium. Understanding the molecular basis of the Ag^+ tolerance trait presented greater challenges compared to the NAg resistance trait[193,194]. Transcriptomic analysis of the Ag^+-treated WT strain identified various primary Ag^+ defence-associated gene expression changes. Enhanced expression of these genes in the tolerant strain, as part of the advanced primary defence system, appeared to be dependent on the concentration of Ag^+ present. Specifically, when exposed to lower (or sub-lethal) cation doses, upregulation of genes related to physical cell surface protection occurred, namely genes encoding OMPs and a lipoprotein-carrier. But upon treatment with higher (lethal) doses of Ag^+, the bacterium predominantly exhibited enhanced activation of antibiotic efflux pumps, along with the lipoprotein-carrier. Similar concentration-dependent expression patterns were also observed in the secondary defence system, which, like with the NAg^R strain, is unique from the WT bacterium and believed to form the basis of Ag^+ tolerance in *A. baumannii* ATCC 19606. In response to low Ag^+ doses, genes which contribute to the general stress response and physical cell surface protection mechanisms were upregulated, while at higher doses, genes related to heavy metal and antibiotic efflux, oxidative stress responses, DNA repair, and respiratory activity, exhibited upregulation. When in optimal conditions (*i.e.* without Ag^+ stress), the tolerant strain exhibited stable and permanent upregulation of several advanced primary and secondary defence-related genes, except for genes requiring the presence of silver for activation. Like the NAg^R strain, this highlighted that the Ag^{+T} bacterium had undergone evolutionary physiological changes and that the stably upregulated genes now permanently contributed to the Ag^+ tolerance trait. Additionally, the constitutively upregulated genes were correlated to the observed changes in biofilm-formation,

oxidative stress defence, and potentially, respiratory activity and morphology characteristics of the Ag^{+T} bacterium. Furthermore, two mutated genes identified in the tolerant bacterium were also constitutively upregulated which indicated their expression was permanently altered due to mutation and suggests they now play pivotal roles in Ag^{+} tolerance of ATCC 19606.

Indeed, several of the identified silver defence mechanisms overlapped between the NAg^{R} and Ag^{+T} variants. While research highlights that both silver agents exert distinct antimicrobial mechanisms from each other, they are known to share similar fundamental toxicity paradigms. Although no cross-adaptation effects were observed between the evolved strains in this study (see **Figure S3**), it is reasonable to suggest that an exhibition of cross-defence from specific mechanisms in ATCC 19606 against both NAg and Ag^{+} is possible. This, of course, will require continual assessment and further experimental work to substantiate this claim. Being that the transcriptomic analysis of the NAg- and Ag^{+}-adapted strains is the first of its kind, there remain an assortment of questions and inconclusive hypotheses. As such, there are number of feasible follow-up studies and future directions which can be implemented to elucidate and better comprehend the molecular basis of NAg resistance and Ag^{+} tolerance in this bacterium.

7.3 Future Directions

The emergence of NAg resistance and Ag^{+} tolerance has not been previously identified in any *A. baumannii* strain. This study has generated substantial knowledge into the molecular basis of silver adaptation in this species, while equally highlighting that the toxicity features of antimicrobial silver and potential concurrent bacterial defence responses are diverse and complex.

Research into bacterial NAg adaptation has expanded in recent years, with many inquiries demonstrating that resistance development is not species specific. Even so, identified mechanisms of NAg resistance are versatile among bacterial species, which can be attributed to the multi-targeting and broad-spectrum antibacterial properties of the nanoparticle. Consequently, the first reported establishment of NAg resistance in *A. baumannii* ATCC 19606 has raised various unresolved queries which could not be fully addressed in this study. Moreover, while the mechanisms of bacterial Ag^{+}

resistance are relatively well-established, the development of Ag^{+} tolerance posed a challenge. This adaptation trait has also not been previously identified in *A. baumannii* and tolerance is overall less researched and considered more biologically complex in comparison to resistance.

The comprehensive phenotypic, genetic, and transcriptomic analyses of the NAg^{R} and Ag^{+T} strains, has ultimately provided valuable insights into the fundamental mechanisms of silver adaptation and defence in this bacterium. However, establishing a direct connection between phenotype and the identified genetic/epigenetic modifications in the silver-adapted strains will help affirm the mechanisms of silver adaptation and defence in *A. baumannii*. This garnered knowledge not only emphasises the importance of implementing strategies to effectively manage the use and disposal of silver agents but also facilitates future research aimed at overcoming bacterial adaptation to these alternative antimicrobial agents.

7.3.1 Follow-up studies

The RNA-Seq work performed within this study provided strong evidential links between gene expression changes in silver-adapted *A. baumannii* ATCC 19606 and potentially encoded silver defence mechanisms. However, it is important that follow-up work is performed to confirm this relationship, as transcriptomic profiling can only reveal the expression patterns of genes of interest but does not conclusively disclose mechanistic gene function.

Firstly, the NAg particulates utilised in this study were synthesised through a specific method (*i.e.* flame spray pyrolysis) with specific physicochemical properties (*i.e.* morphology and surface functionalisation; see **Section 3.1**). As a result, the susceptibility and evolutionary adaptation capabilities of ATCC 19606 may be specific to these nanoparticle properties. While the fundamental toxicity paradigms of NAg (*i.e.* oxidative Ag^{+} leaching, ROS generation, biomolecule degradation) are generally consistent, it is likely that nanoparticles synthesised through alternative methods with different physicochemical characteristics could influence the degree and extent of antibacterial activity against this bacterium (see **Section 2.5**). Consequently, this could also impact the rate at which the bacterium adapts and triggers its defence response/s. Considering this, and the novelty of this study, it may be advantageous to perform

analogous antibacterial and evolution studies as those reported in this thesis with nanoparticles fabricated with different sizes, shapes, and functional surface properties. Additionally, a comparative assessment of the efficacy of variably synthesised nanoparticles against different bacterial species, encompassing both antibiotic-susceptible and -resistant strains (such as WT *versus* MDR strains within Gram-positive and Gram-negatives species) may also yield useful insights into how particular intrinsic and/or acquired antibiotic defence mechanisms impacts the antibacterial activity of NAg and the potential for bacterial evolutionary adaptation.

As described in **Chapter 5** and **Chapter 6**, a common complementary analysis tool to RNA-Seq is RT-qPCR. This tool can be useful in validating the expression patterns of DEGs of interest, particularly those with unclear functional pathways. However, research shows that the data produced through RNA-Seq alone is robust enough to confirm gene expression changes[300,301]. More suitable complementary studies to transcriptomics could include proteomics and metabolomics, which can help dictate the function and regulation of identified defence mechanisms at the protein and metabolite levels. However, the use of omics to study antimicrobial adaptation typically involves bacteria which have evolved to single-target antibacterial agents (*e.g.* antibiotics)[340,341]. While proteomic and metabolomic approaches can help achieve bacterial-wide analyses of defence-related protein and metabolite quantities when treated with antibiotics, both NAg and Ag^{+} are complex and multi-targeting agents (refer to **Figure 2.1**). As seen in this study, both silver-adapted strain exhibited a diverse range of defence-associated gene expression changes, and this would make it extremely difficult to pinpoint the mechanistic origin of identified metabolites, for example. Moreover, most bacterial adaptation-related studies which utilise omics are generally employed to study (antibiotic) resistance, while their applications in investigating tolerance/persistence is rather limited[341,342]. While the phenotypic assessments described in **Chapter 4** (*i.e.* enhanced biofilm formation, oxidative stress defence) are strongly supported by the transcriptomic data outlined in **Chapter 5** and **Chapter 6** (*i.e.* biofilm-related genes, ROS scavenging genes), proteomics and metabolomics could be advantageous in unravelling the stable physiological changes in both strains. Specifically, analysing changes in biofilm-related proteins and metabolites, as well as those involved in cell morphology and respiration, with regard to the Ag^{+T} bacterium (see **Figure 4.2** and **Figure 4.3**), could help better establish what

genes/protein products are involved in these permanent phenotypic modifications[340,342].

Confirming the link between an expressed gene and proposed defence mechanism is critical in proving the extent of adaptation in the evolved strains. One method to enable this includes gene knockout/editing studies (*e.g.* CRISPR-Cas system), which is a relatively simple yet useful tool to observe the loss of a hypothesised defence phenotype when the associated gene is deleted or inactivated[304]. However, a notable limitation to this molecular tool is that only single genes can be targeted at time. Considering that the silver-adapted strains exhibit their evolved defence *via* a myriad of mechanisms, the use of gene knockout studies may be time consuming and inefficient. Alternatively, the implementation of Transposon Directed Insertion Sequencing (TraDIS) can be used to target a broader range of genes of interest. TraDIS involves the insertion of a transposon into a gene, disrupting its function near the insertion site. Bacteria are grown under desired conditions, and the transposon insertion sites are sequenced. This tool helps identify the relationship between gene function and fitness in bacteria, identifying essential and non-essential genes, including those that provide survival advantages under specific environmental conditions, *i.e.* NAg/Ag^{+} defence-related genes within the silver-adapted strains[305].

More specific follow-up work could include the visual assessment of phenotypic changes of the adapted strains. In **Chapter 4**, both the NAg^{R} and Ag^{+T} bacteria exhibited stable physiological increases in their biofilm-forming ability and the transcriptomic work in **Chapter 5** and **Chapter 6** found that both strains experienced expression changes in genes related to biofilm formation. Further biofilm growth studies of the silver-adapted strains *via* fluorescence microscopy when exposed to their respective silver agent could be performed. By comparing the extent of biofilm biomass produced to those shown in **Figure 4.2**, this could help prove that enhanced biofilm formation is an evolved mechanism of silver defence in ATCC 19606. More advanced methods for assessing the biofilm phenotype could include liquid chromatography-mass spectrometry (LC-MS) or employment of biosensors to analyse and quantify the concentration of quorum sensing molecules in biofilm colonies of the adapted strains[343]. This could help determine if cell-to-cell communication has been altered following evolutionary adaptation, potentially supporting improved biofilm formation, population defence, genetic exchange, and even increased virulence.

Furthermore, both the NAg^{R} and Ag^{+T} strains exhibited stable expression increases in OMP genes and *otsA* and *otsB,* which contribute to CPS formation. Super resolution microscopy, such as transmission or scanning electron microscopy (TEM or SEM) or single molecule localisation imaging techniques (*e.g.* photoactivated localisation microscopy or PALM) can help visualise any distinct changes in the integrity and density of the outer membrane and CPS or cell envelope of the adapted bacteria[306,307]. This could also aid in better showcasing the morphological changes observed with the Ag^{+T} bacterium and potentially identify notable alterations in cell surface structure/s.

An assessment of altered virulence and/or pathogenesis of the evolved bacteria may also be beneficial, particularly because of the increasing medical impact of *A. baumannii* globally[17,344]. Given the notable changes in biofilm formation, the oxidative stress response, and, while not specifically discussed in the main body of this thesis, increased expression levels of genes involved in *A. baumannii* virulence, between both the NAg^{R} and Ag^{+T} variants, a comparative mammalian cell infection model involving the silver-adapted and WT strains could be beneficial. This may help assess the potential increased (or decreased) pathogenicity of the evolved bacteria relative to their WT counterpart. Further, these studies could also help determine the therapeutic potential of the respective silver agents and other commercial antibacterial agent (*e.g.* antibiotics) against the infecting populations, and even help facilitate the design of more novel antimicrobial therapies which could overcome the bacterial defence mechanisms (*e.g.* synergistic nanoparticle-antibiotic combinations)[345,346]. For reference, notable detected virulence genes included, the OMP gene *ompA*, the CPS-related genes *otsA/B*, and the stress response genes *bfmR* and *uspA*, each of were in fact stably upregulated in both untreated strains (NRNT and ATNT; see **Figure 5.7** and **Figure 6.7**). The stress response genes reportedly assist in virulence regulation, support *in vivo* survivability of *A. baumannii* and help induce host cell death[264,347,348]. The genes *otsA/B* are known for their involvement in CPS formation *via* trehalose synthesis, and the CPS has been shown to contribute to enhanced biofilm formation and also help improve *in vivo* survivability in *A. baumannii*, specifically conferring defence against immune cells, drugs/toxins, and desiccation[266,349]. The outer membrane protein A gene *ompA* is one of the most highly conserved virulence factors in the *A. baumannii* lineage[250]. OmpA is known to be involved in mammalian cell surface adhesion, invasion, apoptosis, and plays a key role in antibacterial resistance

and biofilm formation, as discussed earlier[248,347]. Furthermore, during infection, *A. baumannii* secretes outer membrane vesicles (OMVs), which are formed from encapsulated OM material, and have been found to contain detached portions of OmpA which subsequently aid in host cell attachment and apoptosis[350,351].

7.3.2 Final remarks

The antimicrobial resistance crisis has emerged as a significant global health emergency, necessitating vital scientific attention. The primary contributing factors to this public health issue are the excessive and inappropriate use of antimicrobials, coupled with declining investments into the research and development of new antimicrobial drugs (including antibiotics and antifungals). The widespread dissemination of multi-drug resistant bacterial organisms in both natural environments and medical settings poses a significant threat to human health. Consequently, there is an urgent need for the development of novel and alternative antimicrobial agents capable of overcoming bacterial resistance. Silver-based products, including silver nanoparticles (NAg) and silver cation (Ag^+) sources (*e.g.* silver nitrate), have gained prominence as valuable alternatives to conventional antimicrobial agents. This is due to their distinct physicochemical properties and diverse and multi-faceted toxicological mechanisms. However, their increased medical, commercial, and consumer utilisation, driven by their lucrative properties, has raised concerns regarding the emergence of silver-resistant bacteria. Numerous research studies have reported on the generation of various silver-adapted bacterial species. Nevertheless, no previous works have investigated the potential for NAg resistance evolution in *A. baumannii*, a critical priority ESKAPE pathogen. Overall, knowledge on the toxicological and defence responses of this bacterium to antimicrobial silver is somewhat limited. It is this knowledge gap which served as the motivation behind the present study.

This work presented in this thesis revealed, for the first time, that *A. baumannii* (strain ATCC 19606) could develop stable NAg resistance following prolonged, repeated exposure. In addition, this work demonstrated that the bacterium could also develop a tolerance trait to Ag^+, a phenotype not previously observed in this species. The work herein identified an abundance of genetic, transcriptomic, and phenotypic modifications in the resistant and tolerant strains which were linked to the evolutionary adaptation of the bacterium and indicated to confer enhanced silver defence. The

knowledge generated from this study, combined with current research evidence, highlights the impact of antimicrobial silver overuse. In practical settings, the use of NAg and other silver agents, as surface coatings, is incorporated at concentrations far higher than those used in *in vitro* susceptibilities studies such as this one[25]. This would imply that the adaptation of bacteria should be near impossible due to the high toxicity of silver. However, studies highlight that the widespread use of silver-coated products can lead to both the systemic absorption of soluble silver into the bloodstream from wound dressings and catheters, or into the environment, due to the disposal of effluent and silver-containing products into wastewater and landfill[25,26,67,68]. The human body, as well as aquatic and terrestrial ecosystems, harbour diverse microbial populations. The introduction of biologically toxic silver into these habitats poses significant risk of prolonged and sub-lethal exposure on potentially pathogenic microbes, in turn perpetuating the evolution and selection of silver-adapted organisms[26,180].

Indeed, the present study has demonstrated this phenomenon. The emergence of NAg resistance and Ag^+ tolerance in *A. baumannii* provides further evidence that bacteria can adapt to antimicrobial silver. While the evolutionary adaptation of ATCC 19606 to silver was notably slower than that of the traditional antibiotic nalidixic acid (Nx) used in this study, it is important to consider that the silver agents are multi-targeting and broad-spectrum by design. Even so, the *in vitro* evolution work performed in this study spanned only 30-days, whereas microorganisms in real-world environments may be exposed to silver for significantly longer durations, thereby exacerbating the potential for a greater number of adaptation occurrences.

Overall, the knowledge gained from this study has helped advance scientific understanding of the NAg resistance phenomena, while equally highlighting that adaptation to silver extends beyond resistance to encompass tolerance as well. The identification of unique physiological changes and defence features exhibited by silver-adapted *A. baumannii* ATCC 19606 can help future research circumvent the potential for evolution of these adaptation mechanisms. Specifically, the design of new antimicrobial nanoparticle (or heavy metal) agents can be guided by this knowledge to ensure that priority bacterial populations are more efficiently targeted, for example, if used in combination with traditional antibiotics. However, the global usage of novel antimicrobial agents like NAg and Ag^+ necessitates careful management. Regulatory bodies must be established to implement strategies to effectively utilise and dispose of

silver-based products, thereby minimising the risk of human and environmental contamination and subsequent microbial adaptation. In the era of AMR, the need for powerful alternative antimicrobial agents for public health safety is dire. Given the lack of newly discovered commercially available antibiotic classes, it is imperative to safeguard the efficacy of valuable alternatives such as NAg and Ag^+ to sustain the battle against opportunistic, drug-resistant microorganisms in the long-term.

References

1 Abdar, M. H. *et al.* Prevalence of extended-spectrum beta-lactamase genes in Acinetobacter baumannii strains isolated from nosocomial infections in Tehran, Iran. *GMS Hygiene and Infection Control* **14** (2019).

2 Murray, C. J. *et al.* Global burden of bacterial antimicrobial resistance in 2019: a systematic analysis. *The Lancet* (2022).

3 O'Neill, J. Tackling drug-resistant infections globally: final report and recommendations. *The Review on Antimicrobial Resistance* (2016).

4 Centers for Disease Control and Prevention. Office of Infectious Disease Antibiotic Resistance Threats in the United States, 2013. *Atlanta, GA: Centers for Disease Control and Prevention* (2013).

5 Ventola, C. L. The antibiotic resistance crisis: part 1: causes and threats. *Pharmacy and Therapeutics* **40**, 277 (2015).

6 Centers for Disease Control and Prevention. Antibiotic resistance threats in the United States, 2019. *Centres for Disease Control and Prevention, US Department of Health and Human Services* (2019).

7 World Health Organization. Prioritization of pathogens to guide discovery, research and development of new antibiotics for drug-resistant bacterial infections, including tuberculosis. (World Health Organization, 2017).

8 Bartlett, J. G., Gilbert, D. N. & Spellberg, B. Seven ways to preserve the miracle of antibiotics. *Clinical Infectious Diseases* **56**, 1445-1450 (2013).

9 Zhen, X., Lundborg, C. S., Sun, X., Hu, X. & Dong, H. Economic burden of antibiotic resistance in ESKAPE organisms: a systematic review. *Antimicrobial Resistance & Infection Control* **8**, 137 (2019).

10 Santajit, S. & Indrawattana, N. Mechanisms of antimicrobial resistance in ESKAPE pathogens. *BioMed Research International* **2016**, 2475067 (2016).

11 Rice, L. B. Federal funding for the study of antimicrobial resistance in nosocomial pathogens: no ESKAPE. *The Journal of Infectious Diseases* **197**, 1079-1081 (2008).

12 Gonzalez-Villoria, A. M. & Valverde-Garduno, V. Antibiotic-resistant Acinetobacter baumannii increasing success remains a challenge as a nosocomial pathogen. *Journal of Pathogens* **2016**, 1-10 (2016).

13 Howard, A., O'Donoghue, M., Feeney, A. & Sleator, R. D. Acinetobacter baumannii: an emerging opportunistic pathogen. *Virulence* **3**, 243-250 (2012).

14 Peleg, A. Y., Seifert, H. & Paterson, D. L. Acinetobacter baumannii: emergence of a successful pathogen. *Clinical Microbiology Reviews* **21**, 538-582 (2008).

15 Gootz, T. D. & Marra, A. Acinetobacter baumannii: an emerging multidrug-resistant threat. *Expert Review of Anti-infective Therapy* **6**, 309-325 (2008).

16 Morris, F. C., Dexter, C., Kostoulias, X., Uddin, M. I. & Peleg, A. Y. The mechanisms of disease caused by Acinetobacter baumannii. *Frontiers in Microbiology* **10**, 1601 (2019).

17 Alsan, M. & Klompas, M. Acinetobacter baumannii: an emerging and important pathogen. *Journal of Clinical Outcomes Management* **17**, 363 (2010).

18 Hamidian, M. & Nigro, S. J. Emergence, molecular mechanisms and global spread of carbapenem-resistant Acinetobacter baumannii. *Microbial Genomics* **5** (2019).
19 Rai, M., Deshmukh, S., Ingle, A. & Gade, A. Silver nanoparticles: the powerful nanoweapon against multidrug-resistant bacteria. *Journal of Applied Microbiology* **112**, 841-852 (2012).
20 Marambio-Jones, C. & Hoek, E. M. A review of the antibacterial effects of silver nanomaterials and potential implications for human health and the environment. *Journal of Nanoparticle Research* **12**, 1531-1551 (2010).
21 Lara, H. H., Ayala-Núñez, N. V., Turrent, L. d. C. I. & Padilla, C. R. Bactericidal effect of silver nanoparticles against multidrug-resistant bacteria. *World Journal of Microbiology and Biotechnology* **26**, 615-621 (2010).
22 Morones, J. R. *et al.* The bactericidal effect of silver nanoparticles. *Nanotechnology* **16**, 2346-2353 (2005).
23 Khan, I., Saeed, K. & Khan, I. Nanoparticles: Properties, applications and toxicities. *Arabian Journal of Chemistry* **2017**, 1-24 (2017).
24 Burdușel, A.-C. *et al.* Biomedical applications of silver nanoparticles: An up-to-date overview. *Nanomaterials* **8**, 681 (2018).
25 Gunawan, C. *et al.* Widespread and indiscriminate nanosilver use: genuine potential for microbial resistance. *ACS Nano* **11**, 3438-3445 (2017).
26 Schaïfer, B., Tentschert, J. & Luch, A. Nanosilver in consumer products and human health: more information required! *Environmental science & technology* **45**, 7589-7590 (2011).
27 Rai, M., Yadav, A. & Gade, A. Silver nanoparticles as a new generation of antimicrobials. *Biotechnology Advances* **27**, 76-83 (2009).
28 Stabryla, L. M. *et al.* Role of bacterial motility in differential resistance mechanisms of silver nanoparticles and silver ions. *Nature Nanotechnology* **16**, 1-8 (2021).
29 Valentin, E. *et al.* Heritable Nanosilver Resistance in Priority Pathogen: A Unique Genetic Adaptation and Comparison with Ionic Silver and Antibiotic. *Nanoscale* **12** (2020).
30 Panáček, A. *et al.* Bacterial resistance to silver nanoparticles and how to overcome it. *Nature Nanotechnology* **13**, 65-71 (2018).
31 Graves Jr, J. L. *et al.* Rapid evolution of silver nanoparticle resistance in Escherichia coli. *Frontiers in Genetics* **6**, 42 (2015).
32 Gunawan, C., Teoh, W. Y., Marquis, C. P. & Amal, R. Induced adaptation of Bacillus sp. to antimicrobial nanosilver. *Small* **9**, 3554-3560 (2013).
33 McNeilly, O., Mann, R., Hamidian, M. & Gunawan, C. Emerging Concern for Silver Nanoparticle Resistance in Acinetobacter baumannii and other Bacteria. *Frontiers in Microbiology* **12**, 894 (2021).
34 Hosny, A. E.-D. M., Rasmy, S. A., Aboul-Magd, D. S., Kashef, M. T. & El-Bazza, Z. E. The increasing threat of silver-resistance in clinical isolates from wounds and burns. *Infection and Drug Resistance* **2019**, 1985-2001 (2019).
35 Deshpande, L. M. & Chopade, B. A. Plasmid mediated silver resistance in Acinetobacter baumannii. *Biometals* **7**, 49-56 (1994).
36 Deshpande, L. M., Kapadnis, B. P. & Chopade, B. A. Metal resistance in Acinetobacter and its relation to β-lactamase production. *Biometals* **6**, 55-59 (1993).
37 Wintachai, P., Paosen, S., Yupanqui, C. T. & Voravuthikunchai, S. P. Silver nanoparticles synthesized with Eucalyptus critriodora ethanol leaf extract

stimulate antibacterial activity against clinically multidrug-resistant Acinetobacter baumannii isolated from pneumonia patients. *Microbial Pathogenesis* **126**, 245-257 (2019).
38 Chen, M. *et al.* Biomedical Potentialities of Silver Nanoparticles for Clinical Multiple Drug-Resistant Acinetobacter baumannii. *Journal of Nanomaterials* **2019** (2019).
39 Singh, R. *et al.* Antibacterial activities of bacteriagenic silver nanoparticles against nosocomial Acinetobacter baumannii. *Journal of Nanoscience and Nanotechnology* **18**, 3806-3815 (2018).
40 Singh, R., Nadhe, S., Wadhwani, S., Shedbalkar, U. & Chopade, B. A. Nanoparticles for control of biofilms of Acinetobacter species. *Materials* **9**, 383 (2016).
41 Łysakowska, M. E., Ciebiada-Adamiec, A., Klimek, L. & Sienkiewicz, M. The activity of silver nanoparticles (Axonnite) on clinical and environmental strains of Acinetobacter spp. *Burns* **41**, 364-371 (2015).
42 Cassini, A. *et al.* Attributable deaths and disability-adjusted life-years caused by infections with antibiotic-resistant bacteria in the EU and the European Economic Area in 2015: a population-level modelling analysis. *The Lancet Infectious Diseases* **19**, 56-66 (2019).
43 Cassini, A. *et al.* Impact of infectious diseases on population health using incidence-based disability-adjusted life years (DALYs): results from the Burden of Communicable Diseases in Europe study, European Union and European Economic Area countries, 2009 to 2013. *Euro Surveill* **23** (2018).
44 Golkar, Z., Bagasra, O. & Pace, D. G. Bacteriophage therapy: a potential solution for the antibiotic resistance crisis. *The Journal of Infection in Developing Countries* **8**, 129-136 (2014).
45 Al-Anazi, K. A. & Al-Jasser, A. M. Infections caused by Acinetobacter baumannii in recipients of hematopoietic stem cell transplantation. *Frontiers in Oncology* **4**, 186 (2014).
46 Heritier, C., Poirel, L. & Nordmann, P. Cephalosporinase over-expression resulting from insertion of ISAba1 in Acinetobacter baumannii. *Clinical Microbiology and Infection* **12**, 123-130 (2006).
47 Chen, N. *et al.* Epidemiological and clinical characteristics of 99 cases of 2019 novel coronavirus pneumonia in Wuhan, China: a descriptive study. *The Lancet* **395**, 507-513 (2020).
48 Towner, K. Acinetobacter: an old friend, but a new enemy. *Journal of Hospital Infection* **73**, 355-363 (2009).
49 Gottesman, T., Fedorowsky, R., Yerushalmi, R., Lellouche, J. & Nutman, A. An outbreak of carbapenem-resistant Acinetobacter baumannii in a COVID-19 dedicated hospital. *Infection Prevention in Practice* **3**, 100113 (2021).
50 Jain, U. Risk of COVID-19 due to shortage of personal protective equipment. *Cureus* **12**, e8837 (2020).
51 Sharifipour, E. *et al.* Evaluation of bacterial co-infections of the respiratory tract in COVID-19 patients admitted to ICU. *BMC Infectious Diseases* **20**, 1-7 (2020).
52 Perez, S. *et al.* Increase in hospital-acquired carbapenem-resistant Acinetobacter baumannii infection and colonization in an acute care hospital during a surge in COVID-19 admissions—new jersey, february–july 2020. *Morbidity and Mortality Weekly Report* **69**, 1827 (2020).

53 Clancy, C. J., Buehrle, D. J. & Nguyen, M. H. PRO: the COVID-19 pandemic will result in increased antimicrobial resistance rates. *JAC-Antimicrobial Resistance* **2**, dlaa049 (2020).
54 Hsu, J. How covid-19 is accelerating the threat of antimicrobial resistance. *BMJ* **369**, m1983 (2020).
55 Hamidian, M. & Hall, R. M. The AbaR antibiotic resistance islands found in Acinetobacter baumannii global clone 1–Structure, origin and evolution. *Drug Resistance Updates* **41**, 26-39 (2018).
56 Asif, M., Alvi, I. A. & Rehman, S. U. Insight into Acinetobacter baumannii: pathogenesis, global resistance, mechanisms of resistance, treatment options, and alternative modalities. *Infection and Drug Resistance* **11**, 1249-1260 (2018).
57 Hujer, K. M. *et al.* Analysis of antibiotic resistance genes in multidrug-resistant Acinetobacter sp. isolates from military and civilian patients treated at the Walter Reed Army Medical Center. *Antimicrobial Agents and Chemotherapy* **50**, 4114-4123 (2006).
58 Michael, C. A., Dominey-Howes, D. & Labbate, M. The antimicrobial resistance crisis: causes, consequences, and management. *Frontiers in Public Health* **2**, 145 (2014).
59 Zheng, W., Sun, W. & Simeonov, A. Drug repurposing screens and synergistic drug-combinations for infectious diseases. *British Journal of Pharmacology* **175**, 181-191 (2018).
60 Fair, R. J. & Tor, Y. Antibiotics and bacterial resistance in the 21st century. *Perspectives in Medicinal Chemistry* **6**, 25-64 (2014).
61 Silva, G. A. Introduction to nanotechnology and its applications to medicine. *Surgical Neurology* **61**, 216-220 (2004).
62 Mody, V. V., Siwale, R., Singh, A. & Mody, H. R. Introduction to metallic nanoparticles. *Journal of Pharmacy and Bioallied Sciences* **2**, 282-289 (2010).
63 Ge, L. *et al.* Nanosilver particles in medical applications: synthesis, performance, and toxicity. *International Journal of Nanomedicine* **9**, 2399-2407 (2014).
64 Rezvani, E., Rafferty, A., McGuinness, C. & Kennedy, J. Adverse effects of nanosilver on human health and the environment. *Acta biomaterialia* **94**, 145-159 (2019).
65 Gupta, A., Matsui, K., Lo, J.-F. & Silver, S. Molecular basis for resistance to silver cations in Salmonella. *Nature Medicine* **5**, 183-188 (1999).
66 Muller, M. & Merrett, N. D. Pyocyanin production by Pseudomonas aeruginosa confers resistance to ionic silver. *Antimicrobial Agents and Chemotherapy* **58**, 5492-5499 (2014).
67 McGillicuddy, E. *et al.* Silver nanoparticles in the environment: Sources, detection and ecotoxicology. *Science of the Total Environment* **575**, 231-246 (2017).
68 Chopra, I. The increasing use of silver-based products as antimicrobial agents: a useful development or a cause for concern? *Journal of Antimicrobial Chemotherapy* **59**, 587-590 (2007).
69 Yun'an Qing, L. C. *et al.* Potential antibacterial mechanism of silver nanoparticles and the optimization of orthopedic implants by advanced modification technologies. *International Journal of Nanomedicine* **13**, 3311-3327 (2018).

70 Zhang, X.-F., Liu, Z.-G., Shen, W. & Gurunathan, S. Silver nanoparticles: synthesis, characterization, properties, applications, and therapeutic approaches. *International Journal of Molecular Sciences* **17**, 1534 (2016).
71 Syafiuddin, A., Salim, M. R., Beng Hong Kueh, A., Hadibarata, T. & Nur, H. A review of silver nanoparticles: Research trends, global consumption, synthesis, properties, and future challenges. *Journal of the Chinese Chemical Society* **64**, 732-756 (2017).
72 Pal, S., Tak, Y. K. & Song, J. M. Does the antibacterial activity of silver nanoparticles depend on the shape of the nanoparticle? A study of the gram-negative bacterium Escherichia coli. *Applied and Environmental Microbiology* **73**, 1712-1720 (2007).
73 Silhavy, T. J., Kahne, D. & Walker, S. The bacterial cell envelope. *Cold Spring Harbor Perspectives in Biology* **2**, a000414 (2010).
74 Fahmy, H. M. *et al.* Coated silver nanoparticles: Synthesis, cytotoxicity, and optical properties. *RSC Advances* **9**, 20118-20136 (2019).
75 El Badawy, A. M. *et al.* Surface charge-dependent toxicity of silver nanoparticles. *Environmental Science & Technology* **45**, 283-287 (2010).
76 Tang, S. & Zheng, J. Antibacterial activity of silver nanoparticles: structural effects. *Advanced Healthcare Materials* **7**, 1701503 (2018).
77 Dakal, T. C., Kumar, A., Majumdar, R. S. & Yadav, V. Mechanistic basis of antimicrobial actions of silver nanoparticles. *Frontiers in Microbiology* **7**, 1831 (2016).
78 Duval, R. E., Gouyau, J. & Lamouroux, E. Limitations of recent studies dealing with the antibacterial properties of silver nanoparticles: fact and opinion. *Nanomaterials* **9**, 1775 (2019).
79 Pazos-Ortiz, E. *et al.* Dose-dependent antimicrobial activity of silver nanoparticles on polycaprolactone fibers against gram-positive and gram-negative bacteria. *Journal of Nanomaterials* **2017** (2017).
80 Limpiteeprakan, P. & Babel, S. Leaching potential of silver from nanosilver-treated textile products. *Environmental monitoring and assessment* **188**, 1-12 (2016).
81 Sotiriou, G. A., Meyer, A., Knijnenburg, J. T., Panke, S. & Pratsinis, S. E. Quantifying the origin of released Ag+ ions from nanosilver. *Langmuir* **28**, 15929-15936 (2012).
82 Xiu, Z.-m., Zhang, Q.-b., Puppala, H. L., Colvin, V. L. & Alvarez, P. J. Negligible particle-specific antibacterial activity of silver nanoparticles. *Nano Letters* **12**, 4271-4275 (2012).
83 Lok, C.-N. *et al.* Proteomic analysis of the mode of antibacterial action of silver nanoparticles. *Journal of Proteome Research* **5**, 916-924 (2006).
84 Vila Domínguez, A., Ayerbe Algaba, R., Miró Canturri, A., Rodríguez Villodres, Á. & Smani, Y. Antibacterial Activity of Colloidal Silver against Gram-Negative and Gram-Positive Bacteria. *Antibiotics* **9**, 36 (2020).
85 Kędziora, A. *et al.* Similarities and differences between silver ions and silver in nanoforms as antibacterial agents. *International Journal of Molecular Sciences* **19**, 444 (2018).
86 Li, W.-R. *et al.* A comparative analysis of antibacterial activity, dynamics, and effects of silver ions and silver nanoparticles against four bacterial strains. *International Biodeterioration & Biodegradation* **123**, 304-310 (2017).

87 Radzig, M. *et al.* Antibacterial effects of silver nanoparticles on gram-negative bacteria: influence on the growth and biofilms formation, mechanisms of action. *Colloids and Surfaces B: Biointerfaces* **102**, 300-306 (2013).
88 Nikaido, H. Porins and specific diffusion channels in bacterial outer membranes. *Journal of Biological Chemistry* **269**, 3905-3908 (1994).
89 Sánchez-López, E. *et al.* Metal-based nanoparticles as antimicrobial agents: an overview. *Nanomaterials* **10**, 292 (2020).
90 Lemire, J. A., Harrison, J. J. & Turner, R. J. Antimicrobial activity of metals: mechanisms, molecular targets and applications. *Nature Reviews Microbiology* **11**, 371-384 (2013).
91 Różalska, B., Sadowska, B., Budzyńska, A., Bernat, P. & Różalska, S. Biogenic nanosilver synthesized in Metarhizium robertsii waste mycelium extract–As a modulator of Candida albicans morphogenesis, membrane lipidome and biofilm. *PLoS One* **13**, e0194254 (2018).
92 Berrisford, J. M., Baradaran, R. & Sazanov, L. A. Structure of bacterial respiratory complex I. *Biochimica et Biophysica Acta (BBA)-Bioenergetics* **1857**, 892-901 (2016).
93 Holt, K. B. & Bard, A. J. Interaction of silver (I) ions with the respiratory chain of Escherichia coli: an electrochemical and scanning electrochemical microscopy study of the antimicrobial mechanism of micromolar Ag+. *Biochemistry* **44**, 13214-13223 (2005).
94 Xu, H. *et al.* Role of reactive oxygen species in the antibacterial mechanism of silver nanoparticles on Escherichia coli O157: H7. *Biometals* **25**, 45-53 (2012).
95 Ezraty, B., Gennaris, A., Barras, F. & Collet, J.-F. Oxidative stress, protein damage and repair in bacteria. *Nature Reviews Microbiology* **15**, 385-396 (2017).
96 Zhao, X. & Drlica, K. Reactive oxygen species and the bacterial response to lethal stress. *Current Opinion in Microbiology* **21**, 1-6 (2014).
97 Ray, P. D., Huang, B.-W. & Tsuji, Y. Reactive oxygen species (ROS) homeostasis and redox regulation in cellular signaling. *Cellular Signalling* **24**, 981-990 (2012).
98 Gunawan, C. *et al.* Nanosilver Targets the Bacterial Cell Envelope: The Link with Generation of Reactive Oxygen Radicals. *ACS Appl Mater Interfaces* **12**, 5557-5568 (2020).
99 Slavin, Y. N., Asnis, J., Häfeli, U. O. & Bach, H. Metal nanoparticles: understanding the mechanisms behind antibacterial activity. *Journal of Nanobiotechnology* **15**, 65 (2017).
100 Feng, Q. L. *et al.* A mechanistic study of the antibacterial effect of silver ions on Escherichia coli and Staphylococcus aureus. *Journal of biomedical materials research* **52**, 662-668 (2000).
101 Guzman, M., Dille, J. & Godet, S. Synthesis and antibacterial activity of silver nanoparticles against gram-positive and gram-negative bacteria. *Nanomedicine: Nanotechnology, Biology and Medicine* **8**, 37-45 (2012).
102 Kirstein, J. & Turgay, K. A new tyrosine phosphorylation mechanism involved in signal transduction in Bacillus subtilis. *Journal of Molecular Microbiology and Biotechnology* **9**, 182-188 (2005).
103 Garcia-Garcia, T. *et al.* Role of protein phosphorylation in the regulation of cell cycle and DNA-related processes in bacteria. *Frontiers in Microbiology* **7**, 184 (2016).

104 Shrivastava, S. *et al.* Characterization of enhanced antibacterial effects of novel silver nanoparticles. *Nanotechnology* **18**, 225103 (2007).
105 Baptista, P. V. *et al.* Nano-strategies to fight multidrug resistant bacteria—"A Battle of the Titans". *Frontiers in Microbiology* **9**, 1441 (2018).
106 Percival, S. L., Bowler, P. G. & Dolman, J. Antimicrobial activity of silver-containing dressings on wound microorganisms using an in vitro biofilm model. *International Wound Journal* **4**, 186-191 (2007).
107 Silva Santos, K. *et al.* Silver nanocomposite biosynthesis: Antibacterial activity against multidrug-resistant strains of Pseudomonas aeruginosa and Acinetobacter baumannii. *Molecules* **21**, 1255 (2016).
108 Cavassin, E. D. *et al.* Comparison of methods to detect the in vitro activity of silver nanoparticles (AgNP) against multidrug resistant bacteria. *Journal of Nanobiotechnology* **13**, 64 (2015).
109 Wan, G. *et al.* Effects of silver nanoparticles in combination with antibiotics on the resistant bacteria Acinetobacter baumannii. *International Journal of Nanomedicine* **11**, 3789 (2016).
110 Gaidhani, S. *et al.* Biofilm disruption activity of silver nanoparticles synthesized by Acinetobacter calcoaceticus PUCM 1005. *Materials Letters* **108**, 324-327 (2013).
111 Salunke, G. R. *et al.* Rapid efficient synthesis and characterization of silver, gold, and bimetallic nanoparticles from the medicinal plant Plumbago zeylanica and their application in biofilm control. *International journal of nanomedicine* **9**, 2635 (2014).
112 Tiwari, V., Tiwari, M. & Solanki, V. Polyvinylpyrrolidone-capped silver nanoparticle inhibits infection of carbapenem-resistant strain of Acinetobacter baumannii in the human pulmonary epithelial cell. *Frontiers in Immunology* **8**, 973 (2017).
113 Ebrahimi, A., Jafferi, H., Habibian, S. & Lotfalian, S. Evaluation of Anti biofilm and Antibiotic Potentiation Activities of Silver Nanoparticles Against some Nosocomial Pathogens. *Iranian Journal of Pharmaceutical Sciences* **14**, 7-14 (2018).
114 McShan, D., Zhang, Y., Deng, H., Ray, P. C. & Yu, H. Synergistic antibacterial effect of silver nanoparticles combined with ineffective antibiotics on drug resistant Salmonella typhimurium DT104. *Journal of Environmental Science and Health, Part C* **33**, 369-384 (2015).
115 Katva, S., Das, S., Moti, H. S., Jyoti, A. & Kaushik, S. Antibacterial synergy of silver nanoparticles with gentamicin and chloramphenicol against Enterococcus faecalis. *Pharmacognosy Magazine* **13**, S828-S833 (2017).
116 Li, P., Li, J., Wu, C., Wu, Q. & Li, J. Synergistic antibacterial effects of β-lactam antibiotic combined with silver nanoparticles. *Nanotechnology* **16**, 1912 (2005).
117 Allahverdiyev, A. M., Kon, K. V., Abamor, E. S., Bagirova, M. & Rafailovich, M. Coping with antibiotic resistance: combining nanoparticles with antibiotics and other antimicrobial agents. *Expert Review of Anti-Infective Therapy* **9**, 1035-1052 (2011).
118 Donlan, R. M. Biofilms: microbial life on surfaces. *Emerging Infectious Diseases* **8**, 881 (2002).
119 O'Toole, G., Kaplan, H. B. & Kolter, R. Biofilm formation as microbial development. *Annual Reviews in Microbiology* **54**, 49-79 (2000).

120 Garrett, T. R., Bhakoo, M. & Zhang, Z. Bacterial adhesion and biofilms on surfaces. *Progress in Natural Science* **18**, 1049-1056 (2008).
121 López, D., Vlamakis, H. & Kolter, R. Biofilms. *Cold Spring Harbor Perspectives in Biology* **2**, a000398 (2010).
122 Romanova, I. & Gintsburg, A. Bacterial biofilms as a natural form of existence of bacteria in the environment and host organism. *Zhurnal Mikrobiologii, Epidemiologii, i Immunobiologii* **3**, 99-109 (2011).
123 Flemming, H.-C. & Wingender, J. The biofilm matrix. *Nature Reviews Microbiology* **8**, 623 (2010).
124 Dufour, D., Leung, V. & Lévesque, C. M. Bacterial biofilm: structure, function, and antimicrobial resistance. *Endodontic Topics* **22**, 2-16 (2010).
125 Lewis, K. Persister cells. *Annual Review of Microbiology* **64**, 357-372 (2010).
126 Miller, M. B. & Bassler, B. L. Quorum sensing in bacteria. *Annual Reviews in Microbiology* **55**, 165-199 (2001).
127 Hausner, M. & Wuertz, S. High rates of conjugation in bacterial biofilms as determined by quantitative in situ analysis. *Applied and Environmental Microbiology* **65**, 3710-3713 (1999).
128 Rutherford, S. T. & Bassler, B. L. Bacterial quorum sensing: its role in virulence and possibilities for its control. *Cold Spring Harbor Perspectives in Medicine* **2**, a012427 (2012).
129 Choi, O., Yu, C.-P., Fernández, G. E. & Hu, Z. Interactions of nanosilver with Escherichia coli cells in planktonic and biofilm cultures. *Water Research* **44**, 6095-6103 (2010).
130 Martinez-Gutierrez, F. *et al.* Anti-biofilm activity of silver nanoparticles against different microorganisms. *Biofouling* **29**, 651-660 (2013).
131 Markowska, K., Grudniak, A. M. & Wolska, K. I. Silver nanoparticles as an alternative strategy against bacterial biofilms. *Acta Biochimica Polonica* **60**, 523-530 (2013).
132 Pompilio, A. *et al.* Electrochemically synthesized silver nanoparticles are active against planktonic and biofilm cells of Pseudomonas aeruginosa and other cystic fibrosis-associated bacterial pathogens. *Frontiers in Microbiology* **9**, 1349 (2018).
133 Qayyum, S., Oves, M. & Khan, A. U. Obliteration of bacterial growth and biofilm through ROS generation by facilely synthesized green silver nanoparticles. *PloS One* **12**, e0181363 (2017).
134 Vaidya, M. Y., McBain, A. J., Butler, J. A., Banks, C. E. & Whitehead, K. A. Antimicrobial efficacy and synergy of metal ions against Enterococcus faecium, Klebsiella pneumoniae and Acinetobacter baumannii in planktonic and biofilm phenotypes. *Scientific reports* **7**, 1-9 (2017).
135 Shih, H.-Y. & Lin, Y. E. Efficacy of copper-silver ionization in controlling biofilm-and plankton-associated waterborne pathogens. *Applied and environmental microbiology* **76**, 2032-2035 (2010).
136 Ramachandran, R. & Sangeetha, D. Antibiofilm efficacy of silver nanoparticles against biofilm forming multidrug resistant clinical isolates. *The Pharma Innovation* **6**, 36 (2017).
137 Loo, Y. Y. *et al.* In vitro antimicrobial activity of green synthesized silver nanoparticles against selected gram-negative foodborne pathogens. *Frontiers in Microbiology* **9**, 1555 (2018).
138 Jelenko 3rd, C. Silver nitrate resistant E. coli: report of case. *Annals of Surgery* **170**, 296-299 (1969).

139 Rosenkranz, H. S., Coward, J. E., Wlodkowski, T. J. & Carr, H. S. Properties of silver sulfadiazine-resistant Enterobacter cloacae. *Antimicrobial Agents and Chemotherapy* **5**, 199-201 (1974).
140 Mchugh, G. L., Moellering, R., Hopkins, C. & Swartz, M. Salmonella typhimurium resistant to silver nitrate, chloramphenicol, and ampicillin: A new threat in burn units? *The Lancet* **305**, 235-240 (1975).
141 Li, X.-Z., Nikaido, H. & Williams, K. E. Silver-resistant mutants of Escherichia coli display active efflux of Ag+ and are deficient in porins. *Journal of Bacteriology* **179**, 6127-6132 (1997).
142 Randall, C. P., Gupta, A., Jackson, N., Busse, D. & O'Neill, A. J. Silver resistance in Gram-negative bacteria: a dissection of endogenous and exogenous mechanisms. *Journal of Antimicrobial Chemotherapy* **70**, 1037-1046 (2015).
143 Mijnendonckx, K., Leys, N., Mahillon, J., Silver, S. & Van Houdt, R. Antimicrobial silver: uses, toxicity and potential for resistance. *Biometals* **26**, 609-621 (2013).
144 Munson, G. P., Lam, D. L., Outten, F. W. & O'Halloran, T. V. Identification of a copper-responsive two-component system on the chromosome of Escherichia coli K-12. *Journal of bacteriology* **182**, 5864-5871 (2000).
145 Franke, S., Grass, G., Rensing, C. & Nies, D. H. Molecular analysis of the copper-transporting efflux system CusCFBA of Escherichia coli. *Journal of bacteriology* **185**, 3804-3812 (2003).
146 Lok, C.-N. *et al.* Proteomic identification of the Cus system as a major determinant of constitutive Escherichia coli silver resistance of chromosomal origin. *Journal of Proteome Research* **7**, 2351-2356 (2008).
147 Koebnik, R., Locher, K. P. & Van Gelder, P. Structure and function of bacterial outer membrane proteins: barrels in a nutshell. *Molecular microbiology* **37**, 239-253 (2000).
148 Cai, S. J. & Inouye, M. EnvZ-OmpR interaction and osmoregulation in Escherichia coli. *Journal of Biological Chemistry* **277**, 24155-24161 (2002).
149 Loh, J. V., Percival, S. L., Woods, E. J., Williams, N. J. & Cochrane, C. A. Silver resistance in MRSA isolated from wound and nasal sources in humans and animals. *International Wound Journal* **6**, 32-38 (2009).
150 Randall, C. P., Oyama, L. B., Bostock, J. M., Chopra, I. & O'Neill, A. J. The silver cation (Ag+): antistaphylococcal activity, mode of action and resistance studies. *Journal of antimicrobial chemotherapy* **68**, 131-138 (2013).
151 Shakibaie, M., Dhakephalker, B., Kapadnis, B. & Chopade, B. Silver resistance in Acinetobacter baumannii BL54 occurs through binding to a Ag-binding protein. *Iranian Journal of Biotechnology* **1** (2003).
152 Alquethamy, S. F. *et al.* The role of the CopA copper efflux system in Acinetobacter baumannii virulence. *International Journal of Molecular Sciences* **20**, 575 (2019).
153 Williams, C. L. *et al.* Copper resistance of the emerging pathogen Acinetobacter baumannii. *Applied Environmental Microbiology* **82**, 6174-6188 (2016).
154 Gupta, A., Phung, L. T., Taylor, D. E. & Silver, S. Diversity of silver resistance genes in IncH incompatibility group plasmids. *Microbiology* **147**, 3393-3402 (2001).
155 Niño-Martínez, N., Salas Orozco, M. F., Martínez-Castañón, G.-A., Torres Méndez, F. & Ruiz, F. Molecular Mechanisms of Bacterial Resistance to Metal

and Metal Oxide Nanoparticles. *International Journal of Molecular Sciences* **20**, 2808 (2019).
156 Silver, S. Bacterial silver resistance: molecular biology and uses and misuses of silver compounds. *FEMS Microbiology Reviews* **27**, 341-353 (2003).
157 Andrade, L. N., Siqueira, T. E., Martinez, R. & Darini, A. L. C. Multidrug-resistant CTX-M-(15, 9, 2)-and KPC-2-producing Enterobacter hormaechei and Enterobacter asburiae isolates possessed a set of acquired heavy metal tolerance genes including a chromosomal *sil* operon (for acquired silver resistance). *Frontiers in Microbiology* **9**, 1-6 (2018).
158 Su, D., Berndt, C., Fomenko, D. E., Holmgren, A. & Gladyshev, V. N. A conserved cis-proline precludes metal binding by the active site thiolates in members of the thioredoxin family of proteins. *Biochemistry* **46**, 6903-6910 (2007).
159 Finley, P. J. *et al.* Unprecedented silver resistance in clinically isolated Enterobacteriaceae: major implications for burn and wound management. *Antimicrobial Agents and Chemotherapy* **59**, 4734-4741 (2015).
160 Gilmour, M. W., Thomson, N. R., Sanders, M., Parkhill, J. & Taylor, D. E. The complete nucleotide sequence of the resistance plasmid R478: defining the backbone components of incompatibility group H conjugative plasmids through comparative genomics. *Plasmid* **52**, 182-202 (2004).
161 Johnson, T. J., Wannemeuhler, Y. M., Scaccianoce, J. A., Johnson, S. J. & Nolan, L. K. Complete DNA sequence, comparative genomics, and prevalence of an IncHI2 plasmid occurring among extraintestinal pathogenic Escherichia coli isolates. *Antimicrobial agents and chemotherapy* **50**, 3929-3933 (2006).
162 Sherburne, C. K. *et al.* The complete DNA sequence and analysis of R27, a large IncHI plasmid from Salmonella typhi that is temperature sensitive for transfer. *Nucleic acids research* **28**, 2177-2186 (2000).
163 Kang, F., Alvarez, P. J. & Zhu, D. Microbial extracellular polymeric substances reduce Ag+ to silver nanoparticles and antagonize bactericidal activity. *Environmental Science & Technology* **48**, 316-322 (2013).
164 Lu, Y. & Swartz, J. R. Functional properties of flagellin as a stimulator of innate immunity. *Scientific Reports* **6**, 18379 (2016).
165 Metlina, A. Bacterial and archaeal flagella as prokaryotic motility organelles. *Biochemistry (Moscow)* **69**, 1203-1212 (2004).
166 Park, S. & Imlay, J. A. High levels of intracellular cysteine promote oxidative DNA damage by driving the fenton reaction. *Journal of bacteriology* **185**, 1942-1950 (2003).
167 Sinha, S. C. *et al.* The purine repressor of Bacillus subtilis: a novel combination of domains adapted for transcription regulation. *Journal of Bacteriology* **185**, 4087-4098 (2003).
168 Ma, Y., Metch, J. W., Yang, Y., Pruden, A. & Zhang, T. Shift in antibiotic resistance gene profiles associated with nanosilver during wastewater treatment. *FEMS Microbiology Ecology* **92** (2016).
169 Siddiqui, M., Mondal, A., Sultan, I., Ali, A. & Haq, Q. Co-occurrence of ESBLs and silver resistance determinants among bacterial isolates inhabiting polluted stretch of river Yamuna, India. *International Journal of Environmental Science and Technology* **16**, 5611-5622 (2019).
170 Koditschek, L. K. & Guyre, P. Resistance transfer fecal coliforms isolated from the Whippany River. *Water Research* **8**, 747-752 (1974).

171 Baker-Austin, C., Wright, M. S., Stepanauskas, R. & McArthur, J. Co-selection of antibiotic and metal resistance. *Trends in Microbiology* **14**, 176-182 (2006).
172 Seiler, C. & Berendonk, T. U. Heavy metal driven co-selection of antibiotic resistance in soil and water bodies impacted by agriculture and aquaculture. *Frontiers in Microbiology* **3**, 399 (2012).
173 Chapman, J. S. Disinfectant resistance mechanisms, cross-resistance, and co-resistance. *International Biodeterioration & Biodegradation* **51**, 271-276 (2003).
174 Nakajima, H., Kobayashi, K., Kobayashi, M., Asako, H. & Aono, R. Overexpression of the *robA* gene increases organic solvent tolerance and multiple antibiotic and heavy metal ion resistance in Escherichia coli. *Applied and Environmental Microbiology* **61**, 2302-2307 (1995).
175 Pal, C. *et al.* Metal resistance and its association with antibiotic resistance. *Advances in Microbial Physiology* **70**, 261-313 (2017).
176 Veress, A. *et al.* Abundance of mobile genetic elements in an Acinetobacter lwoffii strain isolated from Transylvanian honey sample. *Scientific reports* **10**, 1-14 (2020).
177 Vänskä, M. *et al.* Toxic environment of war: maternal prenatal heavy metal load predicts infant emotional development. *Infant Behavior and Development* **55**, 1-9 (2019).
178 Gębka, K., Bełdowski, J. & Bełdowska, M. The impact of military activities on the concentration of mercury in soils of military training grounds and marine sediments. *Environmental Science and Pollution Research* **23**, 23103-23113 (2016).
179 Bazzi, W. *et al.* Heavy metal toxicity in armed conflicts potentiates AMR in A. baumannii by selecting for antibiotic and heavy metal co-resistance mechanisms. *Frontiers in Microbiology* **11**, 68 (2020).
180 Chen, Q.-L. *et al.* Does nano silver promote the selection of antibiotic resistance genes in soil and plant? *Environment International* **128**, 399-406 (2019).
181 Pietsch, F. *et al.* Selection of resistance by antimicrobial coatings in the healthcare setting. *Journal of Hospital Infection* (2020).
182 Yang, Y. & Alvarez, P. J. Sublethal concentrations of silver nanoparticles stimulate biofilm development. *Environmental Science & Technology Letters* **2**, 221-226 (2015).
183 Song, T., Duperthuy, M. & Wai, S. N. Sub-optimal treatment of bacterial biofilms. *Antibiotics* **5**, 23 (2016).
184 Singh, S., Singh, S. K., Chowdhury, I. & Singh, R. Understanding the mechanism of bacterial biofilms resistance to antimicrobial agents. *The Open Microbiology Journal* **11**, 53-62 (2017).
185 Qiu, Z. *et al.* Effects of nano-TiO2 on antibiotic resistance transfer mediated by RP4 plasmid. *Nanotoxicology* **9**, 895-904 (2015).
186 Qiu, Z. *et al.* Nanoalumina promotes the horizontal transfer of multiresistance genes mediated by plasmids across genera. *Proceedings of the National Academy of Sciences* **109**, 4944-4949 (2012).
187 Gunawan, C., Teoh, W. Y., Marquis, C. P., Lifia, J. & Amal, R. Reversible antimicrobial photoswitching in nanosilver. *Small* **5**, 341-344 (2009).
188 Schaub, I. G. & Hauber, F. D. A biochemical and serological study of a group of identical unidentifiable gram-negative bacilli from human sources. *Journal of bacteriology* **56**, 379 (1948).

189 Eng, R., Padberg, F., Smith, S., Tan, E. & Cherubin, C. Bactericidal effects of antibiotics on slowly growing and nongrowing bacteria. *Antimicrobial Agents and Chemotherapy* **35**, 1824-1828 (1991).
190 Wiegand, I., Hilpert, K. & Hancock, R. E. Agar and broth dilution methods to determine the minimal inhibitory concentration (MIC) of antimicrobial substances. *Nature Protocols* **3**, 163 (2008).
191 Luber, P., Bartelt, E., Genschow, E., Wagner, J. & Hahn, H. Comparison of broth microdilution, E test, and agar dilution methods for antibiotic susceptibility testing of Campylobacter jejuni and Campylobacter coli. *Journal of Clinical Microbiology* **41**, 1062-1068 (2003).
192 Andrews, J. M. Determination of minimum inhibitory concentrations. *Journal of Antimicrobial Chemotherapy* **48**, 5-16 (2001).
193 Brauner, A., Fridman, O., Gefen, O. & Balaban, N. Q. Distinguishing between resistance, tolerance and persistence to antibiotic treatment. *Nature Reviews Microbiology* **14**, 320-330 (2016).
194 Balaban, N. Q. *et al.* Definitions and guidelines for research on antibiotic persistence. *Nature Reviews Microbiology* **17**, 441-448 (2019).
195 Gaio, D. *et al.* Hackflex: low cost Illumina sequencing library construction for high sample counts. *BioRxiv*, 779215 (2019).
196 Benjamini, Y. & Hochberg, Y. Controlling the false discovery rate: a practical and powerful approach to multiple testing. *Journal of the Royal statistical society: series B (Methodological)* **57**, 289-300 (1995).
197 Lukovic, B. *et al.* The first nationwide multicenter study of Acinetobacter baumannii recovered in Serbia: emergence of OXA-72, OXA-23 and NDM-1-producing isolates. *Antimicrobial Resistance & Infection Control* **9**, 1-12 (2020).
198 Mann, R. *et al.* Evolution of biofilm-forming pathogenic bacteria in the presence of nanoparticles and antibiotic: adaptation phenomena and cross-resistance. *Journal of Nanobiotechnology* **19**, 1-17 (2021).
199 Hamidian, M. *et al.* Analysis of complete genome sequence of Acinetobacter baumannii strain ATCC 19606 reveals novel mobile genetic elements and novel prophage. *Microorganisms* **8**, 1851 (2020).
200 Durán, N. *et al.* Silver nanoparticles: a new view on mechanistic aspects on antimicrobial activity. *Nanomedicine: Nanotechnology, Biology and Medicine* **12**, 789-799 (2016).
201 Sugino, A., Peebles, C. L., Kreuzer, K. N. & Cozzarelli, N. R. Mechanism of action of nalidixic acid: purification of Escherichia coli nalA gene product and its relationship to DNA gyrase and a novel nicking-closing enzyme. *Proceedings of the National Academy of Sciences* **74**, 4767-4771 (1977).
202 Bohlmann, L. *et al.* Chemical synergy between ionophore PBT2 and zinc reverses antibiotic resistance. *MBio* **9**, e02391-02318 (2018).
203 Chukwu, K. B., Abafe, O. A., Amoako, D. G., Essack, S. Y. & Abia, A. L. Environmental concentrations of antibiotics, biocides, and heavy metals fail to induce phenotypic antimicrobial resistance in Escherichia coli. *Science of the Total Environment* **899**, 165721 (2023).
204 Forbes, S., Dobson, C. B., Humphreys, G. J. & McBain, A. J. Transient and sustained bacterial adaptation following repeated sublethal exposure to microbicides and a novel human antimicrobial peptide. *Antimicrobial Agents and Chemotherapy* **58**, 5809-5817 (2014).

205 Ribera, A. *et al.* Antimicrobial susceptibility and mechanisms of resistance to quinolones and β-lactams in Acinetobacter genospecies 3. *Antimicrobial Agents and Chemotherapy* **48**, 1430-1432 (2004).
206 Ribera, A., Ruiz, J., Jiminez de Anta, M. T. & Vila, J. Effect of an efflux pump inhibitor on the MIC of nalidixic acid for Acinetobacter baumannii and Stenotrophomonas maltophilia clinical isolates. *Journal of Antimicrobial Chemotherapy* **49**, 697-698 (2002).
207 Seward, R. J. & Towner, K. J. Molecular epidemiology of quinolone resistance in Acinetobacter spp. *Clinical microbiology and infection* **4**, 248-254 (1998).
208 Thummeepak, R. *et al.* Essential gene clusters involved in copper tolerance identified in Acinetobacter baumannii clinical and environmental isolates. *Pathogens* **9**, 60 (2020).
209 Klumpp, S., Zhang, Z. & Hwa, T. Growth rate-dependent global effects on gene expression in bacteria. *Cell* **139**, 1366-1375 (2009).
210 Rasouly, A. & Nudler, E. Reactive oxygen species as the long arm of bactericidal antibiotics. *Proceedings of the National Academy of Sciences* **116**, 9696-9698 (2019).
211 Harms, A., Maisonneuve, E. & Gerdes, K. Mechanisms of bacterial persistence during stress and antibiotic exposure. *Science* **354** (2016).
212 Pommier, Y., Leo, E., Zhang, H. & Marchand, C. DNA topoisomerases and their poisoning by anticancer and antibacterial drugs. *Chemistry & Biology* **17**, 421-433 (2010).
213 Ardebili, A., Lari, A. R., Beheshti, M. & Lari, E. R. Association between mutations in gyrA and parC genes of Acinetobacter baumannii clinical isolates and ciprofloxacin resistance. *Iranian Journal of Basic Medical Sciences* **18**, 623 (2015).
214 Park, S. *et al.* Alterations of gyrA, gyrB, and parC and activity of efflux pump in fluoroquinolone-resistant Acinetobacter baumannii. *Osong Public Health and Research Perspectives* **2**, 164-170 (2011).
215 Laubacher, M. E. & Ades, S. E. The Rcs phosphorelay is a cell envelope stress response activated by peptidoglycan stress and contributes to intrinsic antibiotic resistance. *Journal of Bacteriology* **190**, 2065-2074 (2008).
216 Rogov, V. V. *et al.* A new structural domain in the Escherichia coli RcsC hybrid sensor kinase connects histidine kinase and phosphoreceiver domains. *Journal of Molecular Biology* **364**, 68-79 (2006).
217 Crossman, L. C. *et al.* The complete genome, comparative and functional analysis of Stenotrophomonas maltophilia reveals an organism heavily shielded by drug resistance determinants. *Genome Biology* **9**, 1-13 (2008).
218 Gaddy, J. A. & Actis, L. A. Regulation of Acinetobacter baumannii biofilm formation. *Future Microbiology* **4**, 273-278 (2009).
219 Colquhoun, J. M. & Rather, P. N. Insights into mechanisms of biofilm formation in Acinetobacter baumannii and implications for uropathogenesis. *Frontiers in cellular and infection microbiology* **10**, 253 (2020).
220 Lu, S. C. Regulation of glutathione synthesis. *Molecular Aspects of Medicine* **30**, 42-59 (2009).
221 Forman, H. J., Zhang, H. & Rinna, A. Glutathione: overview of its protective roles, measurement, and biosynthesis. *Molecular aspects of medicine* **30**, 1-12 (2009).

222 Wongsaroj, L. *et al.* Pseudomonas aeruginosa glutathione biosynthesis genes play multiple roles in stress protection, bacterial virulence and biofilm formation. *PLoS one* **13**, e0205815 (2018).
223 Ishida, T. Antibacterial mechanism of Ag+ ions for bacteriolyses of bacterial cell walls via peptidoglycan autolysins, and DNA damages. *MOJ Toxicol* **4**, 345-350 (2018).
224 Park, H.-J. *et al.* Silver-ion-mediated reactive oxygen species generation affecting bactericidal activity. *Water research* **43**, 1027-1032 (2009).
225 Coyne, S., Rosenfeld, N., Lambert, T., Courvalin, P. & Périchon, B. Overexpression of resistance-nodulation-cell division pump AdeFGH confers multidrug resistance in Acinetobacter baumannii. *Antimicrobial agents and chemotherapy* **54**, 4389-4393 (2010).
226 Hall-Stoodley, L., Costerton, J. W. & Stoodley, P. Bacterial biofilms: from the natural environment to infectious diseases. *Nature Reviews Microbiology* **2**, 95 (2004).
227 Jung, W. K. *et al.* Antibacterial activity and mechanism of action of the silver ion in Staphylococcus aureus and Escherichia coli. *Applied and environmental microbiology* **74**, 2171-2178 (2008).
228 Zou, J. *et al.* Non-walled spherical Acinetobacter baumannii is an important type of persister upon β-lactam antibiotic treatment. *Emerging microbes & infections* **9**, 1149-1159 (2020).
229 Krishnamurthi, V. R., Chen, J. & Wang, Y. Silver ions cause oscillation of bacterial length of Escherichia coli. *Scientific reports* **9**, 1-11 (2019).
230 Faiz, M. B. *et al.* Nanosilver and the microbiological activity of the particulate solids *versus* the leached soluble silver. *Nanotoxicology* **12**, 263-273 (2018).
231 Monem, S. *et al.* Mechanisms protecting Acinetobacter baumannii against multiple stresses triggered by the host immune response, antibiotics and outside-host environment. *International Journal of Molecular Sciences* **21**, 5498 (2020).
232 Li, F.-J., Starrs, L. & Burgio, G. Tug of war between Acinetobacter baumannii and host immune responses. *Pathogens and disease* **76**, ftz004 (2018).
233 Clarke, D., Joyce, S., Toutain, C., Jacq, A. & Holland, I. Genetic analysis of the RcsC sensor kinase from Escherichia coli K-12. *Journal of bacteriology* **184**, 1204-1208 (2002).
234 Shiba, Y. *et al.* Activation of the Rcs signal transduction system is responsible for the thermosensitive growth defect of an Escherichia coli mutant lacking phosphatidylglycerol and cardiolipin. *Journal of bacteriology* **186**, 6526-6535 (2004).
235 Orman, M. A. & Brynildsen, M. P. Inhibition of stationary phase respiration impairs persister formation in E. coli. *Nature communications* **6**, 1-13 (2015).
236 McBee, M. E. *et al.* Production of superoxide in bacteria is stress-and cell state-dependent: a gating-optimized flow cytometry method that minimizes ROS measurement artifacts with fluorescent dyes. *Frontiers in microbiology* **8**, 459 (2017).
237 Brynildsen, M. P., Winkler, J. A., Spina, C. S., MacDonald, I. C. & Collins, J. J. Potentiating antibacterial activity by predictably enhancing endogenous microbial ROS production. *Nature biotechnology* **31**, 160-165 (2013).
238 Masri, A. *et al.* Transcriptome analysis of Escherichia coli K1 after therapy with hesperidin conjugated with silver nanoparticles. *BMC microbiology* **21**, 1-11 (2021).

239 McQuillan, J. S. & Shaw, A. M. Differential gene regulation in the Ag nanoparticle and Ag+-induced silver stress response in Escherichia coli: a full transcriptomic profile. *Nanotoxicology* **8**, 177-184 (2014).
240 Singh, N., Rajwade, J. & Paknikar, K. Transcriptome analysis of silver nanoparticles treated Staphylococcus aureus reveals potential targets for biofilm inhibition. *Colloids and Surfaces B: Biointerfaces* **175**, 487-497 (2019).
241 Valentin, E. *Staphylococcus aureus Bacterial Resistance to Silver Nanoparticle: The Emergence and the Mechanisms of Resistance*, (2020).
242 Yoneyama, H. & Nakae, T. Protein C (OprC) of the outer membrane of Pseudomonas aeruginosa is a copper-regulated channel protein. *Microbiology* **142**, 2137-2144 (1996).
243 Puchkova, L. V., Broggini, M., Polishchuk, E. V., Ilyechova, E. Y. & Polishchuk, R. S. Silver ions as a tool for understanding different aspects of copper metabolism. *Nutrients* **11**, 1364 (2019).
244 De Villenoisy, T. *et al.* Principles of Design and Synthesis of Metal Derivatives from MOFs. *Advanced Materials*, 2210166 (2023).
245 Bhamidimarri, S. P. *et al.* Acquisition of ionic copper by the bacterial outer membrane protein OprC through a novel binding site. *PLoS Biology* **19**, e3001446 (2021).
246 Arts, I. S., Gennaris, A. & Collet, J.-F. Reducing systems protecting the bacterial cell envelope from oxidative damage. *FEBS letters* **589**, 1559-1568 (2015).
247 Chautrand, T., Souak, D., Chevalier, S. & Duclairoir-Poc, C. Gram-negative bacterial envelope homeostasis under oxidative and nitrosative stress. *Microorganisms* **10**, 924 (2022).
248 Uppalapati, S. R., Sett, A. & Pathania, R. The outer membrane proteins OmpA, CarO, and OprD of Acinetobacter baumannii confer a two-pronged defense in facilitating its success as a potent human pathogen. *Frontiers in microbiology* **11**, 589234 (2020).
249 Kwon, H. I. *et al.* Outer membrane protein A contributes to antimicrobial resistance of Acinetobacter baumannii through the OmpA-like domain. *Journal of Antimicrobial Chemotherapy* **72**, 3012-3015 (2017).
250 Nie, D. *et al.* Outer membrane protein A (OmpA) as a potential therapeutic target for Acinetobacter baumannii infection. *Journal of biomedical science* **27**, 1-8 (2020).
251 Lin, M.-F., Lin, Y.-Y. & Lan, C.-Y. Characterization of biofilm production in different strains of Acinetobacter baumannii and the effects of chemical compounds on biofilm formation. *PeerJ* **8**, e9020 (2020).
252 Wu, X.-B. *et al.* Outer membrane protein OmpW of Escherichia coli is required for resistance to phagocytosis. *Research in microbiology* **164**, 848-855 (2013).
253 Labrador-Herrera, G. *et al.* Virulence role of the outer membrane protein CarO in carbapenem-resistant Acinetobacter baumannii. *Virulence* **11**, 1727-1737 (2020).
254 Cabral, M. P. *et al.* Proteomic and functional analyses reveal a unique lifestyle for Acinetobacter baumannii biofilms and a key role for histidine metabolism. *Journal of proteome research* **10**, 3399-3417 (2011).
255 Shin, J.-H., Lee, H.-W., Kim, S.-M. & Kim, J. Proteomic analysis of Acinetobacter baumannii in biofilm and planktonic growth mode. *The Journal of Microbiology* **47**, 728-735 (2009).

256 Völlmecke, C., Drees, S. L., Reimann, J., Albers, S.-V. & Lübben, M. The ATPases CopA and CopB both contribute to copper resistance of the thermoacidophilic archaeon Sulfolobus solfataricus. *Microbiology* **158**, 1622-1633 (2012).
257 Williams, C. L. *et al.* Characterization of Acinetobacter baumannii copper resistance reveals a role in virulence. *Frontiers in microbiology*, 16 (2020).
258 Tang, Y., Quail, M. A., Artymiuk, P. J., Guest, J. R. & Green, J. Escherichia coli aconitases and oxidative stress: post-transcriptional regulation of sodA expression. *Microbiology* **148**, 1027-1037 (2002).
259 Cunningham, L., Gruer, M. J. & Guest, J. R. Transcriptional regulation of the aconitase genes (acnA and acnB) of Escherichia coli. *Microbiology* **143**, 3795-3805 (1997).
260 Palethorpe, S. *et al.* Acinetobacter baumannii regulates its stress responses via the BfmRS two-component regulatory system. *Journal of Bacteriology* **204**, e00494-00421 (2022).
261 Saulou-Berion, C. *et al.* Escherichia coli under ionic silver stress: an integrative approach to explore transcriptional, physiological and biochemical responses. *PloS one* **10**, e0145748 (2015).
262 Abdollahi, S., Rasooli, I. & Gargari, S. L. M. The role of TonB-dependent copper receptor in virulence of Acinetobacter baumannii. *Infection, Genetics and Evolution* **60**, 181-190 (2018).
263 McNeilly, O. *et al.* Development of Nanoparticle Adaptation Phenomena in Acinetobacter baumannii: Physiological Change and Defense Response. *Microbiology Spectrum* **11**, e02857-02822 (2023).
264 Farrow III, J. M., Wells, G. & Pesci, E. C. Desiccation tolerance in Acinetobacter baumannii is mediated by the two-component response regulator BfmR. *PloS One* **13** (2018).
265 Zeidler, S. *et al.* Trehalose, a temperature-and salt-induced solute with implications in pathobiology of Acinetobacter baumannii. *Environmental microbiology* **19**, 5088-5099 (2017).
266 Crippen, C. S., Glushka, J., Vinogradov, E. & Szymanski, C. M. Trehalose-deficient Acinetobacter baumannii exhibits reduced virulence by losing capsular polysaccharide and altering membrane integrity. *Glycobiology* **31**, 1520-1530 (2021).
267 Vanaporn, M. & Titball, R. W. Trehalose and bacterial virulence. *Virulence* **11**, 1192-1202 (2020).
268 Nyström, T. & Neidhardt, F. C. Expression and role of the universal stress protein, UspA, of Escherichia coli during growth arrest. *Molecular microbiology* **11**, 537-544 (1994).
269 Elhosseiny, N. M., Amin, M. A., Yassin, A. S. & Attia, A. S. Acinetobacter baumannii universal stress protein A plays a pivotal role in stress response and is essential for pneumonia and sepsis pathogenesis. *International journal of medical microbiology* **305**, 114-123 (2015).
270 O'Toole, R. & Williams, H. D. Universal stress proteins and Mycobacterium tuberculosis. *Research in Microbiology* **154**, 387-392 (2003).
271 Lorenz, C., Dougherty, T. J. & Lory, S. Correct sorting of lipoproteins into the inner and outer membranes of Pseudomonas aeruginosa by the Escherichia coli LolCDE transport system. *Mbio* **10**, e00194-00119 (2019).
272 Kaplan, E., Greene, N. P., Crow, A. & Koronakis, V. Insights into bacterial lipoprotein trafficking from a structure of LolA bound to the LolC periplasmic

domain. *Proceedings of the National Academy of Sciences* **115**, E7389-E7397 (2018).
273 Campanacci, V., Bishop, R. E., Blangy, S., Tegoni, M. & Cambillau, C. The membrane bound bacterial lipocalin Blc is a functional dimer with binding preference for lysophospholipids. *FEBS letters* **580**, 4877-4883 (2006).
274 Bishop, R. E. The bacterial lipocalins. *Biochimica Et Biophysica Acta (BBA)-Protein Structure and Molecular Enzymology* **1482**, 73-83 (2000).
275 Macedo-Marquez, A. *et al.* Overexpression of a monomeric form of the bovine odorant-binding protein protects Escherichia coli from chemical-induced oxidative stress. *Free Radical Research* **48**, 814-822 (2014).
276 Choi, A. H., Slamti, L., Avci, F. Y., Pier, G. B. & Maira-Litrán, T. The pgaABCD locus of Acinetobacter baumannii encodes the production of poly-β-1-6-N-acetylglucosamine, which is critical for biofilm formation. *Journal of bacteriology* **191**, 5953-5963 (2009).
277 Jones, L. S. & Howe, R. A. in *Biofilms in Infection Prevention and Control* 257-285 (Elsevier, 2014).
278 Gupta, P. & Diwan, B. Bacterial exopolysaccharide mediated heavy metal removal: a review on biosynthesis, mechanism and remediation strategies. *Biotechnology Reports* **13**, 58-71 (2017).
279 Haque, M. M., Mosharaf, M. K., Haque, M. A., Tanvir, M. Z. H. & Alam, M. K. Biofilm formation, production of matrix compounds and biosorption of copper, nickel and lead by different bacterial strains. *Frontiers in Microbiology* **12**, 615113 (2021).
280 Brossard, K. A. & Campagnari, A. A. The Acinetobacter baumannii biofilm-associated protein plays a role in adherence to human epithelial cells. *Infection and immunity* **80**, 228-233 (2012).
281 Loewen, P. C., Switala, J. & Triggs-Raine, B. L. Catalases HPI and HPII in Escherichia coli are induced independently. *Archives of Biochemistry and Biophysics* **243**, 144-149 (1985).
282 Srinivasa Rao, P., Yamada, Y. & Leung, K. Y. A major catalase (KatB) that is required for resistance to H2O2 and phagocyte-mediated killing in Edwardsiella tarda. *Microbiology* **149**, 2635-2644 (2003).
283 Sun, D. *et al.* KatG and KatE confer Acinetobacter resistance to hydrogen peroxide but sensitize bacteria to killing by phagocytic respiratory burst. *Life sciences* **148**, 31-40 (2016).
284 Schellhorn, H. Regulation of hydroperoxidase (catalase) expression in Escherichia coli. *FEMS microbiology letters* **131**, 113-119 (1995).
285 Tainer, J. A., Getzoff, E. D., Richardson, J. S. & Richardson, D. C. Structure and mechanism of copper, zinc superoxide dismutase. *Nature* **306**, 284-287 (1983).
286 da Silva Neto, J. F., Negretto, C. C. & Netto, L. E. Analysis of the organic hydroperoxide response of Chromobacterium violaceum reveals that OhrR is a cys-based redox sensor regulated by thioredoxin. *PloS One* (2012).
287 Reeve, W. G., Tiwari, R. P., Kale, N. B., Dilworth, M. J. & Glenn, A. R. ActP controls copper homeostasis in Rhizobium leguminosarum bv. viciae and Sinorhizobium meliloti preventing low pH-induced copper toxicity. *Molecular microbiology* **43**, 981-991 (2002).
288 Ohno, K., Clausen, C., Green, F. & Stanosz, G. The copper-transporting ATPase pump and its potential role in copper-tolerance. *The International*

Research Group on Wood Protection, section 1, Biology, IRG/WP 16-10859. (2016).
289 Nimse, S. B. & Pal, D. Free radicals, natural antioxidants, and their reaction mechanisms. *RSC advances* **5**, 27986-28006 (2015).
290 Cox, M. M. Regulation of bacterial RecA protein function. *Critical reviews in biochemistry and molecular biology* **42**, 41-63 (2007).
291 Ajiboye, T. O., Skiebe, E. & Wilharm, G. Contributions of RecA and RecBCD DNA repair pathways to the oxidative stress response and sensitivity of Acinetobacter baumannii to antibiotics. *International journal of antimicrobial agents* **52**, 629-636 (2018).
292 Aranda, J. *et al.* Acinetobacter baumannii RecA protein in repair of DNA damage, antimicrobial resistance, general stress response, and virulence. *Journal of bacteriology* **193**, 3740-3747 (2011).
293 Kvint, K., Nachin, L., Diez, A. & Nyström, T. The bacterial universal stress protein: function and regulation. *Current opinion in microbiology* **6**, 140-145 (2003).
294 Meng, J., Young, G. & Chen, J. The Rcs system in Enterobacteriaceae: envelope stress responses and virulence regulation. *Frontiers in Microbiology* **12**, 627104 (2021).
295 Melnyk, A. H., Wong, A. & Kassen, R. The fitness costs of antibiotic resistance mutations. *Evolutionary applications* **8**, 273-283 (2015).
296 Zhu, L. J., Chen, X. Y. & Hou, P. F. Mutation of CarO participates in drug resistance in imipenem-resistant Acinetobacter baumannii. *Journal of clinical laboratory analysis* **33**, e22976 (2019).
297 Ye, Y. *et al.* Roles of outer membrane protein W (OmpW) on survival, morphology, and biofilm formation under NaCl stresses in Cronobacter sakazakii. *Journal of dairy science* **101**, 3844-3850 (2018).
298 Alcalde-Rico, M., Hernando-Amado, S., Blanco, P. & Martínez, J. L. Multidrug efflux pumps at the crossroad between antibiotic resistance and bacterial virulence. *Frontiers in microbiology* **7**, 1483 (2016).
299 Ebbensgaard, A. E., Løbner-Olesen, A. & Frimodt-Møller, J. The role of efflux pumps in the transition from low-level to clinical antibiotic resistance. *Antibiotics* **9**, 855 (2020).
300 Coenye, T. Do results obtained with RNA-sequencing require independent verification? *Biofilm* **3** (2021).
301 Wang, Z., Gerstein, M. & Snyder, M. RNA-Seq: a revolutionary tool for transcriptomics. *Nature reviews genetics* **10**, 57-63 (2009).
302 Mahamad Maifiah, M. H., Velkov, T., Creek, D. J. & Li, J. Global Metabolic Analyses of Acinetobacter baumannii. *Acinetobacter baumannii: Methods and Protocols*, 321-328 (2019).
303 Dong, Y., Hu, J., Fan, L. & Chen, Q. RNA-Seq-based transcriptomic and metabolomic analysis reveal stress responses and programmed cell death induced by acetic acid in Saccharomyces cerevisiae. *Scientific reports* **7**, 1-16 (2017).
304 Nakashima, N. & Miyazaki, K. Bacterial cellular engineering by genome editing and gene silencing. *International journal of molecular sciences* **15**, 2773-2793 (2014).
305 Barquist, L. *et al.* The TraDIS toolkit: sequencing and analysis for dense transposon mutant libraries. *Bioinformatics* **32**, 1109-1111 (2016).

306 Coltharp, C. & Xiao, J. Superresolution microscopy for microbiology. *Cellular microbiology* **14**, 1808-1818 (2012).
307 Golding, C. G., Lamboo, L. L., Beniac, D. R. & Booth, T. F. The scanning electron microscope in microbiology and diagnosis of infectious disease. *Scientific reports* **6**, 1-8 (2016).
308 El-Halfawy, O. M. *et al.* Antibiotic capture by bacterial lipocalins uncovers an extracellular mechanism of intrinsic antibiotic resistance. *MBio* **8**, e00225-00217 (2017).
309 Sugawara, E. & Nikaido, H. Properties of AdeABC and AdeIJK efflux systems of Acinetobacter baumannii compared with those of the AcrAB-TolC system of Escherichia coli. *Antimicrobial agents and chemotherapy* **58**, 7250-7257 (2014).
310 Alav, I., Sutton, J. M. & Rahman, K. M. Role of bacterial efflux pumps in biofilm formation. *Journal of Antimicrobial Chemotherapy* **73**, 2003-2020 (2018).
311 Blair, J. M. & Piddock, L. J. Structure, function and inhibition of RND efflux pumps in Gram-negative bacteria: an update. *Current opinion in microbiology* **12**, 512-519 (2009).
312 Nguyen, T. H. T. *et al.* Efflux Pump Inhibitors in Controlling Antibiotic Resistance: Outlook under a Heavy Metal Contamination Context. *Molecules* **28**, 2912 (2023).
313 Delcour, A. H. Outer membrane permeability and antibiotic resistance. *Biochimica et Biophysica Acta (BBA)-Proteins and Proteomics* **1794**, 808-816 (2009).
314 Porcheron, G., Garénaux, A., Proulx, J., Sabri, M. & Dozois, C. M. Iron, copper, zinc, and manganese transport and regulation in pathogenic Enterobacteria: correlations between strains, site of infection and the relative importance of the different metal transport systems for virulence. *Frontiers in cellular and infection microbiology* **3**, 90 (2013).
315 Choi, S.-H. *et al.* Zinc-dependent regulation of zinc import and export genes by Zur. *Nature communications* **8**, 15812 (2017).
316 Xu, C., Bilya, S. & Xu, W. adeABC efflux gene in Acinetobacter baumannii. *New microbes and new infections* **30**, 100549 (2019).
317 Hui, D., Khaiat, S., Uy, T. & Xu, H. Partial confirmation of single katG and katE knockouts and double katG/katE knockouts created from isogenic background of Escherichia coli K-12 strains. *J. Exp. Microbiol. Immunol* **18**, 139-145 (2014).
318 Seitz, E. M., Brockman, J. P., Sandler, S. J., Clark, A. J. & Kowalczykowski, S. C. RadA protein is an archaeal RecA protein homolog that catalyzes DNA strand exchange. *Genes & development* **12**, 1248-1253 (1998).
319 Borisov, V. B. *et al.* Bacterial oxidases of the cytochrome bd family: Redox enzymes of unique structure, function, and utility as drug targets. *Antioxidants & redox signaling* **34**, 1280-1318 (2021).
320 Pearson, S. A. & Cowan, J. Glutathione-coordinated metal complexes as substrates for cellular transporters. *Metallomics* **13**, mfab015 (2021).
321 Helbig, K., Bleuel, C., Krauss, G. J. & Nies, D. H. Glutathione and transition-metal homeostasis in Escherichia coli. *Journal of bacteriology* **190**, 5431-5438 (2008).

322 Van Laar, T. A. *et al.* Pseudomonas aeruginosa gshA mutant is defective in biofilm formation, swarming, and pyocyanin production. *Msphere* **3**, e00155-00118 (2018).
323 Ku, J. W. K. & Gan, Y.-H. New roles for glutathione: Modulators of bacterial virulence and pathogenesis. *Redox Biology* **44**, 102012 (2021).
324 VanDrisse, C. M. & Escalante-Semerena, J. C. Protein acetylation in bacteria. *Annual review of microbiology* **73**, 111-132 (2019).
325 Marciano, D. C. *et al.* Negative feedback in genetic circuits confers evolutionary resilience and capacitance. *Cell reports* **7**, 1789-1795 (2014).
326 Michalska, K. *et al.* Conservation of the structure and function of bacterial tryptophan synthases. *IUCrJ* **6**, 649-664 (2019).
327 Itoh, Y. *et al.* Roles of pgaABCD genes in synthesis, modification, and export of the Escherichia coli biofilm adhesin poly-β-1, 6-N-acetyl-D-glucosamine. *Journal of bacteriology* **190**, 3670-3680 (2008).
328 Kröger, C., Kary, S. C., Schauer, K. & Cameron, A. D. Genetic regulation of virulence and antibiotic resistance in Acinetobacter baumannii. *Genes* **8**, 12 (2016).
329 Tomaras, A. P., Flagler, M. J., Dorsey, C. W., Gaddy, J. A. & Actis, L. A. Characterization of a two-component regulatory system from Acinetobacter baumannii that controls biofilm formation and cellular morphology. *Microbiology* **154**, 3398-3409 (2008).
330 Park, J. S. *et al.* Mechanism of anchoring of OmpA protein to the cell wall peptidoglycan of the gram-negative bacterial outer membrane. *The FASEB Journal* **26**, 219 (2012).
331 Vollmer, W., Blanot, D. & De Pedro, M. A. Peptidoglycan structure and architecture. *FEMS microbiology reviews* **32**, 149-167 (2008).
332 Huang, K. C., Mukhopadhyay, R., Wen, B., Gitai, Z. & Wingreen, N. S. Cell shape and cell-wall organization in Gram-negative bacteria. *Proceedings of the National Academy of Sciences* **105**, 19282-19287 (2008).
333 Kana, B. D. *et al.* Characterization of the cydAB-encoded cytochrome bd oxidase from Mycobacterium smegmatis. *Journal of Bacteriology* **183**, 7076-7086 (2001).
334 Voggu, L. *et al.* Microevolution of cytochrome bd oxidase in Staphylococci and its implication in resistance to respiratory toxins released by Pseudomonas. *Journal of bacteriology* **188**, 8079-8086 (2006).
335 Huemer, M., Mairpady Shambat, S., Brugger, S. D. & Zinkernagel, A. S. Antibiotic resistance and persistence—Implications for human health and treatment perspectives. *EMBO reports* **21**, e51034 (2020).
336 Friedlander, R. S. *et al.* Bacterial flagella explore microscale hummocks and hollows to increase adhesion. *Proceedings of the National Academy of Sciences* **110**, 5624-5629 (2013).
337 Grabowicz, M. Lipoprotein Transport: Greasing the Machines of Outer Membrane Biogenesis: Re-Examining Lipoprotein Transport Mechanisms Among Diverse Gram-Negative Bacteria While Exploring New Discoveries and Questions. *BioEssays* **40**, 1700187 (2018).
338 Cussiol, J. R., Alegria, T. G., Szweda, L. I. & Netto, L. E. Ohr (organic hydroperoxide resistance protein) possesses a previously undescribed activity, lipoyl-dependent peroxidase. *Journal of Biological Chemistry* **285**, 21943-21950 (2010).

339 Zhu, Y. *et al.* Complete genome sequence and genome-scale metabolic modelling of Acinetobacter baumannii type strain ATCC 19606. *International Journal of Medical Microbiology* **310**, 151412 (2020).
340 Kok, M., Maton, L., van der Peet, M., Hankemeier, T. & van Hasselt, J. C. Unraveling antimicrobial resistance using metabolomics. *Drug Discovery Today* (2022).
341 Sulaiman, J. E. & Lam, H. Proteomics in antibiotic resistance and tolerance research: mapping the resistome and the tolerome of bacterial pathogens. *Proteomics* **22**, 2100409 (2022).
342 Fortuin, S. & Soares, N. C. The integration of proteomics and metabolomics data paving the way for a better understanding of the mechanisms underlying microbial acquired drug resistance. *Frontiers in Medicine* **9**, 849838 (2022).
343 Miller, C. & Gilmore, J. Detection of quorum-sensing molecules for pathogenic molecules using cell-based and cell-free biosensors. *Antibiotics* **9**, 259 (2020).
344 Antunes, L., Visca, P. & Towner, K. J. *Acinetobacter baumannii*: evolution of a global pathogen. *Pathogens and Disease* **71**, 292-301 (2014).
345 Brunetti, J., Falciani, C., Bracci, L. & Pini, A. Models of in-vivo bacterial infections for the development of antimicrobial peptide-based drugs. *Current topics in medicinal chemistry* **17**, 613-619 (2017).
346 Shi, D., Mi, G., Wang, M. & Webster, T. J. In vitro and ex vivo systems at the forefront of infection modeling and drug discovery. *Biomaterials* **198**, 228-249 (2019).
347 Shadan, A., Pathak, A., Ma, Y., Pathania, R. & Singh, R. P. Deciphering the virulence factors, regulation, and immune response to Acinetobacter baumannii infection. *Frontiers in Cellular and Infection Microbiology* **13**, 156 (2023).
348 Gebhardt, M. J. *et al.* Joint transcriptional control of virulence and resistance to antibiotic and environmental stress in Acinetobacter baumannii. *MBio* **6**, e01660-01615 (2015).
349 Geisinger, E. & Isberg, R. R. Antibiotic modulation of capsular exopolysaccharide and virulence in Acinetobacter baumannii. *PLoS pathogens* **11**, e1004691 (2015).
350 Bonnington, K. & Kuehn, M. Protein selection and export via outer membrane vesicles. *Biochimica et Biophysica Acta (BBA)-Molecular Cell Research* **1843**, 1612-1619 (2014).
351 Jin, J. S. *et al.* Acinetobacter baumannii secretes cytotoxic outer membrane protein A via outer membrane vesicles. *PloS one* **6**, e17027 (2011).

Appendix

Table A1 Gene ontology enrichment analysis of statistically significant differentially expressed genes (DEGs) mapped to functional biological pathways identified in the RNA-Seq comparisons of WT and NAg^R *A. baumannii* ATCC 19606.

Enrichment FDR[1]	No. of DEGs[2]	No. of Pathway Genes[3]	Fold Enrichment	Functional Pathway
		WTLA vs WTNT		
		Upregulated		
0.003856942	1	4	713	Aconitase/3-isopropylmalate dehydratase large subunit, alpha/beta/alpha domain
0.003856942	1	4	713	Aconitase/3-isopropylmalate dehydratase large subunit, alpha/beta/alpha, subdomain
0.003856942	1	4	713	Aconitase, iron-sulfur domain
0.003856942	1	4	713	Aconitase family (aconitate hydratase)
0.004407934	1	5	356.5	Mixed, incl. PrpF protein, and citrate synthase-like, small alpha subdomain
0.004407934	1	4	356.5	Aconitase/3-isopropylmalate dehydratase, swivel
0.004407934	1	3	356.5	Aconitase C-terminal domain
0.034712482	1	49	39.61111111	Mixed, incl. pyruvate, and tricarboxylic acid cycle
0.04628331	1	72	26.40740741	Mixed, incl. pyruvate, and NAD(p)-binding domain superfamily
		Downregulated		
		N/A[4]		
		NRLN vs WTLN		
		Upregulated		
		N/A		
		Downregulated		
0.007863504	4	4	6.79047619	CF(1)
0.000173287	6	8	6.79047619	ATP synthesis, and ATP synthase A chain
0.000173287	6	6	6.79047619	ATP synthesis
0.000173287	6	6	6.79047619	Hydrogen ion transport
0.04496184	3	5	6.79047619	Mixed, incl. ribosomal protein S8, and ribosomal protein L1
0.006199586	5	6	5.658730159	Mixed, incl. stress response, and Hsp90 protein
0.029675761	4	5	5.432380952	Translation protein SH3-like domain superfamily
0.029675761	4	6	5.432380952	Fatty acid biosynthesis
1.61E-13	23	32	5.206031746	rRNA-binding
3.80E-21	37	60	5.024952381	Ribonucleoprotein
2.63E-21	38	61	4.962271062	Ribosomal protein

1.27E-20	38	67	4.778483245	Ribosomal protein, and elongation factor Tu domain 2
1.04E-18	40	85	4.115440115	Ribosomal protein, and elongation factor
0.018354727	6	11	4.074285714	Chaperone, and Hsp90 protein
8.15E-20	44	102	3.983746032	Ribosomal protein, and protein biosynthesis
3.01E-20	54	161	3.333506494	Mixed, incl. ribonucleoprotein, and protein biosynthesis
6.29E-08	24	61	3.325947522	RNA-binding

NRHN vs NRNT				
Upregulated				
0.007760048	7	13	4.401234568	Mixed, incl. histidine metabolism, and HutD
0.038706688	5	6	4.401234568	Histidine metabolism, and HutD
0.000493409	11	29	4.034465021	Dioxygenase
0.007760048	9	108	3.601010101	Mostly uncharacterized, incl. dioxygenase, and sugar (and other) transporter
0.007760048	9	89	3.601010101	Mixed, incl. dioxygenase, and sugar transporter, conserved site
0.017992297	8	63	3.520987654	Mixed, incl. dioxygenase, and coenzyme A transferase
0.031939557	11	120	2.689643347	Mixed, incl. LysR substrate binding domain, and LysE type translocator
0.008084264	16	110	2.514991182	Transcription regulation
0.019823374	14	101	2.464691358	Winged helix DNA-binding domain superfamily
0.013984614	17	115	2.338155864	Transcription
0.017992297	17	125	2.267302656	Winged helix-like DNA-binding domain superfamily
0.007760048	21	174	2.254290876	DNA-binding
Downregulated				
0.001954735	17	46	2.774954212	Mixed, incl. ATP synthesis, and proton-conducting membrane transporter
0.008435284	15	39	2.671078921	Mixed, incl. ATP synthesis, and quinone
0.042330184	12	36	2.611721612	Protein biosynthesis
0.014657461	19	74	2.255577756	Ligase

NRHN vs NRLN				
Upregulated				
0.008443366	7	13	4.570512821	Mixed, incl. histidine metabolism, and HutD
0.031438958	5	6	4.570512821	Histidine metabolism, and HutD
0.006785941	10	29	3.808760684	Dioxygenase
0.031438958	8	108	3.324009324	Mostly uncharacterized, incl. dioxygenase, and sugar (and other) transporter
0.031438958	8	89	3.324009324	Mixed, incl. dioxygenase, and sugar transporter, conserved site
0.029993603	11	53	2.793091168	Mostly uncharacterized, incl. histidine metabolism, and nickel insertion
0.029993603	11	120	2.793091168	Mixed, incl. LysR substrate binding domain, and LysE type translocator
0.027762545	14	101	2.559487179	Winged helix DNA-binding domain superfamily
0.027762545	15	110	2.448489011	Transcription regulation
0.029993603	16	115	2.28525641	Transcription
0.020356756	20	174	2.229518449	DNA-binding

0.031438958	16	125	2.216006216	Winged helix-like DNA-binding domain superfamily
			Downregulated	
0.021195614	16	46	2.41285956	Mixed, incl. ATP synthesis, and proton-conducting membrane transporter
0.021195614	20	74	2.193508691	Ligase
			NRNT vs WTNT	
			Upregulated	
0.03855924	11	181	3.267916667	Signal
0.000179797	33	235	2.262403846	Oxidoreductase
			Downregulated	
0.002725011	5	6	5.941666667	Fatty acid biosynthesis
0.012851779	5	6	4.951388889	Mixed, incl. stress response, and Hsp90 protein
0.012851779	5	8	4.951388889	Fatty acid metabolism
5.18E-23	40	59	4.850340136	Ribosomal protein
9.19E-23	40	60	4.753333333	Ribonucleoprotein
5.18E-23	42	67	4.621296296	Ribosomal protein, and Elongation factor Tu domain 2
4.47E-12	23	32	4.555277778	rRNA-binding
2.05E-21	48	102	3.802666667	Ribosomal protein, and protein biosynthesis
0.042815578	6	11	3.565	Chaperone, and Hsp90 protein
2.24E-22	60	161	3.240909091	Mixed, incl. ribonucleoprotein, and protein biosynthesis
2.21E-07	25	61	3.031462585	RNA-binding

[1] FDR = false discovery rate (adjusted *P*-value of 0.05). [2] Number of DEGs identified in functional pathway. [3] Number of total genes within functional pathway. [4] N/A = not applicable (no DEGs identified in pathway).

Table A2 Gene ontology enrichment analysis of statistically significant differentially expressed genes (DEGs) mapped to functional biological pathways identified in the RNA-Seq comparisons of WT and Ag^{+T} *A. baumannii* ATCC 19606.

Enrichment FDR[1]	No. of DEGs[2]	No. of Pathway Genes[3]	Fold Enrichment	Functional Pathway
			WTLA vs WTNT	
			Upregulated	
0.035818682	1	3	101.8571429	Glycosyl transferase family 21
0.035818682	1	3	101.8571429	Glycosyl transferase family group 2
0.035818682	1	5	101.8571429	Glycosyltransferase like family 2
0.010080967	2	7	67.9047619	Mixed, incl. PGAD-like protein, and hypothetical glycosyl hydrolase family 13
0.010080967	2	18	50.92857143	Mixed, incl. glycosyltransferase like family 2, and glycoside hydrolase/deacetylase
0.040082851	1	5	50.92857143	Mixed, incl. NAD kinase, and Sir2 family
0.040082851	1	6	50.92857143	Mixed, incl. proton-conducting membrane transporter, and Na^+/H^+ antiporter subunit
0.040082851	1	4	50.92857143	NodB homology domain
0.040082851	1	6	50.92857143	Glycoside hydrolase/deacetylase, beta/alpha-barrel
0.040082851	1	4	50.92857143	Polysaccharide deacetylase
0.022352934	2	81	18.51948052	Mixed, incl. response regulator receiver domain, and histidine kinase A (phosphoacceptor)
0.013792393	3	46	12.73214286	Mixed, incl. ATP synthesis, and proton-conducting membrane transporter
0.040082851	2	39	9.25974026	Mixed, incl. ATP synthesis, and quinone
0.040182649	2	181	8.488095238	Signal
0.013792393	5	617	4.428571429	Transmembrane helix
0.013792393	5	625	4.390394089	Transmembrane
0.022352934	5	668	3.663926002	Membrane
			Downregulated	
0.044394351	1	8	118.8333333	Mixed, incl. protein of unknown function, DUF485, and sodium:solute symporter family
0.044394351	1	7	118.8333333	Mixed, incl. glyoxalase/fosfomycin resistance/dioxygenase domain, and fumarylace
0.044394351	1	5	118.8333333	Mixed, incl. citrate transporter, and Cyclin M, transmembrane domain
0.013147271	2	4	59.41666667	Histidine metabolism
0.044394351	1	29	59.41666667	Mostly uncharacterized, incl. phosphoesterase, and protein of unknown function
0.044394351	1	11	59.41666667	Mostly uncharacterized, incl. ligase N family, and citrate transporter
0.044394351	1	5	59.41666667	Glyoxalase/fosfomycin resistance/dioxygenase domain
0.044394351	1	4	59.41666667	Amidohydrolase-related
0.044394351	1	4	59.41666667	Metal-dependent hydrolase, composite domain superfamily
0.044394351	1	6	59.41666667	Glyoxalase/bleomycin resistance protein/dihydroxybiphenyl dioxygenase
0.044394351	1	6	59.41666667	Vicinal oxygen chelate (VOC) domain
0.044394351	1	5	59.41666667	Glyoxalase/Bleomycin resistance protein/Dioxygenase superfamily

0.044394351	1	5	59.41666667	Amidohydrolase family
0.013147271	2	6	47.53333333	Histidine metabolism, and HutD
0.01826809	2	13	33.95238095	Mixed, incl. histidine metabolism, and HutD
0.044394351	2	53	13.2037037	Mostly uncharacterized, incl. histidine metabolism, and nickel insertion

ATLA vs WTLA

Upregulated

0.01775664	4	14	7.059405941	Mixed, incl. thiosulphate/sulfate-binding protein, and phosphoadenosine phosphosulfate
0.01775664	4	34	7.059405941	Mixed, incl. alcohol dehydrogenase groES-like domain, and iron-type alcohol dehydrogenase
0.016173219	5	20	5.882838284	Mixed, incl. ion transport, and cation transporter
0.000538968	9	68	5.294554455	Mostly uncharacterized, incl. NMT1-like family, and MetI-like superfamily
0.009938189	6	42	5.294554455	Mostly uncharacterized, incl. molybdenum cofactor biosynthesis, and molybdopterin
0.001534206	8	37	5.134113411	Short chain dehydrogenase
0.001534206	8	34	5.134113411	KR domain
0.000423979	10	85	5.042432815	Mostly uncharacterized, incl. MetI-like superfamily, and NMT1-like family
0.034530239	5	36	5.042432815	Mixed, incl. TonB-dependent receptor-like, beta-barrel, and ACP-like superfamily
0.005602223	7	32	4.941584158	Short-chain dehydrogenase/reductase SDR
0.005602223	7	21	4.941584158	Short-chain dehydrogenase/reductase, conserved site
0.005602223	7	34	4.941584158	Enoyl-(Acyl carrier protein) reductase
0.000210346	14	181	4.117986799	Signal
0.021188637	11	85	2.876054272	NAD(P)-binding domain superfamily
0.01775664	27	235	1.832730388	Oxidoreductase

Downregulated

0.002219513	4	4	8.695121951	Histidine metabolism
0.016622938	3	5	8.695121951	Mixed, incl. ribosomal protein S8, and ribosomal protein L1
0.008946135	4	6	6.956097561	Histidine metabolism, and HutD
2.22E-16	23	32	6.666260163	rRNA-binding
3.73E-26	37	60	6.434390244	Ribonucleoprotein
1.77E-26	38	61	6.35412758	Ribosomal protein
0.004039135	5	13	6.210801394	Mixed, incl. histidine metabolism, and HutD
7.38E-26	38	67	6.118789521	Ribosomal protein, and elongation factor Tu domain 2
2.18E-23	43	118	4.732787897	Ribosomal protein, and protein biosynthesis
9.41E-24	46	131	4.444173442	Mixed, incl. ribonucleoprotein, and protein biosynthesis
1.12E-10	24	61	4.258835241	RNA-binding

ATHA vs ATNT

Upregulated

3.80E-08	27	32	2.556573705	rRNA-binding
3.90E-05	19	39	2.453277798	Mixed, incl. ATP synthesis, and quinone
2.03E-08	40	60	2.27250996	Ribonucleoprotein

2.55E-08	39	59	2.260915522	Ribosomal protein
1.45E-07	40	67	2.104175889	Ribosomal protein, and elongation factor Tu domain 2
5.19E-06	35	61	2.02902675	RNA-binding
3.24E-08	54	118	1.941701548	Ribosomal protein, and protein biosynthesis
6.88E-07	45	85	1.936798261	Ribosomal protein, and elongation factor
3.24E-08	61	138	1.863213811	Mixed, incl. ribonucleoprotein, and protein biosynthesis
			Downregulated	
0.04735129	9	84	3.363207547	Mixed, incl. TonB dependent receptor, and protein transport
0.04735129	10	32	3.203054807	Mixed, incl. pseudouridine synthase, catalytic domain superfamily, and s-adenosylmethionine
			ATHA vs ATLA	
			Upregulated	
3.51E-08	27	32	2.619183673	rRNA-binding
0.000252326	18	39	2.381076067	Mixed, incl. ATP synthesis, and quinone
2.08E-08	39	59	2.316284881	Ribosomal protein
2.63E-08	39	60	2.269959184	Ribonucleoprotein
7.57E-08	40	67	2.155706727	Ribosomal protein, and elongation factor Tu domain 2
1.28E-05	34	61	2.019325281	RNA-binding
2.92E-07	45	85	1.984230056	Ribosomal protein, and elongation factor
4.39E-08	53	118	1.952415397	Ribosomal protein, and protein biosynthesis
1.62E-07	57	131	1.843129252	Mixed, incl. ribonucleoprotein, and protein biosynthesis
			Downregulated	
			N/A[4]	
			ATNT vs WTNT	
			Upregulated	
0.0102631	5	20	5.991596639	Mixed, incl. ammonium/urea transporter, and GlnD PII-uridylyltransferase
0.002466615	6	20	5.991596639	Mixed, incl. ion transport, and cation transporter
0.030271401	4	14	5.991596639	Mixed, incl. thiosulphate/sulfate-binding protein, and phosphoadenosine phosphosulfate
0.030271401	4	34	5.991596639	Mixed, incl. alcohol dehydrogenase groES-like domain, and iron-type alcohol dehydrogenase
0.002466615	7	42	5.242647059	Mostly uncharacterized, incl. molybdenum cofactor biosynthesis, and molybdopterin
0.0102631	6	36	5.135654262	Mixed, incl. TonB-dependent receptor-like, beta-barrel, and ACP-like superfamily
0.000136111	10	68	4.992997199	Mostly uncharacterized, incl. NMT1-like family, and MetI-like superfamily
0.000136111	11	85	4.707683073	Mostly uncharacterized, incl. MetI-like superfamily, and NMT1-like family
0.0102631	8	84	3.994397759	Mixed, incl. TonB dependent receptor, and protein transport
0.02602932	7	37	3.812834225	Short chain dehydrogenase
0.02602932	7	34	3.812834225	KR domain
0.000136111	15	181	3.744747899	Signal
0.02602932	12	85	2.662931839	NAD(P)-binding domain superfamily

0.014492569	31	235	1.78595669	Oxidoreductase
			Downregulated	
0.036616266	3	5	7.427083333	Mixed, incl. ribosomal protein S8, and ribosomal protein L1
0.005481389	4	4	7.427083333	Histidine metabolism
0.022426063	4	6	5.941666667	Histidine metabolism, and HutD
5.88E-23	37	59	5.608205782	Ribosomal protein
6.89E-23	37	60	5.496041667	Ribonucleoprotein
0.011370031	5	13	5.305059524	Mixed, incl. histidine metabolism, and HutD
7.59E-12	21	32	5.198958333	rRNA-binding
3.18E-21	37	67	5.088927469	Ribosomal protein, and elongation factor Tu domain 2
1.52E-17	40	102	3.961111111	Ribosomal protein, and protein biosynthesis
1.40E-18	45	131	3.713541667	Mixed, incl. ribonucleoprotein, and protein biosynthesis
2.35E-06	21	61	3.183035714	RNA-binding

[1] FDR = false discovery rate (adjusted *P*-value of 0.05). [2] Number of DEGs identified in functional pathway. [3] Number of total genes within functional pathway. [4] N/A = not applicable (no DEGs identified in pathway).